

**Ore Genesis and Geochemical Characteristics of Carbonate-hosted Talc
Deposits in Nangarhar Province, Afghanistan**

(アフガニスタン, Nangarhar州における炭酸塩岩胚胎-
滑石鉱床の成因と地球化学的特徴)

Muhammad Tahir

ID No.9515101



Department of Geosciences, Geotechnology, and Materials Engineering for Resources,
Graduate School of Engineering and Resource Science,
Akita University, JAPAN

2018

Ore Genesis and Geochemical Characteristics of Carbonate-hosted Talc Deposits in Nangarhar Province, Afghanistan

Muhammad Tahir, ID # 9515101

Abstract

Talc occurs as economic deposits in amphibolite facies metamorphosed dolomite marble and magnesite rocks in the Spinghar Fault Block in Afghanistan. This block is composed of various Proterozoic gneisses, schists, quartzites, marbles and amphibolites metamorphosed to amphibolite facies which were intruded by Early Cretaceous igneous rocks such as migmatite-granite and gabbro-monzonite-diorite. Eight deposits and two prospects were chosen from three areas. Six quarries and outcrops among ten from the western part i.e., Anarokas, Kherwasti, Dar, Janinaw, Kotikhel (Dawood mine and Noor mine), three from the middle part i.e., Wachalgad, Lesho, Sargare and one from the most eastern part i.e., Mamond dara in Spinghar Fault Block were studied. The objective of this study is to understand the talc mineralization and formation processes in these areas on the basis of field relations, petrography, X-ray diffractometry (XRD), X-ray fluorescence spectroscopy (XRF), inductively coupled plasma mass spectrometry (ICP-MS), scanning electron microscope energy-dispersive X-ray spectroscopy (SEM-EDX) and electron probe micro analysis (EPMA).

In this block, talc ore bodies occur parallel to subparallel to host magnesite rocks, dolomite marble and gneiss. Intrusive rocks such as dolerite and diorite cross cut the talc ore bodies, host carbonate rocks and gneiss, and are also parallel to sub parallel to the beddings of host carbonate rocks and talc ore bodies. Tremolite was observed with most of talc, and

Carbonate-hosted talc deposits, 2018

antigorite (serpentine) in the altered dolerite and host carbonate rocks. Quartz veins follow the gneissosity of gneiss all over the study areas. Quartz veins were cross cut by granitic rocks at Anarokas. Talc was mainly formed by alteration of magnesite and tremolite in Kherwasti, Anarokas, Dar, Wachalgad, Lesho and Sargare, while in Janinaw, Kotikhel and Mamond dara, talc was formed by alteration of dolomite and tremolite. Common mineral assemblages in the study area of talc ores are (a) talc + magnesite, (b) talc + tremolite, in magnesite rocks (c) magnesite \pm olivine and (d) magnesite + antigorite in Dar, Anarokas and Kherwasti, (e) talc + magnesite, in talc ores and (f) dolomite + calcite + tremolite in dolomite marble in Wachalgad, (g) talc + magnesite, in talc ores, (h) dolomite + tremolite \pm talc in dolomite marble, and (i) hornblende + quartz + plagioclase in amphibolites in Lesho and Sargare, (j) talc + dolomite, in talc ores, (k) tremolite + dolomite in dolomite marble and (l) quartz + talc in quartz veins in Kotikhel and Janinaw, and (m) dolomite + talc + quartz \pm calcite, in host dolomite marble (n) quartz + microcline + muscovite + biotite + allanite in gneiss in Mamond dara, and (o) quartz + muscovite + biotite in gneiss in Anarokas, Wachalgad and Kotikhel. On the basis of the mineral assemblages, the formation temperatures of different minerals such as talc, tremolite and antigorite were estimated. In Mamond dara, the temperature ranged from 360 to 460°C. In Anarokas, Dar and Kherwasti, the temperature was 380 to 460°C. In Janinaw and Kotikhel, it ranged from 405 to 500°C.

The SiO₂ contents of talc rocks from all deposits range from 56.1 to 65.1 wt% and carbonate rocks of Kotikhel are 16.2 wt%, those from Kherwasti range from 1.6 to 25.8 wt%, Anarokas range from 16.6 to 45.5 wt%, Dar range from 6.9 to 8.9 wt%, Wachalgad range from 5.6 to 22.2 wt%, Lesho are 31.0 wt%, Sargare range from 9.6 to 13.9 wt% and Mamond dara range from 10.9 to 15.7 wt%. It is evident that SiO₂ content increased to form talc from

Carbonate-hosted talc deposits, 2018

magnesite rocks and dolomite marble. The whole-rock MgO contents of those range from 30.2 to 35.5 wt% and 27.1 wt%, from 25.1 to 46.3 wt%, from 37.3 to 47.7 wt%, from 43.7 to 46.0 wt%, 23.1 to 53.5 wt%, 37.5 wt%, 26.2 to 48.1 wt%, and 19.3 to 21.9 wt%, respectively. The whole-rock CaO contents of talc rocks and magnesite rocks of all deposits are less than 1 wt%, while those of dolomite marbles of Kotikhel, Kherwasti, Wachalgad, Sargare and Mamond dara range from 17.0 to 33.5 wt%. The Σ REE contents of talc rocks, magnesite rocks and dolomite marbles in Wachalgad and Sargare are 0.4, 1.3, 3.5 ppm and 2.1, 1.7 and 6.6 ppm respectively. The Σ REE contents of talc rocks and magnesite rocks in Kherwasti range from 0.2 to 1.2 ppm, 0.7 to 18.6 ppm respectively, in Anarokas 0.5 ppm, 1.0 to 4.2 ppm respectively, in Dar from 0.2 to 0.8 ppm, 1.1 to 4.7 ppm respectively and in Lesho 2.6 ppm and 13.0 ppm respectively. The Σ REE contents of talc rocks and dolomite marble in Kotikhel are 0.12 ppm and 14.0 ppm respectively, in Janinaw from 0.08 to 6.6 ppm and 2.5 ppm respectively, while in Mamond dara it ranges from 0.04 to 3.2 ppm and 23.5 ppm respectively. EPMA analysis of carbonate minerals from all deposits shows that dolomite and magnesite compositions are close to the ideal composition with FeCO_3 ranging from 0.2 to 0.6 wt% and from 0.2 to 0.5 wt%, and MnCO_3 ranging from 0.02 to 0.06 wt% and from 0.01 to 0.09 wt%, respectively. The chemical compositions of talc and tremolite slightly deviate from ideal compositions with FeO, Na_2O , K_2O , MnO, Al_2O_3 , TiO_2 and Cr_2O_3 contents less than 1 wt%. Concentrations of Al, Ta, Th, Cr, Ni, Co and Σ REE in talc ores and carbonates rocks are comparatively very low with mafic and ultramafic rocks, so inconsistent with mafic and ultramafic rocks protolith. Therefore, the metamorphosed sedimentary carbonate rocks were likely the protolith of talc ores. Magnesium has been derived from pre-existing Mg-rich carbonate host rocks, *i.e.*, magnesite and dolomite marbles.

Table of Contents

Chapter 1	Page No.
Introduction.....	1-13
1.1 Talc.....	1
1.2 Types of Talc Deposits.....	3
1.3 Uses of Talc.....	5
1.4 Magnesite Rocks and Dolomite Marble.....	6
1.5 Location of Study Areas.....	7
1.6 Aims and Objectives.....	8
1.7 Previous Works.....	8
1.8 Climate and Vegetation.....	9
1.9 Demographics.....	10
1.10 Topography and Geomorphology.....	10
1.11 Surface Water.....	12
1.12 Ground Water.....	13
 Chapter 2	
Tectonic Setting.....	14-22
2.1 Geological Units and Faulting.....	17
2.2 Geology of the Study Area (Spinghar Fault Block).....	20
 Chapter 3	
Mode of Occurrence of Talc Deposits.....	23-37
 Chapter 4	
Analytical Methods.....	38-54
 Chapter 5	
Petrography.....	55-74
 Chapter 6	
Geochemistry.....	75-83
6.1 Major Elements.....	75

Carbonate-hosted talc deposits, 2018

6.2 Trace Elements.....	78
6.3 Carbonate Minerals Chemistry.....	81
6.4 Silicate Minerals Chemistry.....	81

Chapter 7

Discussion.....	84-99
7.1 Evidences in Field.....	84
7.2 Phase Relations and Reactions.....	86
7.3 Geochemical Behavior of Elements.....	90
7.4 Genetic Model.....	98

Chapter 8

Tectonic Evolution of Spinghar Block.....	100-108
8.1 Regional Metamorphism.....	100
8.2 Tectonic Evolution.....	101

Chapter 9

Comparison with Other Talc Deposits.....	109-110
--	---------

Chapter 10

Conclusions.....	111-112
Acknowledgements.....	113
References.....	114-125
Appendices.....	126-165

List of Figures

Figures	Page No.
1.1 Different colors of talc ores.....	1

Carbonate-hosted talc deposits, 2018

1.2 Tectonic sketch of Afghanistan showing the major sutures, locations of ophiolitic rocks, basic intrusions and talc deposits.....	3
1.3 Districts of Nangarhar province showing the study areas.....	8
1.4 Topography and generalized geology of the study area.....	12
2.1 Greater Alpine-Himalaya orogenic belt of Asia. Vectors show relative plate motions and velocities between the Indian, Eurasian, and Arabian plates.....	16
2.2 Locations of faults.....	19
2.3 Geological map of Spinghar Fault Block.....	22
3 Beddings in Dolomite marble and magnesite rocks.....	25
3.1 (a) Outcrop of Dawood mine and (b) Outcrop of Noor mine.....	27
3.2 Outcrop sketch of Janinaw deposit.....	28
3.3 Outcrop of Kherwasti deposit.....	29
3.4A Replacement of magnesite by antigorite in Anarokas deposit.....	30
3.4B Outcrop of Anarokas deposit.....	30
3.4C A granitic intrusion cross cut the gneiss and the quartz vein within the gneiss at Anarokas deposit.....	31
3.5 Outcrop of Dar deposit.....	32
3.6 Outcrop sketch of Wachalgad prospect.....	33
3.7 Outcrop of Lesho deposit.....	34
3.8 Outcrop of Sargare prospect.....	35
3.9 Outcrop of Mamond dara deposit.....	36
4.1 (a) Clinometer, (b) laser range finder.....	38
4.2 (a) Different sizes of powder for polishing the sample chips and thin sections, (b) Mounted slide glass with polished chip, (c) Cutting the rock portion with secondary cutter and (d) Ready thin sections for microscopic observations.....	39
4.3 Nikon Eclipse LV100N POL microscope.....	40
4.4 Sample preparation for XRD analysis.....	41

Carbonate-hosted talc deposits, 2018

4.5 Rigaku Multi Flex X-ray Diffractometer at Department of Earth Science and Technology, Akita University.....	41
4.6 Sample (powder pellets) preparation for XRF analysis.....	42
4.7 Electric furnace used for loss on ignition.....	43
4.8 (a) Rigaku ZSX primus II in Akita University, (b) Powder pellet for XRF analysis.....	44
4.9 Samples digestion for ICP-MS analysis.....	45
4.10 Agilent Technologies 7500 Series ICP-MS at Department of Resource Science Akita University.....	46
4.11 (a) JEOL JEC-560 Auto Carbon Coater, (b) JEOL-JXA-8800R Superprobe microanalyser (EPMA), at Akita University, Japan.....	47
4.12 JEOL JSM-6610 Scanning Electron Microscope at Faculty of Education, Akita University.....	54
5.1 Photomicrographs of (a) Talc rock, (b) Dolomite marble showing well developed talc crystals along the boundaries of dolomite, (c) Tremolitite showing replacement of dolomite by tremolite, (d) Antigorite showing replacement of dolomite by antigorite, (e) replacement of quartz by talc, (f) Gneiss having quartz and abundant of muscovite.....	56
5.2 X-ray diffractogram of quartz vein (16KTI11) from Kotikhel showing the presence of quartz and talc.....	57
5.3 Photomicrographs of (a) Talc rock having tremolite replaced by talc, (b) Talc rock showing idiomorphic crystals of tremolite in ground mass of talc, (c) Host dolomite marble, showing abundant of calcite and tremolite, (d) Quartz vein showing replacement of quartz by talc.....	58
5.4 Photomicrographs of (a) Talc rock having relict of magnesite (b) Magnesite rock showing well developed talc crystals, (c) Magnesite rock showing olivine replaced magnesite, (d) Altered diorite, (e) Tremolitite showing coarse grained tremolite crystals , (f) Magnesite rock, replaced by antigorite.....	60

Carbonate-hosted talc deposits, 2018

5.5 Photomicrographs of (a) Talc rock, (b)) Magnesite rock having well developed talc crystals showing poikiloblastic texture, (c) Highly metamorphosed amphibolite having porphyroclast of pyroxene, (d) Magnesite replaced by antigorite , (e) Gneiss having abundant of biotite with muscovite and quartz, (f) Granite.....	62
5.6 X-ray diffractograms of (a) talc-bearing dolomite marble (16ANK10) from Anarokas showing peaks of talc, antigorite and dolomite, (b) magnesite rock (16ANK05B) from Anarokas showing peaks of magnesite and talc with minor dolomite.....	63
5.7 Photomicrographs of (a) Magnesite rock having talc and olivine, (b)) Dolomite marble replaced dolomite by tremolite, (c) Talc rock having relicts of tremolite and magnesite, (d) Altered dolerite, (e) Dolerite showing ophitic texture, (f) Serpentine showing alteration of olivine by serpentine.....	65
5.7A SEM-EDX results show the interstices in tremolite filled by talc.....	66
5.8 Photomicrographs of (a) Magnesite rock replaced by talc, (b)) Talc rock having relicts of magnesite, (c) Dolomite marble having tremolite showing poikiloblastic texture, (d) Gneiss having abundant of biotite and muscovite.....	67
5.9 Photomicrographs of (a) Magnesite rock having well developed talc crystals, (b) Dolomite marble replaced by tremolite and talc, (c) Dolomite marble having coarse grained tremolite, (d) Highly metamorphosed amphibolite.....	68
5.10 Photomicrographs of (a) Magnesite rock replaced by talc, (b) Talc rock, (c) Dolomite marble having tremolite replaced by talc.....	69

Carbonate-hosted talc deposits, 2018

5.11 Photomicrographs of (a) Dolomite marble showing veins of quartz in dolomite to form talc, (b)) Talc rock having relict of dolomite, (c) Quartz chlorite schist, (d) Gneiss showing porphyroblastic texture, (e) Allanite in gneiss.....	71
7.1 Photographs showing typical examples of field observation of talc mineralization at Spinghar Fault Block (a) granitic intrusion into gneiss cross cutting the quartz vein at Anarokas, (b) quartz veins in gneiss at Anarokas, (c) replacement of magnesite by antigorite at Kherwasti, (d) replacement of dolomite by antigorite at Kotikhel, (e) fresh diabase cross cutting the talc veins and host magnesite rocks at Dar, (f) alternating layers of talc and dolomite marble with parallel intrusive rock, strongly altered to quartz chlorite schist at Mamond dara.....	85
7.2 Isobaric temperature- X_{CO_2} diagram showing the stability field of talc at $P_{fluid} > 2$ MPa.....	89
7.3a CaO-MgO-SiO ₂ ternary diagram showing the molecular ratio of bulk chemical compositions of talc rocks, magnesite rocks, talc-bearing magnesite, dolomite marble and talc-bearing dolomite marble, compared with ideal mineral compositions.....	90
7.3b FeCO ₃ -CaCO ₃ -MgCO ₃ ternary diagram showing the compositions of (a) magnesite from Kherwasti, Anarokas, Dar, Wachalgad and Lesho and (b) dolomite from Kotikhel, Wachalgad, Sargare and Mamond dara, (c) calcite from Janinaw.....	92
7.3c (a) FeCO ₃ and (b) MnCO ₃ concentrations in carbonate rocks.....	93
7.3d CaO-MgO-SiO ₂ ternary diagrams showing the molecular ratio of talc and tremolite minerals.....	94
7.3e REE patterns normalized to post-Archean Australian shale (PAAS, Taylor et al., 1985) for talc rocks, magnesite rocks and dolomite marbles while normalized to C1 chondrite	

Carbonate-hosted talc deposits, 2018

(McDonough & Sun, 1995) for intrusive rocks, metamorphic rocks, altered rocks and quartz veins. A) Talc rocks, B) Magnesite rocks and dolomite marble, C) Intrusive rocks, metamorphic rocks and quartz veins.....96

7.4 Genetic model for talc formation in Nangarhar Province, Afghanistan.....99

8.1 Regional metamorphism in Spinghar Block, based on mineral assemblages.....101

8.2 Tectonic sketch map of the Afghan orogenic segment.....104

8.3 Collision history of the Gondwana terrane between the Indian and Turan plates.....107

8.4 Overview map of NW Pakistan SE Afghanistan showing the southward thrusting of the northern units over southern units.....108

List of Tables

Tables	Page No.
1 Mode of occurrence of talc deposits and related rocks in Spinghar Fault Block, Afghanistan..	37
2 Mineral assemblages based on microscopic observations and XRD analysis from different rocks of each deposit in Spinghar Fault Block, Afghanistan.....	72
3 Replacement and intergrowth minerals in talc deposits from Nangarhar province, Afghansitan.....	74
4 Whole-rock chemical composition of talc rocks.....	76
5 Whole-rock chemical composition of magnesite rocks and dolomite marble.....	77
6 Whole-rock chemical analysis of rare earth elements (REE).....	79
7 Bulk trace elements concentration of talc rocks, magnesite rocks, dolomite marble, metamorphic rocks, intrusive rocks and quartz veins.....	80
8 EPMA data of carbonate rocks from Nangarhar talc deposits, Afghanistan.....	82
9 EPMA data of silicate minerals from Nangarhar talc deposits, Afghanistan.....	83

List of Appendices

Appendix	Page No.
1 List of hand specimens from each deposit.....	126
2 List of minerals in each rock from each deposit.....	138
3 List of XRD analysis of each rock from each deposit.....	141
4 List of SEM-EDS analysis of different minerals.....	153
5 Histograms of Fe and Mn concentrations in magnesite, calcite and dolomite minerals from each deposit.....	155

Dedication

I dedicate my efforts to my dear parents and teachers who guided me till this position. I also dedicate this dissertation to my many friends who have supported me throughout the process; I will always appreciate all they have done.

I also dedicate this work to my brothers and sisters and my dear family who always supported me in all conditions.

1. Introduction

1.1 Talc

Talc is a hydrous magnesium silicate inert industrial mineral composed of magnesium, silicon and oxygen, and water. Talc has a great economic significance but its deposits are relatively poorly understood with respect to their occurrence, genesis and timing of formation compared to precious and base metal deposits. Its chemical formula is $Mg_3Si_4O_{10}(OH)_2$. Specific gravity varies from 2.58 to 2.83 gm/cm^3 . Talc is relatively pure in its composition but can contain small amounts of aluminum, iron, manganese, and titanium. Talc can be white, apple green, dark green, pink, brown or black, depending on its composition (Fig. 1.1).

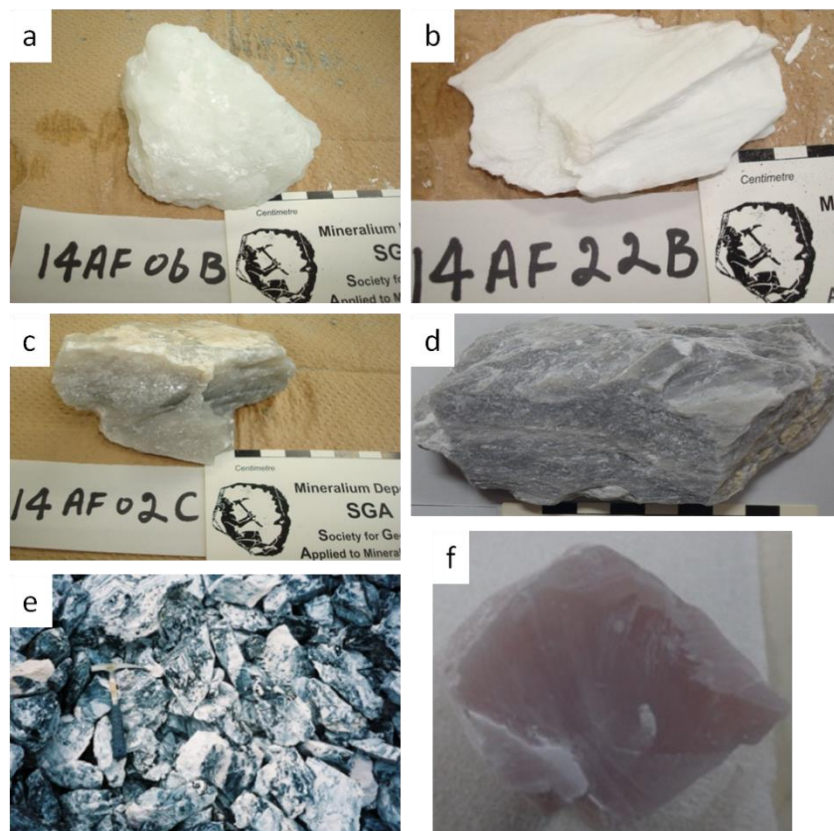


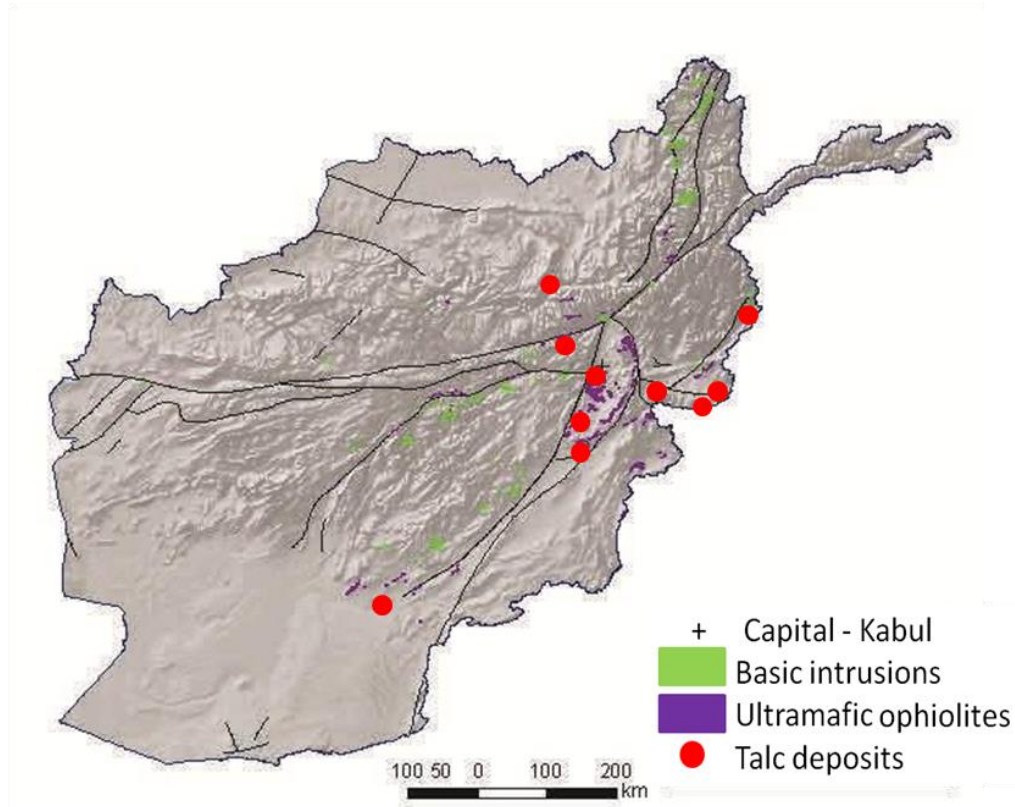
Figure 1.1 Different colors of talc ores (a) greenish white, (b) milky white, (c) light grey, (d) dark grey, (e) black “Shokozan Mining Company”, and (f) pink “Shokozan Mining Company”.

Carbonate-hosted talc deposits, 2018

Talc is the softest mineral, with Moh's hardness being 1. It is composed of microscopic platelets, and the bonds holding the platelets together are very weak. This enables the platelets to slide by one another and results in the soft and greasy feeling. Talc is also used as a term to describe a rock that contains mineral talc. Other names for talc-rich rocks are steatite, a high-purity massive variety and soapstone, an impure rock containing talc and other minerals.

When most people think of talc, they probably envision talcum and baby powder. Since talc is very soft and easily carved, one might also think of sculptures in soapstone (massive talc). In fact, these uses of talc are quite minor compared to its wide variety of applications in manufacturing and agriculture. High-quality (pure) talc has many physical and chemical properties favorable for its use, such as its softness, purity, fragrance retention, whiteness, luster, moisture content, oil and grease adsorption, chemical inertness, low electrical conductivity and high dielectric strength (Virta, 1998).

Talc deposits in Afghanistan are related to mafic and ultramafic rocks and also metamorphosed dolomite marbles and magnesite rocks in different provinces such as Kabul, Konar, Maydan, Parvan, Baghlan, Logar, Ghazni, Kandahar and Nangarhar (Fig.1.2).



<http://afghanistanmines.blogspot.jp/2017/01/chromite-mines-in-afghanistan.html>

Figure 1.2 Tectonic sketch of Afghanistan showing the major sutures, locations of ophiolitic rocks, basic intrusions and talc deposits.

1.2 Types of Talc Deposits

The genesis of talc/soapstone which is formed by the metamorphic/hydrothermal process is still debated. Some workers suggested that talc is a product of hydrothermal replacement (Nautiyal, 1947; Muktinath and Wakhaloo, 1962) while others contended that it represents a low-grade metamorphic reaction product of magnesite and silica (Valdiya, 1968; Sengupta, and Yadav, 2002).

In nature talc is originated from solutions and colloid where magnesium in magnesium-rich rocks reacts with hydrothermal silica and is formed as the final phase of regional or contact

Carbonate-hosted talc deposits, 2018

metamorphism (green schist to amphibolites facies). The most common accompanying mineral is tremolite [$\text{Ca}_2\text{Mg}_5\text{Si}_8\text{O}_{22}(\text{OH})_2$]. Other common magnesium silicates in commercial talc are chlorite, serpentine, anthophyllite and diopside. Quartz, calcite, dolomite, magnesite and pyrophyllite are usually present (McCarthy *et al.* 2006). Four types of talc deposits have been recognized as follows:

1.2.1 Ultramafic Rock Origin

In this case the host rocks are ultramafic rocks e.g. peridotite. At first step, the serpentinization of host rocks take place by hydration at high temperature ($>600\text{ }^\circ\text{C}$) and pressure with little loss of magnesium and silica to form serpentine. At step two, carbonization of serpentinite takes place by influx of fluid containing carbon dioxide to form talc and carbonate. In this case the impurities are magnesite, chlorite, serpentine, mica, and sulfides (McCarthy *et al.* 2006).

1.2.2 Mafic Rock Origin

In this case the host rocks are mafic rocks e.g. gabbro. At first step, the serpentinization of host rocks take place by hydration with little loss of silica and magnesium to form serpentinite. At step two, carbonization of serpentinite takes place by influx of fluid containing carbon dioxide to form talc and carbonate. In this case the impurities are magnesite, chlorite, serpentine, and relicts of mafic host rocks (McCarthy *et al.* 2006).

1.2.3 Metasedimentary Rock Origin

In this case the host rocks are dolomite or magnesite rocks. The process takes place by hydrothermal alteration of host rock by influx of silica-containing fluid. The impurities in this case are dolomite, calcite, quartz, and feldspar (McCarthy *et al.* 2006).

1.2.4 Metamorphic Rock Origin

In this case the host rocks are dolomite or silica-containing dolomite marbles. At first step, amphibolites facies metamorphism of host rocks take place at temperature and pressure and recrystallization of the host rocks to form tremolite or actinolite within the marble. At step two, steatization of tremolite or actinolite occurs at lower temperature (300 – 460 °C) and pressure to talc and carbonate. The impurities in this case are tremolite, carbonate minerals, serpentine, actinolite, and quartz (McCarthy *et al.* 2006).

Steatization- the formation of talc-rich rock in places has even altered granite and siliceous strata to talc. Favorable sites for talc formation include igneous-sedimentary contacts, faults and shear zones. Dolomitic strata selectively tremolitized when granitic rocks were emplaced nearby, may have been selectively altered to talc schist during retrograde metamorphism (Harben *et al.* 1989).

Alteration of ultramafic or mafic bodies to talc in the Spinghar range has not been recognized or reported.

1.3 Uses of Talc

Talc is used in the production of ceramics (the main domestic use), paint, paper (for improving several paper qualities and in recycling processes), plastics (as functional filler, providing rigidity to the plastic), roofing, rubber, flooring, caulking, and agricultural applications. Due to inert, soft and fragrance-retentive nature, it is used in cosmetic products and in soap. As examples, talc is used in the ceramic substrate of catalytic convertors, and is found in wire and cable insulation, auto body putty, asphalt shingles, caulks, sealants, joint compounds, foam

Carbonate-hosted talc deposits, 2018

packaging, animal feed, pharmaceuticals, chewing gum, candy, gaskets, hoses, belts, flooring (providing softness and flexibility), insecticide carriers, baby and body powders.

1.4 Magnesite Rocks and Dolomite Marble

It is believed that metasomatic and metamorphic magnesite deposits form by the interaction of magnesium-rich fluids with the host rocks. These fluids can be extract from low grade or contact metamorphism or may be hydrothermal (Koons, 1981; Harben and Kuzvart, 1996). Such type of replacement is selective and mineralization depends on the host rock composition. Crystalline magnesite deposits form by such process are strata bound to stratiform and hosted by dolomite marbles and sometimes limestone (Simandl and Handcock, 1998).

Magnesite deposits can also be found in association with ultramafic rocks, in sedimentary rocks, or in metasedimentary rocks. Magnesite deposits in sedimentary or metasedimentary rocks are also known as sparry (Veitsch-type) magnesite, carbonate-hosted magnesite, or crystalline magnesite (Pohl, 1990; Harben and Kuzvart, 1996; Simandl and Handcock, 1999). The talc deposits hosted by such rocks are known as carbonate-hosted or dolomite hosted talc deposits (Simandl and Paradis, 1999). In case of the sparry magnesite deposits, talc and magnesite can occur together in metasediments, especially dolostone or dolomitic marble. Illustration and classifications of carbonate-hosted magnesite and talc deposits and their origin are found in Pohl (1989, 1990), Pohl and Siegl (1986), Harben and Kužvart (1996), Simandl and Handcock (1999), and Simandl and Paradis (1999). Hypotheses regarding the genesis of these types of deposits are (1) metasomatic replacement of dolomitized, permeable carbonates by magnesite and (2) diagenetic recrystallization of magnesia-rich chemical sediment in a marine or lacustrine setting (Simandl and Hancock, 1999). In a metamorphic environment, a dolomitic limestone and

Carbonate-hosted talc deposits, 2018

magnesite become dolomite marble and recrystallized magnesite, respectively (Simandl and Handcock, 1999).

The Nangarhar deposits include two generations of magnesite. The first generation is the replacement of dolomite by micritic and laminated magnesite during diagenesis and then recrystallized the magnesite during amphibolite facies metamorphism (Melezhik *et al.*, 2001). Primary dolomite was deposited under evaporitic conditions in sabkha to playa-lake environment, but later altered to magnesite, by reaction with Mg-bearing, hypersaline brines derived from seawater. The dolomite marbles in Spinghar Block is considered to be an altered sequence of stromatolites. It was formed in shallow-marine and non-marine, evaporitic environments (Melezhik *et al.*, 2001).

1.5 Locations of Study Areas

The study area is located about 30 km southwest of Jalalabad city, the capital city of Nangarhar province, Afghanistan (Fig.1.3). There is about 10 to 20 km paved road from the Jalalabad city to the study areas and the rest of the road is very rough and at some places there is no road at all. The stockpiles of talc are located about 3 to 10 km from the deposits. Nangarhar province consists of 20 districts and the study area is located in Shirzad, Khugyani, Pachir wa Agam and Achin districts (Fig.1.3).

Carbonate-hosted talc deposits, 2018

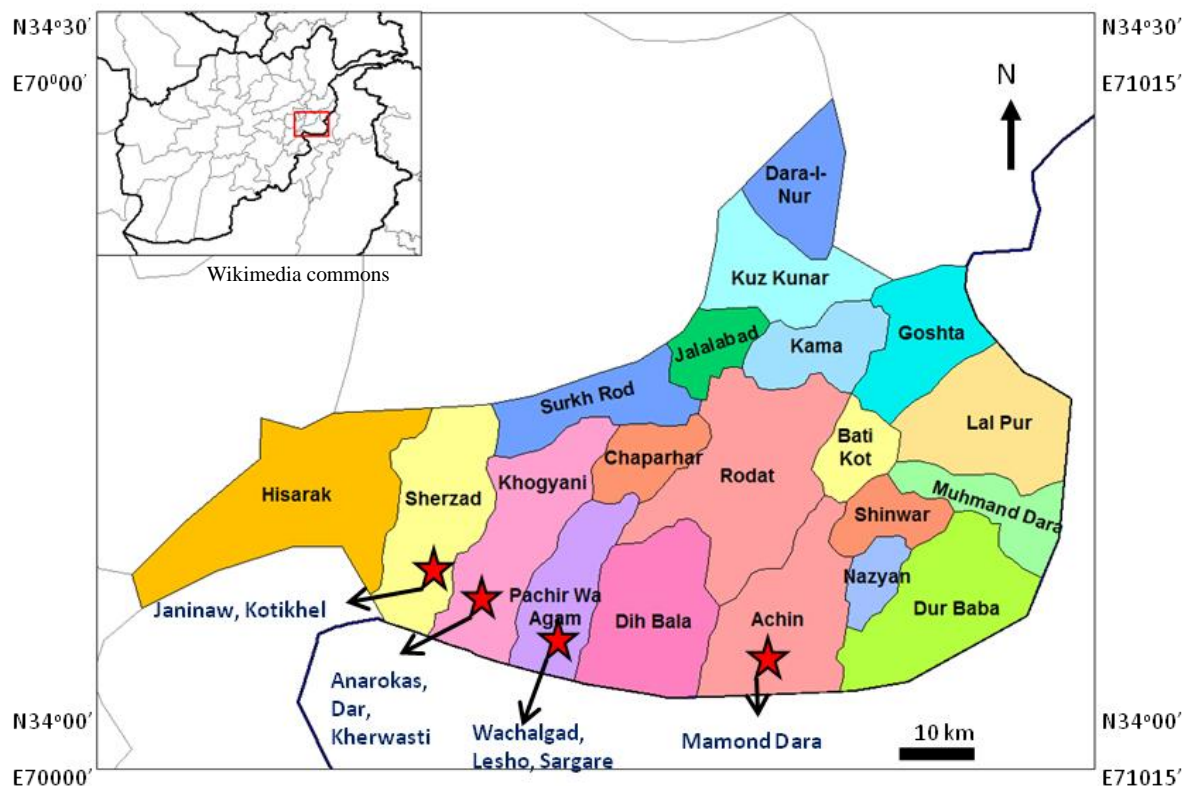


Figure 1.3 Districts of Nangarhar province showing the study areas.

1.6 Aims and Objectives

Very less or no work has been done on the talc deposits in the Nangarhar province except a small data available on Achin area (Lednev, 1977). Currently there is no mining activity in Achin area while in other areas talc exploitation is informal. The aims of this study are to elucidate the characteristics of talc mineralization in the Nangarhar province, to figure out the genesis and formation process of talc deposits in this area and to construct a model for talc mineralization based on the field observations and systematic geochemical analyses.

1.7 Previous Works

The geology of the area is very uncertain, partly due to the complexity of the geology and less geological work on the area due to its frontier location to Pakistan. Geologists from the former

Carbonate-hosted talc deposits, 2018

USSR and Afghanistan mapped the deposits and parts of the surrounding areas and excavated several trenches and exploration tunnels, shallow drill holes (Lednev, 1977). They collected chip samples from the trenches and adits and MgO, SiO₂ and CaO contents of talc were analyzed. Filippov (1974) and Nielson (1976) wrote brief reports on these deposits. The Economic and Social Commission for Asia and the Pacific (ESCAP) published a compilation of the geology and mineral resources of Afghanistan in 1995 based mainly on studies by Soviet and Afghanistan geologists (ESCAP 1995). Orris and Bliss (2002) compiled a database of known Afghan mines and mineral occurrences. Peters *et al.* (2007) discussed the industrial uses of talc and magnesite and general models of metasomatic and metamorphic magnesite and talc deposits. They defined a permissive tract for these types of deposits which includes both the Achin and Ghunday deposits based on a lithologic unit that contains both amphibolite dikes and carbonate rocks. Abdullah *et al.* (1977) and Abdullah and Chmyriov (2008) described the general geology of the Achin and Ghunday deposits, as well as the surrounding geologic terrain. A large scale map of Nangarhar province of 1:25000 has been compiled by Bohannon and Turner (2005). USGS, the Task Force for Business and Stability Operations (TFBSO) of the Department of Defense and Afghanistan Geological Survey (AGS) (2009 to 2011) classified the magnesite rocks as sparry magnesite and these larger bodies of talc are suggested to be formed by the process of regional metamorphism of beds of siliceous dolomite. The talc rocks are of high quality with average whiteness ranges from 92.4 to 95.6 % (Shokozan Mining Co. Ltd. 2014, unpublished).

1.8 Climate and Vegetation

According to Afghanistan Agro Meteorological Seasonal Bulletin (Ministry of Agriculture, Irrigation, and Livestock, 2010), the annual precipitation in the study area is 196.5mm with monthly minimum 0.9 mm in June and monthly maximum 38.9 mm in April. The minimum

Carbonate-hosted talc deposits, 2018

temperature is 8.3°C in January and maximum 33.1°C in June. The snow-depth map ([Ministry of Agriculture, Irrigation, and Livestock, 2010, map 7](#)) shows less than 2 cm of snow in the study area with the amount of snow increasing from east to west.

The vegetation in the study area as classified by [Breckle \(2007\)](#) is mostly Sclerophyllous oak forests. The lower elevations in the northern part of the study area are classified as subtropical dry scrub and savannah and the southwest corner of the study area is Rhododendron-Krummholz ([Breckle, 2007](#)). The high mountain areas along the southern border of the study area reach elevations in excess of 4,000 m above sea level ([Bohannon, 2005](#)). These areas are classified as thorny cushions, subalpine and alpine semi deserts and meadows. There are perennial snowfields at the higher elevations. Much of the upland surface of the study area is bedrock outcrop with thin alluvial cover. Azonal riverine vegetation likely was present in the stream valleys, but the trees have been harvested for fuel and building materials. Most land suitable for farming has been plowed and planted, especially along major stream valleys and some of the ephemeral tributary stream valleys. Irrigated fields are present in many of the valleys in the study area.

1.9 Demographics

The lower elevations of the study area, occupied by the city of Jalalabad are densely populated, with many areas having 501 to 2,500 inhabitants per square km as mapped by Land Scan ([Oak Ridge National Laboratory, 2010](#)). The city of Jalalabad is estimated to have more than 190,000 people ([Central Statistics Organization, 2010](#)). Higher elevation areas, essentially the bedrock uplands have few to no inhabitants.

1.10 Topography and Geomorphology

Carbonate-hosted talc deposits, 2018

The topography of the study area consists of a northerly sloping high plain in the northern part of the study area that gradually transitions to high, rugged mountain in the southern part (Bohannon, 2005). The elevations along the northern border of the study area range from about 450 m above sea level in the east to 2,000 m in the extreme northwest corner. The break in slope between the high plain and the mountain foothills is at about 1,400 m (Bohannon, 2005). The highest peaks form the international border between Afghanistan and Pakistan. The highest peak is mapped as being 4,520 m above sea level, and several other peaks are higher than 4,000 m. The relief between the high plain and the mountains is as much as 2,600 m in much of the study area. The geomorphology of the high mountain areas is dominated by alpine glacial features. The international boundary follows an arête and there are several cirques. The high plain appears to have been formed by sediments discharged from the mountain streams, forming coalescing alluvial fans. The alluvial fans have been dissected by perennial and ephemeral streams flowing from the mountains onto the high plain (Fig. 1.4).

Carbonate-hosted talc deposits, 2018

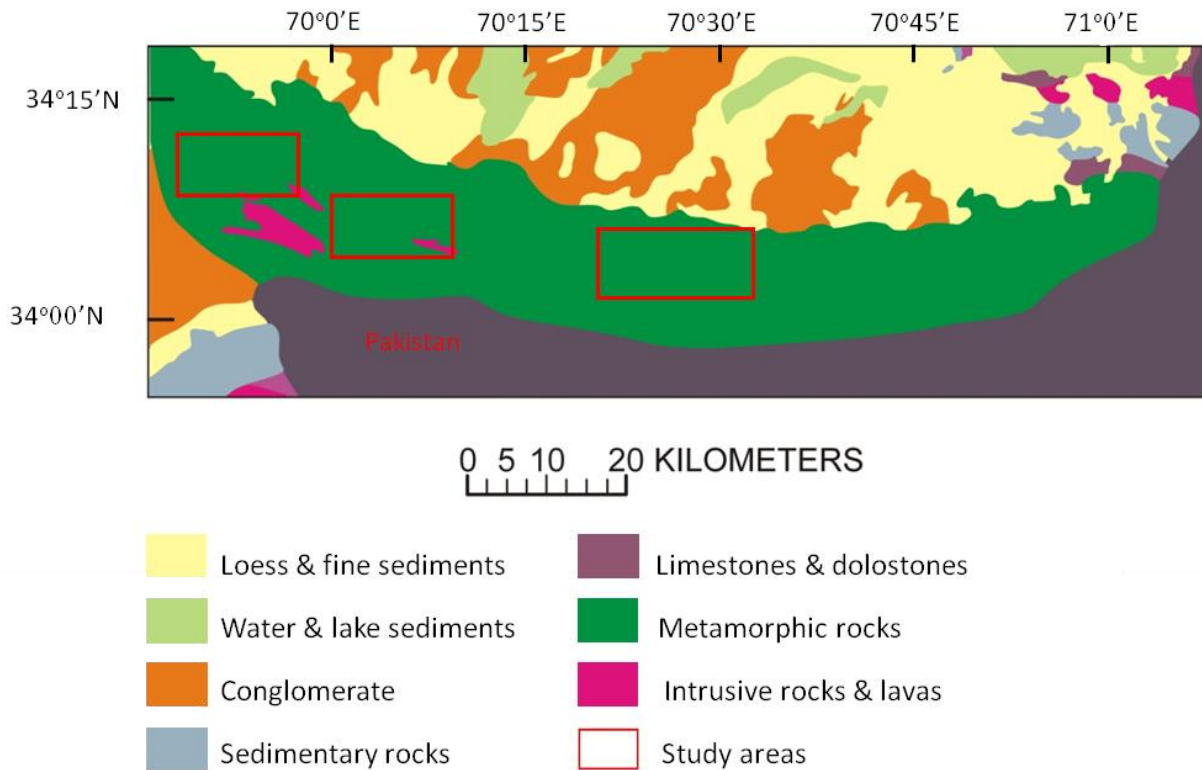


Figure 1.4 Topography and generalized geology of the study area (Geohydrology modified from Doeblich and Wahl, 2006).

1.11 Surface Water

There is one stream gage within the study area. The Kabul River at Dakah stream gage station (Afghanistan identification number 1-0.000-1M) is located in the northeast corner of the study area. This station is at an elevation of 420 m above sea level and has a drainage area of 67,370 km² and a period of record that extends from 21 February, 1968, to 22 July, 1980 (Olson and Williams-Sether, 2010). The annual mean stream flow per unit area for this station is 0.0091 m³/s/km² (cubic meters per second per square km). The seasonal timing of maximum and minimum monthly stream flow is high flows in the late spring through summer and low flows in winter.

Carbonate-hosted talc deposits, 2018

The Surkhrud River near Sultanpur stream gage station (Afghanistan identification number 1-5.R00-1A) is 18 km north of the study area and approximately 9 km upstream from the confluence with the Kabul River. This station is at an elevation of 700 m above sea level and has a drainage area of 2,590 km² and a period of record that extends from 8 March, 1968, to 30 September, 1975, and from 15 January, 1976, to 31 March, 1980 (Olson and Williams-Sether, 2010). The annual mean stream flow per unit area for this station is 0.0010 m³/s/km². The seasonal timing of maximum and minimum monthly stream flow is high flows in the spring through early summer and low flows in fall and winter.

The Konar River at Pul-i-Kama stream gage station (Afghanistan identification number 1-5.R00-1A) is 25 km north of the study area and approximately 7 km upstream from the confluence with the Kabul River. This station is at an elevation of 555 m above sea level and has a drainage area of 26,005 km² and a period of record that extends from 28 December, 1966, to 30 September, 1979 (Olson and Williams-Sether, 2010). The annual mean stream flow per unit area for this station is 0.018 m³/s/km². The seasonal timing of maximum and minimum monthly stream flow is high flows in the summer and low flows in the winter and early spring.

1.12 Ground Water

More than 3,085 shallow community groundwater-supply wells have been installed in the study area by Non-governmental organizations (NGOs). Information about these wells can be found in a database maintained by DACAAR (Danish Committee for Aid to Afghan Refugees, 2011). Well-depth and static-water-level information is available for most of the wells in this database. About 80 percent of the supply wells are less than 30 m deep and 95 percent are less than 50 m deep. The median well depth is 16.8 m. The depth to water in 60 percent of the supply wells in the study area is less than 15 m. The median depth to water is 12.8 m.

2. Tectonic Setting

Afghanistan has complex and varied geology, and the ages have been determined as from Archean, Proterozoic and all Phanerozoic Eras. Afghanistan forms the most stable part of a promontory that projects south from the Eurasian Plate (Ambraseys *et al.*, 2003; DeMets *et al.*, 1990) (Fig. 2.1). West of Afghanistan, the Arabian Plate is subducted northward beneath Eurasian Plate, and east of Afghanistan the Indian Plate does the same. South of Afghanistan, the Arabian and Indian Plates adjoin and both are subducted northward beneath the Eurasian Promontory. The plate boundaries west, south, and east of Afghanistan are hundreds of km wide. They involve the contractional deformation of large parts of the Eurasian Promontory.

More specifically, south of Afghanistan at the Makran subduction zone, the plate boundary between the overriding Eurasian Plate and the subducting Arabian and Indian Plates crops out along a line beneath the Gulf of Oman and the Arabian Sea (Fig. 2.1). Within the plate boundary and north of the plate contact, southwestern Pakistan and southeastern Iran, together with southernmost Afghanistan, make up a broad deformation zone of north-dipping thrust faults and associated folds that trend east west (Kazmi, 1979; Shareq, 1981; Haghypour *et al.*, 1984a, b; Hessami *et al.*, 2003). The north-trending direction of plate convergence is nearly perpendicular to the east-west plate contact (Fig. 2.1). Thus, the deformation zone north of the contact includes dominantly reverse faults and associated folding, with strike-slip faulting (Kazmi, 1979; Hessami *et al.*, 2003).

In contrast, east and west of Afghanistan, the plate boundaries trend north-northeast and north-northwest, respectively. Subduction is oblique, and plate convergence is transpressional. The western plate boundary between Arabia and Eurasia is roughly a mirror image of the eastern boundary between India and Eurasia. The western boundary is entirely within Iran and largely

Carbonate-hosted talc deposits, 2018

outside the area shown on Figure 2.1. Within the eastern boundary, upper crustal strain of the deformation zone is partitioned into a broad complex of thrust faults at and near the plate boundary and a wide, north-northeast-trending belt of left-lateral, strike-slip faults farther inside the Eurasian Plate (Kazmi, 1979; Sarwar and De Jong, 1979; Kazmi and Rana, 1982; Haghypour *et al.*, 1984a). The plate boundary follows the curved traces of the outermost thrust faults in Pakistan (Fig. 2.1), and the strike-slip belt extends west as far as the left-lateral Chaman Fault of Afghanistan. The strike-slip belt contains many large, left-lateral faults that strike north and northeast, and fewer, smaller reverse faults that strike east-west and northeast and dip northerly (Kazmi, 1979; Sarwar and De Jong, 1979; Kazmi and Rana, 1982).

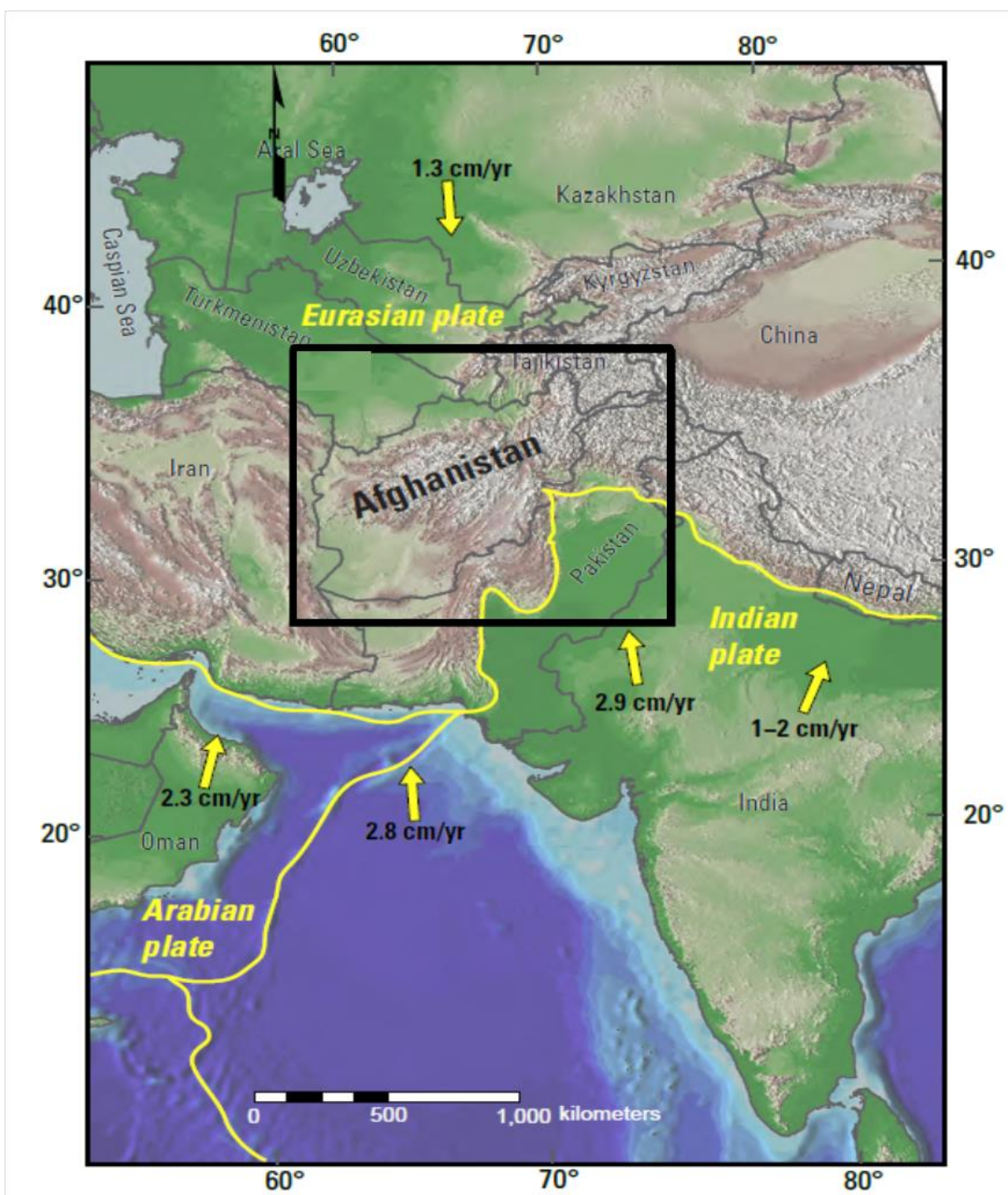


Figure 2.1 Greater Alpine-Himalaya orogenic belt of Asia. Vectors show relative plate motions and velocities between the Indian, Eurasian, and Arabian Plates (plate boundaries shown and labeled in yellow). Plate velocities from [Jade \(2004\)](#), [Bird \(2003\)](#), [Vernant *et al.*, 2004](#) and [Sella *et al.*, 2002](#) by [Ruleman *et al.*, 2007](#).

Carbonate-hosted talc deposits, 2018

2.1 Geological Units and Faulting

Afghanistan, north of the Hari Rod Fault and west of the Central Badakhsan Fault, comprises the North Afghan Platform (Fig. 2.2 Turan platform of [Shareq, 1981](#) and [Tapponnier *et al.*, 1981](#); [Tadjhik platform of Treloar and Izatt, 1993](#)). The basement of platform of metamorphic and igneous rocks was developed during the Carboniferous-Permian Hercynian orogeny and the basement has been comparatively stable since then ([Shareq, 1981](#); [Tapponnier *et al.*, 1981](#)). A cover sequence of Mesozoic and Tertiary strata overlying the basement, is 6 km thick at the Pakistan-Afghan border, and thickens northward to as much as 16 km ([Brookfield and Hashmat, 2001](#)). The cover sequence hosts the mature Amu-Darya gas-oil province of Turkmenistan and Uzbekistan ([Kingston and Clarke, 1995](#)). Most faults within the platform strike east-west or west-northwest, and lack significant offset ([Brookfield and Hashmat, 2001](#)). Petroleum traps are folds that are thought to overlie the reactivated basement faults.

Mapped faults on the platform are more numerous near its southern and eastern edges than within its interior (Fig. 2.2). However, geologic and tectonic maps show that the Precambrian and Paleozoic basement rocks of the platform are exposed throughout this belt, from northernmost Afghanistan southwest to approximately longitude 67° E ([Shareq and Chmyriov, 1977](#); [United Nations Economic and Social Commission for Asia and the Pacific, 1995](#)).

In contrast to the platform, the evolution of Afghanistan south and east of the platform was dominated by collisions of Gondwanan fragments with Laurasia that began during the Mesozoic Era and which continues today in the form of Indian subduction ([Exxon Production Research Company, 1985](#); [Haghipour *et al.*, 1984b](#); [Wittekindt *et al.*, 1997](#)). [Shareq \(1981\)](#) showed igneous rocks immediately south of the Hari Rod Fault and [Exxon Production Research](#)

Carbonate-hosted talc deposits, 2018

[Corporation \(1985\)](#) interpreted them as ophiolites. The presence of ophiolites implies subduction of oceanic or marginal basin crust beneath the continental crust of the North Afghan Platform. [Sengor \(1984\)](#) interpreted these relations to conclude that the subducted oceanic crust underlay an early part of the Tethyan Ocean and was subducted during late Early Carboniferous to Triassic time. The rifting that initiated this part of the Tethyan Ocean must have predated subduction of the oceanic crust. Presumably, the rifting postdated the Carboniferous-Permian orogeny that formed the North Afghan Platform.

[Sengor \(1984\)](#) noted that continued subduction and final closure of the Tethyan Ocean produced the widespread Mesozoic Cimmerian orogeny. South and east of the platform, Afghanistan is laced with hundreds of faults that are large enough to be mapped geologically at a scale of 1:500,000, except where the faults are covered by young Quaternary and some Pliocene strata, as in southwestern Afghanistan (Fig. 2.2) and adjacent Iran and Pakistan ([Chmyriov and Mirzad, 1972](#); [Kazmi and Rana, 1982](#); [Exxon Production Research Company, 1985](#); [Shareq and Chmyriov, 1977](#)). Crustal fragments south of the Hari Rod Fault and east of the Central Badakhsan Fault, but northwest of the Chaman and Konar Faults (Fig. 2.2), rifted away from Gondwana before India did, crossed the Tethyan Ocean, and accreted to Eurasia before India did, during the Cimmerian orogeny ([Treloar and Izatt, 1993](#)). Fragments accreted successively southward and most or all subduction zones dipped north ([Tapponnier et al., 1981](#)). Additional fragments accreted east of the Chaman and Konar Faults until the arrival of India ([Wittekindt et al., 1997](#)).

The Hari Rod Fault (Fig. 2.2) was reactivated in transtension during Oligocene-Miocene time, and most large faults south of the Hari Rod Fault were reactivated during the Tertiary Period as strike slip faults ([Treloar and Izatt, 1993](#)). Today, the 20 to 60 km-wide zone between

Carbonate-hosted talc deposits, 2018

the Hari Rod Fault on the north, and the Qarghanaw, Bande Bayan and Onay Faults on the south, contains what [Shareq \(1981\)](#) regarded as the most structurally complex rocks in Afghanistan. He named these rocks the “Middle Afghanistan geosuture zone”. Fault bounded, lens-shaped rock masses trend roughly east-west throughout Middle Afghanistan (Fig. 2.2). This fabric strongly indicates considerable strike slip, and [Brookfield and Hashmat \(2001\)](#) reported that Paleozoic rocks are displaced right laterally by about 600 km across the Hari Rod Fault. Despite the original north dip of most or all of the Afghan subduction zones, most large faults within the accreted terranes now dip steeply ([Tapponnier *et al.*, 1981](#)).

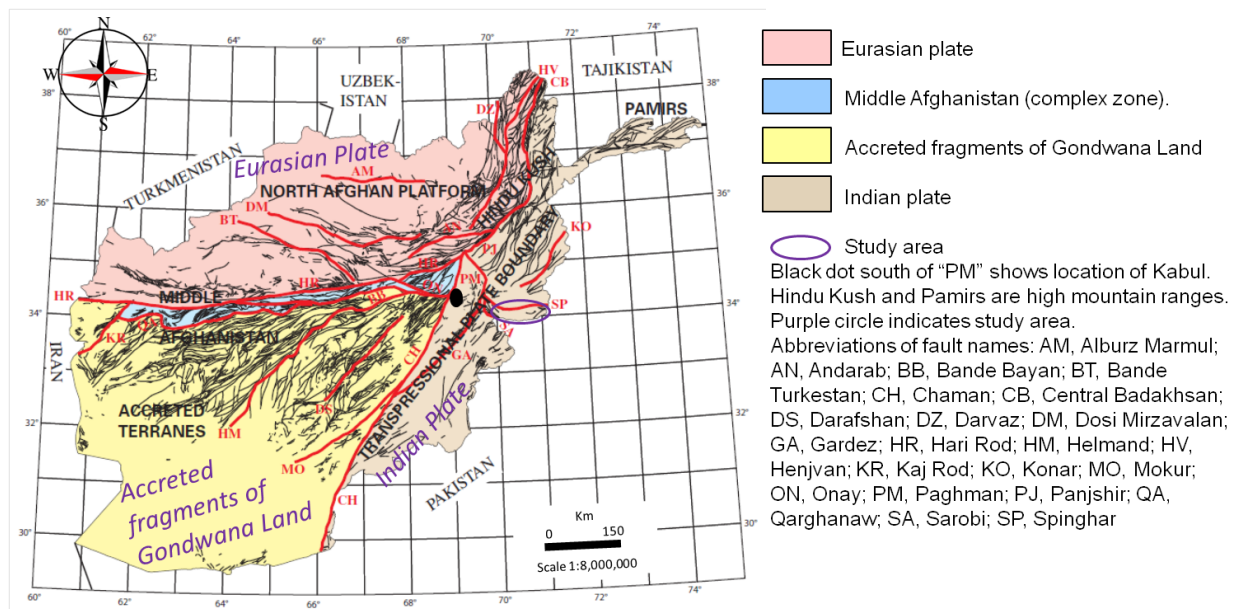


Figure 2.2 Locations of faults named in the text (red). Fault traces from USGS-funded digitization of the geologic map of [Shareq and Chmyriov \(1977\)](#) (black). Abbreviations of fault names: AM, Alburz Marmul; AN, Andarab; BB, Bande Bayan; BT, Bande Turkestan; CH, Chaman; CB, Central Badakhsan; DS, Darafshan; DZ, Darvaz; DM, Dosi Mirzavalan; GA, Gardez; HR, Hari Rod; HM, Helmand; HV, Henjvan; KR, Kaj Rod; KO, Konar; MO, Mokur; ON, Onay; PM, Paghman; PJ, Panjshir; QA, Qarghanaw; SA, Sarobi; SP, Spin Ghar. Transverse Mercator projection with scale factor 0.999600 at central meridian 66° E., projection origin is 34° N., false easting and northing are zero. Tectonic regions of Afghanistan (quoted from [Wheeler *et al.* 2005](#)).

Carbonate-hosted talc deposits, 2018

2.2 Geology of the Study Area (Spinghar Fault Block)

In the south-eastern part of Afghanistan, enclosed between the valleys of the Kabul and Tarnak rivers and separated from the Hazarajat region by the Ghazni-Kandahar Plateau, there are the Suleiman Mountains which are bounded in the north by the Spinghar Ridge of almost east-west trend. The Suleiman-Kirthar Folded Region includes the Spinghar Fault Block, the Kabul Stable Mass, the Khost- Matun Uplift, the Katawaz and Ras Koh Mirjawar Troughs. The Spinghar Fault Block covers most of the Spinghar Ridge. The area of the fault block is underlain by metamorphosed Proterozoic rocks, 4,500-8,000 meters in thickness, intruded by sub concordant bodies of Proterozoic granites. Small gabbro-diorite bodies of supposedly Early Cretaceous age occur in the western part of the block. Folds encountered within the block are mostly of brachyform shape and of east-west trend. Some of the folds traceable in the western part of the block have a northwestern strike. Minor folds are much more complex being represented by isoclinal and flow folds. The highest elevation of the Spinghar Ridge is 4,755 meters (Abdullah and Chmyriov, 2008).

Spinghar Fault Block was distinguished by Denikaev *et al.* (1972), Sborshchikov *et al.* (1972, 1975) within the limits of the Spinghar Ridge in the south-eastern part of Afghanistan. The block has been studied inadequately owing to its position at the border. In the north, the block borders on the Hinduraj-Hazar Folded Region along the Spinghar Fault, in the south, on the Suleiman Uplift along the Safed Koh Fault (Weippert *et al.*, 1970) and in the west, on the Katawaz Trough along the Sarobay Fault. The trend of the block is nearly east-western. It extends for 125 km, the maximum width being 15 km. The block is composed of compositionally variable gneisses, schists, quartzites, marbles and amphibolites metamorphosed to an amphibolite facies. Intrusive rocks are derivatives of migmatite-granite and gabbro-

Carbonate-hosted talc deposits, 2018

monzonite-diorite. The former are tentatively dated as Proterozoic and the latter as Early Cretaceous (Weippert *et al.*, 1970). The trend of folding is approximately eastwest. The major folds are relatively simple, broad, shallow, linear and brachyform. The minor folds are commonly complex, narrow, and steep-limbed. In the recent structural pattern the block appears as horst-type uplift.

The Spinghar Fault is the third link of the fault chain under consideration. This fault separates the Spinghar Fault Block from the structures of the Konar Zone located to the north (Weippert *et al.*, 1970). The fault is traceable over its whole extent at the northern foothills of the Spinghar Range. It extends for 125 km. from east to west and appears as a right-lateral fault along which the rock units of the Konar Zone have been displaced eastward relative to the metamorphosed rocks of the Spinghar Fault Block shifted westward. Most of the fault is concealed under the Pliocene-Quaternary cover; nevertheless it is well apparent in all the available air photographs (Fig.2.3).

Carbonate-hosted talc deposits, 2018

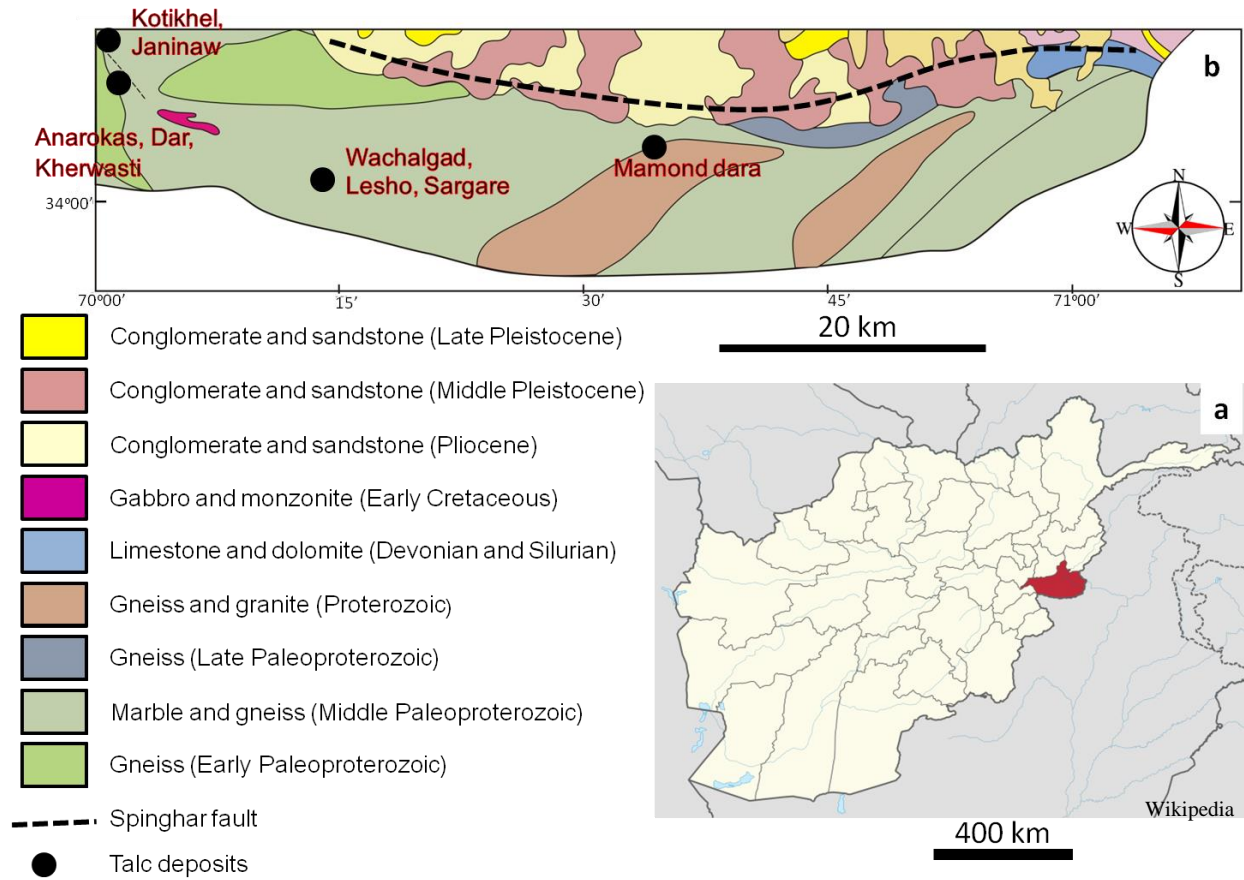
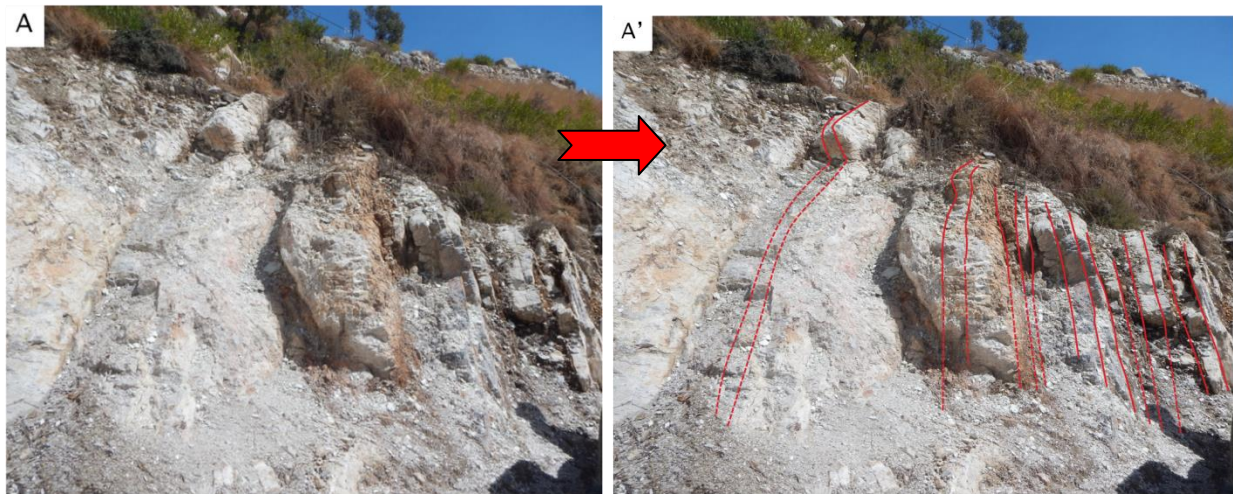


Figure 2.3 (a) Location of the study area on the map of Afghanistan, (b) Geological map of Spinghar Fault Block. Modified after [Bohannon and Turner \(2005\)](#).

3. Mode of Occurrence of Talc Deposits

Ten talc deposits including two prospects i.e. Kotikhel (Dawood mine and Noor mine), Janinaw, Kherwasti, Anarokas, Dar, Wachalgad (prospect), Lesho, Sargare (prospect) and Mamond dara (Fig.2.3) in different parts of the Spinghar Fault Block were studied. Within each deposit, talc rocks, magnesite rocks, talc-bearing magnesite, dolomite marble, talc-bearing dolomite marble, metamorphic rocks, intrusive rocks, quartz veins and altered intrusive and carbonate rocks were collected for petrographic and geochemical analyses. List of hand specimen samples is given in appendix 1. Talc mineralization is confined to carbonate rocks such as magnesite rocks and dolomite marbles. Beddings in dolomite marble and magnesite rocks were marked in all deposits and prospects and talc veins are parallel to sub-parallel to these beddings (Fig. 3). According to [Lednev, 1977a](#), the amphibolite, and talc bodies are roughly parallel to subparallel to the bedding of the dolomite marble and magnesite rocks.



Carbonate-hosted talc deposits, 2018



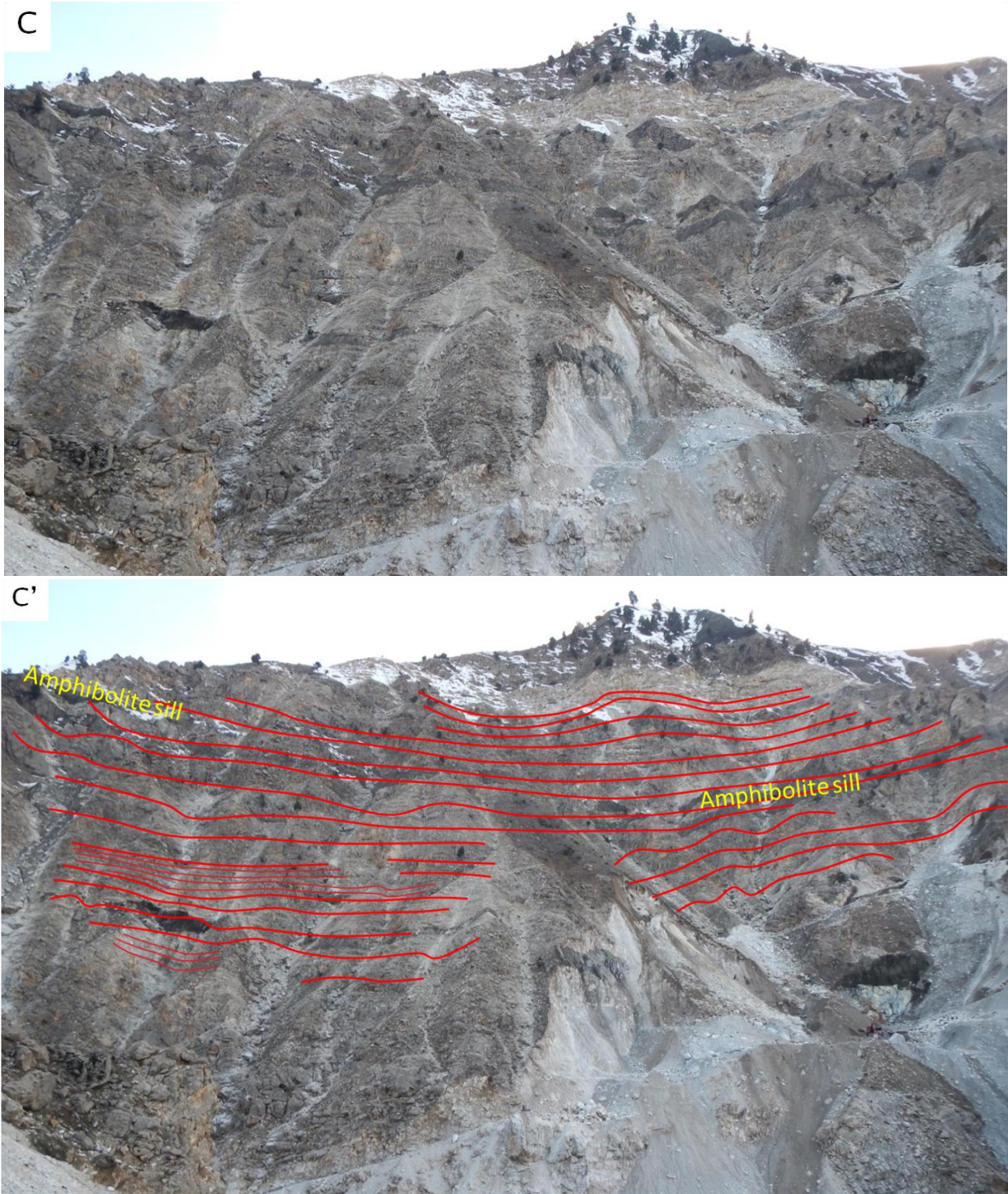


Figure 3 Beddings in (A, A') dolomite marble in Mamond dara, (B) magnesite rocks in Dar and (C, C') magnesite rocks in Kherwasti.

3.1 Kotikhel (Dawood mine and Noor mine)

Location of the Dawood mine is $N34^{\circ} 14' 17.6''$ and $E69^{\circ} 57' 25.7''$, while the location of the Noor mine is $N34^{\circ} 12' 38.0''$ and $E69^{\circ} 57' 09.1''$. In this area, talc ore bodies in the form of veins are hosted by dolomite marble. Talc veins 1.5 to 2 meters thick in the Dawood mine are parallel to sub parallel to the beddings of host dolomite marble. Very thin layer to massive tremolitite bodies were also marked in dolomite marble (Fig. 3.1a). Serpentine (antigorite) was also marked in dolomite marble about 150 m away from talc veins. In the Noor mine, about 0.5 meters thick talc veins are hosted and parallel to sub parallel to the beddings of dolomite marble having sharp contact with gneiss. Massive and folded quartz bodies were marked in the contact between talc and dolomite marble (Fig. 3.1b).

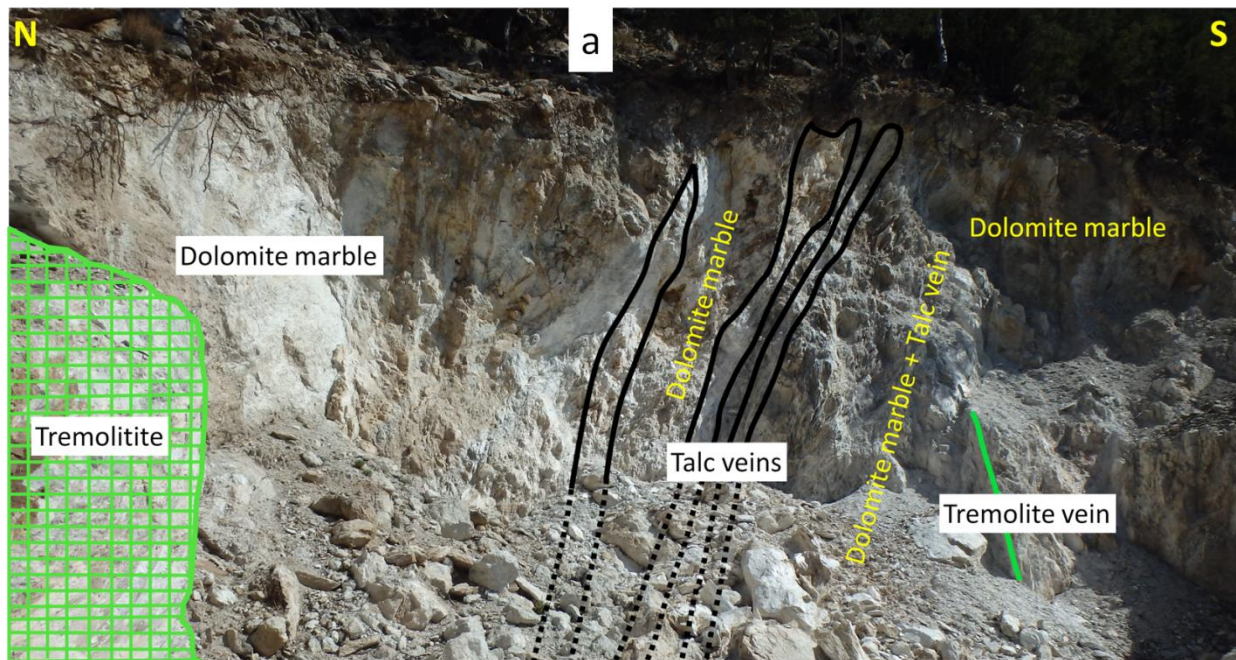




Figure 3.1 (a) Outcrop at the Dawood mine and (b) Outcrop at the Noor mine.

3.2 Janinaw

This deposit is in the Kutikhel area, Sherzad district, Nangarhar province. Its location is $N34^{\circ} 12' 51.3''$ and $E69^{\circ} 56' 25.1''$. In this deposit different colors of talc veins such as milky white, grayish white and greenish white are hosted by dolomite marble and the talc ores are parallel to sub parallel to the beddings of dolomite marble. Talc also occurs as a mixture with tremolite. Needle like tremolite crystals occur randomly in the talc matrix and a thin layer of talcose quartz was also observed in talc ore. No intrusive and metamorphic rocks were observed in this deposit (Fig. 3.2).

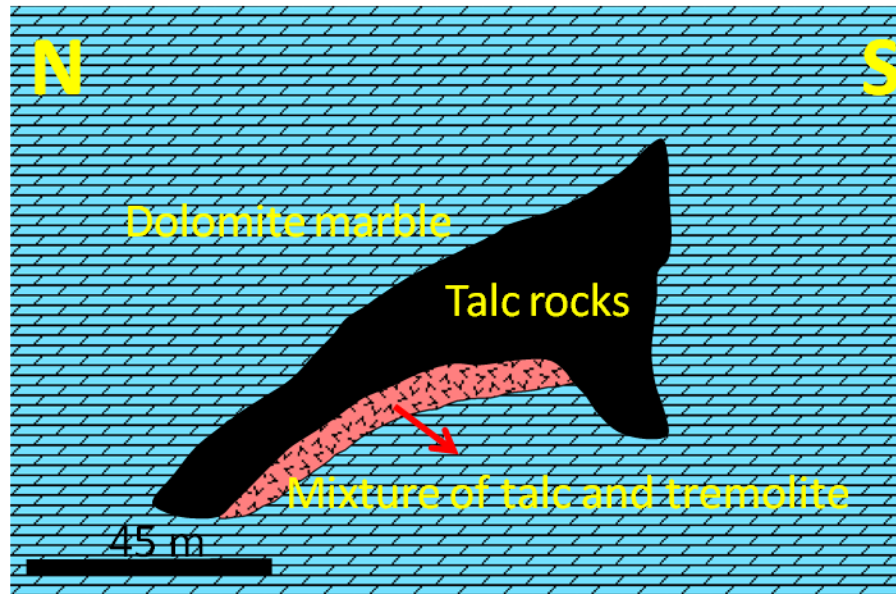


Figure 3.2 Outcrop sketch of the Janinaw deposit.

3.3 Kherwasti

Location of the Kherwasti deposit is $N34^{\circ} 08' 50.5''$ and $E69^{\circ} 59' 55.1''$. The host rock in this deposit is magnesite, and talc veins are parallel to sub parallel to the beddings of magnesite rock. Both talc ore and magnesite rock are crosscut perpendicularly by diorite and also parallel to sub parallel to those rocks. Altered diorite was also marked cross cutting magnesite rock. Magnesite rock is crystalline, white to gray in color characterized by lustrous grains having no contact with gneiss. Deformation in the form of reverse fault was observed (Fig. 3.3). Tremolitite observed were massive, milky white and dark green in color. A mixture of magnesite and serpentine (antigorite) was marked at the contact between amphibolite and magnesite rock. Massive dolomite marble was also marked in this area between the Dar and Kherwasti deposits.

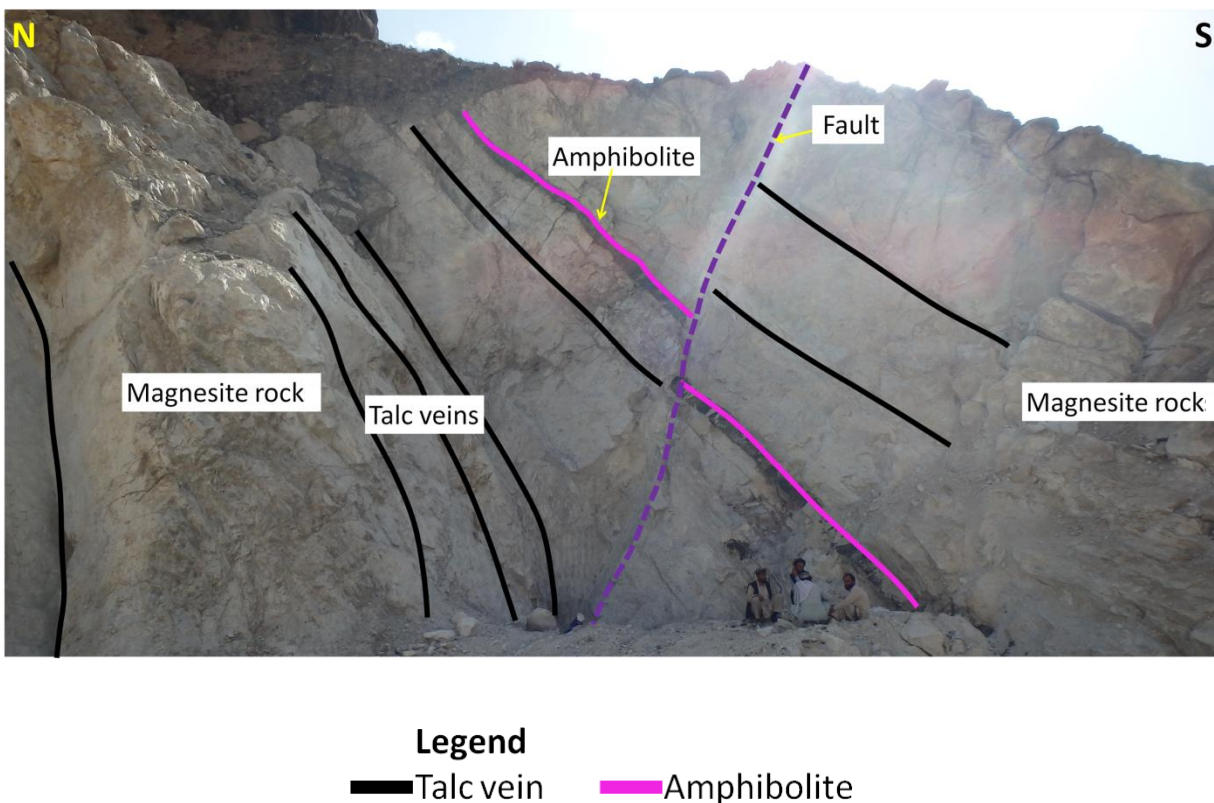


Figure 3.3 Outcrop of Kherwasti deposit.

3.4 Anarokas

Location of the Anarokas deposit is $N34^{\circ} 10' 47.9''$ and $E70^{\circ} 00' 57.1''$. Host rock in this deposit is also magnesite and talc veins are parallel to sub parallel to the beddings of magnesite rock. Magnesite rock has a sharp contact with gneiss but talc is not related with this gneiss. Quartz veins are aligned parallel to the gneissosity of gneiss. Both magnesite rock and gneiss are cross cut by mafic intrusive rocks metamorphosed to amphibolites. A mixture of magnesite and serpentine (antigorite) was also marked at the contact between amphibolites and magnesite (Fig. 3.4A and B). Tremolite was marked at the contact between magnesite rock and amphibolites. A granitic intrusion was also observed in this area about 200 m away from talc veins. The granite cross cut the gneiss and quartz veins in gneiss (Fig. 3.4C).

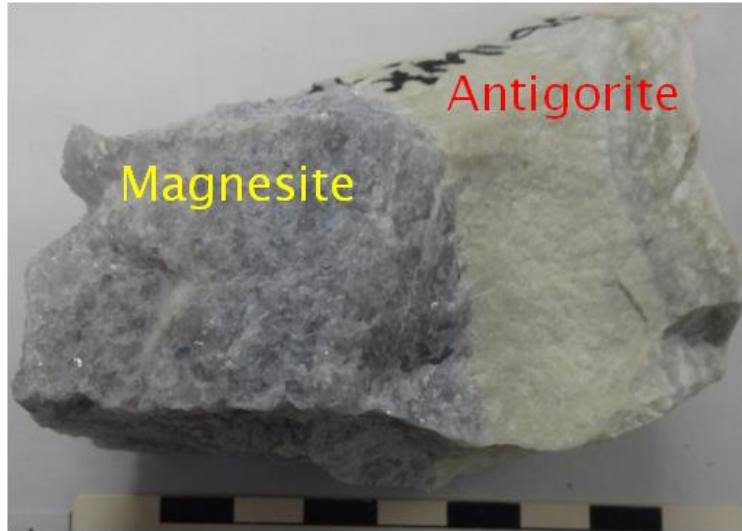
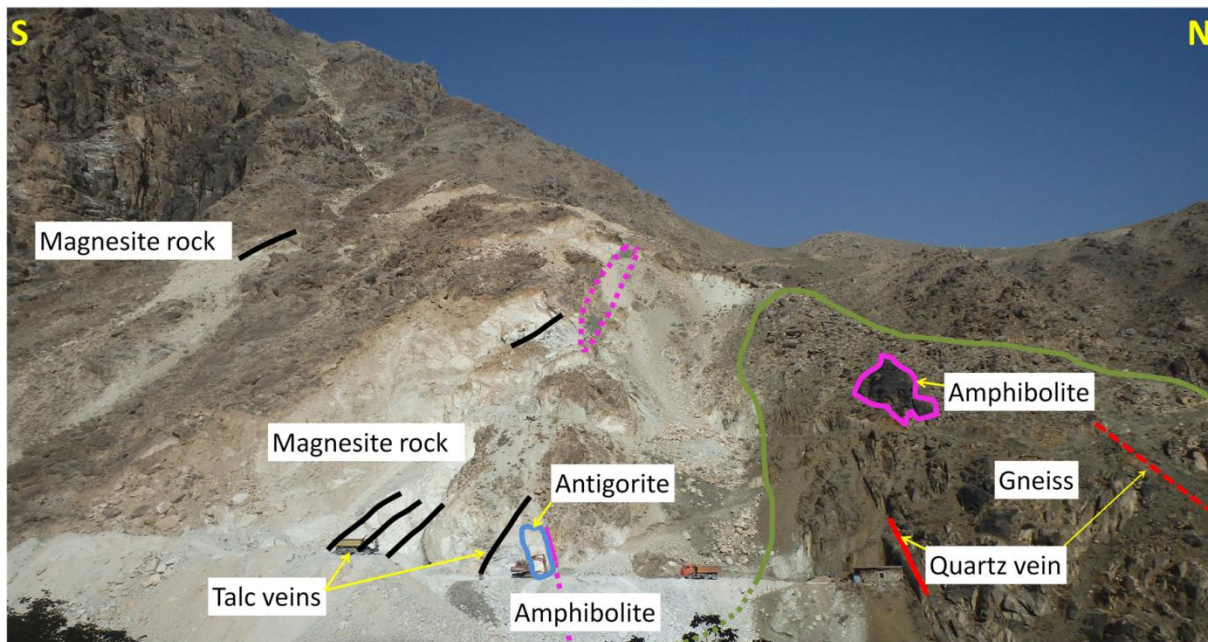


Figure 3.4A Replacement of magnesite by antigorite in Anarokas deposit.



- Legend**
- Talc vein
 - Quartz vein
 - Intrusive rocks
 - Gneiss
 - Serpentine

Figure 3.4B Outcrop of the Anarokas deposit.



Figure 3.4C A granitic intrusion cross cut the gneiss and the quartz vein within the gneiss at Anarokas deposit.

3.5 Dar

Location of this deposit is $N34^{\circ} 09' 56''$ and $E70^{\circ} 00' 29.1''$. The host rock is magnesite extended hundred of meters and talc occurs as complex vein network parallel to sub parallel to the beddings of magnesite rock with a thickness ranging from 3 to 4 meters. A layer of about 0.2 meter dolomite marble in magnesite rock was also marked and confirmed by XRD analysis. Many altered and fresh diabase/dolerite cross cut talc veins and magnesite rock and also parallel to sub parallel to this rock. A serpentinite layer of about 30 to 60 cms thick was also marked parallel to sub parallel to the beddings of magnesite rock (Fig. 3.5).

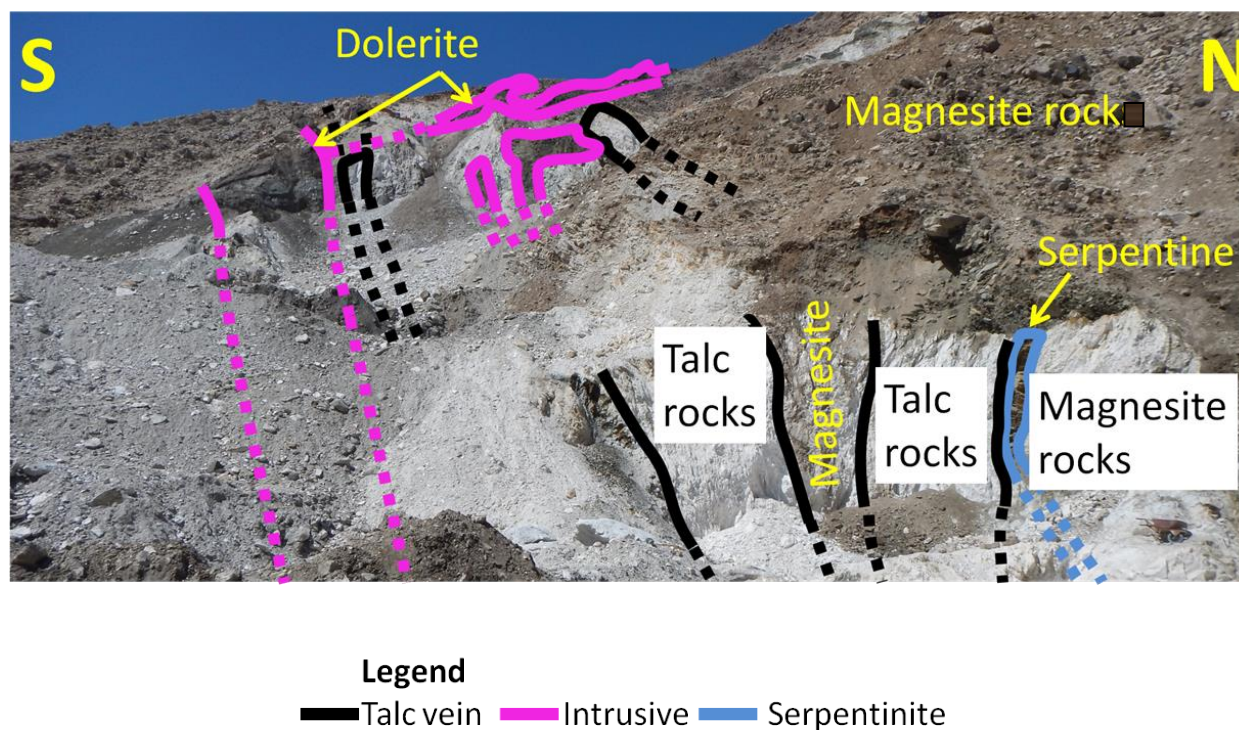


Figure 3.5 Outcrop of Dar deposit.

3.6 Wachalgad

Location of this prospect is $N34^{\circ} 02' 33.37''$ and $E70^{\circ} 14' 50.32''$. The host rock in this prospect is pure magnesite to talc-bearing magnesite rock having no contact with gneiss. Thick talc veins ranging in thickness from 1 to 14 meters are parallel to sub parallel to the beddings of magnesite rocks (Fig. 3.6). Massive layers of dolomite marble were also observed having sharp contact with gneiss about 700 meters from talc veins but talc was not related to those dolomite marbles. Quartz veins are aligned parallel to sub parallel to the gneissosity of gneiss and beddings of dolomite marble. Quartz veins also show lenticular structure. Tremolitite was not observed unlike other magnesite hosted deposits.

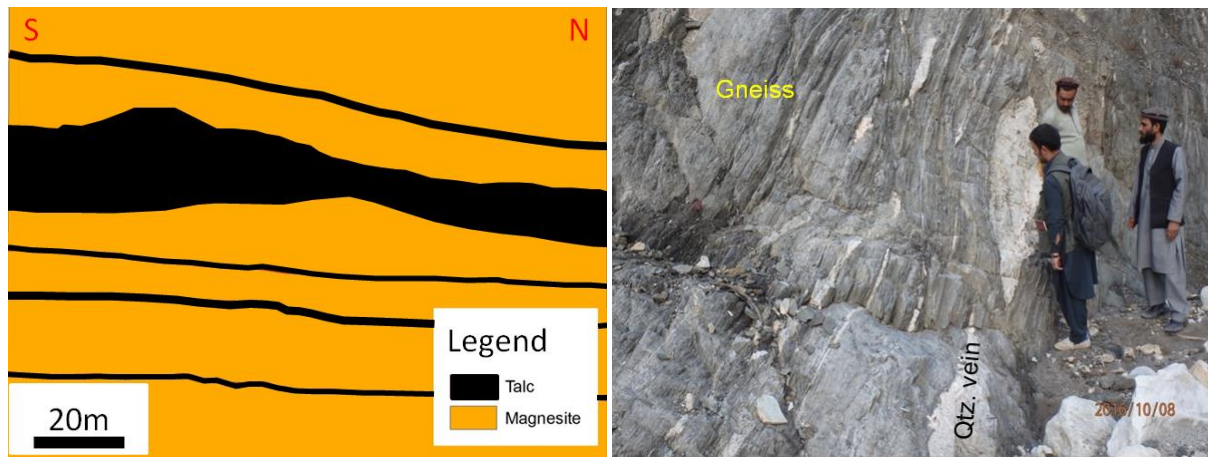


Figure 3.6 Outcrop sketch of the Wachalgad prospect and lenticular quartz veins in gneiss.

3.7 Lesho

Location of this deposit is $N34^{\circ} 01' 40.1''$ and $E70^{\circ} 14' 07.3''$. Host rocks in this deposit are magnesite and dolomite marble. Talc is massive, powdery and milky white to black in color. Occasionally talc and magnesite occurred as a mixture. Tremolite was also observed at the contact between dolomite marble and amphibolite (Fig. 3.7). Gneiss was not marked in this deposit but massive layers of dolomite marble parallel to sub parallel to the beddings of magnesite rocks were marked about 400 m away from talc veins.

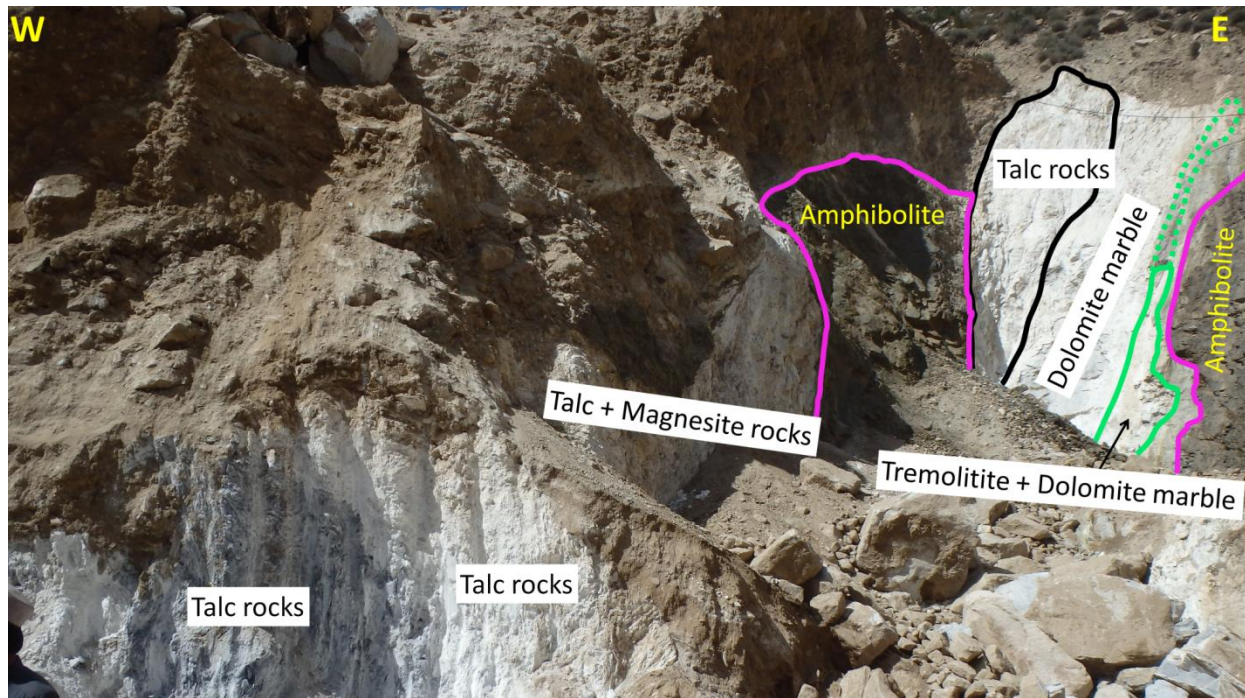


Figure 3.7 Outcrop of the Lesho deposit.

3.8 Sargare

Location of this prospect is $N34^{\circ} 01' 23.6''$ and $E70^{\circ} 14' 53.34''$. Host rock in this prospect is also magnesite and a talc vein is parallel to sub parallel to the beddings of magnesite rock. Talc was also observed as small veinlets originated from the main vein (Fig. 3.8). About 0.5 meter thick dolomite bed parallel to sub parallel to the beddings of magnesite rock was marked. Gneiss and tremolite were not marked in this prospect.

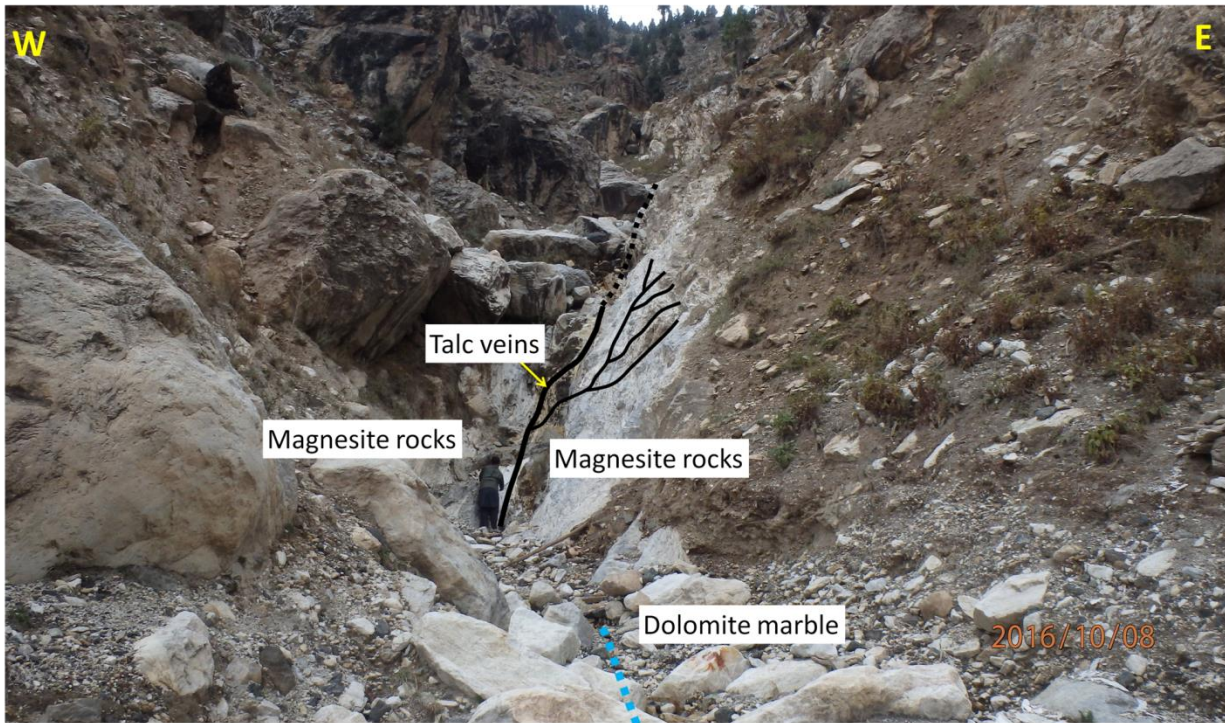


Figure 3.8 Outcrop of the Sargare prospect.

3.9 Mamond dara

This deposit is named as “Chengas” in the Mamond Tangai area, Achin district, Nangarhar province. Its location is $N34^{\circ} 03' 19.7''$ and $E70^{\circ} 34' 38.3''$. In this deposit, talc occurs as alternating layers of talc and dolomite marble. Dolomite marble has a sharp contact with gneiss. Intrusive rocks were also observed metamorphosed to quartz chlorite schist. Tremolitite was not observed in this deposit, unlike the Kotikhel and Jainaw deposits. Beddings of dolomite marble, talc veins and gneissosity of gneiss are parallel to sub parallel to each other (Fig. 3.9a & b).

Carbonate-hosted talc deposits, 2018

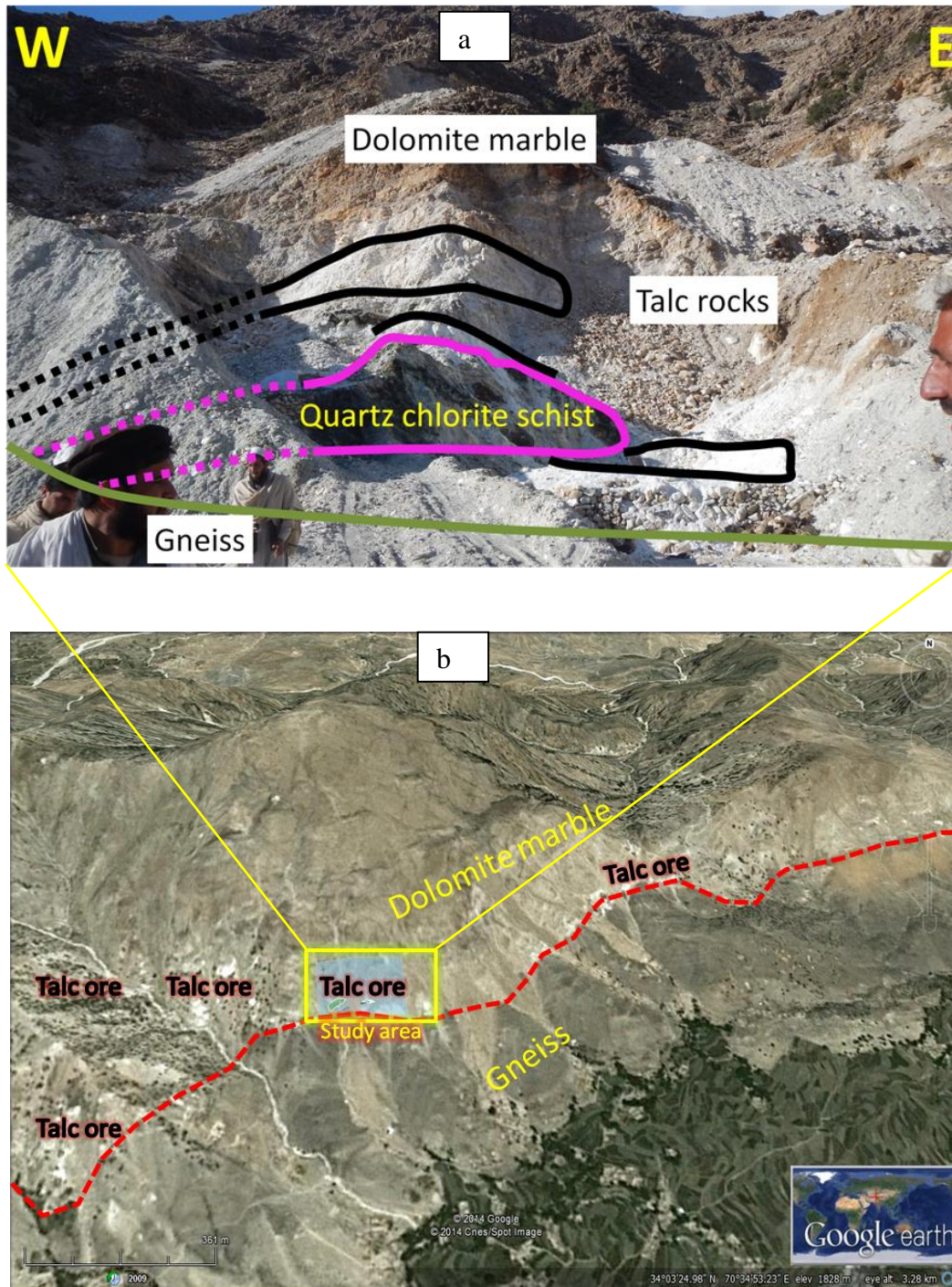


Figure 3.9 (a) Outcrop of the Mamond dara deposit, (b) Contact between dolomite marble and gneiss and different talc ore bodies along that contact.

Mode of occurrence of all rocks in each deposit is summarized in Table 1.

Carbonate-hosted talc deposits, 2018

Table 1. Mode of occurrence of talc deposits and related rocks in Spinghar Fault Block, Afghanistan.

No	Deposits	Type of rocks	Thickness (m)	Host rocks	Mode of occurrence
1	Kotikhel (Dawood mine and Noor mine)	Talc rocks	0.5 to 2	Dolomite marble	Parallel to sub parallel to the beddings of dolomite marble
		Dolomite maarble	Hundreds of meters		Parallel to sub parallel beddings with gneissosity of gneiss
		Tremolite	0.2	Dolomite marble	Parallel to sub parallel to the beddings of dolomite marble
		Antigorite	5 to 8	Dolomite marble	Occurred at the contact of dolomite marble and amphibolite
		Quartz veins	1.5		Folded and occurred at the contact of dolomite marble and talc
		Gneiss	Thousands of meters		Sharp contact with host dolomite marble
2	Janinaw	Talc rocks	1.5 to 2.5	Dolomite marble	Parallel to sub parallel to the beddings of dolomite marble
		Dolomite maarble	Hundreds of meters		No contact with gneiss
		Talc and tremolite	3	Dolomite marble	Needle like tremolite crystals occur randomly in the soft talc matrix
		Quartz veins	0.1	Talc rocks	Thin layer of talcose quartz observed in talc ore
3	Kherwasti	Talc rocks	0.3 to 1	Magnesite rocks	Parallel to sub parallel to the beddings of magnesite rocks
		Magnesite rocks	Hundreds of meters	Dolomite marble	No contact with gneiss
		Amphibolite	0.5 to 5		Cross cutting and parallel to sub parallel to magnesite rocks
		Altered diorite	2.5		Cross cutting magnesite rocks
		Tremolite	2 to 5.5	Magnesite rocks	Parallel to sub parallel to the beddings of magnesite rocks
		Antigorite	0.2 to 3	Magnesite rocks	Occurred at the contact of magnesite rocks and amphibolite
4	Anarokas	Talc rocks	1 to 1.5	Magnesite rocks	Parallel to sub parallel to the beddings of magnesite rocks
		Magnesite rocks	Hundreds of meters	Dolomite marble	Sharp contact with gneiss
		Amphibolite	2.5 to 20		Cross cutting magnesite rocks and gneiss
		Antigorite	2 to 3	Magnesite rocks	Occurred at the contact of magnesite rocks and amphibolite
		Tremolite	0.4 to 2.5		Occurred at the contact of magnesite rocks and amphibolite
		Granite	Hundreds of meters	Gneiss	Cross cutting the gneiss and quartz veins in gneiss
		Quartz veins	0.1 to 0.2	Gneiss	Parallel to sub parallel to the gneissosity of gneiss
5	Dar	Talc rocks	3 to 4	Magnesite rocks	Parallel to sub parallel to the beddings of magnesite rocks
		Magnesite rocks	Hundreds of meters	Dolomite marble	No contact with gneiss
		Diabase	0.1 to 10		Cross cutting and parallel to sub parallel to talc and magnesite rocks
		Serpentinite	0.3 to 0.6	Magnesite rocks	Parallel to sub parallel to the beddings of magnesite rocks
6	Wachalgad	Talc rocks	1 to 14	Magnesite rocks	Parallel to sub parallel to the beddings of magnesite rocks
		Magnesite rocks	Hundreds of meters	Dolomite marble	No contact with gneiss
		Dolomite maarble	Hundreds of meters		Sharp contact with gneiss
		Quartz veins	0.1 to 1	Gneiss	Lenticular veins parallel to sub parallel to the gneissosity of gneiss
7	Lesho	Talc rocks	2 to 8	Magnesite rocks and Dolomite marble	Massive, powdery and milky white to black in color. Occasionally talc and magnesite occurred as a mixture
		Tremolite	0.6 to 1	Dolomite marble	Occurred at the contact of dolomite marble and amphibolite
8	Sargare	Talc rocks	0.1 to 0.6	Magnesite rocks	Parallel to sub parallel to the beddings of magnesite rocks
		Magnesite rocks	Hundreds of meters		No contact with gneiss
		Dolomite maarble	0.5	Magnesite rocks	Parallel to sub parallel to the beddings of magnesite rocks
9	Mamond Dara	Talc rocks	0.1 to 2	Dolomite marble	alternating layers of talc and dolomite marble
		Dolomite maarble	Hundreds of meters		Sharp contact with gneiss
		Quartz chlorite schist	0.2 to 3.5	Dolomite marble	Parallel to sub parallel to the beddings of dolomite marble and talc veins
		Gneiss	Hundreds of meters		Sharp contact with host dolomite marble

4. Analytical Methods

Total 107 samples were collected including host carbonate rocks, talc rocks, gneiss, intrusive rocks, altered intrusive and carbonate rocks and quartz veins, among which representative samples were selected for analyses. In the field work, a clinometer (Fig. 4.1a) was used to measure dip and strike of the talc veins, intrusive and metamorphic rocks and host carbonate rocks. Laser range finder (Fig. 4.1b) was used to sketch each studied quarry and was digitized using computer software.

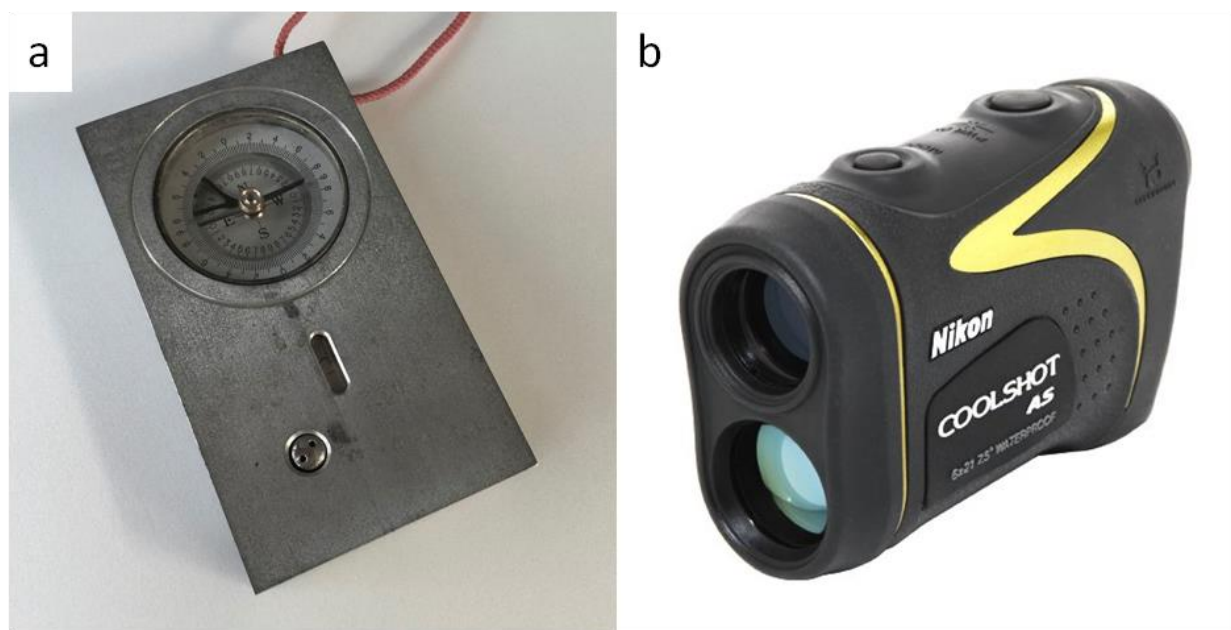


Figure 4.1 (a) Clinometer, (b) laser range finder.

The samples were cut down to the size of slide glass and were polished with powder of size ranges from 100 to 3000 (Fig 4.2a). Most of the samples contain carbonate minerals so a special cementing material was used to make thin sections for microscopic study and later on EPMA and SEM-EDX analyses. “PETROPOXY 154” cannot be used for making thin sections because it can react with carbonate minerals to produce bubbles, so a low viscosity “E205”

Carbonate-hosted talc deposits, 2018

mounting material was used to make the mounds and chips of samples, while “Semedine super” glue was used to mount the samples chips on slide glasses but the slide glasses were made rough before mounting the chips with the glue. Samples were cut from glass slides (Fig. 4.2b) by secondary cutter and then were polished until 1 μ m diamond polish (Fig. 4.2c, d).

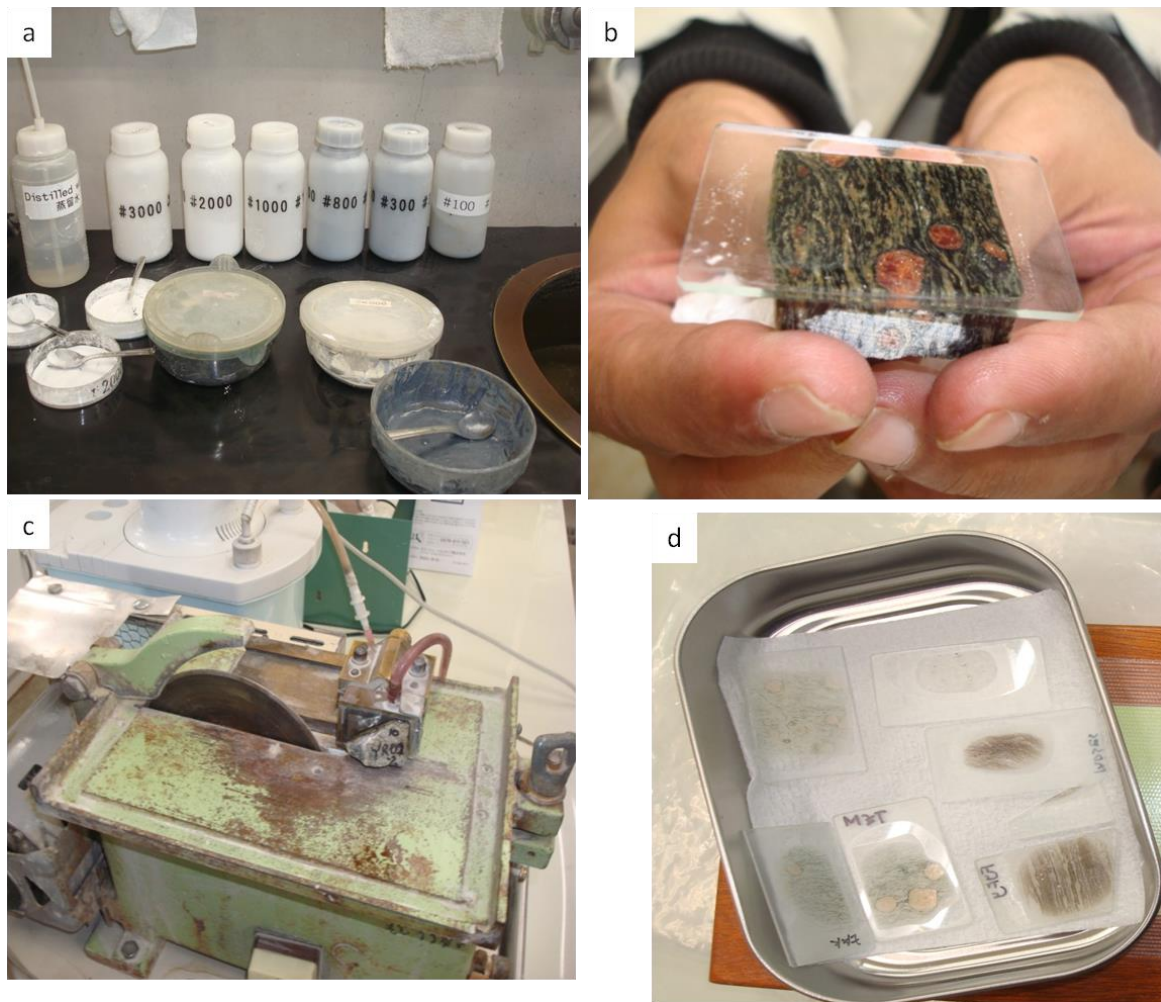


Figure 4.2 (a) Different sizes of powder for polishing the sample chips and thin sections, (b) Mounted slide glass with polished chip, (c) Cutting the rock portion with secondary cutter and (d) Ready thin sections for microscopic observations.

Carbonate-hosted talc deposits, 2018

A Nikon Eclipse LV100N POL microscope (Fig. 4.3) was used to identify the minerals and determine properties of minerals under one polar and crossed polars at Akita University, Japan.



Figure 4.3 Nikon Eclipse LV100N POL microscope.

A proper amount of each rock sample was crushed and pulverized in agate mortar. Samples were prepared (Fig. 4.4) and X-ray diffraction (XRD) analyses were conducted using a Rigaku Multi Flex X-ray diffractometer at Akita University, Japan (Fig. 4.5). Measurement of scan ranged from 2° to 60° (2θ) in steps of 0.01° at $2^\circ/\text{min}$ scan speed, using a monochromated Cu K α ($\lambda = 1.54178 \text{ \AA}$) radiation. 30kV voltages and 16 mA current were used.

Carbonate-hosted talc deposits, 2018



Figure 4.4 Sample preparation for XRD analyses.



Figure 4.5 Rigaku Multi Flex X-ray Diffractometer at Department of Earth Science and Technology, Akita University.

Carbonate-hosted talc deposits, 2018

For XRF analyses, first of all some amount of sample powder was put in the plastic ring mold (30mm diameter) and it was pressed in the powder pellets making machine and pressed for about one minute at 20 MPa pressure (Fig. 4.6). 20% binder was used for very soft samples.

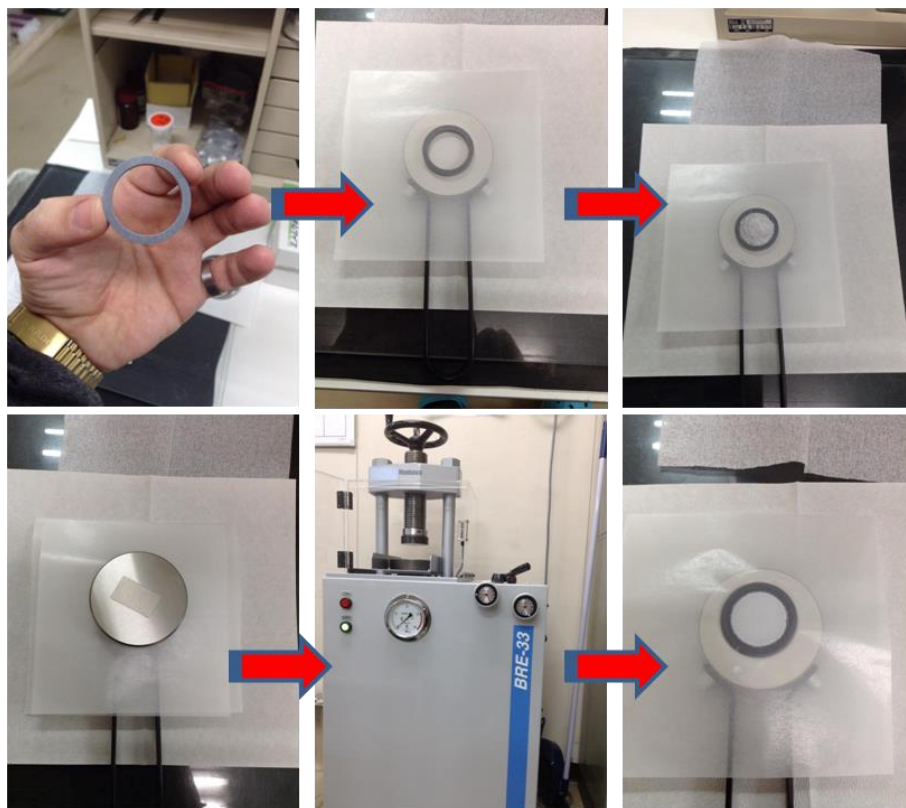


Figure 4.6 Sample (powder pellets) preparation for XRF analyses.

Procedure to obtain loss on ignition (LOI) is as follows:

For drying the samples, temperature was 110°C for 2 hours in an oven, using small alumina crucibles. The alumina crucibles containing samples were put in KDF Electric Furnace 1500-Plus at Akita University (Fig. 4.7) and increased the temperature to 900°C. The temperature has been kept for one hour then turned off the furnace and waited to cool down to 400°C for about 4 hours. The samples have been cooled down to 200°C on the brick in the open air (Fig. 4.7) and then put it in a dry decicator to cool down to room temperature.

Carbonate-hosted talc deposits, 2018

LOI has been calculated by the given formula:

a = weight of crucible

b = weight of crucible + weight of sample

c = total mass after combustion

$$\text{LOI} = \frac{b-c}{b-a} \times 100$$

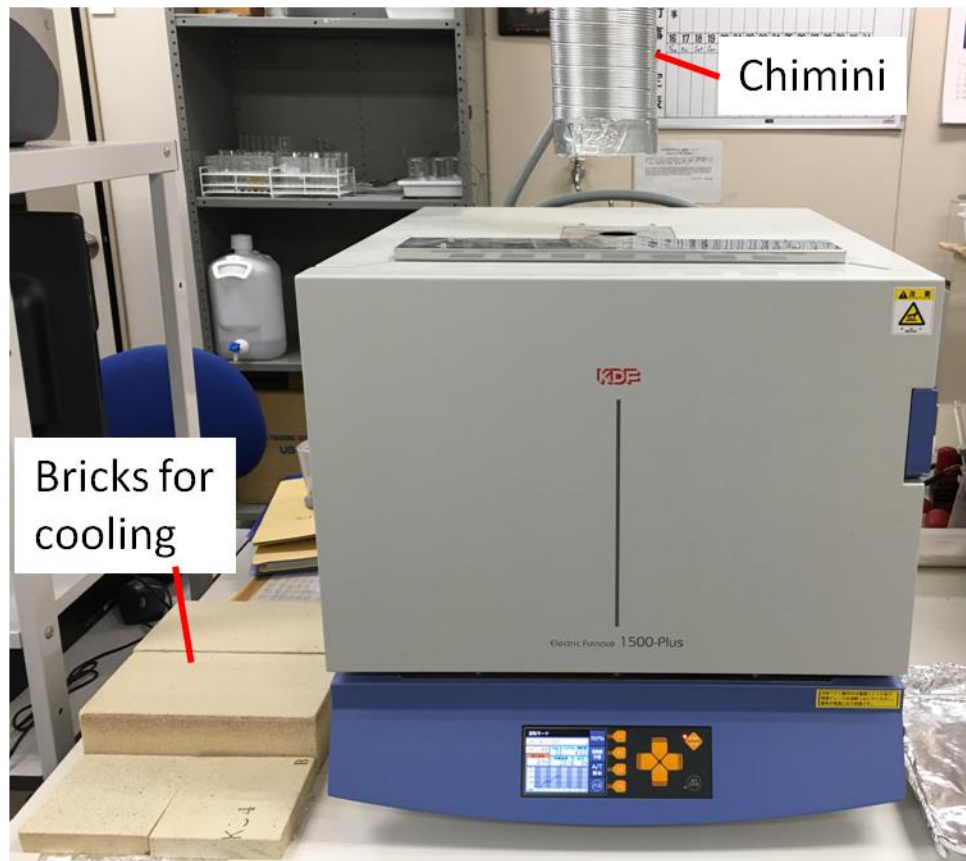


Figure 4.7 Electric furnace used for loss on ignition.

Bulk chemical compositions of major elements were determined using a Rigaku ZSX Primus II X-ray Fluorescence (XRF) spectrometer at Akita University, Japan (Fig.4.8a). Powder pellets were used (Fig.4.8b) and the operating conditions of XRF were 50 kV voltages and 60 mA current. Calibration curves were used using standards distributed by Geological Survey of

Carbonate-hosted talc deposits, 2018

Japan, such as JG-3, JDo-1, JH-1, JA-2, JG-2, JB-3, JP-1, JA-1, JGB-2, JLS-1 and JF-2.

Detection limits of SiO_2 , CaO , MgO , TiO_2 , Al_2O_3 , Fe_2O_3 , MnO , Na_2O , K_2O and P_2O_5 are 0.6, 0.06, 0.2, 0.03, 0.01, 0.11, 1.8, 0.04, 0.03 and 0.001 wt%, respectively.

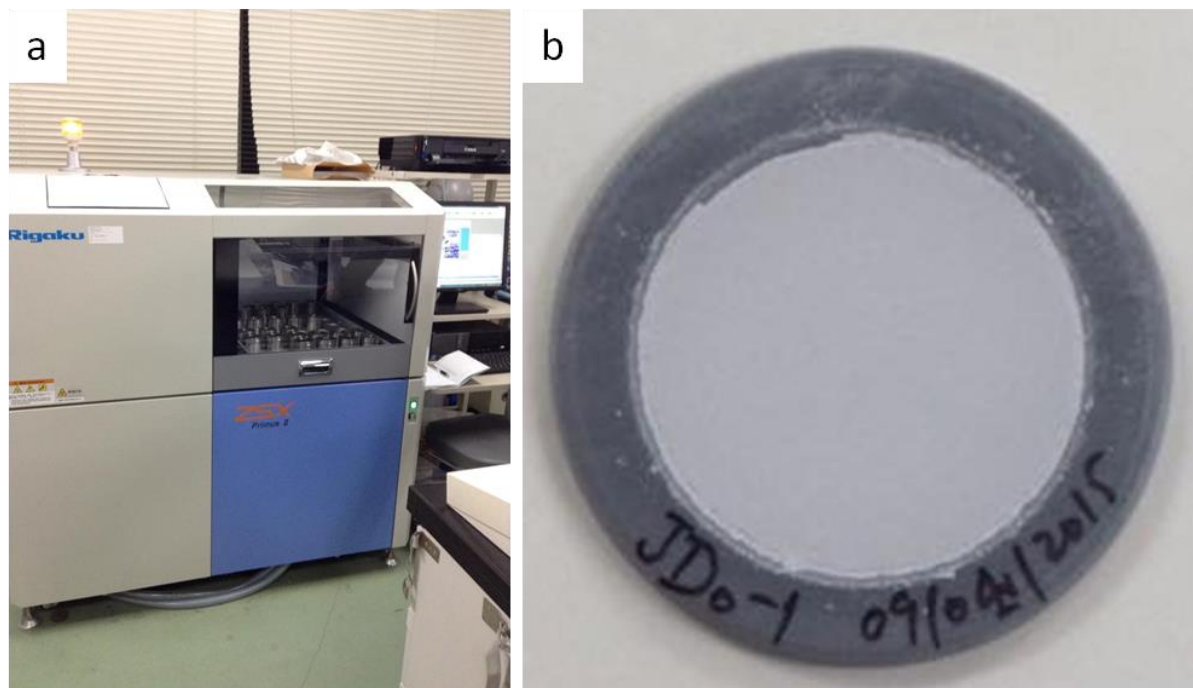


Figure 4.8 (a) Rigaku ZSX primus II in Akita University, (b) Powder pellet for XRF analyses.

For whole rock trace and rare-earth elements (REE) composition analyses, the samples were digested using HClO_4 , HF and HNO_3 (Fig. 4.9) and diluted solutions were analyzed using an Agilent Technologies 7500 Series Inductively Coupled Plasma Mass Spectrometry (ICP-MS) at Akita University, Japan (Fig. 4.10).

Carbonate-hosted talc deposits, 2018

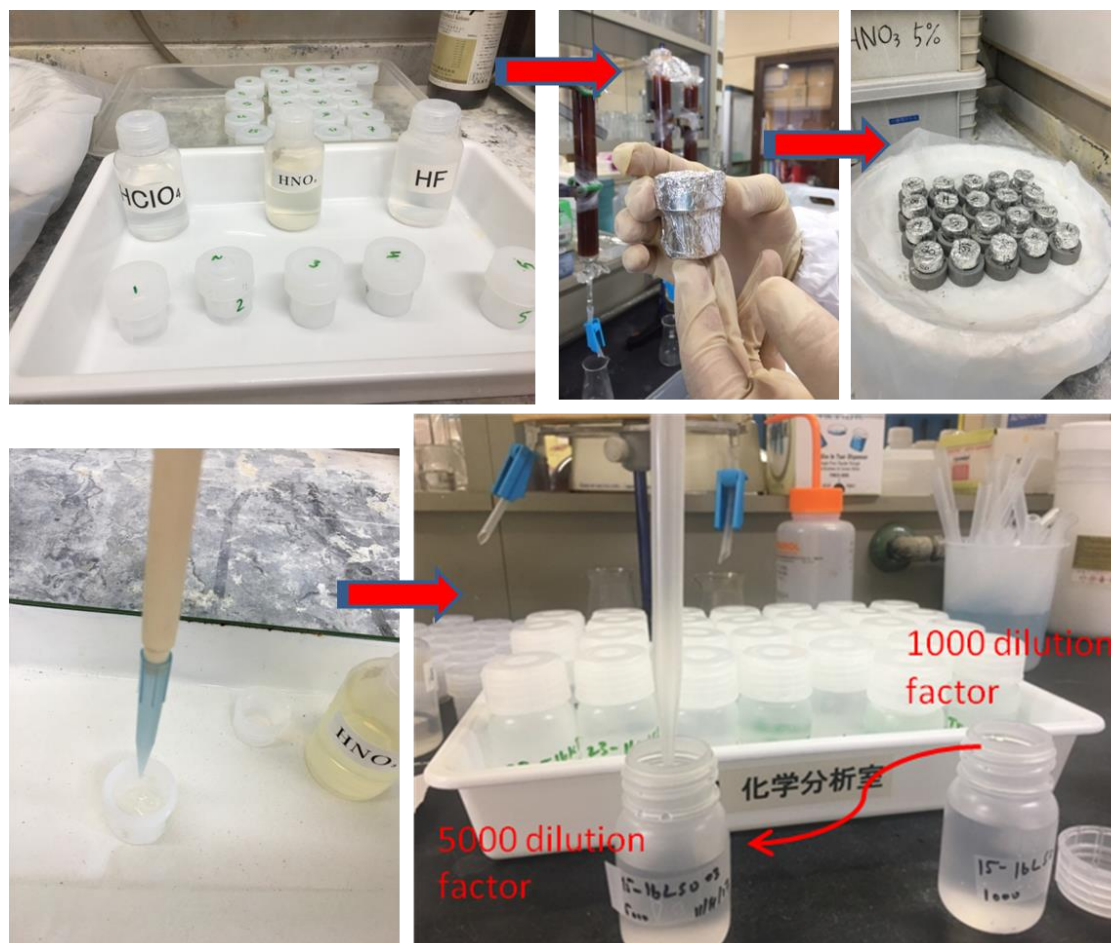


Figure 4.9 Samples digestion for ICP-MS analyses.

Detection limits of trace elements of Co, Y, Sb, Cs, Ta, Re, Th is 0.001 ppb, those of Ni and Sn is 0.004 ppb while Cr = 0.008 ppb, Zr = 0.006 ppb, Ba = 0.15 ppb, Hf = 0.002 ppb. The detection limits of REEs of Ce, Gd, Tb, Dy, Ho, Er, Tm, Yb and Lu is 0.001 ppb and those of La and Eu is 0.0002 ppb, Pr is 0.0001 ppb while those of Nd and Sm is 0.002 ppb. For ICP-MS analyses, Geological Survey of Japan standards were also used to ensure the accuracy of analyses.

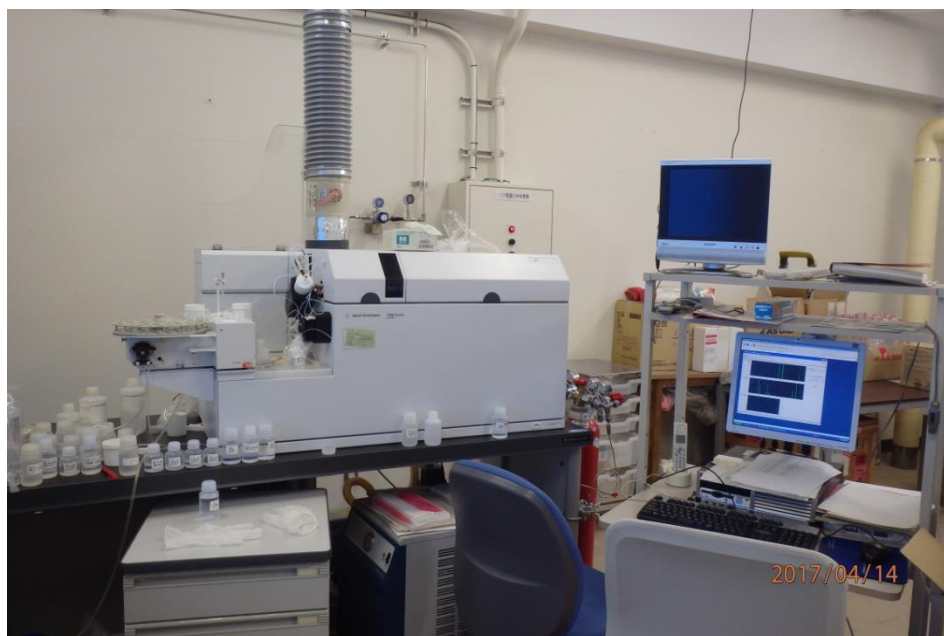


Figure 4.10 Agilent Technologies 7500 Series ICP-MS at Department of Resource Science Akita University.

The representative thin sections of carbonate rocks were carbon-coated with JEOL JEC-560 Auto Carbon Coater (Fig. 4.11a) and chemical compositions of minerals were measured using a JEOL-JXA-8800R Superprobe an electron probe microanalyser (EPMA), at Akita University, Japan (Fig. 4.11b) with 15 kV voltages, 20 nA beam current and 10 μm spot size. Detection limits of Ca, Fe, Mg and Mn in case of magnesite were 122, 212.75, 129.67 and 210.67 ppm, respectively, for calcite, it was 187.45, 248.60, 119.15 and 252.20 ppm, respectively, while those of dolomite was 244.45, 242.55, 121.30 and 222.10 ppm, respectively. Standard materials used were natural minerals and pure metals.

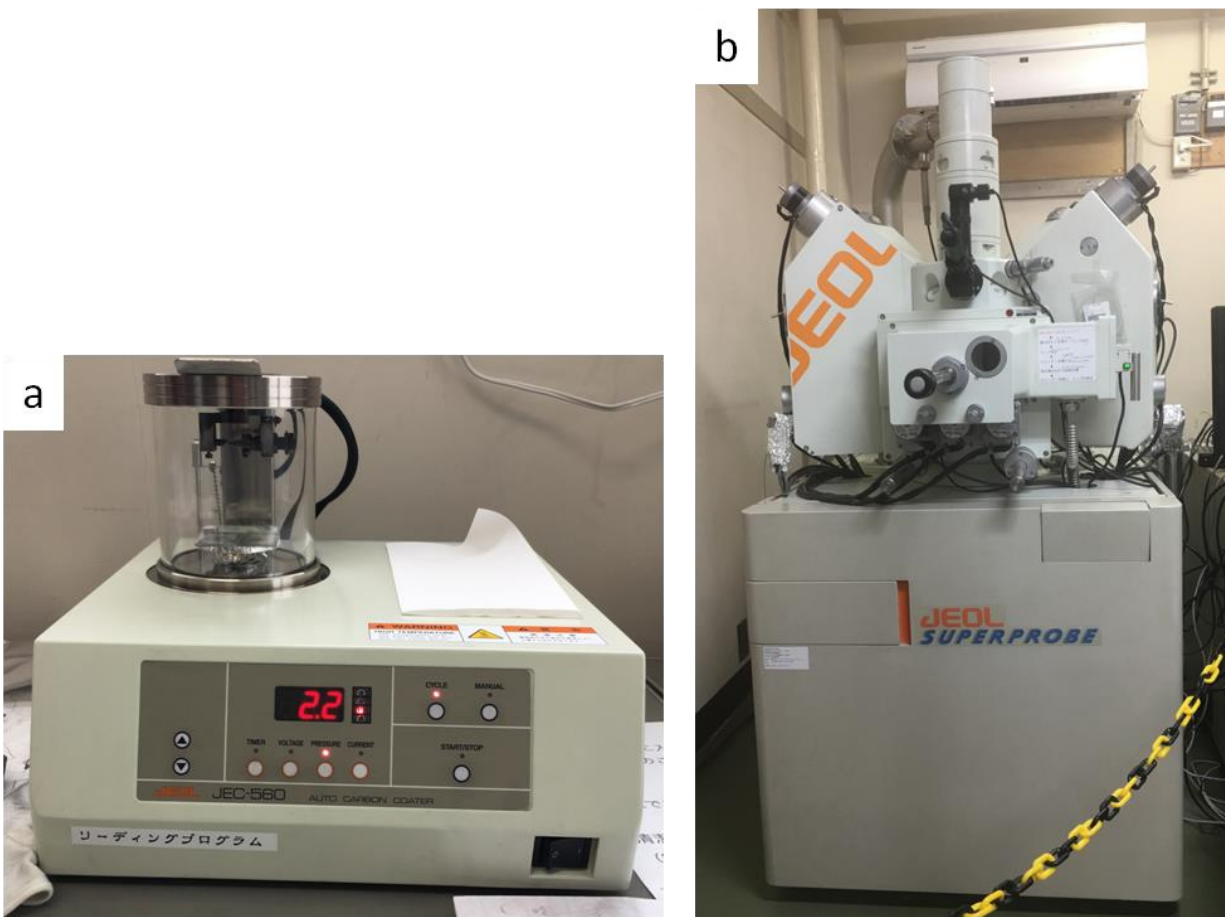


Figure 4.11 (a) JEOL JEC-560 Auto Carbon Coater, (b) JEOL-JXA-8800R Superprobe microanalyser (EPMA), at Akita University, Japan.

Molecular proportion of oxides in carbonates was calculated using the relation:

Molecular proportion of oxide = EPMA data/molecular weight of each oxide present (Table B)

Sample number 16KHTI01A is shown as an example, SD stands for standard deviation.

Carbonate-hosted talc deposits, 2018

Table (A) Weight percent of a magnesite mineral analyzed by EPMA

16KHTI01A

Wt.%

Sample Name	No.	CaO	FeO	MgO	MnO	CO ₂	Total
16KHTI01A1	1	0.1	1.9	44.9	0.0	53.1	100.0
16KHTI01A2	2	0.2	0.5	48.1	0.1	51.2	100.0
16KHTI01A3	3	0.5	0.5	47.9	0.0	51.1	100.0
16KHTI01A4	4	0.0	0.3	48.5	0.0	51.2	100.0
16KHTI01A5	5	0.1	0.9	48.5	0.0	50.5	100.0
16KHTI01A6	6	0.1	0.8	48.3	0.0	50.8	100.0
16KHTI01A7	7	0.5	0.4	49.1	0.0	49.9	100.0
16KHTI01A8	8	0.2	0.7	46.9	0.1	52.1	100.0
16KHTI01A9	9	0.1	0.4	49.8	0.0	49.7	100.0
16KHTI01A10	10	0.0	0.5	49.2	0.1	50.2	100.0
16KHTI01A11	11	0.3	0.6	48.9	0.0	50.2	100.0
16KHTI01A12	12	0.3	0.5	48.9	0.0	50.3	100.0
16KHTI01A13	13	0.6	0.4	48.9	0.0	50.2	100.0
16KHTI01A14	14	0.5	0.4	49.5	0.1	49.5	100.0
16KHTI01A15	15	0.5	0.5	49.5	0.0	49.6	100.0
	Average	0.3	0.6	48.5	0.0		
	SD	0.2	0.4	1.2	0.0		

Carbonate-hosted talc deposits, 2018

Table (B) Molecular proportion of oxides

Molecular proportion of Oxides					
Sample Name	CaO	FeO	MgO	MnO	Total
16KHTI01A1	0.0	0.0	1.1	0.0	46.9
16KHTI01A2	0.0	0.0	1.2	0.0	48.8
16KHTI01A3	0.0	0.0	1.2	0.0	48.9
16KHTI01A4	0.0	0.0	1.2	0.0	48.8
16KHTI01A5	0.0	0.0	1.2	0.0	49.5
16KHTI01A6	0.0	0.0	1.2	0.0	49.2
16KHTI01A7	0.0	0.0	1.2	0.0	50.1
16KHTI01A8	0.0	0.0	1.2	0.0	47.9
16KHTI01A9	0.0	0.0	1.2	0.0	50.3
16KHTI01A10	0.0	0.0	1.2	0.0	49.8
16KHTI01A11	0.0	0.0	1.2	0.0	49.8
16KHTI01A12	0.0	0.0	1.2	0.0	49.7
16KHTI01A13	0.0	0.0	1.2	0.0	49.8
16KHTI01A14	0.0	0.0	1.2	0.0	50.5
16KHTI01A15	0.0	0.0	1.2	0.0	50.4

Then the atomic proportion of oxygen in each molecule was calculated (Table C), which is:

[(EPMA data/molecular weight of each oxide present)*No. of oxygen in each oxide or molecule].

Then all the atomic proportions were sum as (T1) (Table C).

Carbonate-hosted talc deposits, 2018

Table (C) Atomic proportion of Oxygen in each molecule

Sample Name	CaO	FeO	MgO	MnO	Total(T1)
16KHTI01A1	0.0	0.0	1.1	0.0	1.2
16KHTI01A2	0.0	0.0	1.2	0.0	1.2
16KHTI01A3	0.0	0.0	1.2	0.0	1.2
16KHTI01A4	0.0	0.0	1.2	0.0	1.2
16KHTI01A5	0.0	0.0	1.2	0.0	1.2
16KHTI01A6	0.0	0.0	1.2	0.0	1.2
16KHTI01A7	0.0	0.0	1.2	0.0	1.2
16KHTI01A8	0.0	0.0	1.2	0.0	1.2
16KHTI01A9	0.0	0.0	1.2	0.0	1.3
16KHTI01A10	0.0	0.0	1.2	0.0	1.2
16KHTI01A11	0.0	0.0	1.2	0.0	1.2
16KHTI01A12	0.0	0.0	1.2	0.0	1.2
16KHTI01A13	0.0	0.0	1.2	0.0	1.2
16KHTI01A14	0.0	0.0	1.2	0.0	1.3
16KHTI01A15	0.0	0.0	1.2	0.0	1.3

Then cation normalization factor approach was used (Table D). On the basis of 6 oxygens, the molecular formula for carbonates require 2 cations of charge 2^+ each to balance the two CO_3^{2-} anions i.e., $(\text{R}_1^{2+}, \text{R}_2^{2+})(\text{CO}_3)_2$, Where R_1, R_2 represents a combination of any of the cations $\text{Ca}^{2+}, \text{Fe}^{2+}, \text{Mg}^{2+}$ or Mn^{2+} . Since total number of cations in the carbonates must be 2 in this case, it means that $\text{Fe}+\text{Mn}+\text{Mg}+\text{Ca} = 2.0$. For example, dolomite $\text{CaMg}(\text{CO}_3)_2$ or magnesite $\text{Mg}_2(\text{CO}_3)_2$.

Therefore, cation normalization factor is given as:

Total number of cations (in the carbonates, on the basis of 6 oxygens)/T1 = 2/T1.

This cation normalization factor approach is also used in the textbook “An Introduction to the Rock-Forming Minerals” by [Deer et al. \(1966, 2nd Edition, 1992\)](#).

Carbonate-hosted talc deposits, 2018

Table (D) Cation normalization factor

Sample Name	Cation Normalization
16KHTI01A1	1.7
16KHTI01A2	1.6
16KHTI01A3	1.6
16KHTI01A4	1.6
16KHTI01A5	1.6
16KHTI01A6	1.6
16KHTI01A7	1.6
16KHTI01A8	1.7
16KHTI01A9	1.6
16KHTI01A10	1.6
16KHTI01A11	1.6
16KHTI01A12	1.6
16KHTI01A13	1.6
16KHTI01A14	1.6
16KHTI01A15	1.6

After that, atomic proportion of oxygen in each molecule was multiplied by the cation normalization factor, i.e., $[(2/T1) \times \text{atomic proportion of oxygen in each molecule}]$, and summed the results to have a total value (T2) - approximately equal to 2.0, which represents the total number of cations in the carbonates based on 6 oxygens i.e., $\text{Fe}+\text{Mn}+\text{Mg}+\text{Ca} = 2.0$, as shown in Table E.

Carbonate-hosted talc deposits, 2018

Table (E) Total number of cations in the carbonates based on 6 oxygens

Sample Name	Ca	Fe	Mg	Mn	Total(T2)
16KHTI01A1	0.0	0.0	2.0	0.0	2.0
16KHTI01A2	0.0	0.0	2.0	0.0	2.0
16KHTI01A3	0.0	0.0	2.0	0.0	2.0
16KHTI01A4	0.0	0.0	2.0	0.0	2.0
16KHTI01A5	0.0	0.0	2.0	0.0	2.0
16KHTI01A6	0.0	0.0	2.0	0.0	2.0
16KHTI01A7	0.0	0.0	2.0	0.0	2.0
16KHTI01A8	0.0	0.0	2.0	0.0	2.0
16KHTI01A9	0.0	0.0	2.0	0.0	2.0
16KHTI01A10	0.0	0.0	2.0	0.0	2.0
16KHTI01A11	0.0	0.0	2.0	0.0	2.0
16KHTI01A12	0.0	0.0	2.0	0.0	2.0
16KHTI01A13	0.0	0.0	2.0	0.0	2.0
16KHTI01A14	0.0	0.0	2.0	0.0	2.0
16KHTI01A15	0.0	0.0	2.0	0.0	2.0
Average	0.0	0.0	2.0	0.0	
SD	0.0	0.0	0.0	0.0	

Finally, the molecular proportion of carbonates, i.e.,

$[(2/T1) * \text{atomic proportion of oxygen in each molecule}/T2]$ was calculated and then normalized to 100% (Fig. F).

Carbonate-hosted talc deposits, 2018

Table F Molecular proportion of each carbonate

Sample Name	CaCO ₃	FeCO ₃	MgCO ₃	MnCO ₃	Total	CaCO ₃	FeCO ₃	MgCO ₃	MnCO ₃	Total
16KHTI01A1	0.0	0.0	1.0	0.0	1.0	0.2	2.3	97.5	0.0	100.0
16KHTI01A2	0.0	0.0	1.0	0.0	1.0	0.3	0.5	99.1	0.1	100.0
16KHTI01A3	0.0	0.0	1.0	0.0	1.0	0.7	0.5	98.7	0.0	100.0
16KHTI01A4	0.0	0.0	1.0	0.0	1.0	0.1	0.3	99.6	0.0	100.0
16KHTI01A5	0.0	0.0	1.0	0.0	1.0	0.1	1.0	98.9	0.0	100.0
16KHTI01A6	0.0	0.0	1.0	0.0	1.0	0.1	0.9	98.9	0.0	100.0
16KHTI01A7	0.0	0.0	1.0	0.0	1.0	0.7	0.5	98.8	0.0	100.0
16KHTI01A8	0.0	0.0	1.0	0.0	1.0	0.4	0.8	98.8	0.1	100.0
16KHTI01A9	0.0	0.0	1.0	0.0	1.0	0.2	0.4	99.4	0.0	100.0
16KHTI01A10	0.0	0.0	1.0	0.0	1.0	0.1	0.5	99.4	0.1	100.0
16KHTI01A11	0.0	0.0	1.0	0.0	1.0	0.4	0.6	99.0	0.0	100.0
16KHTI01A12	0.0	0.0	1.0	0.0	1.0	0.4	0.6	99.0	0.0	100.0
16KHTI01A13	0.0	0.0	1.0	0.0	1.0	0.8	0.4	98.8	0.0	100.0
16KHTI01A14	0.0	0.0	1.0	0.0	1.0	0.7	0.5	98.7	0.1	100.0
16KHTI01A15	0.0	0.0	1.0	0.0	1.0	0.7	0.5	98.8	0.0	100.0
					Average	0.4	0.7	98.9	0.0	100.0
					SD	0.3	0.5	0.5	0.0	

Selected samples were carbon coated with a JEOL JEC-560 Auto Carbon Coater and then qualitative analyses was conducted for the identification of carbonates and silicate minerals using JEOL JSM-6610 Scanning Electron Microscope (Fig. 4.12) with energy dispersive spectrometers (SEM) at Faculty of Education, Akita University with following conditions:

Accelerating Voltage = 15 kv, Filament Load current (L.C.) = 60 μ A, Spot size = 72, Z-axis distance = 10 mm and Working distance = 10 mm with good beam stability.

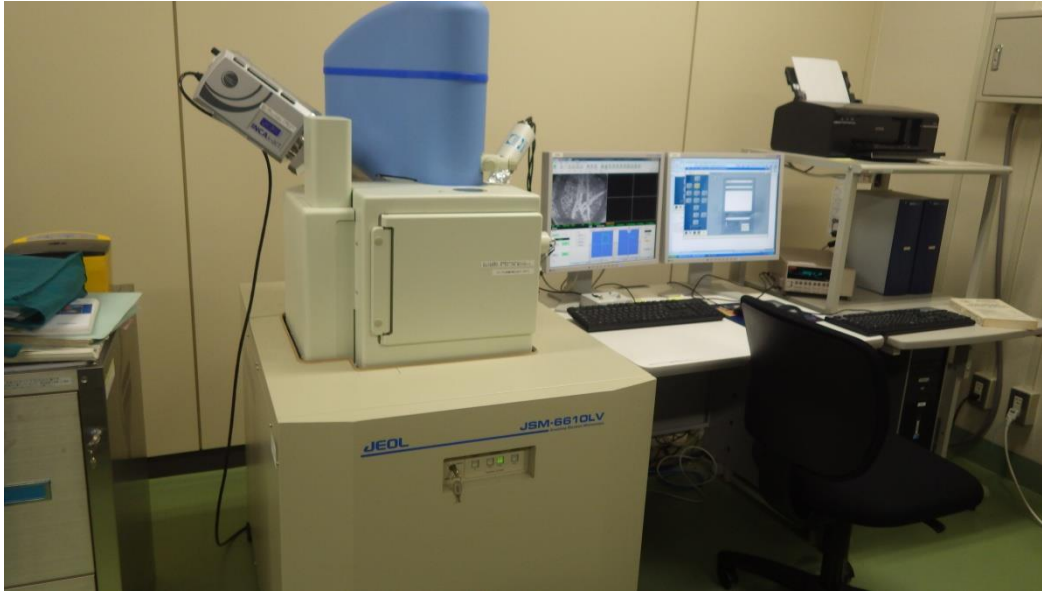


Figure 4.12 JEOL JSM-6610 Scanning Electron Microscope at Faculty of Education, Akita University.

Whiteness of talc samples from each deposit and from its stock piles were measured with a TR-600 machine using JIS M8016 method in Shokozan Mining Co. LTD. Laboratories, Japan.

- ❖ Fluid inclusion micro thermometry was not successful because of too small inclusions in quartz veins and decrepitating of inclusion in dolomite, magnesite and calcite prior to homogenization temperature.

5. Petrography

On the basis of microscopic observations, talc paragenetically coexists with magnesite, tremolite, dolomite and quartz. Well developed talc flakes were observed along the coarse magnesite, dolomite and tremolite. Sporadic talc and tremolite development was also observed within recrystallized magnesite. List of minerals, based on microscopic observations in each rock from each deposit is given in appendix 2.

Abbreviations used in this study are follows:

A = allanite, Atg = antigorite, Bt = biotite, Cc = calcite, Chl = chlorite, Do = dolomite, Ep = epidote, Hbl = hornblende, Mag = magnesite, Mc = microcline, Mu = muscovite, Ol = olivine, Pl = plagioclase, Px = pyroxene, Qz = quartz, Srp = serpentine, Tc = talc, Tr = tremolite.

5.1 Kotikhel (Dawood mine and Noor mine)

Talc ores usually consist of anhedral fibrous talc crystals ranging in length from cryptocrystalline to 0.2 mm (Fig. 5.1a), occasionally having anhedral dolomite ranging in length from 0.01 to 0.7 mm. Dolomite marble, mostly talc-bearing, consists mainly of euhedral dolomite crystals ranging in length from cryptocrystalline to 0.8 mm. Talc crystals are well developed along the boundaries with dolomite ranging in length from 0.01 to 2 mm (Fig. 5.1b). Tremolite was formed by replacement of dolomite (Fig. 5.1c). Antigorite (serpentine) ranging in length from cryptocrystalline to 0.8 mm was formed by replacement of dolomite (Fig. 5.1d). Quartz was rarely observed in the matrix of talc and dolomite marble. Microscopically massive quartz bodies at the contact with talc bodies show mosaic texture ranging in length from 0.02 to 0.4 mm replaced by talc crystals ranging in length from 0.01 to 0.3 mm (Fig. 5.1e). XRD also showed the presence of talc with quartz (Fig. 5.2). Lists of XRD analysis of each rock from each deposit are given in appendix 3. Microscopically gneiss is composed of highly aligned mosaic to elongated

Carbonate-hosted talc deposits, 2018

quartz ranging in length from 0.01 to 0.1 mm and abundant muscovite ranging in length from 0.1 to 0.2 mm (Fig. 5.1f). This high abundance mica causes cleavages bandings of gneiss.

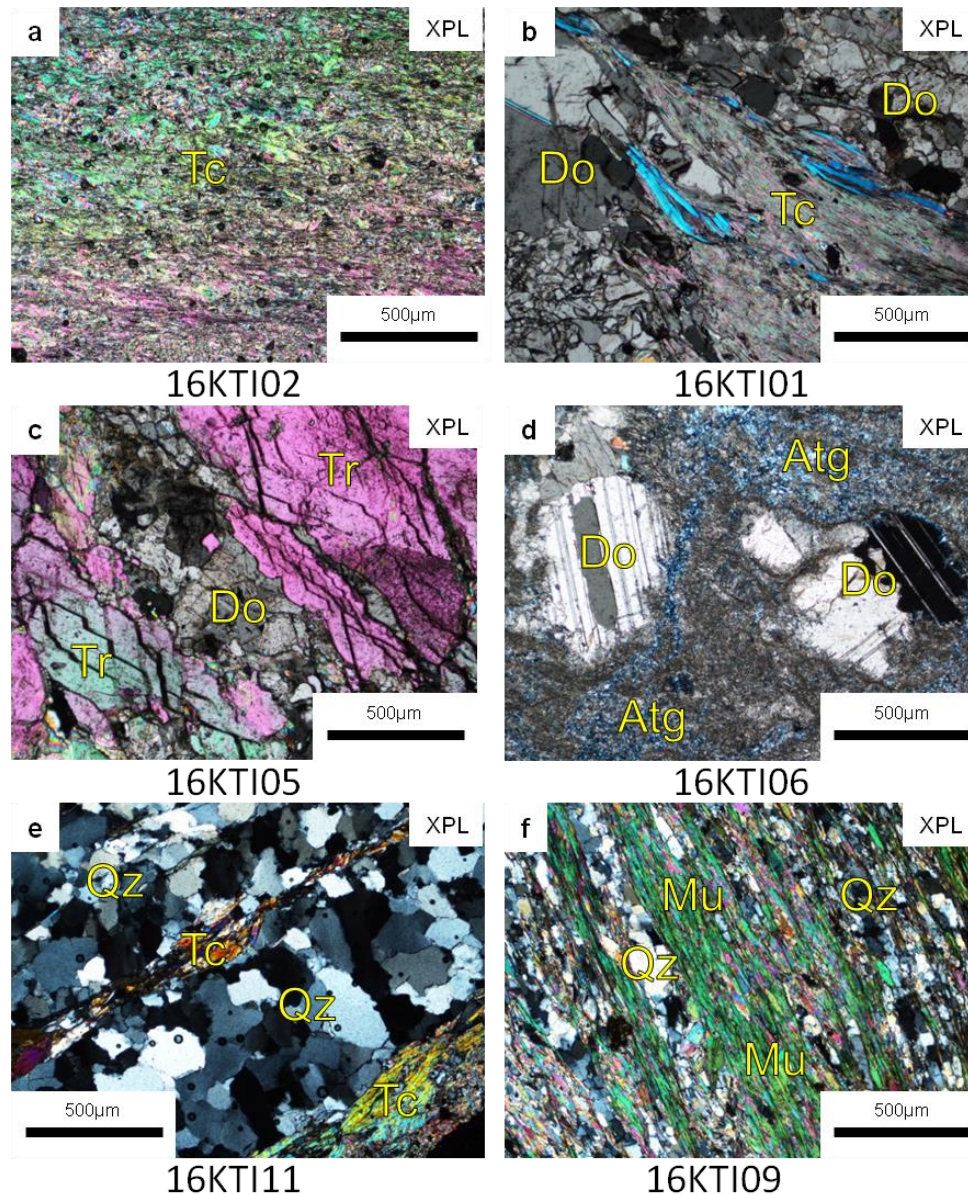


Figure 5.1 Photomicrographs of (a) talc rock, (b) dolomite marble showing well developed talc crystals along the boundaries of dolomite, (c) tremolite that replaced dolomite, (d) antigorite that replaced dolomite, (e) quartz cut by talc, (f) Gneiss consisting of quartz and abundant muscovite from the Kotikhel deposits.

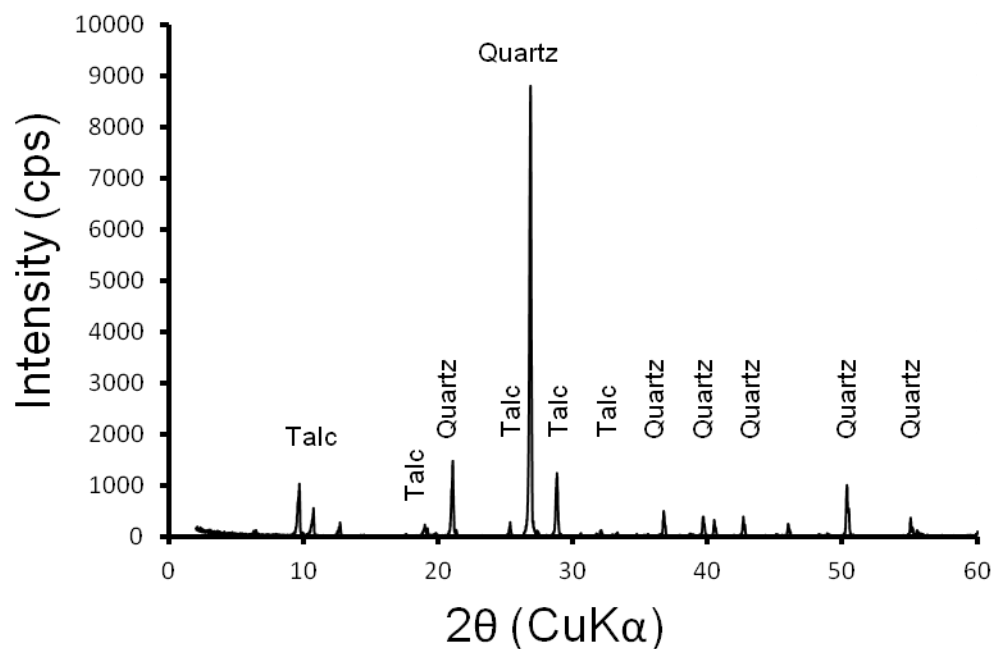


Figure 5.2 X-ray diffractogram of quartz vein (16KT111) from Kotikhel showing the presence of quartz and talc.

5.2 Janinaw

In Janinaw, talc ore is microscopically composed of euhedral, fibrous elongated talc ranging in length from cryptocrystalline to 0.1 mm with subhedral prismatic tremolite ranging in length from 0.3 to 0.6 mm (Fig. 5.3a). The layer of talc contains needle like radiating tremolite crystals visible with naked eye. Talc ore is microscopically composed of light brown color fine grained prismatic talc 0.2 to 0.4 mm and euhedral acicular tremolites ranging in length from 0.01 to 1 mm which are mostly fractured and filled by talc and anhedral dolomite ranging in length from 0.1 to 1.1 mm (Fig. 5.3b). The host dolomite marbles are composed of anhedral calcite 0.2 to 0.5 mm showing lamellar twinning with other minerals including colorless anhedral dolomite ranging in length from 0.2 to 0.4 mm, anhedral, fibrous tremolite ranging in length from 0.02 to 1 mm (Fig. 5.3c). Talcose quartz vein shows an alignment of alternating layers of quartz and talc

Carbonate-hosted talc deposits, 2018

and is microscopically composed of anhedral quartz ranging in length from 0.03 to 0.5 mm with anhedral fibrous talc ranging in length from cryptocrystalline to 0.8 mm and anhedral fibrous chlorite ranging in length from 0.01 to 0.5 mm. The mosaic quartz shows lenticular structure (Fig. 5.3d).

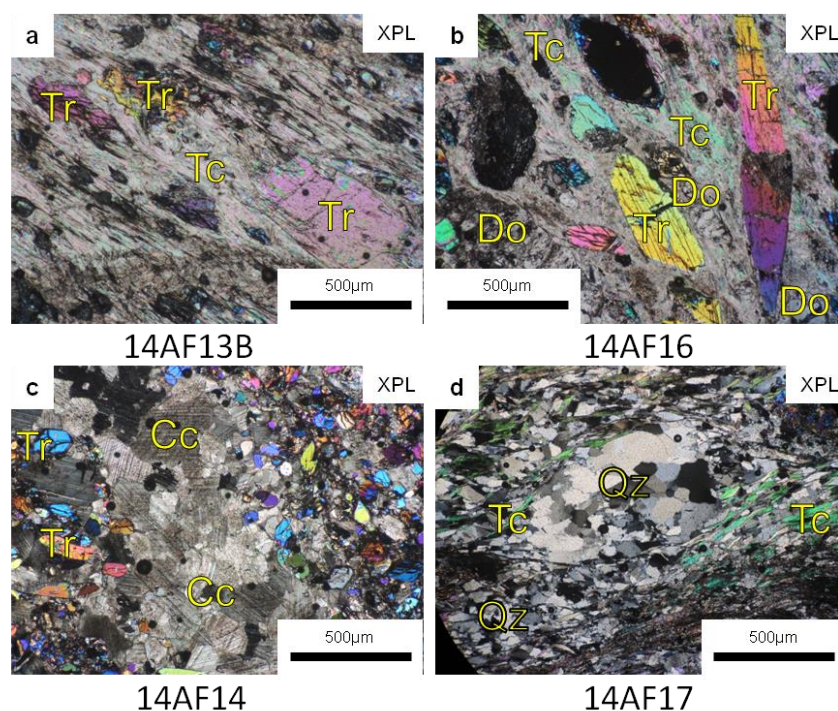


Figure 5.3 Photomicrographs of (a) talc rock having tremolite replaced by talc, (b) talc rock showing idiomorphic crystals of tremolite in ground-mass of talc, (c) host dolomite marble, with abundant calcite and tremolite, (d) quartz vein, quartz was replaced by talc from the Janinaw deposit.

5.3 Kherwasti

In Kherwasti, talc ore is microscopically composed of euhedral to subhedral fibrous talc ranging in length from 0.02 to 2.8 mm having relicts of magnesite (Fig. 5.4a). Magnesite rocks are mostly talc-bearing and are microscopically composed of light to dark brown anhedral magnesite

Carbonate-hosted talc deposits, 2018

ranging in length from 0.01 to 2.8 mm. Euhedral to subhedral fibrous talc ranges in length from 0.1 to 0.5 mm (Fig. 5.4b). Anhedral equant olivine ranges in length from cryptocrystalline to 0.5 mm replaced magnesite (Fig. 5.4c). Cryptocrystalline epidote showing lineation replaced magnesite. Diorite is mostly altered to anhedral fibrous chlorite ranges in length from cryptocrystalline to 0.24 mm, with other minerals including subhedral prismatic plagioclase about 0.02 mm, opaque minerals, biotite and epidote (Fig. 5.4d). Massive tremolites, white and green in color, sheaf like aggregates in hand specimen are microscopically composed of anhedral to euhedral acicular tremolite ranging in length from 0.4 to 2 mm (Fig. 5.4e). Serpentine (antigorite) rock is microscopically consists of cryptocrystalline antigorite showing a mesh texture and magnesite ranging from 0.01 to 0.4 mm (Fig. 5.4f). Amphibolite is microscopically composed of cryptocrystalline hornblende, quartz and plagioclase. Dolomite marble is composed of anhedral dolomite ranging in length from cryptocrystalline to 0.4 mm, and acicular tremolite ranging in length from 0.01 to 0.3 mm while calcite was not found.

Carbonate-hosted talc deposits, 2018

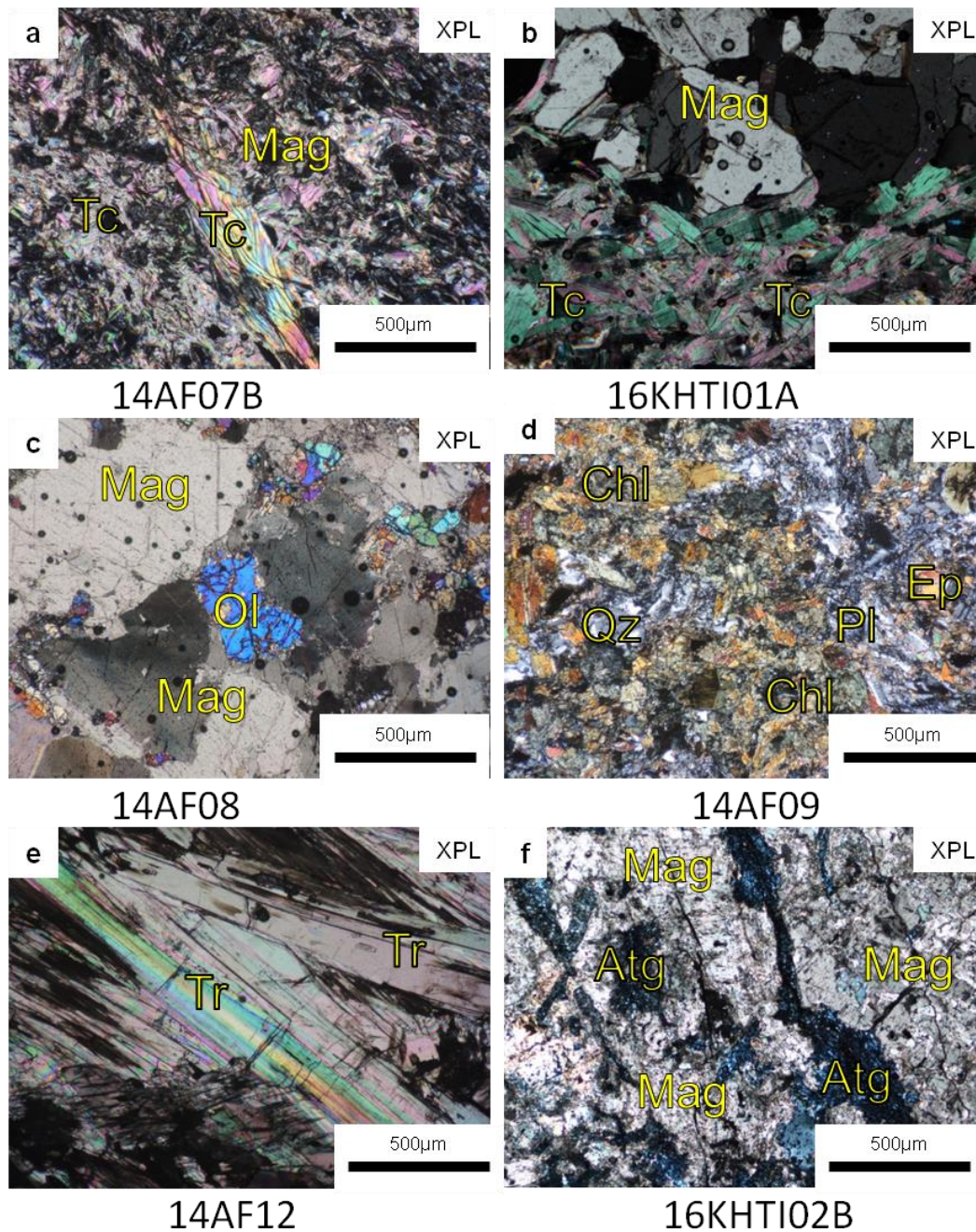


Figure 5.4 Photomicrographs of (a) talc rock having relict of magnesite (b) magnesite rock showing well developed talc crystals, (c) magnesite rock with olivine that replaced magnesite, (d) altered diorite, (e) tremolite consisting of coarse-grained tremolite crystals, (f) magnesite rock, replaced by antigorite from Kherwasti deposit.

5.4 Anarokas

In Anarokas, talc is microscopically composed of euhedral fibrous talc ranging in length from cryptocrystalline to 1 mm (Fig. 5.5a). Talc-bearing dolomite marble was also marked and magnesite rock is mostly talc-bearing marked by XRD (Fig. 5.6a and b) with some dolomite. Magnesite rock is microscopically composed of light to dark brown anhedral to euhedral magnesite ranging in length from 0.01 to 3 mm, euhedral fibrous talc ranging in length from 0.01 to 1.1 mm. Magnesite mostly shows poikiloblastic texture, having inclusions of talc (Fig. 5.5b). Amphibolites are mostly composed of anhedral hornblende ranging in length from 0.01 to 0.1 mm, euhedral prismatic plagioclase about 0.1 mm in length, anhedral quartz ranging in length from 0.01 to 0.15 mm and occasionally porphyroclast of clinopyroxene about 0.3 mm in length (Fig. 5.5c). Serpentinite is composed of anhedral to euhedral fibrous antigorite ranging in length from cryptocrystalline to 0.3 mm, cryptocrystalline talc and euhedral magnesite ranging in length from 0.005 to 0.9 mm (Fig. 5.5d). Anhedral tremolite is very coarse grained about 5 to 6 mm. Quartz veins are microscopically composed of anhedral quartz ranging in length from 0.05 to 0.6 mm and occasionally anhedral plagioclase about 0.1 mm in length. Gneiss is composed of anhedral quartz ranging in length from 0.02 to 0.7 mm, anhedral to euhedral biotite ranging in length from 0.05 to 0.3 mm, anhedral muscovite about 0.05 mm in length, anhedral prismatic plagioclase ranging in length from 0.1 to 0.3 mm and anhedral microcline about 0.4 mm in length (Fig. 5.5e). Granite is mostly composed of anhedral quartz ranging in length from 0.1 to 0.5 mm, microcline ranging in length from 0.01 to 0.3 mm, biotite about 0.01 mm and muscovite about 0.1 mm (Fig. 5.5f).

Carbonate-hosted talc deposits, 2018

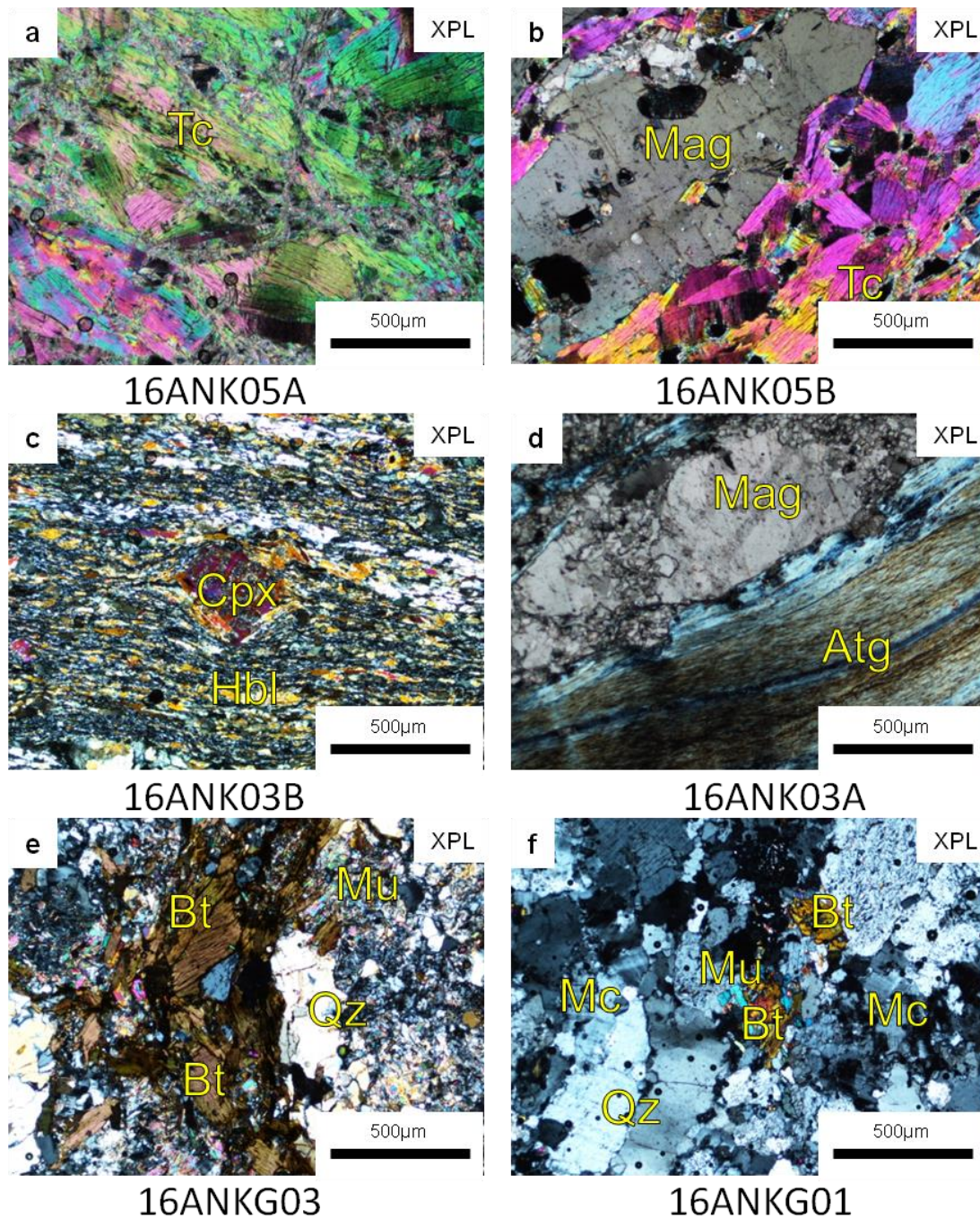


Figure 5.5 Photomicrographs of (a) talc rock, (b) magnesite rock having well developed talc crystals showing poikiloblastic texture, (c) highly metamorphosed amphibolite having porphyroclast of clinopyroxene, (d) magnesite replaced by antigorite, (e) gneiss having abundant biotite with muscovite and quartz, (f) granite from the Anarokas deposit.

Carbonate-hosted talc deposits, 2018

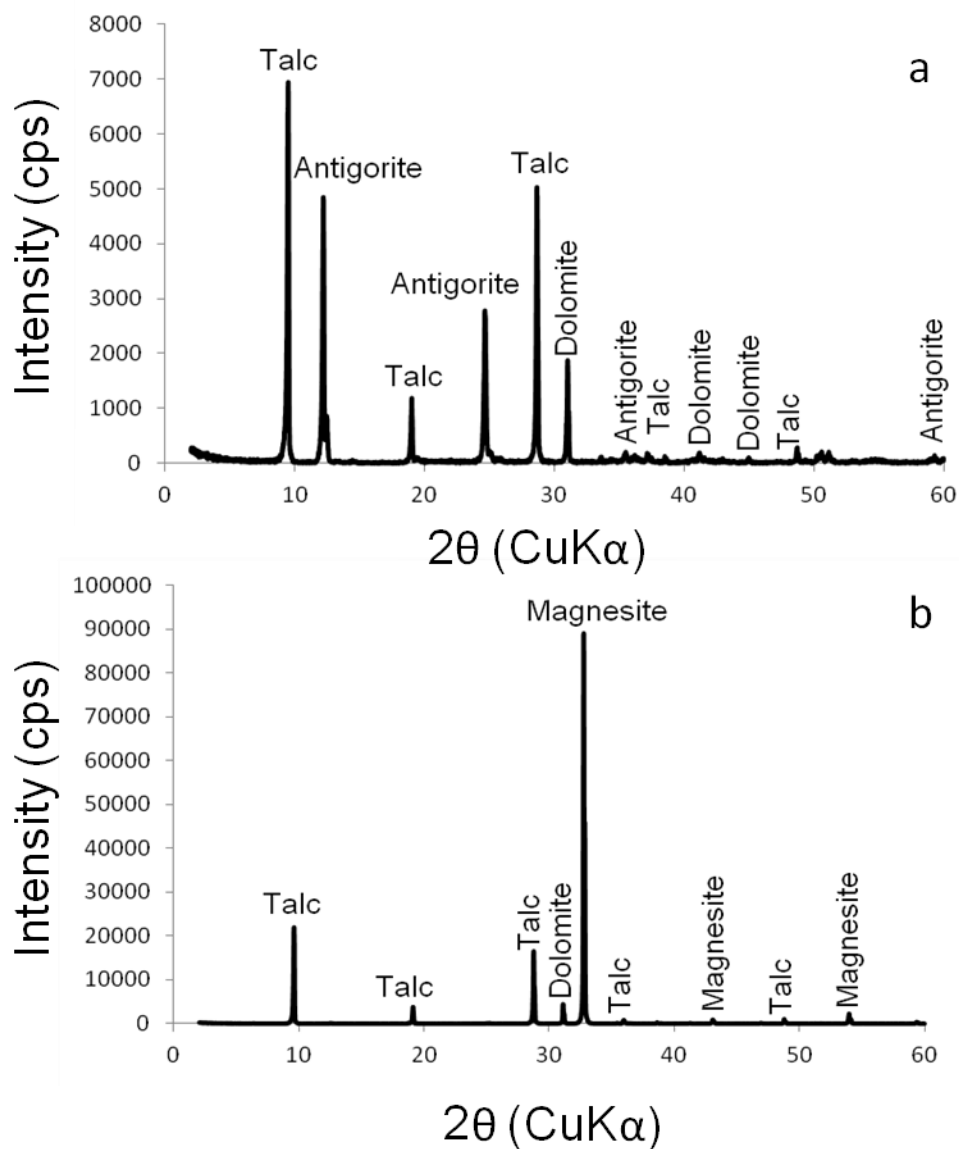


Figure 5.6 X-ray diffractograms of (a) talc-bearing dolomite marble (16ANK10) from Anarokas showing peaks of talc, antigorite and dolomite, (b) magnesite rock (16ANK05B) from Anarokas showing peaks of magnesite and talc with minor dolomite.

5.5 Dar

In Dar, the talc-bearing magnesite rocks are composed of anhedral magnesite ranging in length from 0.7 to 0.8 mm showing mosaic texture. Magnesite shows poikiloblastic texture, having

Carbonate-hosted talc deposits, 2018

inclusions of talc (Fig. 5.7a). Magnesite is replaced by anhedral equant olivine ranging in length from 0.01 to 0.02 mm. Dolomite marble is consists of anhedral dolomite ranging from 0.01 to 0.3 mm in length with anhedral acicular tremolite ranging from 0.05 to 0.9 mm (Fig. 5.7b). Talc ore bodies consist of anhedral fibrous talc ranging in length from 0.8 to 1.6 mm, euhedral acicular relict of tremolite about 4 mm and relicts of anhedral magnesite of about 0.2 mm in length. Tremolite is fractured and interstices between tremolite are filled with talc (Fig. 5.7c), confirmed by SEM-EDX (Fig. 5.7A). SEM-EDX analyses of other minerals is given in appendix 4. Dolerite is mostly altered to chlorite and microscopically consists of euhedral lath-shaped plagioclase about 0.24 mm and anhedral pyrite ranging in length from 0.01 to 0.7 mm (Fig. 5.7d). Unaltered dolerite shows typical ophitic texture having olivine ranging in length from 0.2 to 0.8 mm, anhedral ortho and clinopyroxene ranging in length from 0.2 to 0.7 mm and euhedral lath-shaped plagioclase ranging in length from 0.3 to 0.8 mm (Fig. 5.7e). Serpentinite is composed of colorless euhedral vermiculite ranging in length from 0.02 to 0.8 mm, colorless lizardite, having the relicts of anhedral orthopyroxene ranging in length from 0.001 to 0.2 mm and anhedral olivine ranging from 0.002 to 0.4 mm (Fig. 5.7f).

Carbonate-hosted talc deposits, 2018

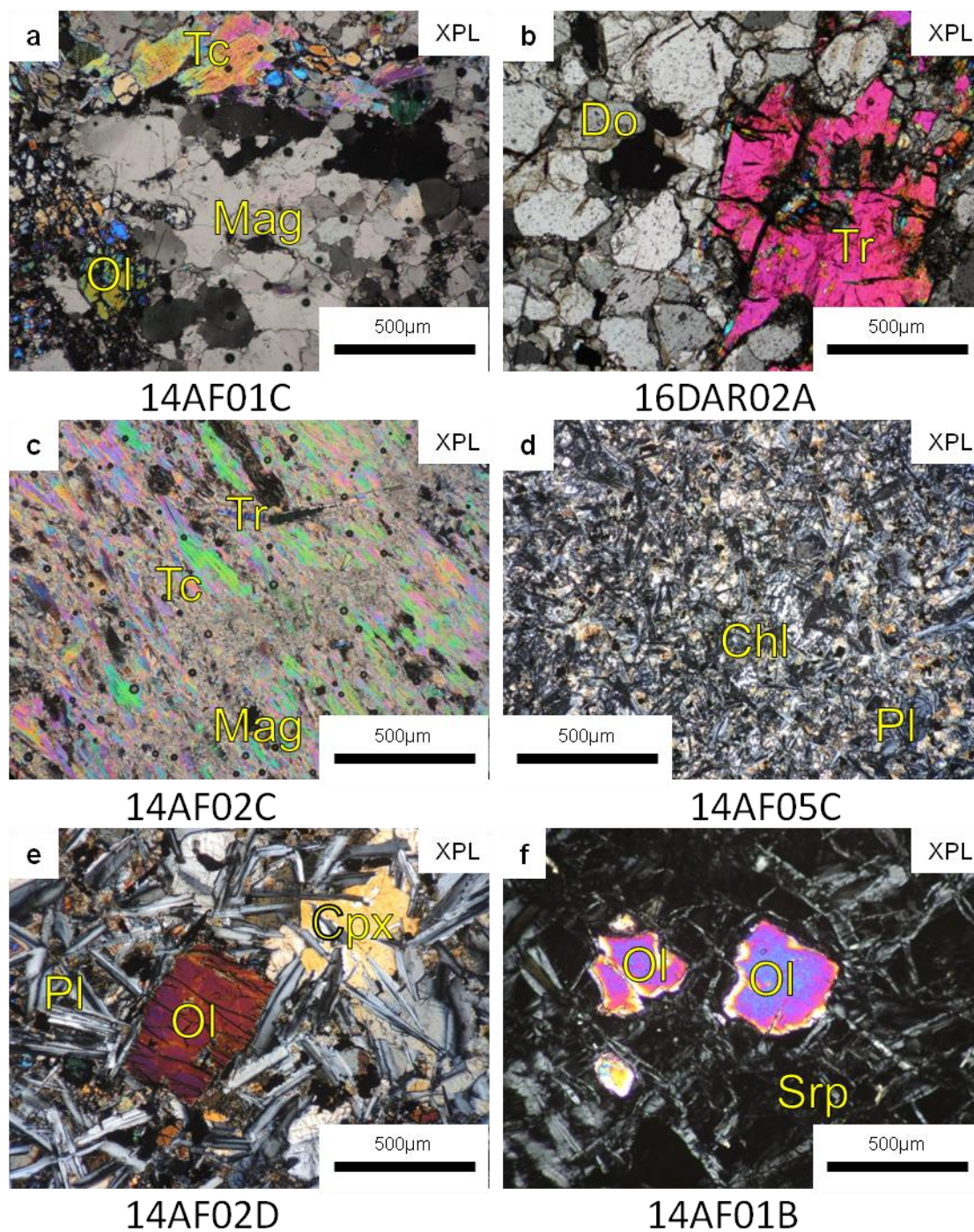


Figure 5.7 Photomicrographs of (a) magnesite rock having talc and olivine, (b) dolomite marble replaced dolomite by tremolite, (c) talc rock having relicts of tremolite and magnesite, (d)

Carbonate-hosted talc deposits, 2018

altered dolerite, (e) dolerite showing ophitic texture, (f) serpentinite showing alteration of olivine by serpentine from the Dar deposit.

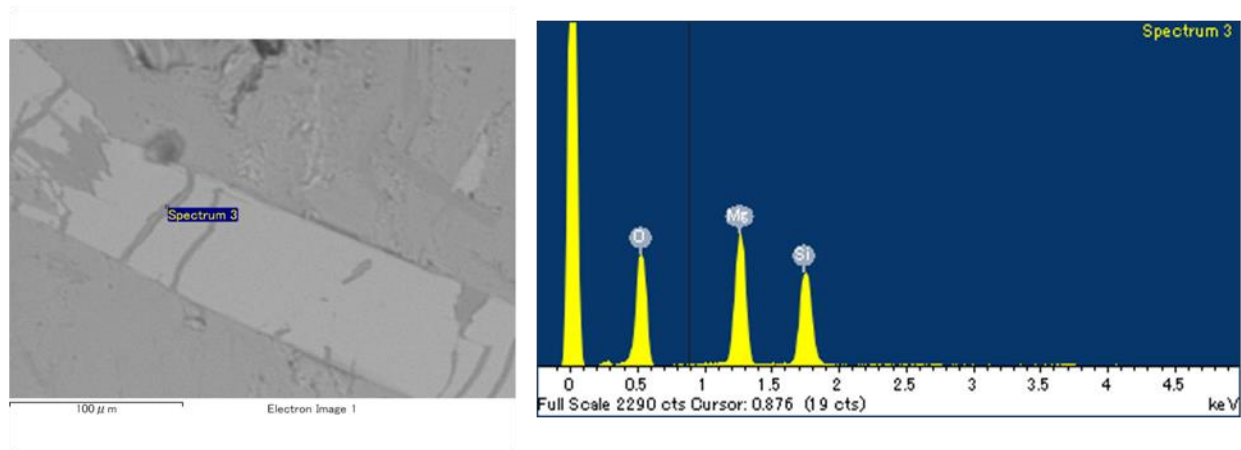


Figure 5.7A SEM-EDX results show the interstices in tremolite filled by talc from the Dar deposit.

5.6 Wachalgad

Host magnesite rocks in Wachalgad are composed of anhedral magnesite ranging in length from 0.1 to 1.6 mm and euhedral fibrous talc ranging in length from 0.01 to 0.8 mm (Fig. 5.8a). Magnesite crystals mostly show poikiloblastic texture having talc inclusions. Talc ore is composed of fibrous talc ranging in length from cryptocrystalline to 0.1 mm, anhedral magnesite ranging in length from 0.001 to 0.6 mm and occasionally chlorite about 0.5 mm in length (Fig. 5.8b). Dolomite marble is composed of anhedral dolomite ranging in length from 0.01 to 1.4 mm and anhedral tremolite ranging in length from 0.1 to 0.9 mm (Fig. 5.8c). Both dolomite and tremolite show poikiloblastic textures having inclusions of calcite and dolomite, respectively. Quartz veins show mosaic texture and are composed of euhedral quartz ranging in length from 0.1 to 1.3 mm and anhedral microcline about 2 mm in length. Gneiss is mostly composed of euhedral and elongated quartz ranging in length from 0.01 to 0.7 mm, euhedral to subhedral

Carbonate-hosted talc deposits, 2018

biotite ranging from 0.01 to 0.4 mm in length, euhedral muscovite ranging in length from 0.01 to 0.5 mm and anhedral microcline about 0.8 mm in length (Fig. 5.8d).

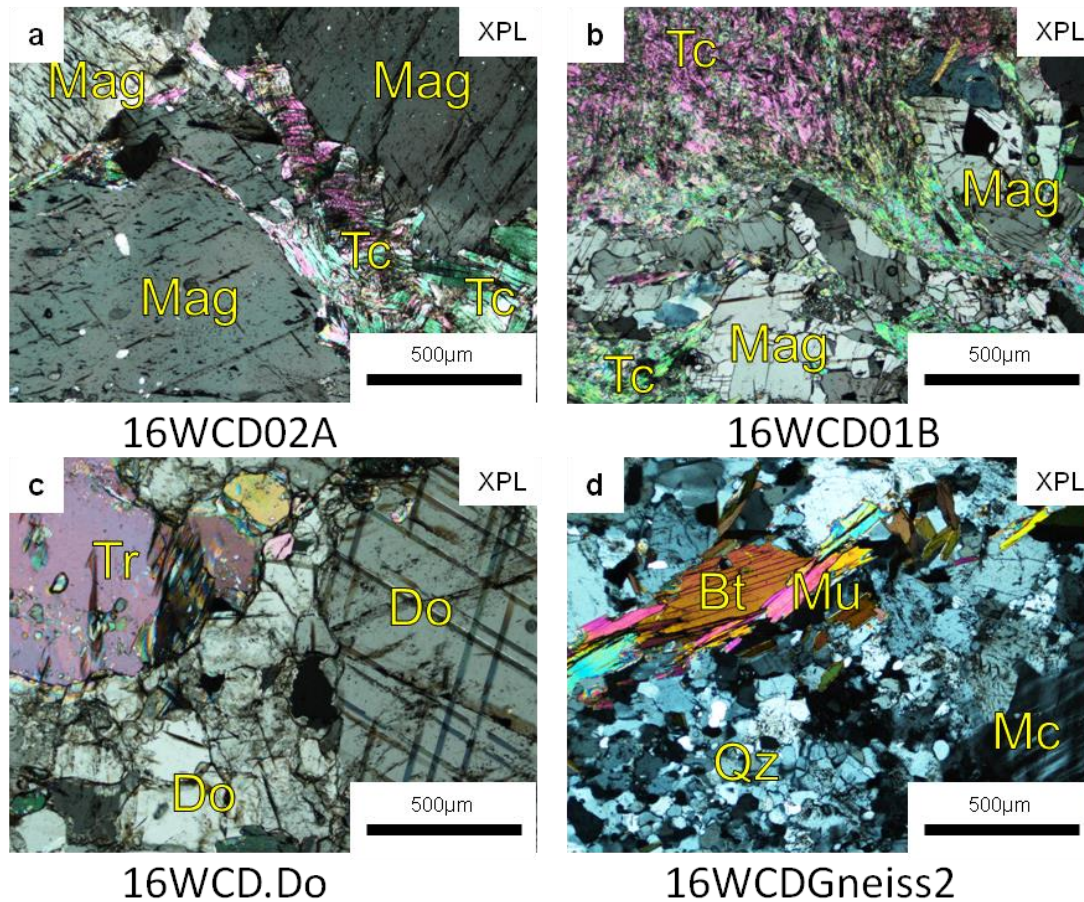


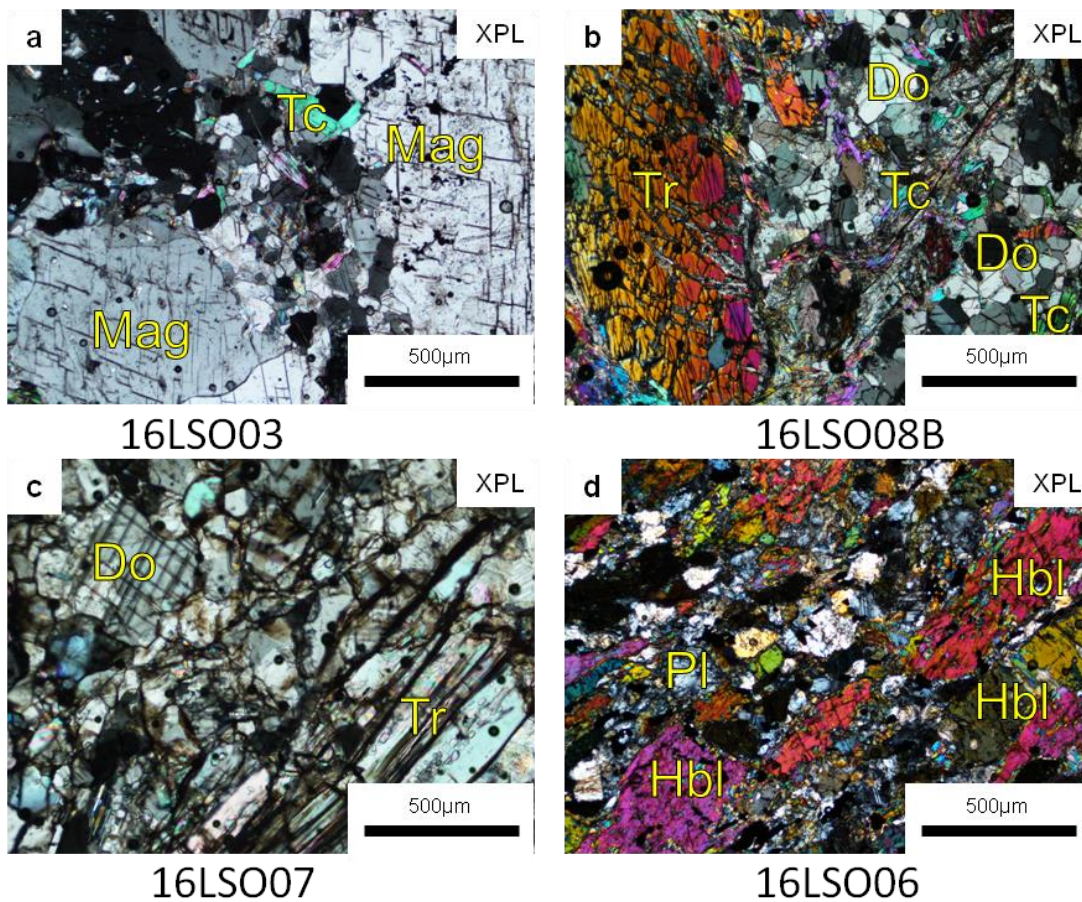
Figure 5.8 Photomicrographs of (a) magnesite rock replaced by talc, (b) talc rock having relicts of magnesite, (c) dolomite marble having tremolite showing poikiloblastic texture, (d) gneiss having abundant biotite and muscovite from the Wachalgad deposit.

5.7 Lesho

Host magnesite rocks in the Lesho are microscopically composed of anhedral magnesite ranging in length from 0.02 to 1 mm and euhedral fibrous talc from 0.05 to 0.7 mm in length (Fig. 5.9a). Magnesite exhibits poikiloblastic texture, having inclusions of talc. Dolomite marble is

Carbonate-hosted talc deposits, 2018

composed of anhedral dolomite ranging in length from 0.02 to 0.4 mm, euhedral fibrous talc about 0.2 mm in length mostly formed at the boundaries between dolomite and tremolite, and anhedral tremolite about 1.5 mm in length (Fig. 5.9b). Talc is powdery and cryptocrystalline. Tremolite is very coarse grained ranging in length from 0.3 to 2 mm and also having dolomite about 0.3 mm in length and calcite about 0.2 mm in length (Fig. 5.9c). Amphibolite is composed of mostly hornblende ranging in length from 0.1 to 0.7 mm, tremolite about 0.3 mm in length and plagioclase about 0.1mm in length (Fig. 5.9d). Massive dolomite marble is composed of anhedral dolomite ranging from 0.2 to 0.4 mm in length and anhedral tremolite ranging from 0.1 to 0.6 mm in length.

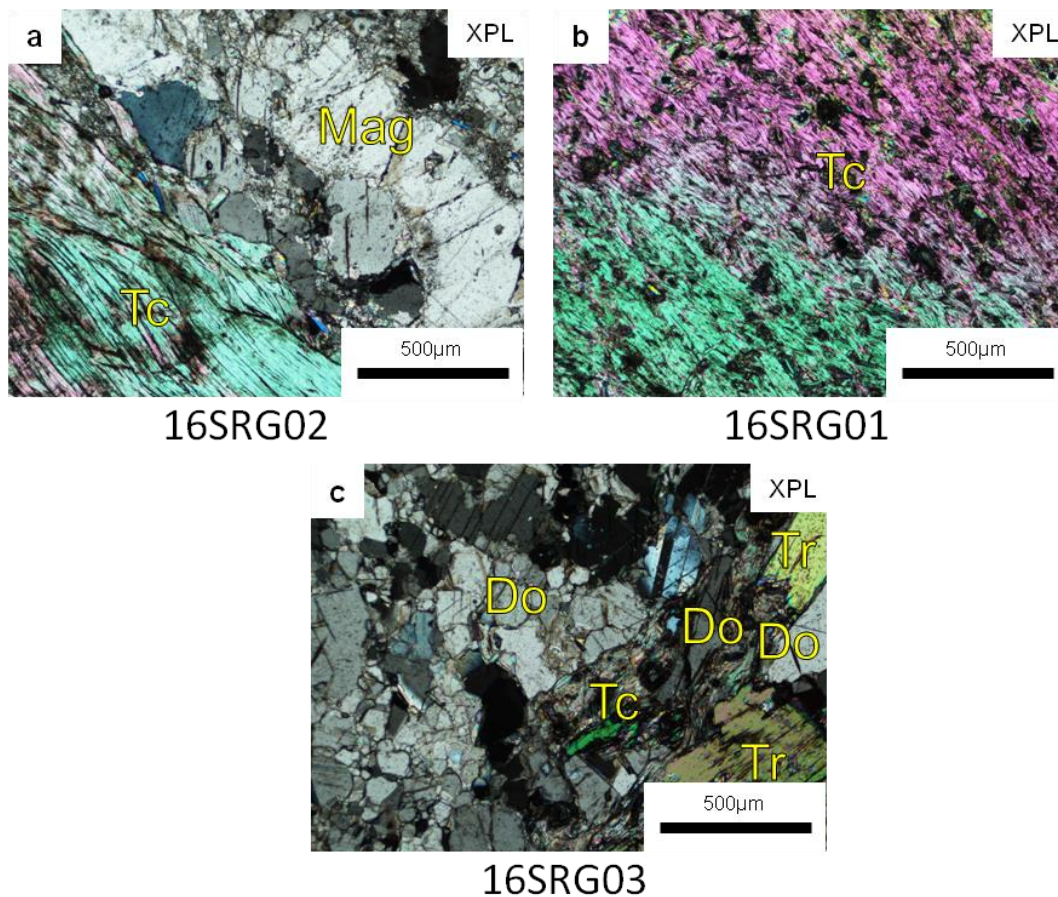


Carbonate-hosted talc deposits, 2018

Figure 5.9 Photomicrographs of (a) magnesite rock having well developed talc crystals, (b) dolomite marble replaced by tremolite and talc, (c) dolomite marble having coarse grained tremolite, (d) highly metamorphosed amphibolites from the Lesho deposit.

5.8 Sargare

Host magnesite rocks are microscopically composed of anhedral magnesite about 0.6 mm in length, showing poikiloblastic texture, having inclusions of talc and euhedral fibrous talc crystals about 1 mm in length (Fig. 5.10a). Talc ores consist of euhedral talc about 0.2 mm in length (Fig. 5.10b). Dolomite marble is composed of anhedral dolomite ranging in length from 0.02 to 0.5 mm, subhedral fibrous tremolite ranging in length from 0.2 to 0.7 mm and anhedral fibrous talc about 0.1 mm in length replaced dolomite and tremolite (Fig. 5.10c).



Carbonate-hosted talc deposits, 2018

Figure 5.10 Photomicrographs of **(a)** magnesite rock replaced by talc, **(b)** talc rock, **(c)** dolomite marble having tremolite replaced by talc from the Sargare prospect.

5.9 Mamond dara

Host dolomite marbles in this deposit are microscopically composed of anhedral calcite about 0.2 mm in length, showing lamellar twinning, anhedral dolomite ranging in length from 0.02 to 0.7 mm, quartz veins of anhedral equant quartz about 0.02 mm in length, anhedral to subhedral fibrous talc ranging in length from 0.3 to 1.1 mm and subhedral fibrous chlorite about 0.1 mm in length (Fig. 5.11a). Talc ore is composed of anhedral prismatic talc ranging in length from cryptocrystalline to 0.02 mm with anhedral dolomite ranging in length from 0.06 to 0.7 mm (Fig. 5.11b). Quartz chlorite schist is composed of equigranular quartz and chlorite about 0.01 mm in length (Fig. 5.11c). Gneiss is composed of anhedral elongated quartz ranging in length from 0.01 to 0.9 mm, anhedral porphyroblasts of microcline about 1.2 mm in length, anhedral fibrous muscovite of 0.8 to 1.1 mm in length, anhedral biotite ranging in length from 0.01 to 1 mm (Fig. 5.11d) and prismatic allanite about 0.02 mm in length (Fig. 5.11e). The rock shows porphyroblastic texture. Quartz crystals are distinctly elongated and aligned.

Carbonate-hosted talc deposits, 2018

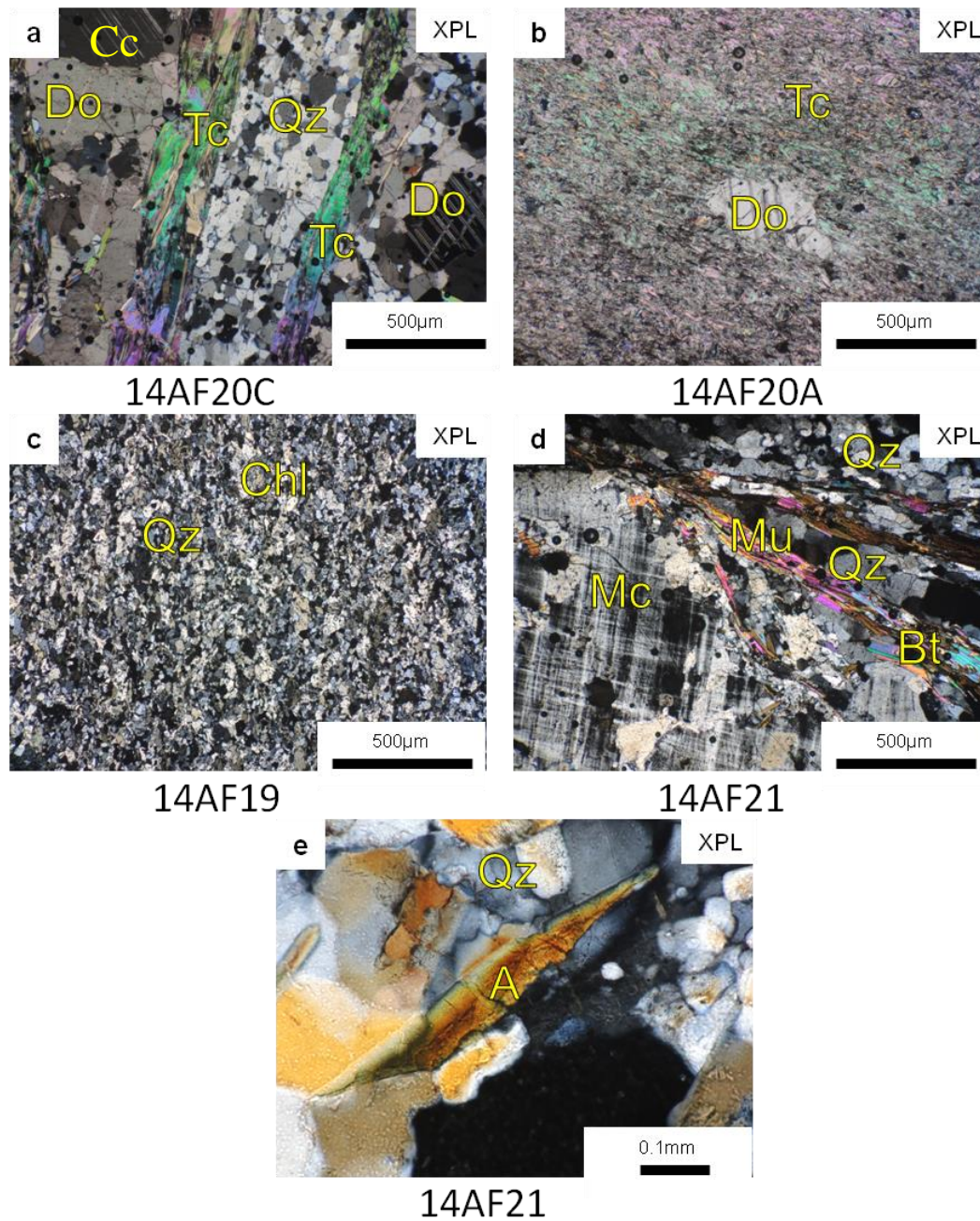


Figure 5.11 Photomicrographs of (a) dolomite marble showing veins of quartz in dolomite to form talc, (b) talc rock having relict of dolomite, (c) quartz chlorite schist, (d) gneiss showing porphyroblastic texture, (e) allanite in gneiss from the Mamond dara deposit.

Minerals assemblages of each rock from each deposit and prospect are summarized in Table 2.

Carbonate-hosted talc deposits, 2018

Table 2. Mineral assemblages based on microscopic observations and XRD analysis from different rocks of each deposit in Spinghar Fault Block, Afghanistan.

No	Deposits	Rock type	Mineral	Size (mm)	Crystal morphology
1	Kotikhel (Dawood mine & Noor mine)	Talc rock	Talc	Cryptocrystalline to 0.2	Anhedral fibrous
			Dolomite	0.01 to 0.7	Anhedral
		Dolomite marble	Dolomite	Cryptocrystalline to 0.8	Euhedral
			Talc	0.01 to 2	Euhedral
			Tremolite	0.01 to 100	Euhedral
			Antigorite	Cryptocrystalline to 0.8	Fibrous
		Quartz veins	Quartz	0.02 to 0.4	Granular
			Talc	0.01 to 0.3	Euhedral
		Gneiss	Quartz	0.01 to 0.1	Granular
Muscovite	0.1 to 0.2		Fibrous		
2	Janinaw	Talc rock	Talc	Cryptocrystalline to 0.1	Euhedral fibrous
			Tremolite	0.3 to 0.6	Subhedral prismatic
			Dolomite	0.1 to 1.1	Anhedral
		Dolomite marble	Calcite	0.2 to 0.5	Anhedral
			Dolomite	0.2 to 0.4	Anhedral
			Tremolite	0.02 to 1	Anhedral fibrous
		Talcose quartz vein	Quartz	0.03 to 0.5	Anhedral
			Talc	Cryptocrystalline to 0.8	Anhedral fibrous
			Chlorite	0.01 to 0.5	Anhedral fibrous
3	Kherwasti	Talc rock	Talc	0.08 to 2.8	Euhedral to subhedral
			Magnesite	0.1	Anhedral
		Magnesite rocks	Magnesite	0.01 to 2.8	Anhedral
			Talc	0.1 to 0.5	Euhedral to subhedral
			Olivine	Cryptocrystalline to 0.5	Anhedral equant
		Tremolite	Tremolite	0.4 to 2	Acicular
		Serpentinite	Antigorite	Cryptocrystalline	Fibrous
			Magnesite	0.01 to 0.4	Anhedral
		Amphibolite	Hornblende	Cryptocrystalline	Anhedral
			Quartz	Cryptocrystalline	Anhedral
			Plagioclase	Cryptocrystalline	Anhedral
4	Anarokas	Talc rock	Talc	Cryptocrystalline to 1	Euhedral fibrous
		Magnesite rocks	Magnesite	0.01 to 3	Euhedral
			Talc	0.01 to 1.1	Euhedral
		Amphibolite	Hornblende	0.01 to 0.1	Anhedral
			Plagioclase	0.1	Euhedral
			Quartz	0.01 to 0.1	Anhedral
			clinopyroxene	0.3	Anhedral
		Serpentinite	Antigorite	Cryptocrystalline to 0.3	Fibrous
			Talc	Cryptocrystalline	Anhedral
			Magnesite	Cryptocrystalline to 0.9	Euhedral
		Tremolite	Tremolite	5 to 6	Anhedral
		Quartz veins	Quartz	0.05 to 0.6	Anhedral
			Plagioclase	0.1	Anhedral
		Gneiss	Quartz	0.02 to 0.7	Anhedral
Biotite	0.05 to 0.3		Euhedral		
Muscovite	0.05		Anhedral		
Plagioclase	0.1 to 0.3		Anhedral		
Microcline	0.4		Anhedral		

(continued on next page)

Carbonate-hosted talc deposits, 2018

No	Deposits	Rock type	Mineral	Size (mm)	Crystal morphology
5	Dar	Talc rock	Talc	0.8 to 1.6	Fibrous
			Tremolite	4	Acicular
			Magnesite	0.2	Anhedral
		Magnesite rock	Magnesite	0.7 to 0.8	Anhedral
			Olivine	0.01 to 0.02	Anhedral equant
		Dolomite marble	Dolomite	0.01 to 0.3	Anhedral
			Tremolite	0.05 to 0.9	Acicular
		Diabase	Olivine	0.2 to 0.8	Anhedral equant
			Clinopyroxene	0.2 to 0.7	Anhedral
			Plagioclase	0.3 to 0.8	Euhedral
		Serpentinite	Vermiculite	0.02 to 0.8	Euhedral
			Lizardite	0.01	Anhedral
Orthopyroxene	Cryptocrystalline to 0.2		Anhedral		
Olivine	Cryptocrystalline to 0.4		Anhedral		
6	Wachalgad	Talc rock	Talc	Cryptocrystalline to 0.1	Fibrous
			Magnesite	Cryptocrystalline to 0.6	Anhedral
			Chlorite	0.5	Anhedral
		Magnesite rock	Magnesite	0.1 to 1.6	Anhedral
			Talc	0.01 to 0.8	Euhedral
		Dolomite marble	Dolomite	0.01 to 1.4	Anhedral
			Tremolite	0.1 to 0.9	Anhedral
		Quartz vein	Quartz	0.1 to 1.3	Euhedral
			Microcline	2	Anhedral
		Gneiss	Quartz	0.01 to 0.7	Euhedral
			Biotite	0.01 to 0.4	Subhedral
			Muscovite	0.01 to 0.5	Euhedral
Microcline	0.8		Anhedral		
7	Lesho	Talc rock	Talc	Cryptocrystalline	Powdery
		Magnesite rock	Magnesite	0.02 to 1	Anhedral
			Talc	0.05 to 0.7	Euhedral
		Tremolitite	Tremolite	0.2 to 2	Acicular
			Dolomite	0.3	Anhedral
			Calcite	0.2	Anhedral
		Amphibolite	Hornblende	0.1 to 0.7	Euhedral
			Tremolite	0.3	Acicular
Plagioclase	0.1	Anhedral			
8	Sargare	Talc rock	Talc	0.2	Euhedral
		Magnesite rock	Magnesite	0.6	Anhedral
			Talc	1	Euhedral
		Dolomite marble	Dolomite	0.02 to 0.5	Anhedral
			Tremolite	0.2 to 0.7	Acicular
9	Mamond Dara	Talc rock	Talc	Cryptocrystalline to 0.02	Anhedral
			Dolomite	0.06 to 0.7	Anhedral
		Dolomite Marble	Dolomite	0.02 to 0.7	Anhedral
			Calcite	0.2	Anhedral
			Quartz	0.02	Anhedral
			Talc	0.3 to 1.1	Subhedral
			Chlorite	0.1	Subhedral
		Quartz chlorite schi	Chlorite	0.01	Anhedral
			Quartz	0.01	Granular
		Gneiss	Quartz	0.01 to 0.9	Anhedral
			Microcline	1.2	Anhedral
			Muscovite	0.8 to 1.1	Anhedral
Biotite	0.01 to 1		Anhedral		
Allanite	0.02		Euhedral		

Also the list of replacement minerals and intergrowth minerals is given in Table 3

Carbonate-hosted talc deposits, 2018

Table 3. Replacement and intergrowth minerals in talc deposits from Nangarhar province, Afghansitan

No.	Replacement	Kotikhel	Janinaw	Kherwasti	Anarokas	Dar	Wachalgad	Lesho	Sargare	Mamond dara	Rock type
1	Mag → Tc			X1	X1	X1	X1	X1	X1		Magnesite & talc
2	Mag → Atg			X3	X3						Magnesite rock
3	Mag → Ol			X4		X4					Magnesite rock
4	Do → Atg	X3									Dolomite marble
5	Cpx → Hbl			X4	X4			X4			Amphibolite
6	Ol → Tc					X4					Magnesite rock
7	Ol → Srp					X4					Serpentinized peridotite
8	Tr → Tc	X3	X3		X3	X3		X3			Talc rock
9	Qz → Tc		X4							X4	Talcosite quartz vein
10	Plg → Chl			X4		X4				X4	Diorite
11	Mag → Ep			X4							Magnesite rock
12	Do → Tr	X2	X2	X3		X4	X4	X3	X4		Dolomite marble
13	Do → Tc	X1	X1							X1	Dolomite marble
Intergrowths											
1	Tc – Tr	X3	X3			X4		X4			Talc rock
2	Tc – Qz		X4							X4	Talcosite quartz vein
3	Cc – Do	X4	X4					X4			Dolomite marble
4	Tr – Cc		X3								Dolomite marble

X1	Major
X2	Minor
X3	Rare
X4	Trace

6. Geochemistry

6.1 Major Elements

The SiO₂ contents of talc rocks from all deposits range from 56.1 to 65.1 wt% and carbonate rocks of Kotikhel are 16.2 wt%, those from Kherwasti range from 1.6 to 25.8 wt%, Anarokas range from 16.6 to 45.5 wt%, Dar range from 6.9 to 8.9 wt%, Wachalgad range from 5.6 to 22.2 wt%, Lesho are 31.0 wt%, Sargare range from 9.6 to 13.9 wt% and Mamond dara range from 10.9 to 15.7 wt% (Table 4 and 5). It is evident that SiO₂ content increased to form talc from magnesite rocks and dolomite marble. The whole-rock MgO contents of those range from 30.2 to 35.5 wt% and 27.1 wt%, from 25.1 to 46.3 wt%, from 37.3 to 47.7 wt%, from 43.7 to 46.0 wt%, 23.1 to 53.5 wt%, 37.5 wt%, 26.2 to 48.1 wt%, and 19.3 to 21.9 wt%, respectively. The whole-rock CaO contents of talc rocks and magnesite rocks of all deposits are less than 1 wt%, while those of dolomite marbles of Kotikhel, Kherwasti, Wachalgad, Sargare and Mamond dara range from 17.0 to 33.5 wt% (Tables 4 and 5). Dolomite marble of Kotikhel, Janinaw, Kherwasti, Wachalgad, Lesho and Sargare commonly contains tremolite and that of Mamond dara contains talc. Magnesite rocks at Kherwasti contain olivine, those at Anarokas contain talc, and those at Dar are mostly pure but also contain talc and tremolite, while those at Wachlagad, Lesho and Sargare contain talc. The presence of these minerals in host carbonate rocks and talc ores is in accordance with lower and high loss on ignition (LOI) values, respectively (Tables 4 and 5).

Carbonate-hosted talc deposits, 2018

Table 4. Whole-rock chemical composition of talc rocks.

Samples	16KTI02	16KTI10	14AF13A	14AF13B	14AF15	14AF06B	14AF07B	16KHTI01D	16ANK05A	14A02C	14AF02E	14AF04	14AF05B	16WCD02B	16LSO02	16SRG01	14AF18B	14AF20A	14AF20B	14A022A	14A022B	
Location	<i>Kotikhel</i>		<i>Janinaw</i>			<i>Kherwasti</i>			<i>Anarokas</i>		<i>Dar</i>			<i>Wachalgad</i>	<i>Lesho</i>	<i>Sargare</i>	<i>Mamond Dara</i>					
(wt%)																						
SiO ₂	63.6	63.6	61.8	62.4	60.3	61.7	62.0	63.8	63.6	64.3	65.1	61.6	61.7	63.4	62.1	64.3	61.4	56.1	62.1	62.6	61.4	
TiO ₂	0.0	0.0	0.0	0.0	0.0	0.0	0.0	0.0	0.0	0.0	0.0	0.0	0.0	0.0	0.0	0.0	0.0	0.1	0.0	0.0	0.0	
Al ₂ O ₃	0.2	0.2	0.1	0.2	0.5	0.0	0.0	0.1	0.1	0.5	0.2	0.1	0.1	0.1	0.2	0.1	0.2	2.5	0.2	0.7	0.2	
Fe ₂ O ₃	0.4	1.6	0.2	0.4	1.9	0.2	0.1	0.2	0.1	0.4	0.2	0.3	0.2	0.3	0.1	0.0	0.1	0.2	0.1	0.1	0.4	
MnO	0.0	0.0	0.0	0.0	0.0	0.0	0.0	0.0	0.0	0.0	0.0	0.0	0.0	0.0	0.0	0.0	0.0	0.0	0.0	0.0	0.0	
MgO	33.5	32.7	31.7	31.8	30.2	31.8	32.2	33.8	33.9	32.8	32.9	31.9	31.7	33.7	33.2	34.0	31.9	31.9	31.9	31.2	31.5	
CaO	0.0	0.0	0.1	0.1	0.1	0.1	0.1	0.0	0.0	0.3	0.0	0.2	0.1	0.0	0.1	0.1	0.1	1.0	0.1	0.1	0.1	
Na ₂ O	0.1	0.1	0.0	0.0	0.0	0.0	0.0	0.1	0.0	0.1	0.0	0.0	0.0	0.1	0.1	0.0	0.0	0.0	0.0	0.1	0.0	
K ₂ O	0.0	0.0	0.0	0.0	0.0	0.0	0.0	0.0	0.0	0.0	0.0	0.0	0.0	0.0	0.0	0.0	0.0	0.0	0.0	0.0	0.0	
P ₂ O ₅	0.0	0.0	0.0	0.0	0.0	0.0	0.0	0.0	0.0	0.0	0.0	0.0	0.0	0.0	0.0	0.0	0.0	0.0	0.0	0.0	0.0	
LOI	2.0	1.6	4.8	4.9	5.0	4.9	5.1	1.9	2.2	5.1	4.9	5.0	4.9	2.4	4.2	1.4	5.9	8.5	5.0	5.2	4.9	
Total	99.8	99.8	98.9	99.8	98.1	98.8	99.6	99.9	99.9	103.4	103.4	99.1	98.8	100.0	99.9	99.9	99.7	100.0	99.3	100.1	98.4	
Trace elements																						
Ba (ppm)	9.4	8.2	8.6	5.1	16.2	9.6	6.2	8.6	7.8	2.0	0.0	0.0	0.0	9.5	13.0	11.3	2.0	0.3	0.0	14.8	3.1	
Cu	4.0	3.6	2.5	2.8	1.6	2.6	2.6	3.1	3.7	0.0	0.0	2.8	3.1	3.9	4.3	3.7	2.1	1.5	3.4	4.8	3.0	
Nb	0.0	0.1	0.0	0.0	0.0	0.0	0.0	0.0	0.0	0.0	0.0	0.0	0.0	0.0	0.0	0.0	0.0	0.0	0.0	0.3	0.0	
Pb	0.4	0.5	7.1	8.1	6.2	8.1	8.1	0.1	0.1	0.0	0.0	8.2	6.4	0.5	0.0	0.2	6.3	7.1	6.1	0.4	5.8	
Rb	0.0	0.0	0.1	0.0	1.8	0.0	0.1	0.0	0.0	4.0	4.0	0.0	0.0	0.0	0.1	0.0	0.0	0.2	0.1	0.1	0.0	
S	0.0	0.0	23.5	22.3	21.8	19.7	49.5	0.0	0.0	0.0	0.0	26.3	28.5	0.0	0.0	0.0	26.2	30.1	27.9	0.0	21.9	
Sr	1.3	1.3	2.1	1.8	2.3	1.6	1.7	1.1	1.6	3.0	2.0	2.3	2.0	1.1	1.6	2.1	1.5	6.8	1.9	1.8	1.6	
V	6.3	2.9	5.4	7.9	3.7	3.3	0.2	4.6	0.6	24.0	9.0	3.1	0.9	2.4	3.5	3.1	5.2	8.3	5.0	8.9	0.7	
Y	0.3	0.3	0.4	0.2	1.3	0.0	0.7	0.2	0.4	0.0	0.0	0.2	0.1	0.4	0.4	0.4	0.0	0.9	0.4	0.8	0.3	
Zn	6.0	41.0	33.9	42.4	63.7	1.4	0.1	1.8	2.1	0.0	0.0	3.2	2.2	7.4	1.6	5.0	9.6	5.2	4.4	8.1	7.3	

Carbonate-hosted talc deposits, 2018

Table 5. Whole-rock chemical composition of magnesite rocks and dolomite marble.

Type	(i) Magnesite rocks													(ii) Dolomite marble					
	14AF06A	14AF07A	16KHTI01A	16ANK03A	16ANK04A	16ANK05B	16ANK05C	14A01C	14A02B	14AF05D	16WCD01A	16LSO03	16SRG02	16KTI01	16KHTI03	16WCDDo	16SRG03	14AF18A	14A20C
Samples	Kherwasti			Anarokas				Dar			Wachalgad	Lesho	Sargare	Kotikhel	Kherwasti	Wachalgad	Sargare	Mamond Dara	
Location	(wt%)																		
SiO ₂	5.0	1.6	25.8	16.6	36.7	34.1	45.5	6.9	8.4	8.9	5.6	31.0	13.9	16.2	5.2	22.2	9.6	11.0	15.7
TiO ₂	0.0	0.0	0.0	0.0	0.0	0.0	0.0	0.0	0.0	0.0	0.0	0.0	0.0	0.0	0.0	0.0	0.0	0.0	0.0
Al ₂ O ₃	0.0	0.0	0.1	0.1	0.1	0.1	0.1	0.2	0.5	0.1	0.1	0.3	0.1	0.9	0.3	0.1	0.3	0.1	1.7
Fe ₂ O ₃	0.4	0.2	0.5	1.8	0.5	0.2	2.4	0.3	1.2	0.3	0.4	0.3	0.2	0.4	0.2	0.1	0.5	0.2	0.2
MnO	0.0	0.0	0.0	0.0	0.0	0.0	0.0	0.0	0.0	0.0	0.0	0.0	0.0	0.0	0.0	0.0	0.0	0.0	0.0
MgO	45.0	46.3	43.1	47.7	43.5	37.3	38.9	46.0	43.7	45.7	53.5	37.5	48.1	27.1	25.1	23.1	26.2	21.9	19.3
CaO	0.9	0.3	0.3	0.2	0.1	2.7	0.3	0.3	0.3	0.3	0.3	2.2	0.7	24.0	33.3	33.5	28.6	18.8	17.0
Na ₂ O	0.0	0.0	0.0	0.0	0.0	0.0	0.0	0.0	0.0	0.0	0.1	0.0	0.0	0.0	0.1	0.0	0.0	0.0	0.0
K ₂ O	0.0	0.0	0.0	0.0	0.0	0.0	0.0	0.0	0.0	0.0	0.0	0.0	0.0	0.0	0.0	0.0	0.0	0.0	0.0
P ₂ O ₅	0.0	0.0	0.0	0.0	0.0	0.0	0.0	0.0	0.0	0.0	0.0	0.0	0.0	0.0	0.0	0.0	0.0	0.0	0.0
LOI	47.6	50.6	30.0	33.5	18.9	25.5	12.5	45.2	46.9	47.4	39.9	28.5	36.8	31.2	35.7	20.9	34.6	41.6	35.7
Total	98.9	99.1	99.9	99.8	99.8	99.9	99.8	98.9	101.1	102.7	99.9	99.9	99.7	99.9	99.9	99.9	99.9	93.5	89.8
Trace elements																			
Ba (ppm)	0.0	0.0	7.7	10.3	4.7	5.0	8.9	24.8	5.7	0.0	8.6	7.3	8.3	9.0	17.8	7.2	13.1	0.0	41.1
Cu	1.6	1.2	3.4	2.8	3.7	3.0	3.3	1.9	1.4	1.5	8.6	3.1	3.9	2.4	2.3	2.8	2.4	2.6	1.7
Nb	0.0	0.0	0.0	0.0	0.0	0.0	0.0	0.0	0.0	0.0	0.0	0.0	0.0	0.6	0.3	0.6	0.3	0.0	0.0
Pb	7.9	10.5	0.2	0.1	0.5	0.4	0.2	17.6	7.6	7.1	0.4	0.1	0.5	0.6	0.6	1.4	1.0	1.4	5.1
Rb	0.0	0.0	0.0	0.0	0.0	0.0	0.0	0.2	0.0	0.0	0.0	0.0	0.0	0.4	0.7	0.6	0.2	0.0	1.0
S	94.2	205	0.0	0.0	34.5	0.0	23.4	79.2	34.4	37.5	0.0	0.0	0.0	0.0	0.0	0.0	0.0	34.4	40
Sr	3.2	3.4	1.2	3.9	2.7	8.7	5.6	3.4	2.7	1.6	2.4	10.8	5.3	86.1	82.5	77.1	91.7	106	66.9
V	0.0	0.6	3.5	2.1	1.3	1.5	1.5	0.0	0.8	1.0	1.2	2.2	0.0	4.1	5.1	0.0	1.7	3.3	0.0
Y	0.0	0.0	0.3	0.4	0.4	0.6	0.2	0.3	0.3	0.3	0.5	2.2	0.3	2.2	0.7	1.1	1.1	1.9	1.4
Zn	0.9	0.1	1.1	4.6	4.6	1.4	11.6	1.6	1.8	0.0	3.4	1.5	3.3	2.1	0.7	5.9	9.6	3.3	2.1

6.2 Trace Elements

The rare earth elements (REE) concentrations of talc rocks, magnesite rocks, dolomite marble and altered carbonate rocks to antigorite (Table 6) are normalized to Post-Archean Australian Shale (PAAS, Taylor *et al.*, 1985) while those of intrusive rocks, metamorphic rocks and quartz veins are normalized to C1 chondrite (McDonough and Sun, 1995) and are plotted on REE pattern diagrams. As compared to the metamorphic rocks of Kotikhel and Mamond dara and intrusive rocks of Anarokas and Dar, talc rocks and carbonate rocks of all deposits have very low REE. Whole-rock trace elements concentrations of talc rocks from all deposits, magnesite rocks from Kherwasti, Anarokas, Dar, Wachalgad, Lesho and Sargare, dolomite marble from Kotikhel, Janinaw, Kherwasti, Wachalgad, Sargare and Mamond dara, intrusive rocks from Anarokas and Dar, metamorphic rocks from Kotikhel and Mamond dara and quartz veins from Kotikhel, Janinaw and Anarokas are given in Table 7.

Carbonate-hosted talc deposits, 2018

Table 6. Whole-rock rare earth elements (REE) contents of talc rocks, magnesite rocks, dolomite marble, intrusive and metamorphic rocks and quartz veins.

Samples	Type/Location	La	Ce	Pr	Nd	Sm	Eu	Gd	Tb	Dy	Ho	Er	Tm	Yb	Lu
Talc rocks (ppm)															
16KTI02	Kotikhel	0.02	0.03	0.00	0.01	0.01	0.00	0.01	0.00	0.01	0.00	0.01	0.00	0.01	0.00
16KTI10		0.01	0.02	0.00	0.01	0.00	0.00	0.01	0.00	0.01	0.00	0.01	0.00	0.01	0.00
14AF13A	Janinaw	0.02	0.04	0.01	0.03	0.01	0.00	0.01	0.00	0.01	0.00	0.00	0.00	0.00	0.00
14AF13B		0.01	0.02	0.00	0.02	0.01	0.00	0.00	0.00	0.01	0.00	0.00	0.00	0.00	0.00
14AF15		1.50	2.80	0.30	1.04	0.19	0.04	0.22	0.03	0.22	0.04	0.12	0.02	0.10	0.01
14AF16		0.46	1.03	0.16	0.75	0.29	0.09	0.45	0.08	0.49	0.10	0.30	0.04	0.30	0.04
16KHTI01D	Kherwasti	0.02	0.05	0.01	0.03	0.01	0.00	0.01	0.00	0.01	0.01	0.00	0.00	0.00	0.00
14AF06B		0.10	0.28	0.03	0.09	0.02	0.00	0.01	0.00	0.01	0.00	0.01	0.00	0.01	0.00
14AF07B		0.16	0.55	0.07	0.26	0.05	0.02	0.04	0.00	0.03	0.01	0.01	0.00	0.01	0.00
16ANK05A	Anarokas	0.08	0.22	0.03	0.11	0.02	0.00	0.02	0.00	0.01	0.00	0.01	0.00	0.00	0.00
14AF02C	Dar	0.04	0.13	0.02	0.08	0.02	0.01	0.02	0.00	0.02	0.00	0.01	0.00	0.01	0.00
14AF02E		0.05	0.12	0.01	0.04	0.01	0.00	0.00	0.00	0.00	0.00	0.00	0.00	0.00	0.00
14AF04		0.14	0.36	0.04	0.15	0.02	0.01	0.01	0.00	0.01	0.00	0.01	0.00	0.01	0.00
14AF05B		0.15	0.40	0.04	0.16	0.03	0.00	0.02	0.00	0.01	0.00	0.00	0.00	0.00	0.00
16WCD02B		Wachalgad	0.09	0.15	0.02	0.09	0.02	0.00	0.02	0.00	0.01	0.00	0.01	0.00	0.01
16LSO02	Lesho	0.10	0.34	0.06	0.24	0.07	0.01	0.07	0.01	0.06	0.01	0.03	0.00	0.02	0.00
16SRG01	Sargare	0.32	0.88	0.12	0.48	0.10	0.03	0.10	0.01	0.06	0.01	0.02	0.00	0.01	0.00
14AF18B	Mamond Dara	0.03	0.03	0.01	0.02	0.01	0.00	0.01	0.00	0.01	0.00	0.01	0.00	0.01	0.00
14AF20B		0.01	0.02	0.00	0.01	0.00	0.00	0.00	0.00	0.00	0.00	0.00	0.00	0.00	0.00
14AF22A		0.43	1.29	0.20	0.81	0.18	0.02	0.13	0.01	0.08	0.01	0.02	0.00	0.01	0.00
14AF22B		0.05	0.14	0.02	0.10	0.02	0.00	0.01	0.00	0.01	0.00	0.01	0.00	0.00	0.00
14AF22B		0.05	0.14	0.02	0.10	0.02	0.00	0.01	0.00	0.01	0.00	0.01	0.00	0.00	0.00
Magnesite rocks (ppm)															
16KHTI01A	Kherwasti	0.07	0.24	0.04	0.14	0.04	0.01	0.05	0.01	0.04	0.01	0.03	0.00	0.03	0.01
14AF06A		0.48	1.09	0.12	0.39	0.06	0.03	0.05	0.01	0.04	0.01	0.02	0.00	0.02	0.00
14AF08		2.61	6.56	0.84	3.64	1.06	0.17	1.43	0.20	1.13	0.20	0.46	0.05	0.22	0.03
16ANK03A	Anarokas	0.14	0.30	0.04	0.17	0.04	0.01	0.05	0.01	0.05	0.01	0.05	0.01	0.07	0.02
16ANK05B		0.53	1.81	0.25	1.01	0.21	0.03	0.19	0.02	0.10	0.02	0.04	0.01	0.03	0.01
14AF01C	Dar	1.06	2.00	0.20	0.72	0.14	0.02	0.13	0.02	0.14	0.03	0.10	0.02	0.11	0.02
14AF02B		0.31	0.61	0.06	0.22	0.03	0.01	0.03	0.00	0.04	0.01	0.04	0.01	0.06	0.01
14AF03		0.40	1.19	0.18	0.76	0.17	0.02	0.14	0.02	0.11	0.02	0.07	0.01	0.07	0.01
14AF05A		0.17	0.49	0.06	0.26	0.05	0.01	0.04	0.00	0.03	0.01	0.02	0.00	0.02	0.00
14AF05D		0.29	0.72	0.09	0.37	0.06	0.01	0.06	0.01	0.06	0.02	0.07	0.01	0.06	0.01
16WCD01A	Wachalgad	0.16	0.50	0.07	0.28	0.05	0.01	0.06	0.01	0.05	0.01	0.04	0.01	0.03	0.01
16LSO03	Lesho	1.43	4.68	0.73	3.09	0.73	0.10	0.78	0.11	0.61	0.11	0.29	0.04	0.24	0.04
16SRG02	Sargare	0.33	0.70	0.09	0.32	0.07	0.03	0.07	0.01	0.07	0.01	0.04	0.01	0.03	0.01
Dolomite marble (ppm)															
16KTI01	Kotikhel	2.32	5.68	0.66	2.50	0.55	0.09	0.63	0.10	0.56	0.12	0.37	0.05	0.34	0.06
14AF14	Janinaw	0.51	1.07	0.13	0.46	0.09	0.02	0.08	0.01	0.07	0.02	0.05	0.01	0.04	0.01
16KHTI03	Kherwasti	0.82	1.87	0.22	0.80	0.14	0.04	0.15	0.02	0.10	0.02	0.06	0.01	0.06	0.01
16WCD00	Wachalgad	0.72	1.39	0.17	0.63	0.12	0.04	0.15	0.02	0.12	0.02	0.06	0.01	0.04	0.01
16SRG03	Sargare	1.16	2.71	0.31	1.21	0.25	0.06	0.29	0.04	0.22	0.04	0.12	0.02	0.11	0.02
14AF18A	Mamond Dara	3.98	9.61	1.23	4.86	1.07	0.28	0.88	0.12	0.69	0.12	0.33	0.04	0.24	0.03
Intrusive rocks (ppm)															
16ANKG01	Anarokas	8.25	15.23	1.68	6.01	1.75	0.29	2.08	0.38	2.42	0.49	1.51	0.23	1.68	0.25
14AF02D	Dar	10.34	23.87	3.22	14.58	3.68	1.23	4.28	0.63	4.09	0.79	2.28	0.31	1.96	0.28
14AF05C		7.52	18.44	2.63	12.55	3.69	1.22	4.75	0.72	4.72	0.94	2.67	0.37	2.29	0.33
Metamorphic rocks (ppm)															
16KTI09	Kotikhel	47.11	85.85	9.27	29.62	4.74	0.52	4.03	0.39	1.41	0.18	0.35	0.04	0.15	0.03
14AF19	Mamond Dara	16.18	38.10	5.30	24.78	7.14	2.43	9.05	1.36	8.93	1.75	5.13	0.70	4.36	0.61
14AF21		76.79	150.70	16.37	57.58	10.07	1.34	7.66	0.99	6.18	1.15	3.27	0.47	2.89	0.41
Quartz vein (ppm)															
16KTI11	Kotikhel	0.27	0.37	0.06	0.28	0.10	0.02	0.19	0.04	0.29	0.07	0.25	0.04	0.35	0.06
14AF17	Janinaw	27.69	26.72	6.58	26.05	4.76	0.64	6.30	0.83	5.41	1.10	2.97	0.38	2.03	0.28
16ANK07	Anarokas	1.78	3.75	0.44	1.58	0.60	0.19	0.69	0.16	1.10	0.19	0.61	0.13	1.06	0.15
16ANKG02		0.02	0.03	0.01	0.02	0.01	0.00	0.01	0.00	0.02	0.00	0.01	0.00	0.01	0.00

Carbonate-hosted talc deposits, 2018

Table 7. Bulk trace elements concentration of talc rocks, magnesite rocks, dolomite marble, metamorphic rocks, intrusive rocks and quartz veins.

Samples	Type/Location	Cr	Co	Ni	Hf	Ta	Th	Zr
Talc rocks (ppm)								
16KTI02	<i>Kotikhel</i>	9.33	1.22	2.78	0.14	0.17	0.04	4.45
16KTI10		10.48	7.09	11.47	0.01	0.01	0.15	0.10
14AF13A		22.76	2.15	1.85	0.00	0.07	0.03	0.00
14AF13B	<i>Janinaw</i>	15.05	2.46	3.56	0.00	0.09	0.02	0.00
14AF15		7.38	11.86	13.61	0.00	0.04	0.35	0.70
14AF16		9.37	10.35	3.12	0.00	0.16	0.04	0.00
14Af06B		9.77	1.36	0.53	0.00	0.12	0.05	0.00
14AF07B	<i>Kherwasti</i>	15.04	1.43	0.54	0.00	0.15	0.10	0.00
16KHTI01D		12.47	0.77	2.13	0.02	0.15	0.06	0.34
16ANK05A	<i>Anarokas</i>	8.33	0.24	1.12	0.05	0.13	0.04	1.66
14AF02C		13.38	2.89	3.64	0.00	0.16	0.07	5.00
14AF02E	<i>Dar</i>	9.31	1.53	0.73	0.00	0.13	0.14	4.00
14AF04		9.90	4.52	2.21	0.00	0.22	0.06	4.00
14AF05B		11.54	1.22	0.62	0.00	0.10	0.06	0.00
16WCD02B	<i>Wachalgad</i>	14.13	1.02	3.10	0.10	0.07	0.66	3.69
16LSO02	<i>Lesho</i>	10.13	0.96	1.18	0.03	0.03	0.12	0.88
16SRG01	<i>Sargare</i>	10.47	0.19	1.54	0.07	0.05	0.12	2.71
14AF18B		12.10	2.39	9.79	0.00	0.17	0.01	0.00
14AF20B	<i>Mamond Dara</i>	11.44	1.51	4.99	0.00	0.08	0.04	0.00
14AF22A		17.31	1.47	9.73	0.00	0.08	0.99	7.20
14AF22B		14.91	1.99	5.80	0.00	0.08	0.02	0.00
Magnesite rocks(ppm)								
16KHTI01A		48.66	0.83	19.92	0.02	0.06	0.09	0.52
14AF06A	<i>Kherwasti</i>	9.95	2.55	1.09	0.03	0.51	0.05	0.00
14AF08		10.45	4.89	2.98	0.00	0.52	0.39	1.60
16ANK03A	<i>Anarokas</i>	47.97	2.90	21.00	0.13	0.17	0.06	4.39
16ANK05B		40.22	0.60	18.23	0.11	0.08	0.13	3.95
14AF01C		31.91	13.44	8.60	0.05	1.09	0.59	4.50
14AF02B		38.37	6.44	7.81	0.00	0.53	0.48	0.00
14AF03	<i>Dar</i>	32.18	2.40	10.50	0.00	0.57	0.29	1.20
14AF05A		43.43	4.92	21.31	0.00	0.40	0.08	0.00
14AF05D		9.73	4.75	1.20	0.00	0.56	0.05	0.00
16WCD01A	<i>Wachalgad</i>	79.24	0.88	29.96	0.05	0.05	0.04	1.72
16LSO03	<i>Lesho</i>	51.32	1.26	21.56	0.14	0.11	0.18	5.18
16SRG02	<i>Sargare</i>	66.47	0.79	28.34	0.05	0.14	0.24	1.59
Dolomite marble (ppm)								
16KTI01	<i>Kotikhel</i>	53.28	1.41	25.39	0.57	0.05	0.98	17.37
14AF14	<i>Janinaw</i>	31.61	3.30	16.12	0.00	0.04	0.06	5.20
16KHTI03	<i>Kherwasti</i>	39.15	1.30	19.45	0.11	0.07	0.14	4.78
16WCDDo	<i>Wachalgad</i>	74.76	1.54	36.32	0.03	0.17	0.10	0.73
16SRG03	<i>Sargare</i>	34.88	1.34	16.65	0.03	0.01	0.44	0.73
14AF18A	<i>Mamond Dara</i>	28.43	2.27	4.35	0.00	0.08	0.17	9.80
Intrusive rocks (ppm)								
16ANKG01	<i>Anarokas</i>	199.00	3.95	166.00	0.20	1.58	24.71	3.66
14AF02D	<i>Dar</i>	504.00	62.94	194.00	1.56	0.94	0.75	0.00
14AF05C		158.00	51.63	93.74	1.87	0.66	0.69	0.00
Metamorphic rocks(ppm)								
16KTI09	<i>Kotikhel</i>	244.00	10.48	121.00	0.04	1.70	29.40	0.93
14AF19	<i>Mamond Dara</i>	168.00	68.34	99.80	0.00	1.60	0.82	0.00
14AF21		13.45	30.26	4.05	0.00	2.78	16.08	0.00
Quartz veins (ppm)								
16KTI11	<i>Kotikhel</i>	378.00	8.31	268.00	0.02	0.02	0.21	0.41
14AF17	<i>Janinaw</i>	95.74	19.16	72.13	0.00	0.80	1.67	0.00
16ANK07	<i>Anarokas</i>	347.00	3.81	165.00	0.06	12.53	0.52	0.64
16ANKG02		512.00	5.48	262.00	0.01	0.01	0.06	0.14

Carbonate-hosted talc deposits, 2018

6.3 Carbonate Minerals Chemistry

Chemical composition of carbonate minerals were normalized by number of cations based on 6 oxygens (Adomako-Ansah *et al.*,2013). Chemical composition of magnesite of Anarokas, Dar, Kherwasti, Wachalgad and Lesho, dolomite of Kotikhel, Wachalgad, Sargare and Mamond dara are close to ideal compositions with FeCO_3 content of dolomite in Kotikhel is 0.6 wt%, in Wachalgad is 0.1 wt%, in Sargare is 0.5 wt% and in Mamond dara ranges from 0.3 to 0.3 wt%. While FeCO_3 of magnesite in Kherwasti is 0.7 wt%, in Anarokas is 0.3 wt%, in Dar is 0.2 wt%, in Wachalgad is 0.4 wt% and in Lesho is 0.4 wt%. MnCO_3 content of dolomite of Kotikhel is 0.1 wt% and of dolomite from other deposits is 0 wt%, while those of magnesite from all deposits is 0 wt%. FeCO_3 and MnCO_3 of calcite in Janinaw is 0 wt% (Table 8).

6.4 Silicate Minerals Chemistry

Chemical composition of silicate minerals such as talc and tremolite is slightly deviate from ideal composition. FeO , Na_2O , K_2O , MnO , Al_2O_3 , TiO_2 and Cr_2O_3 contents in talc and tremolite minerals are less than 1 wt% except FeO content in tremolite from Kherwasti which is 6 wt%. MgO content in talc ranges from 30.1 to 31.4 wt% with highest amount in Sargare (Table 9) while in tremolite it ranges from 20.6 to 24.7 wt%. SiO_2 contents in talc range from 54.4 to 59.6 wt% and in case of tremolite it ranges from 53.7 to 57.2 wt%. CaO contents in talc is 0 wt% while in tremolite, it ranges from 12.8 to 13.6 wt% (Table 9).

Carbonate-hosted talc deposits, 2018

Table 8. EPMA data of carbonate minerals from Nangarhar talc deposits, Afghanistan.

Mineral	(i) Magnesite						(ii) Calcite					(iii) Dolomite										
Sample	16KHTI01A		16ANK05B		14AF01C		16WCD02A		16LSO03		14AF14		16KTI01		16WCD.Do		16SRG03		14AF18A		14AF20C	
Location	Kherwasti		Anarokas		Dar		Wachalgad		Lesho		Janinaw		Kotikhel		Wachalgad		Sargare		Mamond Dara			
No. of ankn	= 15		n = 33		n = 20		n = 23		n = 25		n = 25		n = 20		n = 29		n = 42		n = 61		n = 39	
	Mean	(S.D.)	Mean	(S.D.)	Mean	(S.D.)	Mean	(S.D.)	Mean	(S.D.)	Mean	(S.D.)	Mean	(S.D.)	Mean	(S.D.)	Mean	(S.D.)	Mean	(S.D.)	Mean	(S.D.)
wt%																						
FeO	0.6	0.39	0.27	0.06	0.3	0.04	0.33	0.04	0.38	0.07	0.04	0.06	0.44	0.07	0.11	0.03	0.38	0.07	0.24	0.04	0.24	0.04
MnO	0.03	0.02	0.01	0.02	0.02	0.02	0.01	0.01	0.01	0.01	0.02	0.02	0.04	0.03	0.03	0.02	0.02	0.02	0.02	0.02	0.01	0.02
MgO	48.46	1.23	50.54	0.28	44.48	1.44	46.04	0.94	47.47	2.41	1.68	3.8	22.51	0.62	22.22	0.76	22.76	0.39	20.29	0.34	20.42	0.58
CaO	0.27	0.19	0.2	0.04	0.23	0.06	0.26	0.04	0.76	2.54	52.38	5.27	26.96	0.86	27.94	2.21	26.97	0.44	29.69	0.28	29.53	0.62
Total	49.36	1.83	51.02	0.4	45.03	1.56	46.64	1.03	48.62	5.03	54.12	9.15	49.95	1.58	50.3	3.02	50.13	0.92	50.24	0.68	50.2	1.26
No. of Cations																						
based on 6 oxygens																						
oxygens																						
Fe	0.01	0.01	0.01	0	0	0	0.01	0	0.01	0	0	0	0.01	0	0	0	0.01	0	0.01	0	0.01	0
Mn	0	0	0	0	0	0	0	0	0	0	0	0	0	0	0	0	0	0	0	0	0	0
Mg	1.98	0.01	1.99	0	2	0	1.98	0	1.97	0.08	0.1	0.18	1.07	0.01	1.06	0.03	1.08	0.01	0.97	0.01	0.98	0.01
Ca	0.01	0.01	0.01	0	0	0	0.01	0	0.02	0.08	1.91	0.19	0.92	0.01	0.94	0.03	0.91	0.01	1.02	0.01	1.01	0.01
Total	2	0.03	2	0	2	0	2	0	2	0.16	2	0.37	2	0.02	2	0.06	2	0.02	2	0.02	2	0.02
Molecular proportions of carbonates																						
FeCO ₃	0.69	0.48	0.29	0.07	0.23	0.03	0.4	0.04	0.43	0.07	0.04	0.04	0.58	0.09	0.14	0.04	0.5	0.09	0.32	0.05	0.31	0.05
MnCO ₃	0.04	0.03	0.01	0.02	0.02	0.02	0.01	0.01	0.01	0.01	0.02	0.03	0.05	0.04	0.04	0.03	0.02	0.02	0.02	0.03	0.02	0.02
MgCO ₃	98.88	0.47	99.42	0.09	99.4	0.1	99.19	0.08	98.38	3.93	2.35	0.78	53.55	0.35	52.65	1.84	53.88	0.49	48.73	0.41	49.02	0.45
CaCO ₃	0.4	0.28	0.28	0.06	0.37	0.09	0.4	0.06	1.17	3.96	97.59	0.79	45.82	0.36	47.17	1.82	45.6	0.47	50.93	0.4	50.65	0.45
Total	100	1.26	100	0.24	100	0.24	100	0.19	100	7.97	100	1.64	100	0.84	100	3.73	100	1.07	100	0.89	100	0.97

S.D. = standard deviation

Carbonate-hosted talc deposits, 2018

Table 9. EPMA data of silicate minerals from Nangarhar talc deposits, Afghanistan.

Mineral	Talc												Tremolite						
	Sample No.	14AF06B		14AF13A		14AF20A		16ANK05A		16KTI02		16SRG01		14AF11		16KTI05		16LSO07	
Location	Dar	Janinaw		Mamond dara		Anarokas		Kotikhel		Sargare		Kherwasti		Kotikhel		Lesho			
No. of analyses	n = 30	(S.D.)	n = 13	(S.D.)	n = 16	(S.D.)	n = 25	(S.D.)	n = 7	(S.D.)	n = 22	(S.D.)	n = 24	(S.D.)	n = 26	(S.D.)	n = 29	(S.D.)	
wt%																			
MgO	30.7	0.22	30.6	0.14	30.4	0.26	31.3	0.29	30.1	0.29	31.4	1.07	20.6	0.34	24.1	0.18	24.7	0.15	
CaO	0.0	0.01	0.0	0.01	0.0	0.02	0.0	0.01	0.0	0.01	0.0	0.01	12.8	0.22	13.5	0.13	13.6	0.09	
FeO	0.3	0.04	0.2	0.04	0.2	0.06	0.1	0.04	0.3	0.02	0.1	0.04	6.0	0.31	0.9	0.14	0.2	0.06	
SiO ₂	58.9	0.31	56.4	0.41	54.4	1.87	59.6	0.62	55.1	0.50	57.7	1.53	53.7	0.76	56.8	0.35	57.2	0.24	
Na ₂ O	0.3	0.10	0.2	0.08	0.2	0.10	0.0	0.03	0.0	0.02	0.2	0.10	0.7	0.21	0.1	0.02	0.0	0.02	
K ₂ O	0.0	0.02	0.0	0.01	0.0	0.03	0.0	0.01	0.0	0.01	0.0	0.04	0.0	0.03	0.0	0.01	0.0	0.01	
MnO	0.0	0.02	0.0	0.02	0.0	0.03	0.0	0.02	0.0	0.03	0.0	0.01	0.1	0.03	0.0	0.04	0.0	0.02	
Al ₂ O ₃	0.0	0.02	0.2	0.08	0.8	1.00	0.1	0.02	0.2	0.04	0.7	3.07	0.9	0.12	0.4	0.14	0.2	0.07	
TiO ₂	0.0	0.01	0.0	0.01	0.0	0.02	0.0	0.01	0.0	0.02	0.0	0.05	0.0	0.02	0.0	0.02	0.0	0.02	
Cr ₂ O ₃	0.0	0.03	0.0	0.02	0.0	0.02	0.0	0.03	0.0	0.02	0.0	0.02	0.1	0.13	0.0	0.03	0.0	0.02	
Total	90.3	0.44	87.7	0.31	86.1	1.20	91.2	0.86	85.9	0.71	90.2	0.93	95.0	1.22	95.8	0.40	96.1	0.27	

7. Discussion

7.1 Evidences in Field

Based on the field observations, beddings of magnesite rocks and dolomite marble are parallel to sub-parallel to the gneissosity of gneiss in Kotikhel, Anarokas, Wachalgad and Mamond dara (Figs. 3). A granitic body was observed in Anarokas cross-cutting the gneiss and also quartz veins in gneiss (Fig. 7.1a). The quartz veins ranging from 0.1 to 0.2 m thick are also parallel to sub parallel to the gneissosity of gneiss in Kotikhel, Anarokas and Wachalgad (Fig. 7.1b) and locally appear in lenticular form in Wachalgad. No cross-cutting relationships of quartz veins with magnesite rocks, dolomite marble and gneiss were observed in any deposit except on a minor scale in Anarokas (Fig. 7.1b). It suggests that hydrothermal fluids for the formation of talc were provided through the gneiss to host magnesite rocks and dolomite marble which is also supported by the occurrence of hydrous minerals such as biotite and muscovite in gneiss and talc, tremolite and serpentine (antigorite) in host carbonate rocks, while granitic intrusion was a late activity emplaced after the talc mineralization. Diabase and diorite are mostly metamorphosed to amphibolites. Serpentinite (antigorite) was marked at the contact between magnesite rocks and amphibolites in Kherwasti and Anarokas, and also marked at the contact between dolomite marble and amphibolites in Kotikhel (Fig. 7.1c and d). In Kotikhel, antigorite also occur within dolomite marble having no contact with amphibolites. Fresh diabase cross-cut the magnesite rocks and talc veins at Dar (Fig. 7.1e). Amphibolites in Kherwasti (Fig. 3.3), Anarokas, Dar and Lesho are parallel to sub parallel to the beddings of magnesite and talc veins while quartz chlorite schist and amphibolites are parallel to sub parallel to the beddings of dolomite marble and talc veins in Mamond dara and Lesho (Figs. 3.9 and 7.1f).

Carbonate-hosted talc deposits, 2018

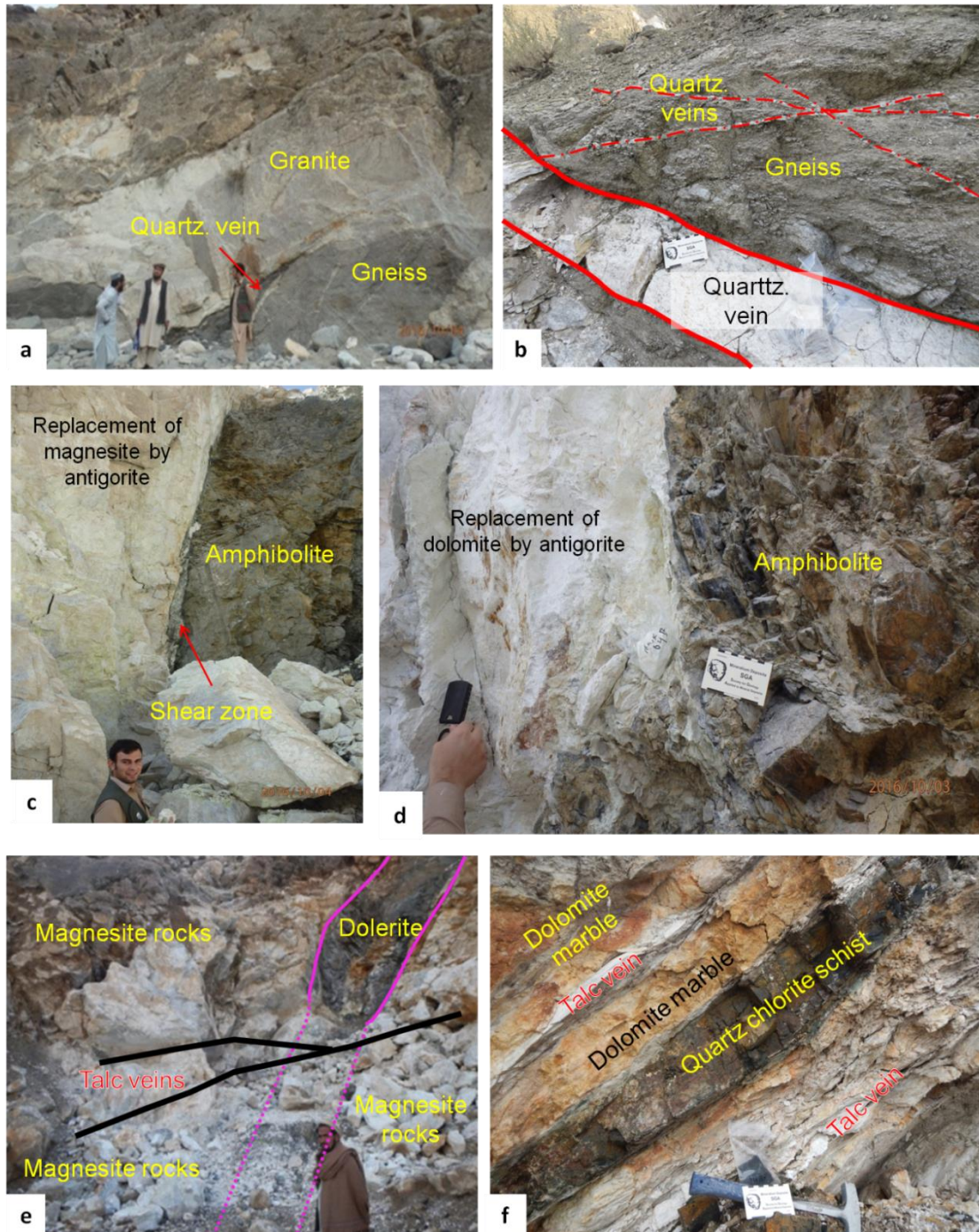


Figure 7.1 Photographs showing typical examples of field observation of talc mineralization at Spinghar Fault Block (a) granitic intrusion into gneiss cross cutting the quartz vein at Anarokas, (b) quartz veins in gneiss at Anarokas, (c) replacement of magnesite by antigorite at Kherwasti, (d) replacement of dolomite by antigorite at Kotikhel, (e) fresh diabase cross cutting the talc

Carbonate-hosted talc deposits, 2018

veins and host magnesite rocks at Dar, (f) alternating layers of talc and dolomite marble with parallel intrusive rock, strongly altered to quartz chlorite schist at Mamond dara.

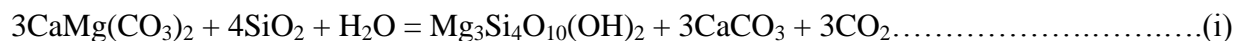
7.2 Phase Relations and Reactions

Based on mineral assemblages, the maximum and minimum formation temperatures were estimated based on T- X_{CO_2} diagram in Figure 7.2 (after Dale *et al.*, 1990; Evans and Guggenheim, 1988) calculated from the thermochemical data (Berman, 1988) and applying the modified Redlich-Kwong expression for non-ideal mixing of H₂O-CO₂ (Kerrick and Jacobs, 1981). The stability field of talc is well defined in terms of pressure (P), temperature (T), and mole fraction of CO₂ (X_{CO_2}) of the fluid phase based on the experimental studies by Gordon and Greenwood (1970), Skippen (1971, 1974), Slaughter *et al.* (1975), and Eggert and Kerrick (1981).

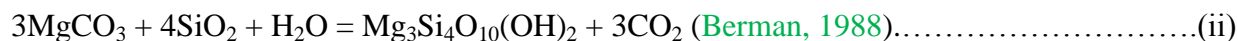
Assuming a mixture of H₂O and CO₂ (Dale *et al.*, 1990) the maximum temperature at which talc can form is approximately 460°C with $X_{\text{CO}_2} > 0.6$, at >200 MPa pressure equal to 6-7 km crustal level. According to this diagram at sufficiently low X_{CO_2} values, talc can form at much lower temperatures. The stability of talc may be affected by other factors such as change in pressure (e.g., Skippen, 1971, 1974; Slaughter *et al.*, 1975; Eggert and Kerrick, 1981), the composition of talc (specifically X_{Mg} and X_{F} ; e.g., Valley *et al.*, 1982; Abercrombie *et al.*, 1987), and non-ideal behavior of H₂O-CO₂-NaCl solutions (Bowers and Helgeson, 1983).

Based on the mineral assemblages, Mamond dara deposit formation followed curve 1 and reaction (i) (Fig. 7.2), where dolomite was replaced by talc due to the supply of silica (Fig. 5.11a). In such a case, talc formed within the temperature range of 360 to 460 °C at X_{CO_2} ranging from 0.01 to 0.6.

Carbonate-hosted talc deposits, 2018



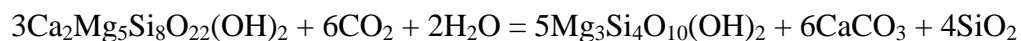
The Wachalgad prospect was probably formed within the same range of temperature and X_{CO_2} , where magnesite rocks are replaced by talc due to the supply of silica (reaction ii).



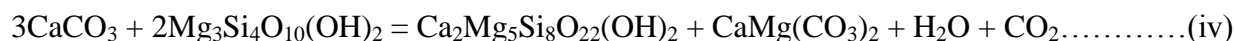
Curve 2 and reaction (iii) (Fig. 7.2) are suggested by the formation of tremolite from talc in the Kherwasti, Anarokas and Dar deposits, where temperature and X_{CO_2} conditions range from 380 to 460 °C and from 0.0 to 0.6, respectively.



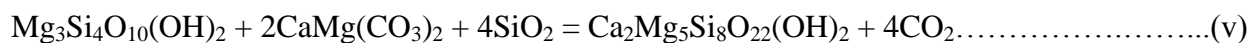
By retrograde metamorphism, tremolite can alter to talc and can be expressed with the help of the above (reaction iii) reversible reaction:



Higher temperatures are estimated for the formation of tremolite and dolomite from talc in the Janinaw deposit. Curve 3 and reaction (iv) (Fig. 7.2) suggest that they were formed within the temperature range of 405 to 460 °C, at X_{CO_2} of 0 to 0.6.

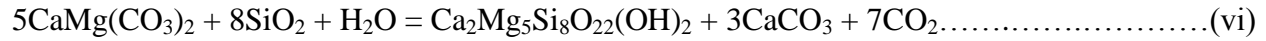


Tremolite in the Kotikhel and Janinaw deposits was formed at a temperature range and X_{CO_2} range of 460 to 490 °C and from 0.6 to 1.0, respectively, following reaction (v) and curve 4 (Fig. 7.2).

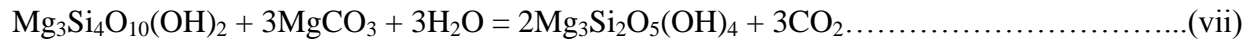


Carbonate-hosted talc deposits, 2018

The formation of tremolite in Kotikhel, Kherwasti, Wachalgad, Lesho and Sargare probably occurred within 460 to 500 °C at X_{CO_2} of 0.6 to 0.9 following curve 5 (Fig. 7.2) and reaction (vi).



Lastly, antigorite was formed from magnesite in Kherwasti and Anarokas following curve 6 (Fig. 7.2) and reaction (vii). The same reaction occurred during the formation of antigorite from the dolomite marble in Kotikhel. The range of temperature for the antigorite formation in Kherwasti and Anarokas was from 450 to 485 °C and the X_{CO_2} varies from 0.0 to 0.04.



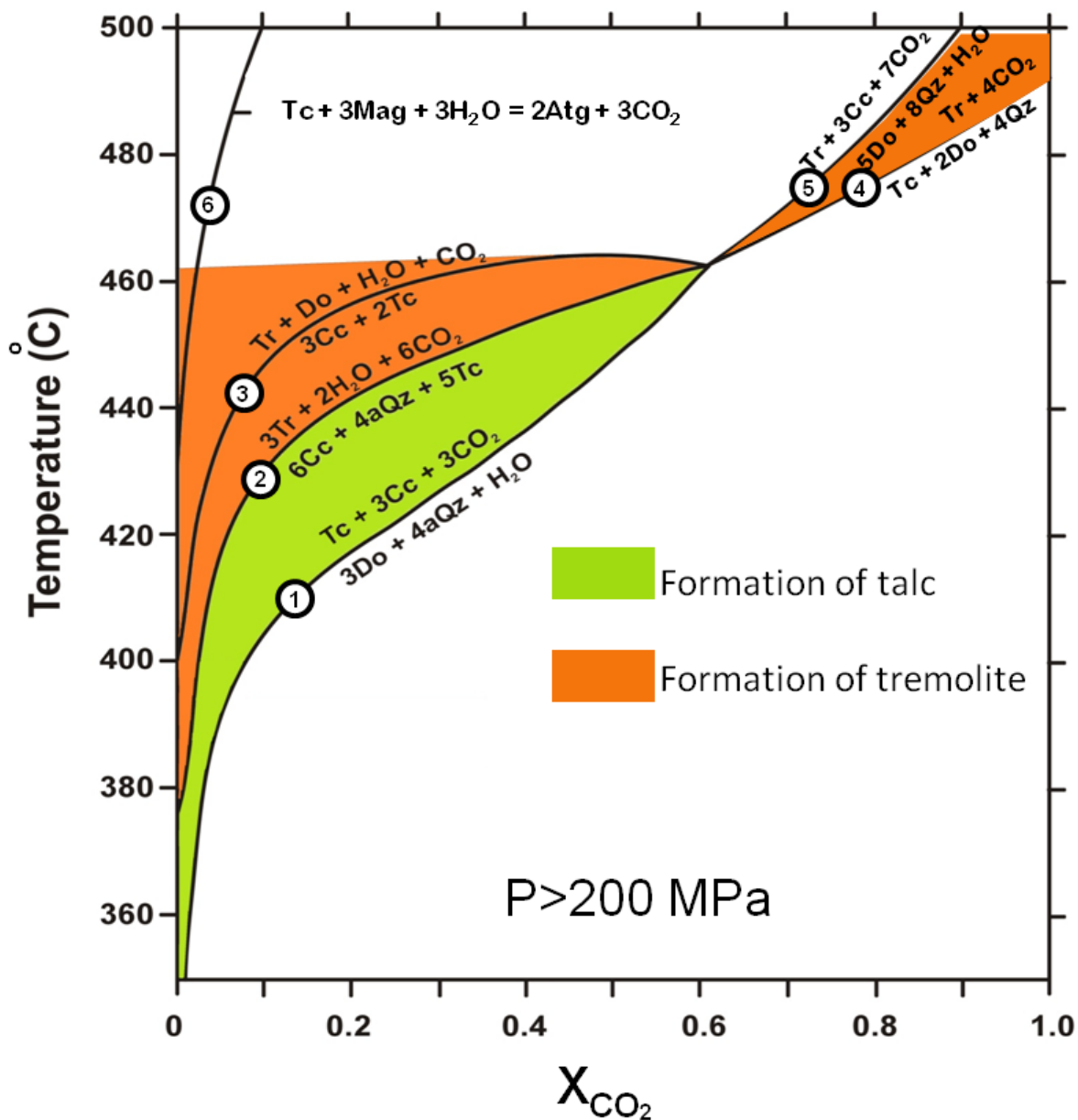


Figure 7.2 Isobaric temperature- X_{CO_2} diagram showing the stability field of talc at $P_{fluid} > 200$ MPa (after Dale *et al.*, 1990 and Evans and Guggenheim, 1988). The green portion can represent the talc stability for most of the deposits in the study area while the orange portion represents the formation temperature of tremolite. Mineral abbreviations used in this diagram are Atg = antigorite, Cc = calcite, Do = dolomite, Mag = magnesite, aQz = alpha quartz, Tc = talc, Tr = tremolite.

7.3 Geochemical Behavior of Elements

The mole ratios of whole-rock MgO, SiO₂ and CaO contents of talc rocks, magnesite rocks, talc bearing magnesite, dolomite marbles and talc bearing dolomite marbles are plotted on the ternary diagram in Figure 7.3a.

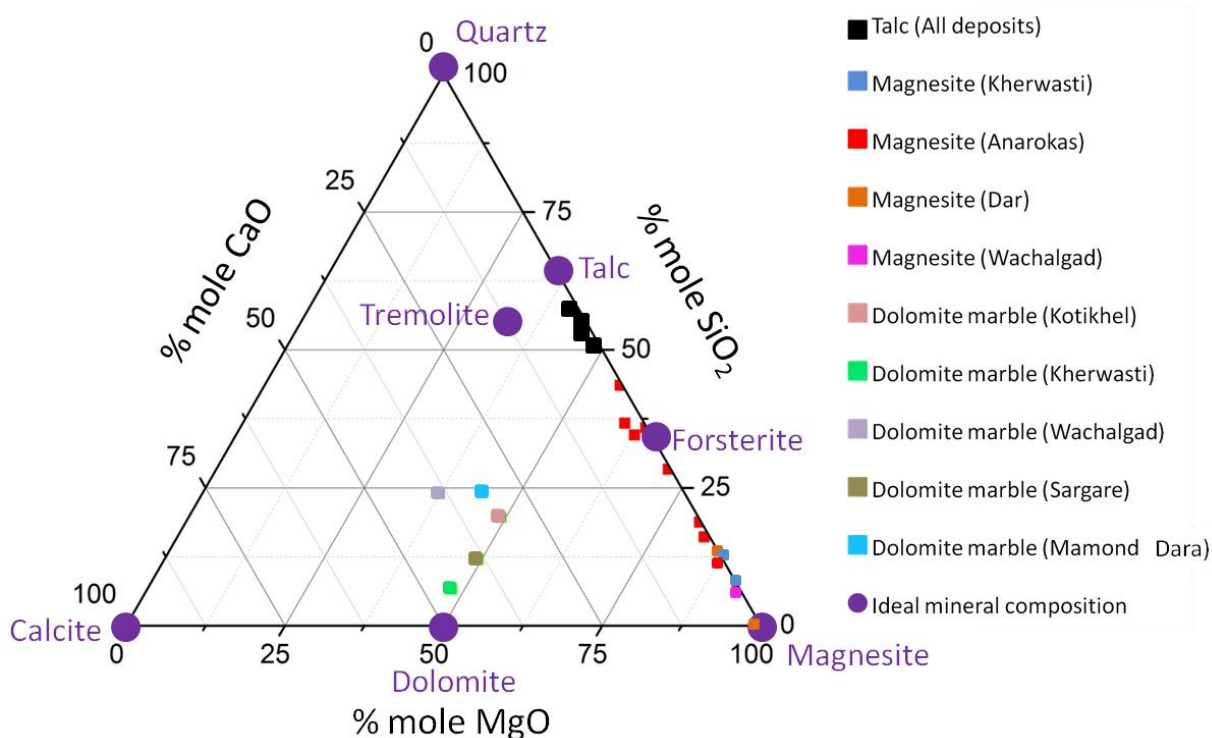


Figure 7.3a CaO-MgO-SiO₂ ternary diagram showing the molecular ratio of bulk chemical compositions of talc rocks, magnesite rocks, talc-bearing magnesite, dolomite marble and talc-bearing dolomite marble, compared with ideal mineral compositions.

The alteration of dolomite marbles and magnesite rocks to form talc are marked by the addition of SiO₂. A significant increase of silica is only possible from an external source and is supported by the common occurrence of quartz veins in the gneiss and talc ore bodies (Figs. 5.3d, 5.11a and 7.1b). The forsterite, tremolite and talc-bearing paragenesis depend on the

Carbonate-hosted talc deposits, 2018

physical conditions of formation rather than composition (Anderson *et al.*, 1990). There is no significant addition or removal of TiO_2 , Al_2O_3 , Fe_2O_3 , MnO , Na_2O , K_2O and P_2O_5 involved during talc formation from magnesite rocks and dolomite marble. The Al_2O_3 content of the talc and carbonate rocks is mostly less than 1 wt%. EPMA data of magnesite, dolomite and calcite are close to ideal mineral compositions with Fe and Mg less than 1wt% (Table 7 and Fig. 7.3b and c). Histograms of FeCO_3 and MnCO_3 from each deposit are given in Appendix 5.

Chemical compositions of talc and tremolite show slightly deviation from ideal minerals compositions (Fig. 7.3d). A little variation generally occurs in the chemical composition of talc mineral. Occasionally small amount of substitution of Al or Ti occurs for Si and a small amount of Mn or Al. Iron (Fe^{2+} and Fe^{3+}) may moderately substitute for Mn (Deer *et al.* 1992). Occasionally some analyses show unusually high amount of water content which can be most probably due to tightly held adsorbed water. Same case is shown by talc minerals in Nangarhar province Afghanistan. The SiO_2 content in talc is about 4 wt% less than ideal composition and water content is about 2 to 7 wt% more than ideal composition. Due to the availability of favorable amount of Ca, tremolite occasionally occurs with talc while chlorite and phlogopite are absent due to lower amount of Al and lack of K, respectively (Deer *et al.* 1992). Tremolite has about 2 wt% less SiO_2 content and high content of water than ideal composition.

Carbonate-hosted talc deposits, 2018

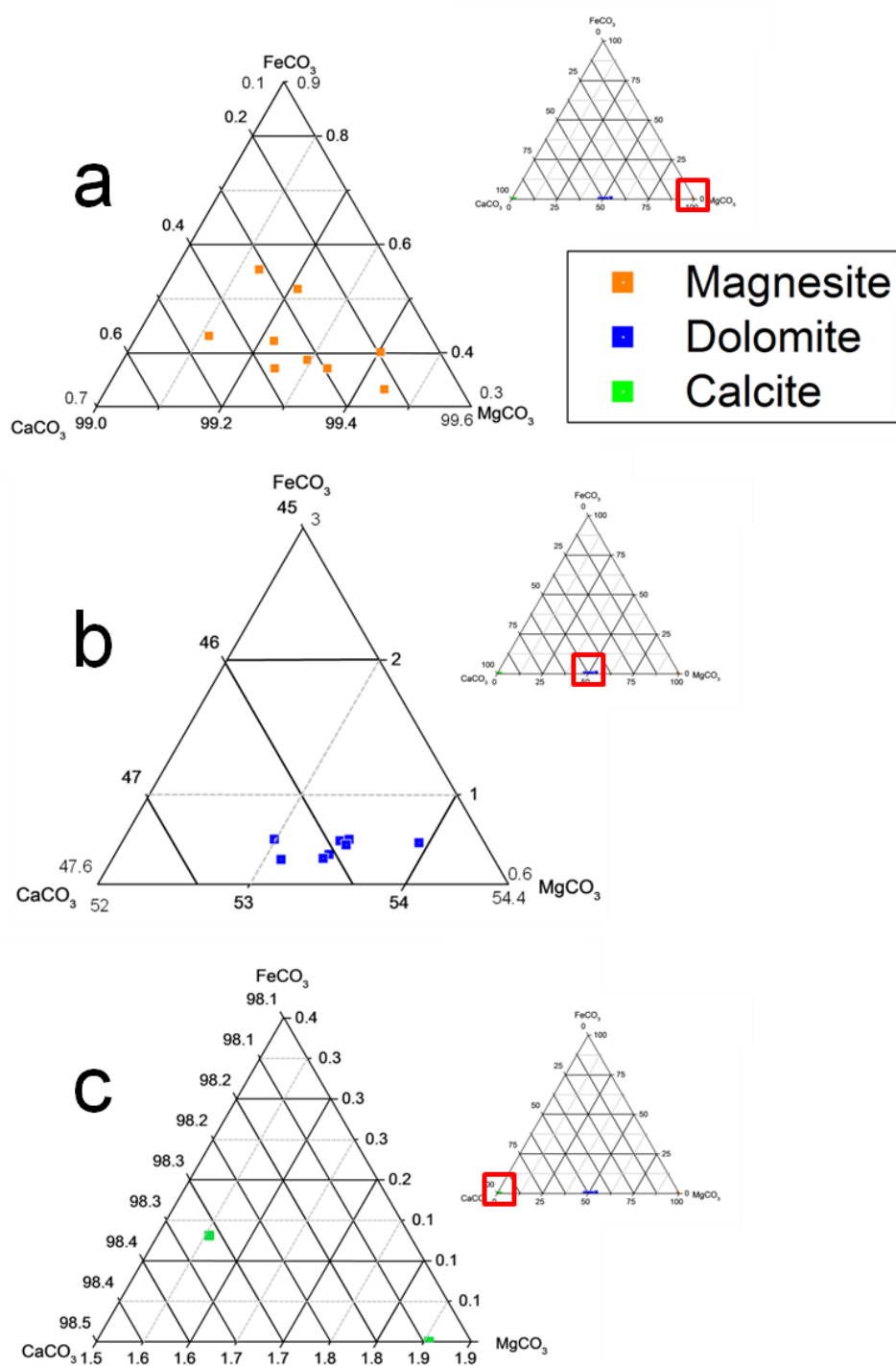


Figure 7.3b FeCO₃-CaCO₃-MgCO₃ ternary diagram of wt% showing the compositions of (a) magnesite from Kherwasti, Anarokas, Dar, Wachalgad and Lesho and (b) dolomite from Kotikhel, Wachalgad, Sargare and Mamond dara, (c) calcite from Janinaw.

Carbonate-hosted talc deposits, 2018

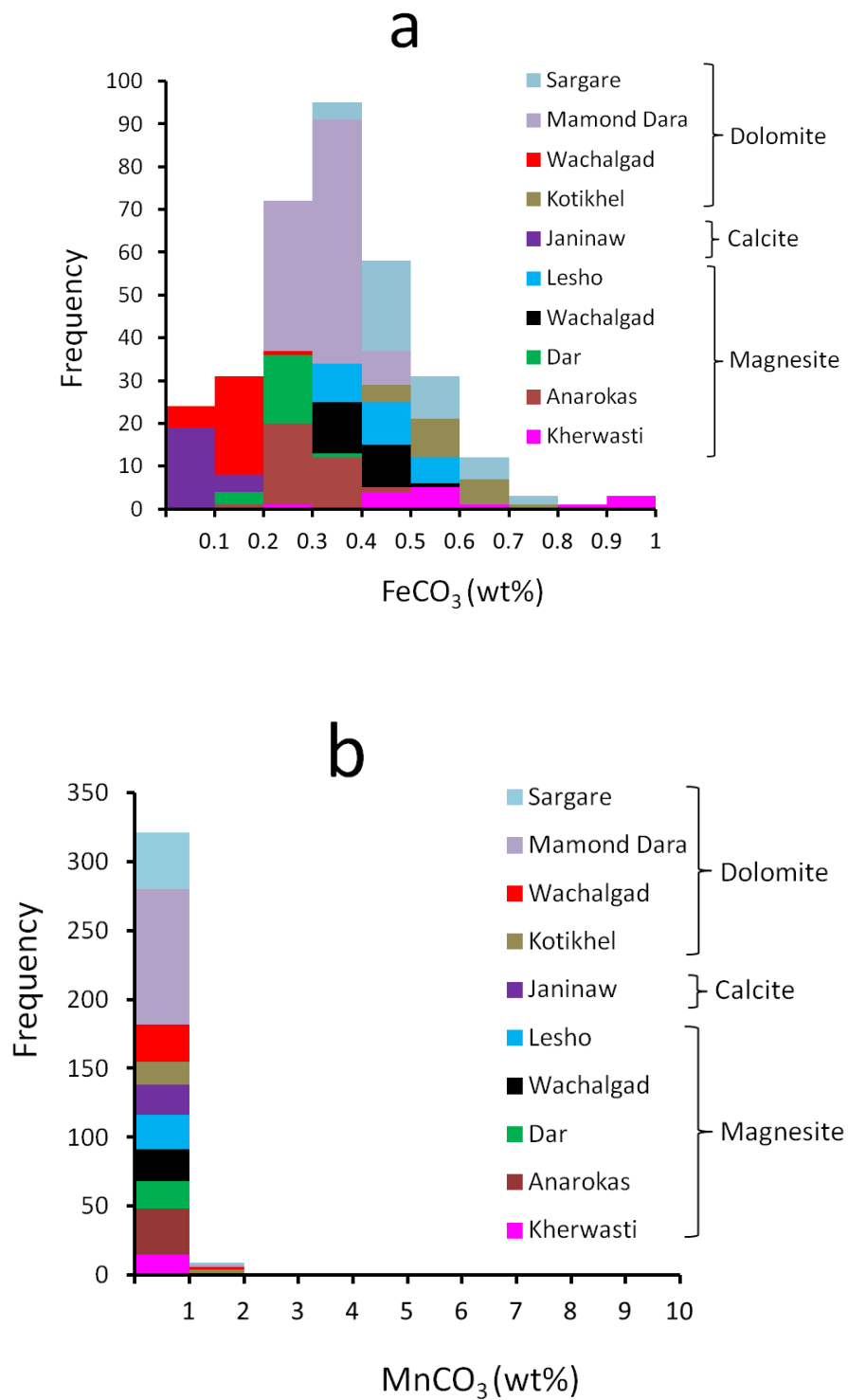


Figure 7.3c (a) FeCO₃ and (b) MnCO₃ concentrations (wt%) in carbonate minerals, based on EPMA analysis.

Carbonate-hosted talc deposits, 2018

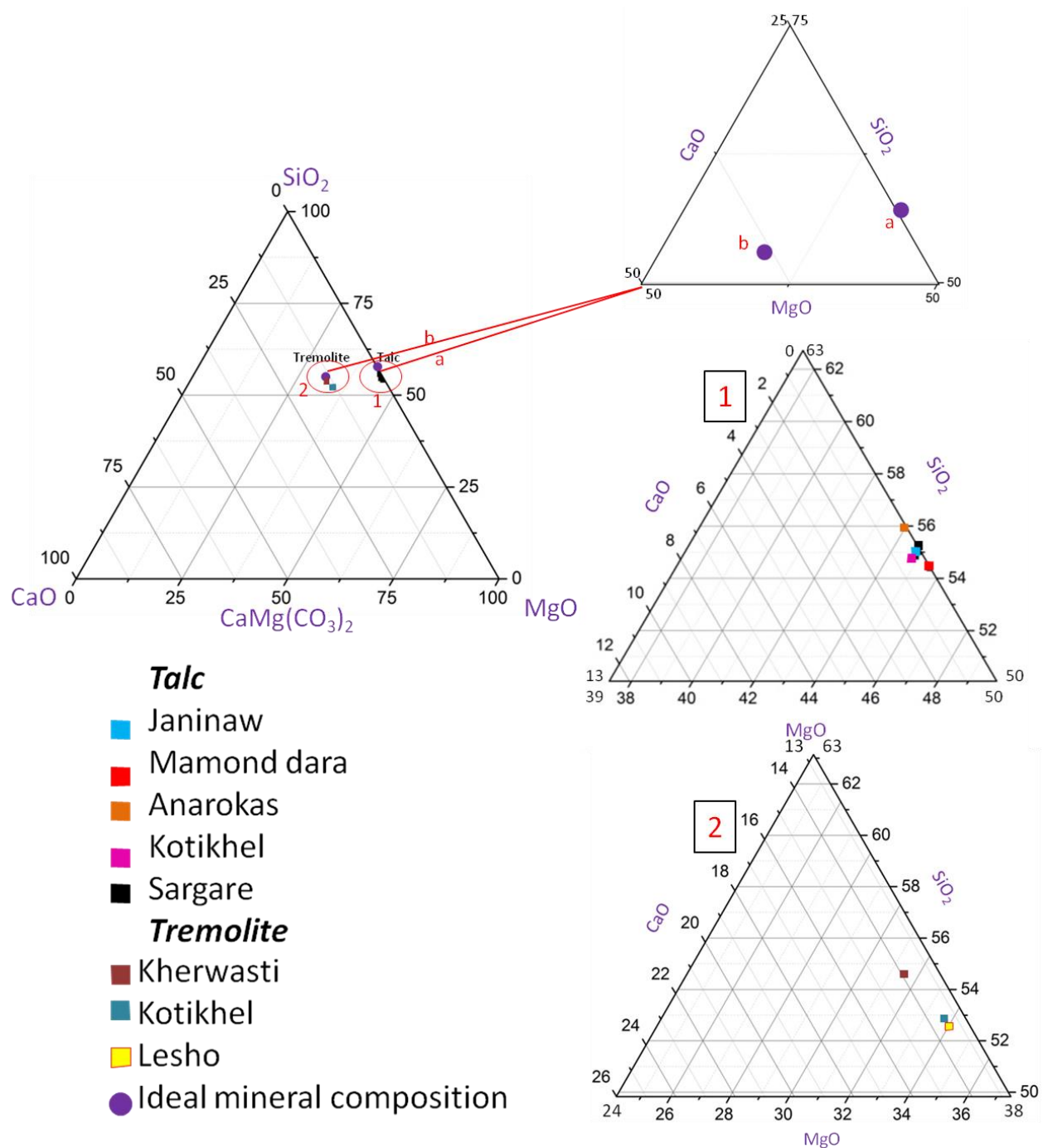


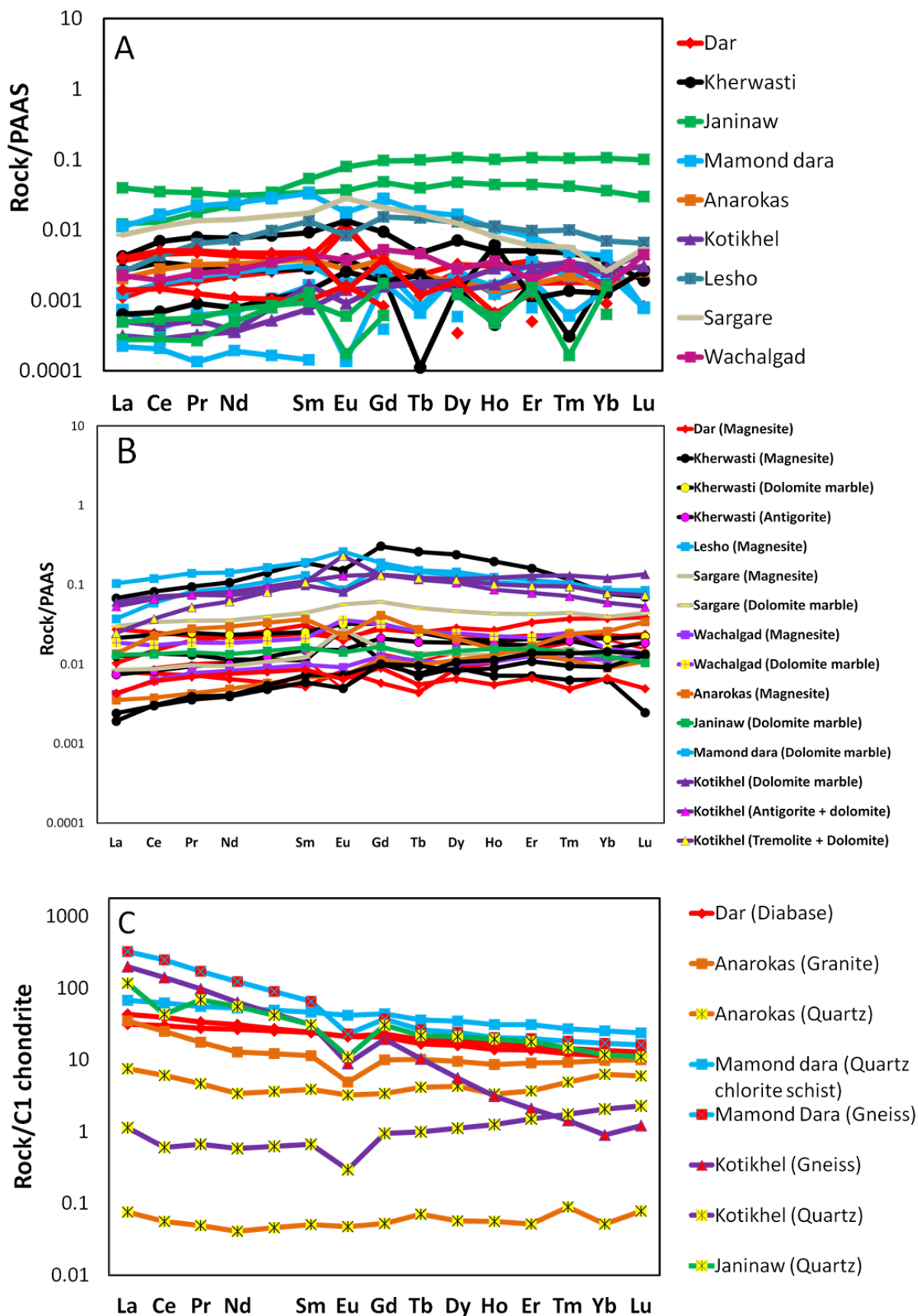
Figure 7.3d CaO-MgO-SiO₂ ternary diagram showing the molecular ratio of (1) talc from Janinaw, Mamond dara, Anarokas, Kotikhel and Sargare, (2) tremolite from Kherwasti, Kotikhel and Lesho, compared with the ideal compositions of (a) talc and (b) tremolite.

Carbonate-hosted talc deposits, 2018

Figure 7.3e showed very low whole-rock REE concentrations of talc rocks, magnesite rocks and dolomite marbles while whole-rock REE of the intrusive rocks and metamorphic rocks were higher. Talc rocks in Kherwasti, Dar and Sargare showed positive Eu anomaly. This positive Eu anomaly may be occurred during formation of magnesite from dolomite during diagenesis (Melezhik *et al.*, 2001). During formation of magnesite there occurred replacement of Ca by Mg, and during this replacement some Ca^{2+} may be replaced by Eu^{2+} . Eu^{2+} can be leached from the rocks and transported by hydrothermal solutions, so hydrothermal solutions are usually enriched with Eu^{2+} (Shikazono, 1999). This positive Eu anomaly is shown by talc formed by replacement of magnesite rocks showing same positive Eu anomaly (Fig. 7.3e).

REE contents of quartz veins in Anarokas and talcose quartz veins in Janinaw were also high due to the presence of REE enriched mineral titanite. Negative Ce anomaly was not exhibited in magnesite rocks and dolomite marble. According to Poul *et al.* (2015), REE contents of Paleoproterozoic sedimentary rocks were low with positive Ce and Eu anomalies. In the early and middle Paleozoic and occasionally in later times (such as the Early Triassic and Cretaceous Anoxic Events), significant volumes of seawater were reducing (Pat *et al.*, 1996). They further concluded that more negative Ce anomaly was found in sediments during warmer climates and transgressive conditions and more positive Ce anomaly was found in sediments during cooler to glacial climates and regressive conditions (Pat *et al.*, 1996).

Carbonate-hosted talc deposits, 2018



Carbonate-hosted talc deposits, 2018

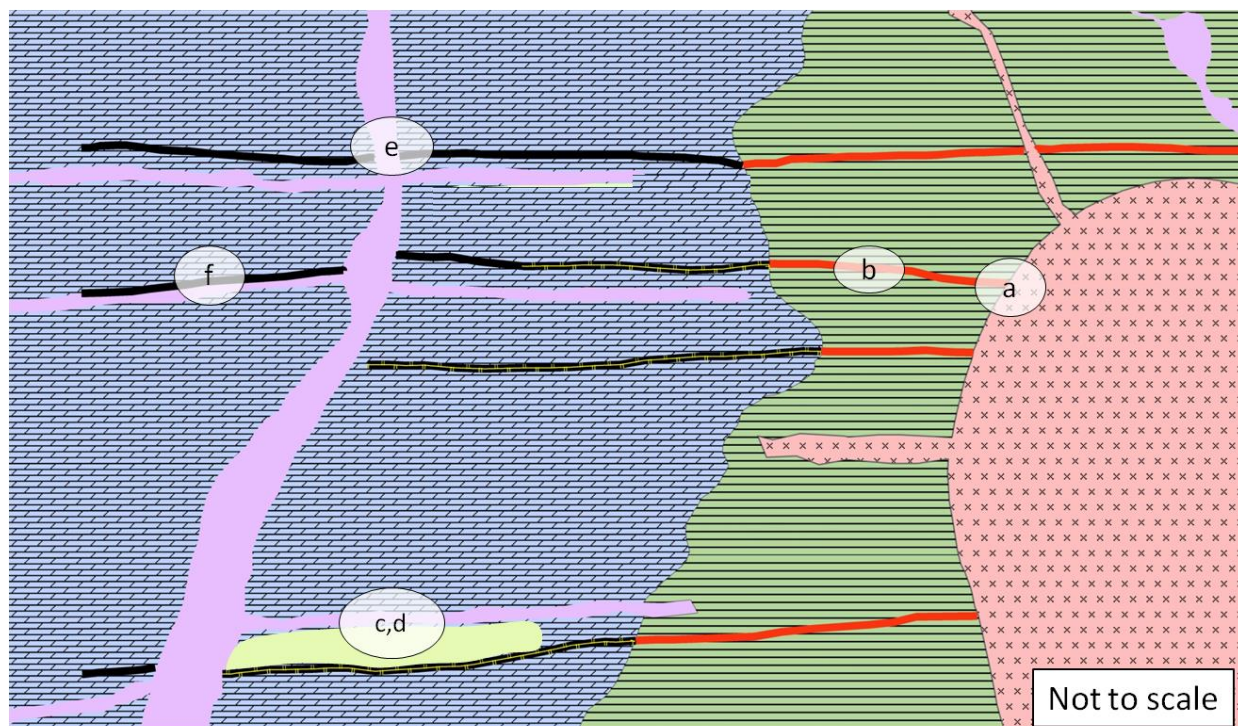
Figure 7.3e REE patterns normalized to post-Archean Australian shale (PAAS, Taylor et al., 1985) for talc rocks, magnesite rocks and dolomite marbles while normalized to C1 chondrite (McDonough & Sun, 1995) for intrusive rocks, metamorphic rocks, altered rocks and quartz veins. A) Talc rocks, B) Magnesite rocks and dolomite marble, C) Intrusive rocks, metamorphic rocks and quartz veins.

As high field strength trace elements such as Ta and Th are inert under most geological conditions (Schandle *et al.*, 1999) so their concentrations must reflect the composition of original rocks. The low concentrations of Al, Ta, Th and REE of talc rocks and carbonate rocks in the study area are inconsistent with those of felsic igneous protolith, whereas the low concentrations of Cr, Ni, and Co of talc rocks and carbonate rocks are inconsistent with those of mafic igneous protolith. Thus these low concentrations of trace elements represent clastic sedimentary rocks as protoliths for talc and carbonate rocks. The whole-rock Ba contents of magnesite rocks in Dar and dolomite marble in Kherwasti, Sargare and Mamonda Dara and also Sr contents of magnesite rocks in Kherwasti, Anarokas, Dar, Lesho and Sargare and dolomite marble in Kotikhel, Kherwasti, Wachalgad, Sargare and Mamond dara are significantly removed during talc formation (Tables 3, 4). The whole-rock V contents of the talc rock, magnesite rocks and dolomite marble are also very low (Table 4). The distinct lower Σ REE and trace elements concentrations of talc and carbonate rocks are very low and it cannot be only due to mobilization during metamorphic process. Marine carbonates usually contain low REE and trace elements, inherited from very low REE abundances in sea water (Piper, 1974; Palmer, 1985). So the lower REE and trace elements of talc are interpreted to be inherited from amphibolites facies metamorphosed carbonate sedimentary rocks such as magnesite rocks and dolomite marble and are suggested as protoliths for talc ores.

7.4 Genetic Model

On the basis of the field observations and geochemical data, I suggest a genetic model for talc formation in Nangarhar province, Afghanistan (Fig. 7.4). Hydrothermal fluids were fed in slightly brittle conditions (Figs. 7.1b and 7.4b) through Early Paleoproterozoic gneiss to Middle Paleoproterozoic host carbonate rocks such as magnesite rocks and dolomite marble, supported by the occurrence of quartz veins in gneiss and hydrous minerals in gneiss such as muscovite and biotite (Figs. 5.1f, 5.5e and 5.8d) and in host carbonate rocks such as talc, tremolite and serpentine (antigorite). Hydrothermal fluids followed the gneissosity of gneiss and replaced magnesite rocks and dolomite marbles into talc and tremolite as the hydrothermal fluids reached these carbonate rocks. Late Paleoproterozoic granitic intrusion cross cut gneiss and quartz veins in gneiss (Figs. 7.1a and, 7.4a) and did not involve in the talc formation in host carbonate rocks. The Early Cretaceous diorite and dolerite dikes cross cut the host carbonate rocks, talc ore bodies and gneiss (Figs. 3.4, 3.5, 7.1e and 7.4e). It also followed the talc ore bodies magnesite rocks and dolomite marble in the form of sills (Figs. 3.1a, 3.3, 3.4, 3.5, 3.9, 7.1f and 7.4f) which may have increased the temperature conditions to form tremolite from talc and serpentinite (antigorite) from magnesite rocks and dolomite marble by contact metamorphism (Fig. 7.1c and d and 7.4c and d).

Carbonate-hosted talc deposits, 2018



Legend

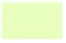
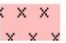






 Antigorite	 Granitic intrusion	 Dolomite marble/Magnesite
 Talc with tremolite	 Talc Vein	 Gneiss
 Diabase/Diorite intrusion	 Quartz Vein	

Figure 7.4 Genetic model for talc formation in Nangarhar province, Afghanistan. a to f in the figure correspond to Figure 7.1.

8. Tectonic Evolution of Spinghar Block

Spinghar (Kohe Safed = white mountain) is a natural fencing between Afghanistan and Pakistan. Spinghar Block is composed of Indian basement crystalline, metamorphosed Paleozoic and relatively unmetamorphosed Mesozoic rocks thrust southward over Indian shelf sediments as young as Miocene. It is mostly composed of Early, Middle to Late Paleoproterozoic gneiss, Middle Paleoproterozoic dolomite marble and magnesite rocks, Late Paleoproterozoic granites, Silurian and Devonian limestone and dolomite, Early Cretaceous intrusive rocks and Pliocene to Late Pleistocene conglomerates (Fig. 2.3). Talc veins most probably formed during Early to Middle Paleoproterozoic time are parallel to sub-parallel to the strike of dolomite marble and magnesite rocks. The Early Cretaceous dolerite or diorite crosscut these host carbonate rocks and talc veins and also parallel to sub-parallel to these rocks (Fig. 7.4). These dolerite and diorite rocks are metamorphosed to amphibolites.

8.1 Regional Metamorphism

Based on field observations and mineral assemblages, the E-W trending Spinghar Block shows regional metamorphism. The most eastern part shows direct replacement of dolomite marble by talc ore. Intrusive rocks metamorphosed to quartz chlorite schist also coexist with talc and dolomite marble but could not increase the temperature to form tremolite. In middle part of the block, talc ore is formed by direct replacement of dolomite and magnesite while tremolite also exists in dolomite marble and talc ore, which shows higher temperature than the most eastern part. The most western part of Spinghar Block has much higher temperature minerals along with talc and tremolite such as antigorite between magnesite rocks and amphibolites and dolomite marble and amphibolites and also in dolomite marble in Kotikhel deposit. Magnesite rocks also contain olivine in Kherwasti deposit (Fig. 5.4c and 8.1).

Carbonate-hosted talc deposits, 2018

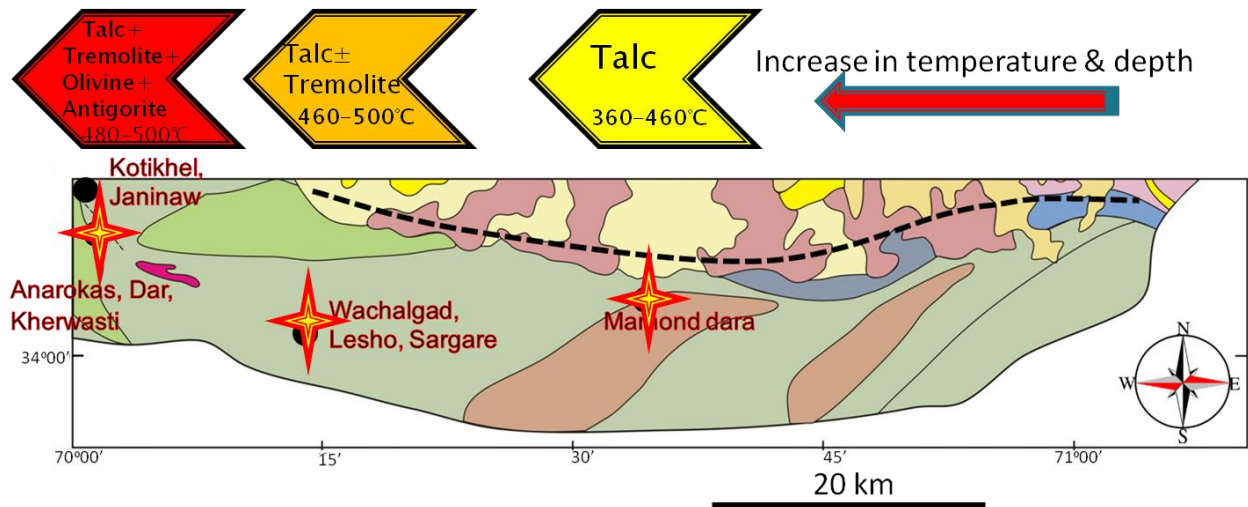


Figure 8.1 Regional metamorphism in Spinghar Block, based on mineral assemblages.

8.2 Tectonic Evolution

The Afghan orogenic block is located within the collision setting of the Eurasian and the Gondwana-derived continental blocks (Brunet *et al.* 2015). The tectonic changes from an area of extreme crustal shortening and deformation in the Pamir–Punjab syntaxis towards the region in the SW where the western Hindu Kush and of Central Afghanistan broadly fan out and comprise a mosaic of internally moderately deformed tectonostratigraphic units.

The collision of the Indian Plate with the Cimmerian Afghan promontory of the Eurasian continent triggered the Himalayan orogenic events and caused a change in the geodynamic setting. This collision started at about 55 Ma in the SE corner of Afghanistan (Khan and Clyde 2013) and the movement of the Indian subcontinent continues northward until today. This movement is indicated by the high seismic activity in the whole region. It was suggested by Khan and Clyde (2013) that the initial India–Asia collision started south of Quetta at about the Paleocene–Eocene boundary and along transpressional margin, proceeded northwards in late

Carbonate-hosted talc deposits, 2018

Early Eocene time to the northern collision sutures of the Main Mantle thrust and the Indus–Yarlung suture in the western Himalaya.

In the Triassic with marine sedimentation occurring as far south as the central Indus basin, break-up of Gondwana started after a Late Permian advance of the Tethyan sea from the north over metamorphosed basement (E Afghanistan, [Kaeffer 1967b](#)) or Paleozoic sediments (Spinghar) (Fig. 8.2). Most possibly the Kabul Block became detached from the Helmand Block in Jurassic times. Since then this block evolved as a micro-craton located offshore of the NW margin of the Indian Plate, surrounded by oceanic crust ([Treolar and Izatt 1993](#)). Along the western side of Greater India, shallow to open marine conditions, deepening to the east, with high energy carbonates dominant are recorded through the Triassic to Middle Jurassic ([Jones 1960](#)). The differences in E-W sedimentation became prominent with the separation of East and West Gondwana in the Late Jurassic (e.g. [Cochran 1988](#)).

The history of collision of the Gondwana terranes between the Turan Plate and the Indian Plate is explained with the help of cartoon (Fig. 8.3). These cartoon sections are not to scale. According to [Brunet *et al.* \(2015\)](#), this is one of the several possible scenarios ([Dercourt *et al.* 1986](#); [Boulin 1990](#); [Treolar and Izatt 1993](#); [Montenat 2009](#)).

M. Triassic: At this time, the subduction of Palaeotethys beneath the southern margin of the Turan Plate was at final stage. Along with this, north Hindu Kush rift basin formation and volcanic arc also occurred. During 240-220 Ma, intrusion of I-type granitoids took place. During the Early Cimmerian orogenic event, in the Late Triassic-Early Jurassic, the Gondwana terrane of the Band-e Bayan (BB)–Helmand (HE) blocks collided with Eurasia. This collision at 210-190 Ma gave rise to post-collisional S-type granitoids (Fig 8.3A).

Carbonate-hosted talc deposits, 2018

M. Jurassic: By back-arc rifting, the opening of the Waras–Panjaw Ocean was caused due to subduction of Neotethys beneath the SE margin of the Helmand Block. During the Late Cimmerian event in the Late Jurassic–Early Cretaceous, the Farah Basin (FB) was filled in by the ‘Panjaw Flysch’ series and later on folded due to collision along the Waras–Panjaw suture with the Helmand Block (Fig. 8.3B).

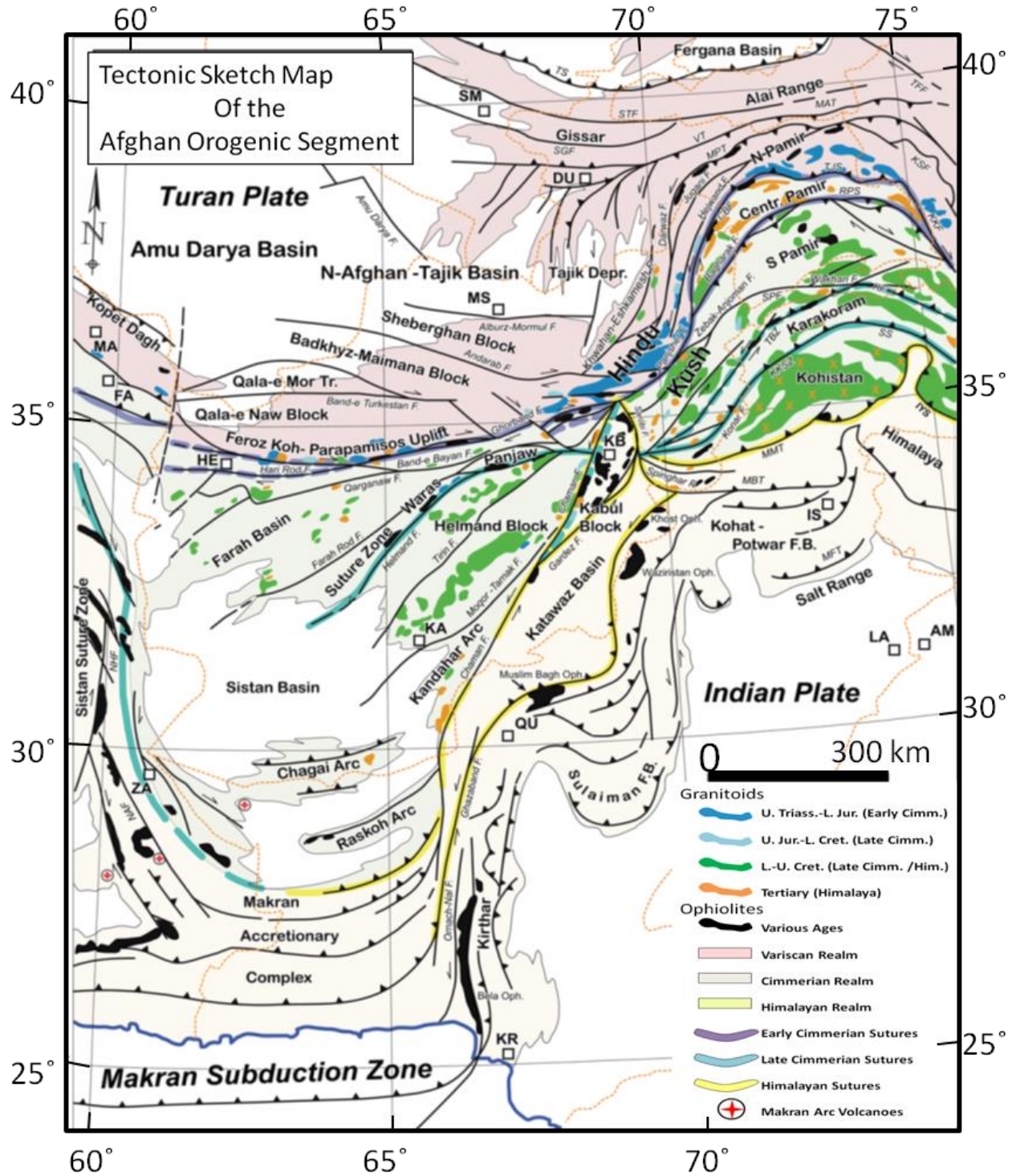


Figure 8.2 Tectonic sketch map of the Afghan orogenic segment. After Brunet *et al.* 2015. CBF, Central Badakhshan/Vanch Akbaytal Fault; KF, Kilik Fault; KKF, Karakoram Fault; KKSZ, Karakoram–Kohistan Suture Zone; KSF, Kongur Shan Fault; MAT, Main Alai Thrust; MBT,

Carbonate-hosted talc deposits, 2018

Main Boundary Thrust; MFT, Main Frontal Thrust; MMT/IYS, Main Mantle Thrust/Indus–Yarlung Suture; MPT, Main Pamir Thrust; NAF, Nostratabad Fault; NHF, Nehbandan Fault; RPS, Rushan Pshart Suture; SGF, South Gissar Fault; SPF, South Pamir Fault; SS, Shyok Suture; STF, Scytho–Turanian Fault; TBZ, Tirich Mir Boundary Zone; TFF, Talas–Fergana Fault; TJS, Tanymas–Jinsha Suture; TS, Turkestan Suture; VT, Vakhsh Thrust.

L. Cretaceous: During this time, intrusion of the mid-Cretaceous granitoids was caused due to continuous subduction beneath the Helmand Block. Also at the SE margin of the Helmand block, the development of the Kandahar forearc basin (KA) took place. According to [Montenant \(2009\)](#), the similarities between the Upper Permian and Upper Triassic of the Helmand and Kabul blocks suggest that the two regions could have been connected during these times. In Jurassic times, the Kabul Block may detach from Helmand Block and evolved as a micro-craton in the NW margin of the Indian Plate ([Treolar and Izatt 1993](#)). This small Gondwana-derived Kabul Block (KB) was assumed to be surrounded by oceanic crust (Fig. 8.3C) between the Helmand Block and the Indian Plate.

U. Cretaceous–Palaeogene: During this time, the collision between Kabul Block, Kandahar forearc basin and the Helmand Block took place and also the Logar ophiolite thrust upon the autochthonous sedimentary cover of the Kabul Block. The Khost–Waziristan ophiolite was thrust over the shelf margin of the Indian Plate during same time (Fig. 8.3D).

Eocene: The Katawaz pull-apart basin opened in the collision zone between the Afghan promontory and India and was then filled in by a thick deltaic sequence. The collision in Neogene times caused the subduction of the Indian Plate together with a series of thrust sheets of

Carbonate-hosted talc deposits, 2018

shelf sediments beneath the Khost–Waziristan ophiolite. The squeezed out Katawaz Basin and its pile of strata moved towards the SE on top of the thrust stack (Fig. 8.3E).

Quaternary: The recent seismic activity shows that the movement of the Indian Plate continues northward along the left-lateral strike-slip faults on both sides of the Kabul Block (Fig. 8.3F).

Miocene-aged southward thrusting of the Spinghar Crystalline unit and covering the rocks over the Murree Formation was resulted due to subduction of the India Plate margin during Himalayan collision. This event may responsible to expose the Early to Middle Paleoproterozoic talc bodies on surface along Spinghar Fault. Southward thrusting of northern units over southern units (Badshah *et al.* 2000), resulted the development of greenschist to amphibolite facies metamorphism in the northern parts of the Kabul Block, along the southern border of the Waziristan ophiolite complex and beneath the Spinghar Thrust (Fig. 8.4). This metamorphic event may cause the metamorphism of dolerites and diorites to amphibolites. A series of stratigraphically discrete episodes of late Paleocene, early Eocene and Neogene deformation during Himalayan contractional tectonism (Beck *et al.* 1995) record many angular unconformities, well documented in eastern Kurram and Waziristan.

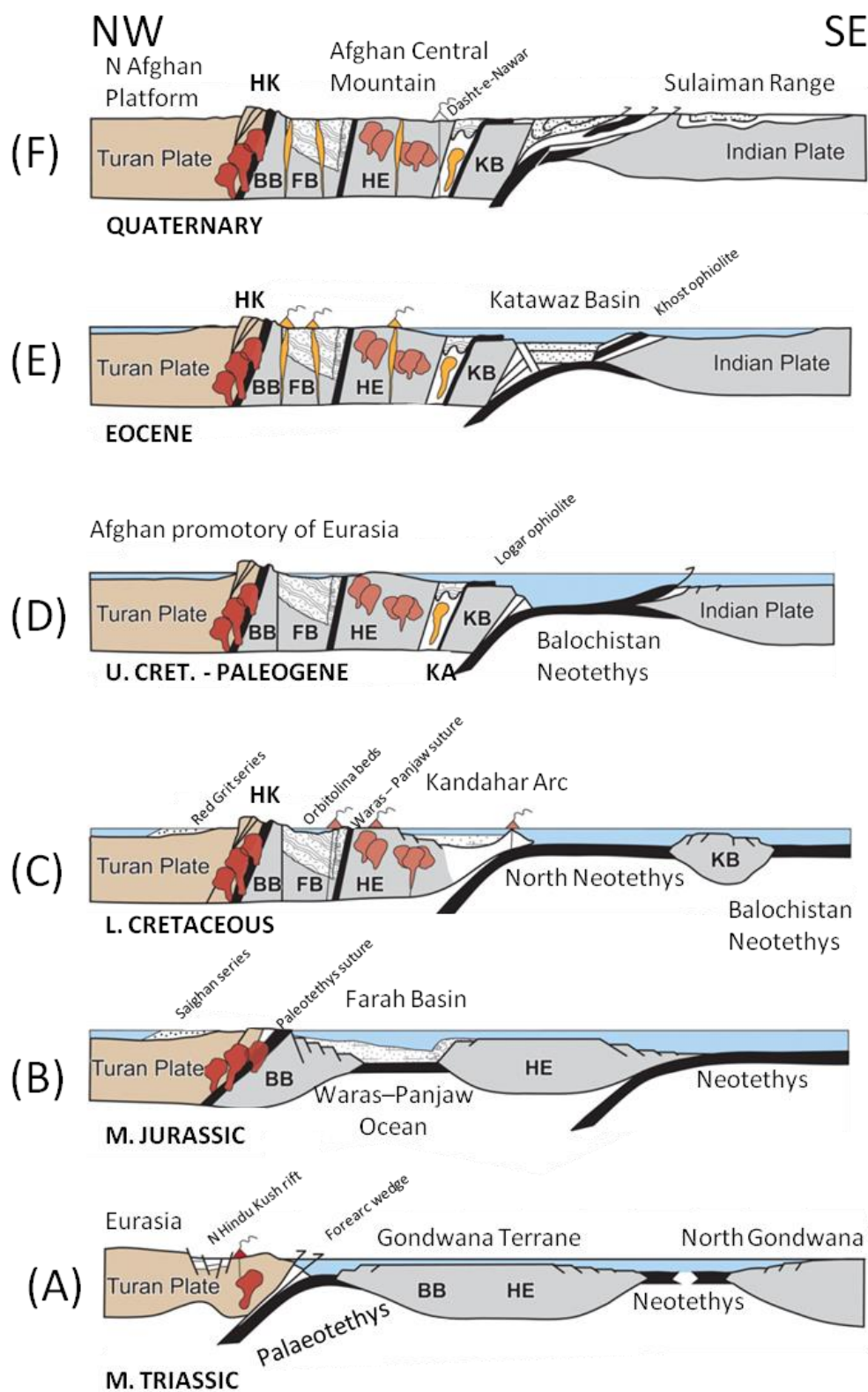


Figure 8.3 Collision history of the Gondwana terrane between the Indian and Turan plates. After Brunet *et al.* 2015.

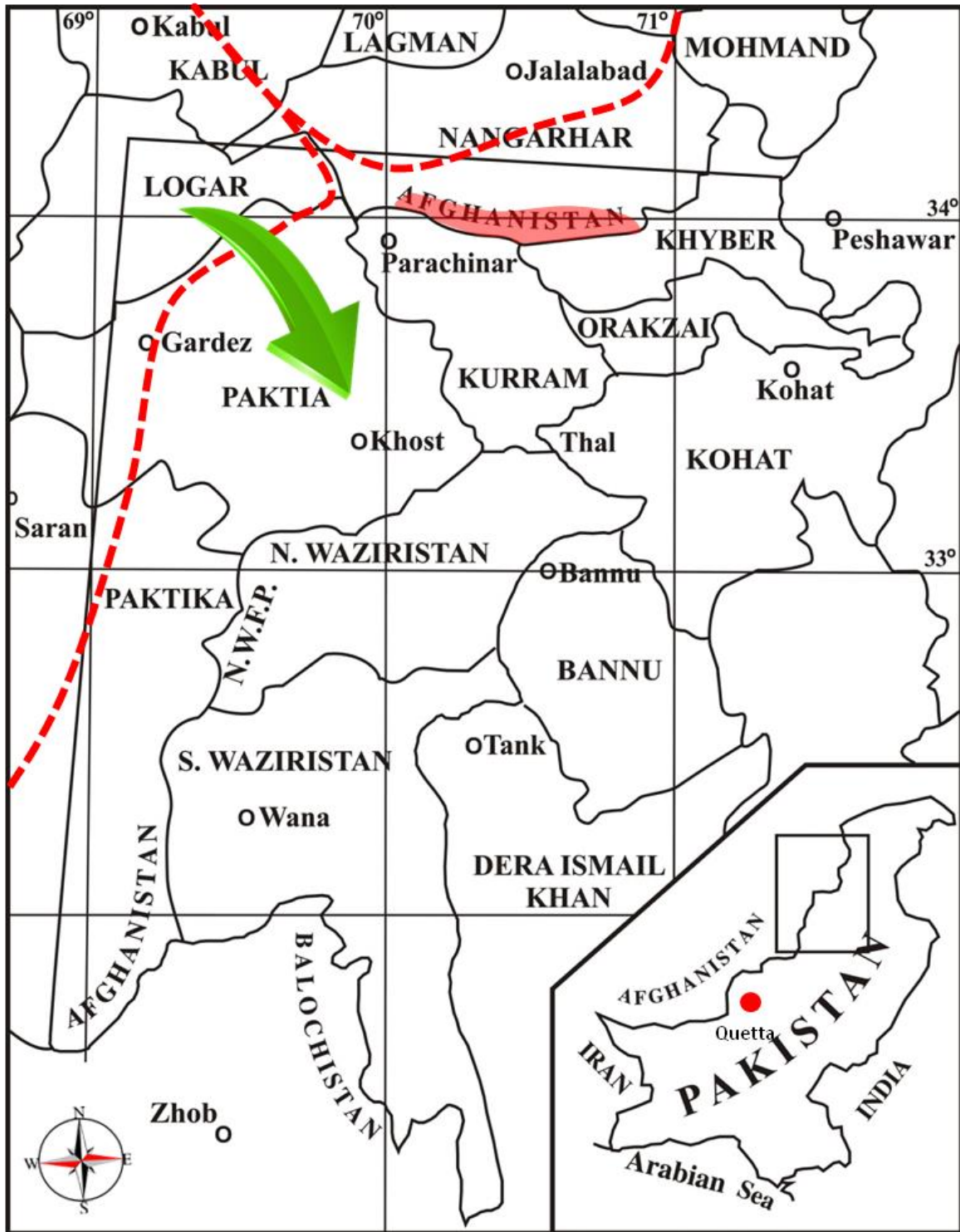


Figure 8.4 Overview map of NW Pakistan SE Afghanistan showing the southward thrusting of the northern units over southern units (modified after [Badshah et al. 2000](#)). Red portion shows the Spinghar Block.

9. Comparisons with Other Talc Deposits

Talc deposits formed by hydrothermal alteration of carbonate rocks include the Rabenwald and Lassing deposits in the eastern Alps of Austria, Gopfersgrun deposits in Germany, within the Bohemian Massif (Hecht *et al.*, 1999), at Atshan in the Hamata area, Egypt, Ruby Range, Southwestern Montana, USA, Winterboro deposit in Alabama, USA, the Trimouns deposit in France and Hwanggangri mineralized zone (HMZ), South Korea. The Rabenwald deposit occurs within a thrust sheet that was transported over the lower Austroalpine gneisses (Prochaska, 1989). The talc orebody at Rabenwald was formed after magnesite, it is intercalated with leucophyllite, and is overlain by mica schists (Prochaska, 1989; Moine *et al.*, 1989). The Lassing deposit occurs within a strongly tectonized block of the Liesing-Palten lineament and consists of shallow-water fossiliferous limestones, dolomites, magnesites, and metasediments (Prochaska, 1989). The Gopfersgrun talc deposit occurs within marbles, graphite schists and metasediments (Schandl *et al.*, 1999), the Atshan talc deposits precursors were impure dolomite limestones locally intercalated with clastic sediments (Schandl *et al.*, 1999). The talc deposits in the Ruby Range have formed in Archean dolomite marbles that were mineralized during retrograde talcification in the Proterozoic (Anderson *et al.*, 1990). The HMZ deposits were formed by replacement of dolomite marble into tremolite during prograde metasomatism due to contact metamorphism by granite intrusion and then tremolite was replaced by talc (Dongbok *et al.*, 2002). Although the talc ore-bodies at all these deposits formed by replacement of carbonates, the Nangarhar talc deposits seem to be significantly different from the Rabenwald and Lassing deposits (Austria), Gopfersgrun deposits, Germany (Schandl *et al.*, 1999) and Atshan deposits, Egypt (Schandl *et al.*, 1999) as mafic silicate minerals such as serpentine, tremolite, olivine and pyroxene are absent in the Rabenwald, Lassing and Gopfersgrun deposits.

Carbonate-hosted talc deposits, 2018

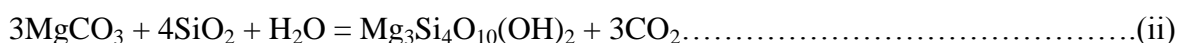
The Atshan deposit occurs within a thick sequence of arc-related volcanic rocks intercalated with some sediments (Abdel-Rahman, 1995; Fafous, 1992) and were intruded by granitic to dioritic rocks. The Ruby Range deposits were related to the rifting of the Belt basin (Wooden *et al.*, 1978). The Lassing carbonate beds were formed in a shallow-water environment (Prochaska, 1989). The Rabenwald magnesite represents a "wedge of upper Australpine Paleozoic rocks" (Prochaska, 1989), and the Gopfersgrun dolomite beds were formed in a marine environment (Hecht *et al.*, 1999). Carbonate minerals were observed in the talc deposits in Nangarhar. On the other hand, due to intense decarbonation reactions of dolomite marble, carbonate minerals are rarely observed in the talc ore of the HMZ (Dongbok *et al.*, 2002). The only features common in all these deposits are the association of chlorite with talc but in Nangarhar and HMZ, this relation is rare with very low concentration of Fe in the carbonates. This last feature would imply that the carbonates at all these deposits are sedimentary and not hydrothermal in origin (Prochaska, 1989), which were metamorphosed to amphibolites facies in Nangarhar prior talc mineralization.

10. Conclusions

The following characteristics and ore genesis of talc in the E-W trending Spinghar Fault Block of Nangarhar province, Afghanistan are revealed based on field observations, petrography and geochemical characteristics.

1. The occurrence of talc deposits is restricted to Middle Paleoproterozoic magnesite rocks and dolomite marble. Talc was formed by replacement of magnesite, dolomite and tremolite.

2. Model reactions suggested for talc formation are:



3. The bulk chemical composition of magnesite rocks suggests an addition of a significant amount of SiO_2 to form talc in Kherwasti, Anarokas, Dar, Wachalgad, Lesho and Sargare deposits.

4. SiO_2 was added and CaO was removed during talc formation from dolomite marble in Kotikhel, Janinaw and Mamond dara deposits.

5. Magnesium has been derived from pre-existing Mg-rich carbonate host rocks, i.e., magnesite rocks and dolomite marbles.

6. The hydrothermal fluids were likely provided through gneiss indicated by the occurrence of parallel to sub parallel quartz veins to the gneissosity of gneiss and hydrous minerals such as biotite and muscovite in gneiss and talc, tremolite and antigorite in host carbonate rocks.

7. The maximum temperature at which talc formed is $460\text{ }^\circ\text{C}$ with $X_{\text{CO}_2} > 0.6$ and the minimum formation temperature is $360\text{ }^\circ\text{C}$ with $0.01 X_{\text{CO}_2}$.

Carbonate-hosted talc deposits, 2018

8. The lower amount of Σ REE, Cr, Co, Ni, Ta, Th, and Fe of talc and host carbonate rocks suggest that talc was formed from magnesite rocks and dolomite marble which were sedimentary in origin.
9. Based on these analyses, unlike Cocker (2011), talc deposits in Nangarhar Province, Afghanistan are suggested to be meta sedimentary in origin.

Acknowledgements

First of all I am very thankful to Allah Almighty who gave me the courage to fulfill this target. This work was supported by the Japanese Government (MONBUKAGAKUSHO: MEXT). I am thankful to the MEXT for providing me the opportunity of this scholarship and Akita University for acceptance my admission and Leading Program (LP) Akita University. I am grateful to Shokozan Mining Company Ltd. and Afghan Talc for their financial and logistic support for field surveys. I would like to express my humble gratitude to my supervisor Prof. Akira Imai and Co-supervisor Dr. Ryohei Takahashi for the arrangements and guidance of laboratory analyses and discussion the problems. I am also indebted to Dr. Hinako Sato for her support in ICP-MS analyses. I am grateful to Dr. Masatsugu Ogasawara, Dr. Yasushi Watanabe, Dr. Antonio Arribas and Dr. Kofi Adomako-Ansah for discussion on data and comments. My humble gratitude to the Ministry of Mines and Petroleum (MoMP), Kabul, Afghanistan for giving me the permission to bring samples to Japan.

References

- Abdel-Rahman, A.F.M. (1995) Tectonic-magmatic stages of shield evolution: the Pan African belt in northeastern Egypt. *Tectonophys.*, 242, 223 -240.
- Abdullah, Sh & Chmyriov, V M (editors in chief) (2008) *Geology and Mineral Resources of Afghanistan*. 2 Volumes. British Geological Survey Occasional Publication No.15.
- Abdullah, Sh. & Chmyriov, V.M. (editors in chief) (1977) *Geology and mineral resources of Afghanistan*, book 2: Afghanistan Ministry of Mines and Industries, Afghanistan Geological Survey, reprinted 2008, British Geological Survey Occasional Publications No. 15, 292.
- Abercrombie, H. J., Skippen, G. B. and Marshall, D. D. (1987) F-OH substitution in natural tremolite, talc, and phlogopite. *Contr. Mineralogy Petrology*, 97, 307-312.
- Adomako-Ansah, K., Mizuta, T., Hammond, N. Q., Ishiyama, D., Ogata, T. and Chiba, H. (2013) Gold mineralization in banded iron formation in the Amalia Greenstone Belt, South Africa: a mineralogical and sulfur isotope study. *Resource Geology*, 63, 119-140.
- Ambraseys, Nicholas, Bilham and Roger. (2003) Earthquakes in Afghanistan: Seismological Research Letters., 74, no. 2, 107–123.
- Anderson, L., Mogk, W. and Childs, F. (1990) Petrogenesis and timing of talc formation in the Ruby Range, Southwestern Montana. *Econ. Geol.*, 85, 585-600.
- Badshah, M. S., Gnos, E., Jan, M. Q. & Afridi, M. I. 2000. Stratigraphic and tectonic evolution of the northwestern Indian plate and Kabul Block. *Geological Society London Special Publications*. In: Khan, M. A., Treloar, P. J., Searle, M. P. & Jan, M. Q. (eds) *Tectonics of the Nanga Parbat Syntaxis and the Western Himalaya*. Geological Society, London, Special Publications, 170, 467–476, <http://doi.org/10.1144/GSL.SP.2000.170.01.25>

Carbonate-hosted talc deposits, 2018

- Beck, R. A. 1995. Late Cretaceous ophiolite obduction and Paleocene India-Asia collision in the western-most Himalaya. PhD thesis, University of Southern California, Los Angeles.
- Berman, R. B. (1988) Internally consistent thermodynamic data for minerals in the system $\text{Na}_2\text{O}-\text{K}_2\text{O}-\text{CaO}-\text{MgO}-\text{FeO}-\text{Fe}_2\text{O}_3-\text{Al}_2\text{O}_3-\text{SiO}_2-\text{TiO}_2-\text{H}_2\text{O}-\text{CO}_2$. *Jour. Petrology*, 29, 445-522.
- Bird, P. (2003) An updated digital model of plate boundaries: G3, *Geochemistry, Geophysics, and Geosystems.*, 4, no. 3, 1–52.
- Bohannon, R.G. (2005) Topographic map of quadrangle 3470 and the northern edge of quadrangle 3370, Jalal-Abad (511), Chaghasaray (512), and Northernmost Jaji-Maydan (517) quadrangles, Afghanistan: U.S. Geological Survey Open-File Report 2005–1108B.
- Boulin, J. 1990. Neocimmerian events in central and western Afghanistan. *Tectonophysics*, 175, 285–315.
- Bowers, T. S. & Helgeson, H. C. (1983) Calculation of the thermodynamic and geochemical consequences of nonideal mixing in the system $\text{H}_2\text{O}-\text{CO}_2-\text{NaCl}$ on phase relations in geological systems. *Metamorphic equilibria at high pressures and temperatures. Am. Mineralogist*, 68, 1059-1075.
- Breckle, S.W. (2007) Flora and vegetation of Afghanistan: Basic and Applied Dryland Research, 1, 2, 155–194.
- Brookfield, M.E. & Hashmat, A. (2001) The geology and petroleum potential of the North Afghan platform and adjacent areas (northern Afghanistan, with parts of southern Turkmenistan, Uzbekistan and Tajikistan): *Earth-Science Reviews*, 55, 41–71.
- Brunet, M.-F., McCann, T. & Sobel, E. R. (eds) 2015. *Geological Evolution of Central Asian Basins and the Western Tien Shan Range*. Geological Society, London, Special Publications, 427.

Carbonate-hosted talc deposits, 2018

Central Statistics Organization. (2010) Afghanistan statistical yearbook 2009–2010: Central Statistics Organization, no. 31, 247.

Chmyriov, V.M. & Mirzad, S.H. (1972) Geologic map of Afghanistan: Kabul, Afghanistan, Ministry of Mines and Industries of Royal Afghanistan, Department of Geology and Mines, 4 sheets, scale 1:1,000,000.

Cochran, J. R. 1988. Somali Basin, Chain Ridge, and origin of the northern Somali Basin gravity and geoid low. *Journal of Geophysical Research*, 93, 11985–12008.

Coshell L., Rosen M.R. and McNamara K.J. 1998. Hydromagnesite replacement of biomineralized aragonite in a new location of Holocene stromatolites, Lake Walyungup, Western Australia. *Sedimentology*, 45 (6), 1005-1018.

Dale, L. A., David, W. M. and John, F. C. (1990) Petrogenesis and timing of talc formation in the Ruby range, Southwestern Montana. *Econ. Geol.*, 85, 585-600.

Danish Committee for Aid to Afghan Refugees. (2011) Update on “National groundwater monitoring wells network activities in Afghanistan” from July 2007 to December 2010: Kabul, Afghanistan, Danish Committee for Aid to Afghan Refugees (DACAAR), 23.

Deer, W.A., Howie, R., A. and Zussman, J. (1966) *An Introduction to the rock forming minerals*. 2nd Edition, 1992. London, Longman, 528 pp.

DeMets, C., Gordon, R.G., Argus, D.F. and Stein, S. (1990) Current plate motions: *Geophysical Journal International*, 101, 425–478.

Denikaev, Sh.Sh. Kafarsky, A.H. Karapetov, S.S. Akhmedzyanov, F.U. Kalimulin, S.M. Slavin, V.I. Sonin, I.I. Stazhilo-Alekseev, K.P. Editors-in-Chief: V.M.Chmyriov, S.H.Mirzad)-
Prin. Cartogr. Inst., Kabul. (1972) 4 sheets.

Carbonate-hosted talc deposits, 2018

Dercourt, J. E. A., Zonenshain, L. P. et al. 1986. Geological evolution of the Tethys belt from the Atlantic to the Pamirs since the Lias. *Tectonophysics*, 123, 241–315.

Doeblich, J.L. & Wahl, R.R., comps., with contributions by Doeblich, J.L., Wahl, R.R., Ludington, S.D., Chirico, P.G., Wandrey, C.J., Bohannon, R.G., Orris, G.J., Bliss, J.D., Wasy, Abdul and Younusi, M.O. (2006) Geologic and mineral resource map of Afghanistan: U.S. Geological Survey Open File Report 2006–1038, scale 1:850,000, available at <http://pubs.usgs.gov/of/2006/1038/>.

Dongbok, S. & Insung, L. (2002) Carbonate-hosted talc deposits in the contact aureole of an igneous intrusion (Hwanggangri mineralized zone, South Korea): geochemistry, phase relationships, and stable isotope studies. *Ore Geology Reviews*, 22, 17-39.

Eggert, R. G. & Kerrick, D. M. (1981) Metamorphic equilibria in the siliceous dolomite system: 6 kbar experimental data and geologic implications *Geochim. Cosmochim. Acta*, 45, 1039-1049.

Evans, B. W. & Guggenheim, S. (1988) Talc, pyrophyllite, and related minerals title of volume *Reviews in Mineralogy*, 19, 225-294.

Exxon Production Research Company. (1985) Tectonic map of the World: 21 sheets, scale 1:10,000,000 at the equator (copyrighted and publicly distributed by American Association of Petroleum Geologists Foundation, Tulsa, Oklahoma, 1994).

Fasfous, B.R.B. (1992) Petrochemical and petrogenetic studies on the steatite mineralization of Hamata and Um Omya areas, Eastern Desert, Egypt. *Mans. Sci Bull.*, 19, 189-212.

Filippov, O.N. (1974) Project of prospecting and explorations at the talc deposits of Achin and Geology and minerals in the south part of Eastern Afghanistan (Report of the Kabul team

Carbonate-hosted talc deposits, 2018

on the work in 1970). (By Sh.Sh.Denikaev, V.P.Feoktistov, I.V. Pyzhyanov, A.A.Adjuruddin, Sh.N.Narbaev, Yu.M.Konev).Kabul, Rec. Off. DGMS, 1971.

Gordon, T. M. & Greenwood, H. J. (1970) The reaction: Dolomite + quartz + water = talc + calcite + carbon dioxide *Am. Jour. Sci.*, 268, 225-242.

Haghipour, A., Ghorashi, M. and Kadjar, M.H. (1984a) Seismotectonic map of Iran, Afghanistan and Pakistan: Commission for the Geological Map of the World, United Nations Educational, Scientific and Cultural Organization, and Geological Survey of Iran, 1 sheet, scale 1:5,000,000, 24. pamphlet.

Haghipour, A., Ghorashi, M. and Kadjar, M.H. (1984b) Explanatory text of the seismotectonic map of Iran, Afghanistan and Pakistan: Tehran, Iran, Commission for the Geological Map of the World, United Nations Educational, Scientific and Cultural Organization, and Geological Survey of Iran, 24.

Harben, P. W., Kuzvart, M., Prochaska, W. (1989) Geochemistry and genesis of Austrian talc deposits. *Appl. Geochem.*4, 511-525.

Harben, P.W., and Kuzvart, Milos, 1996, Sulfur, in *Industrial minerals: A global geology*: London, Industrial Minerals Information Ltd., p. 396-406.

Hecht, L., Freiburger, R., Gilg, H.A., Grundmang, G. and Kosttsyn, Y. A. (1999) Rare earth element and isotope (C, O, Sr) characteristics of hydrothermal carbonates: genetic implications for dolomite-hosted talc mineralization at Gopfersgrun (Fichtelgebirge, Germany). *Chem. Geol.*, 155, 1 15-130.

Hessami, Khaled, Jamali, Farshad and Tabassi, Hadi (2003) Major active faults of Iran: Tehran, Iran, International Institute of Earthquake Engineering and Seismology, 1 sheet, scale

Carbonate-hosted talc deposits, 2018

- 1:2,500,000 (<http://www.iiees.ac.ir/seismology/ActiveFault.pdf>, accessed November 11, 2004).
- Jade & Sridevi (2004) Estimates of plate velocity and crustal deformation in the Indian subcontinent using GPS geodesy: *Current Science*, 86, no. 10, 1443–1448.
- Jones, A. G. 1960. Reconnaissance geology of part of western Pakistan: A Colombo Plan Co-operative Project Report. Government of Canada.
- Kaever, M. 1967b. Untersuchungen zur Schichtfolge im Gebiet Quasim-Khel-Ali-Khel, E-Afghanistan. *Neues Jahrbuch Geologische und Palaontologische Monatshefte*, 5, 284-304.
- Kazmi, A.H. & Rana, R.A. (1982) Tectonic map of Pakistan: Geological Survey of Pakistan, 1 sheet, scale 1:2,000,000.
- Kazmi, A.H. (1979) Preliminary seismotectonic map of Pakistan: Geological Survey of Pakistan, 1 sheet, scale 1:2,000,000.
- Kerrick, D. M. & Jacobs, G. K. (1981) A modified Redlich-Kwong equation for H₂O, CO₂ and H₂O-CO₂ mixtures at elevated pressures and temperatures. *Am. Jour. Sci.*, 281, 735-767.
- Khan, I. H. & Clyde, W. C. 2013. Lower Paleogene tectonostratigraphy of Balochistan: evidence for timetransgressive Late Paleocene-Early Eocene uplift. *Geosciences*, 3, 466–501.
- Kingston, John and Clarke, J.W. (1995) Petroleum geology and resources of Afghanistan: *International Geology Review*, 37, 111–127.
- Koons, P.O., 1981, A study of natural and experimental metasomatic assemblages in an ultramafic-quartzofeldspathic metasomatic system from the Haast Schist, South Island, New Zealand: *Contributions to Mineralogy and Petrology*, v. 78, p. 189–195.

Carbonate-hosted talc deposits, 2018

Lednev, V.V. (1977a) Geological plan of the surface of magnesite body no. 1, longitudinal projection, sections: Kabul, Afghanistan, Ministry of Mines and Industries, graph annex no. 3, scale 1:500.

McCarthy, E. F., Genco, N. A. and Reade, E. H. (2006) Industrial minerals and rocks: Society for Mining, Metallurgy, and Exploration, Inc. (SME), 971-986.

McDonough, W. F. & Sun, S.-s. (1995) The composition of Earth. *Chemical Geology*, 120, 223-253.

Melezhik V. A., Fallick A. E., Medvedev P. V. and Makarikhin V. V. 2001. Palaeoproterozoic magnesite: lithological and isotopic evidence for playa/sabkha environments. *Sedimentology*, 48, 379-397.

Moine, B., Fortune, J.P., Moreal, P. and Viguiet, F. (1989) Comparative mineralogy, geochemistry and conditions of the formation of two metasomatic talc and chlorite deposits: Trimouns (Pyrenees, France) and Rabenwald (eastern Alps, Austria). *Econ. Geol.*, 84, 1398-1416.

Montenat, C. 2009. The Mesozoic of Afghanistan. *GeoArabia*, 14, 147–210.

Muktinath & Wakhaloo, G. L. (1962) A note on the magnesite deposit of Almora district, UP. *Indian Miner.*, 16, 116–123.

Nautiyal, S. P. (1947) General report for the year, 1947. *Rec. Geol. Surv. India*, 1953, 79, 375.

Neilson, J.M. (1976b) Interim evaluation on the Achin talc deposits: UNDP Mineral Evaluation Project AFG/74/002, Watts, Griffis, and McQuat, Ltd., 9.

Oak Ridge National Laboratory. (2010) LandScan global population database 2009: Oak Ridge National Laboratory database, accessed February 1, 2011.

Carbonate-hosted talc deposits, 2018

Olson, S.A. & Williams-Sether, T. (2010) Stream flow characteristics of streamgages in northern Afghanistan and selected locations: U.S. Geological Survey Data Series 529, 512.

Orris, G.J. & Bliss, J.D. (2002) Mines and mineral occurrences of Afghanistan: U.S. Geological Survey Open-File Report 2002, 110, 95.

Palmer, M. R. (1985) Rare earth elements in foraminifera tests. *Earth Planet. Sci. Lett.*, 73, 287-298.

Pat, W., Mary, S. Q. H. and Bernd, D. E. (1996) The whole-rock cerium anomaly: a potential indicator of eustatic sea-level changes in shales of the anoxic facies. *Sedimentary Geology*, 101, 43-53.

Peters, S.G., Ludington, S.D., Orris, G.J., Sutphin, D.M., Bliss, J.D. and Rytuba, J.J., eds., and the U.S. Geological Survey-Afghanistan Ministry of Mines Joint Mineral Resource Assessment Team (2007) Preliminary non-fuel mineral resource assessment of Afghanistan: U.S. Geological Survey Open-File Report 2007, 1214, 810, 1 CD-ROM. (Also available at <http://pubs.usgs.gov/of/2007/1214/>).

Piper, D. Z. (1974) Rare earth elements in sedimentary cycle: a summary. *Chem. Geol.*, 14, 285-304.

Pohl, W., 1990, Genesis of magnesite deposits—models and trends: *Geologische Rundschau*, v. 79, n. 2, p. 291–299.

Poul, E., Patrick, I. M., George, N. B., Edward, A. B. and Alan, E. K. (2015) Rare earth elements in sedimentary phosphate deposits: Solution to the global REE crisis?. *Gondwana Research*, 27, 776-785.

Prochaska, W. (1989) Geochemistry and genesis of Austrian talc deposits. *Appl. Geochem.*, 4, 1-21.

Carbonate-hosted talc deposits, 2018

- Ruleman C.A., Crone A.J., Machette M.N., Haller K.M. and Rukstales K.S. (2007) Open-File Report 2007-1103,
- Ruleman, C.A. Crone, A.J. Machette, M.N. Haller, K.M. and Rukstales, K.S. (2007): Map and Database of Probable and Possible Quaternary Faults in Afghanistan: USGS Afghanistan Project Product No. 150 , U.S. Department of the Interior,U.S. Geological Survey.
- Sarwar, G. & De Jong, K.A. (1979) Arcs, oroclines, syntaxes—The curvatures of mountain belts in Pakistan, in Farah, Abul, and De Jong, K.A., eds., *Geodynamics of Pakistan*: Quetta, Pakistan, Geological Survey of Pakistan, 341–349.
- Sborshchikov, I.M. & Dronov, V.I. (1972) Tectonic Map of Afghanistan. Scale 1,000.000.
- Sborshchikov, I.M. Dronov, V.I. Chmyriov, V.M. Kafarsky, A.Kh. Kazikhani, A.R. Salah, A.S. Slavin, G.I. Teleshev, V.I. and Abdullah, Sh. (1975) *Geology and Mineral Resources of Afghanistan*. Prin. Kabul Times, Kabul, 1975.
- Schandle, E.S., Sharara, N.A. and Gorton, M.P. (1999) The origin of the Atshan talc deposit in the Hamata area, eastern desert, Egypt: a geochemical and mineralogical study. *Can. Mineral.* 37, 1211-1227.
- Sella, G.F., Dixon, T.H. and Mao, A. (2002) REVEL—A model for recent plate velocities from space geodesy: *Journal of Geophysical Research*, 107, 1 pl. doi:10.1029/2000JB000033.
- Sengor, A.M.C. (1984) The Cimmeride orogenic system and the tectonics of Eurasia: *Geological Society of America Special Paper* 195, 82.
- Sengupta, H. P. & Yadav, R. N. (2002) Genesis of Jhiroli magnesite, District Almora, Uttaranchal: Petrological and scanning electron microscope (SEM) approach. *Indian J. Geol.*, 74, 261–274.

Carbonate-hosted talc deposits, 2018

Shareq & Abdullah (1981) Geological and geophysical investigations carried out in Afghanistan over the period 1972–1979, in Gupta, H.K., and Delany, F.M., eds., *Zagros, Hindu Kush, Himalaya—Geodynamic evolution: American Geophysical Union Geodynamics Series 3*, 75–86, 1 folded plate, scale 1:2,500,000.

Shareq, Abdullah, and Chmyriov, V.M. (1977) *Map of mineral resources of Afghanistan: Ministry of Mines and Industries of the Democratic Republic of Afghanistan, Department of Geological and Mineral Survey*, scale 1:500,000.

Shikazono, N. (1999) Rare earth element geochemistry of Kuroko ores and altered rocks: implication for evolution of submarine geothermal system at back-arc basin. *Resource Geology Special Issue*, 20, 23–30.

Simandl, G.J. and Hancock, K., 1998, Sparry magnesite, in *Geological Fieldwork 1997: British Columbia Ministry of Employment and Investment Paper 1998-1*, p. 24E.1 to 24e.3.

Simandl, G.J., and Paradis, S. 1999, Carbonate-hosted talc, in Simandl, G.J., Hora, Z.D., and Lefebure, eds., *Selected British Columbia mineral deposit profiles, volume 3: British Columbia Ministry of Energy and Mines*.

Skippen, G. (1971) Experimental data for reactions in siliceous marbles. *Jour. Geology*, 79, 457-481.

Skippen, G. (1974) An experimental model for low pressure metamorphism of siliceous dolomitic marble: *Am. Jour. Sci.*, 274, 487-509.

Slaughter, J., Kerrick, D. M. and Wall, V. J. (1975) Experimental study of equilibria in the system $\text{CaO-MgO-SiO}_2\text{-H}_2\text{O-CO}_2$ *Am. Jour. Sci.*, 275, 143-162.

Carbonate-hosted talc deposits, 2018

- Tapponnier, P., Mattauer, M., Proust, F. and Cassaigneau, C. (1981) Mesozoic ophiolites, sutures, and large-scale tectonic movements in Afghanistan: *Earth and Planetary Science Letters*, 52, 355–371.
- Taylor, S. R. & McLennan, S. M. (1985) *The Continental Crust: Its Composition and Evolution* Blackwell Scientific Publication, Carlton, 312.
- Treloar, P.J. & Izatt, C.N. (1993) Tectonics of the Himalayan collision between the Indian Plate and the Afghan Block—A synthesis, in Treloar, P.J., and Searle, M.P., eds., *Himalayan tectonics: Geological Society, London, Special Publications*, 74, 69–87.
- U.S. Geological Survey (USGS), the Task Force for Business and Stability Operations (TFBSO) of the Department of Defense, and the Afghanistan Geological Survey (AGS) (2009 to 2011) *Geologic and compilation activities*, 1421-1434.
- United Nations Economic and Social Commission for Asia and the Pacific. (1995) *Geology and Mineral Resources of Afghanistan, Atlas of Mineral Resources of the ESCAP Region*, v. 11: New York, United Nations, 4 maps, scales 1:2,000,000, 1:2,500,000, 85.
- Valdiya, K. S. (1968) Origin of the magnesite deposits of Southern Pithoragarh, Kumaon Himalaya. *Econ. Geol.*, 63, 924–934.
- Valley, J. W., Petersen, E. U., Essence, E. J. and Bowman, J. R. (1982) Fluorophlogopite and fluortremolite in Adirondack marbles and calculated C-O-H-F fluid compositions *Am. Mineralogist*, 67, 545-557.
- Vernant, P., Nilforoushan, F., Masson, F., Hatzfeld, D., Abbassi, M., Vigny, C., Tavakoli, F., Bayer, R., Martinod, J., Ashtiani, M. and Chery, J. (2004) Contemporary crustal deformation and plate kinematics in the Middle East constrained by GPS measurements in Iran and north Oman: *Geophysical Journal International*, 157, 381–398.

Carbonate-hosted talc deposits, 2018

Virta, R.L. (1998) Talc and pyrophyllite, in *Minerals yearbook, metals and minerals 1996*, vol. I: U.S. Geological Survey, 891–897.

Weippert, D., Wittekindt H., Wolfart R. (1970) Zur geologischen Entwicklung von Zentral- und Südafghanistan .- *Bh. Geol. Jb.*, Hannover, 90, 99.

Wheeler, R.L., Bufe, C.G., Johnson, M.L. and Dart, R.L. (2005) Seismotectonic map of Afghanistan, with annotated bibliography, U.S. Geological Survey Open–File Report 2005–1264, accessed (09/01/2006) at <http://pubs.er.usgs.gov/usgspubs/ofr/ofr20051264>.

Wittekindt, H.P., Wolfart, R. and Moores, E.M. (1997) Afghanistan, in Moores, E.M., and Fairbridge, R.W., eds., *Encyclopedia of European and Asian regional geology*: London, Chapman and Hall, 1–7.

Wooden, J. L., Vitaliano, C. J., Koehler, S. W. and Ragland, P. C. (1978) The late Precambrian mafic dikes of the southern Tobacco Root Mountains, Montana: Geochemistry, Rb-Sr geochronology and relationship to Belt tectonics. *Canadian Jour. Earth Sci.*, 15, 467-479.

Carbonate-hosted talc deposits, 2018

Appendix

Appendix 1: List of hand specimens from each deposit.



List of samples from Kotikhel deposits.

Carbonate-hosted talc deposits, 2018



List of samples from Janinaw deposits.

Carbonate-hosted talc deposits, 2018

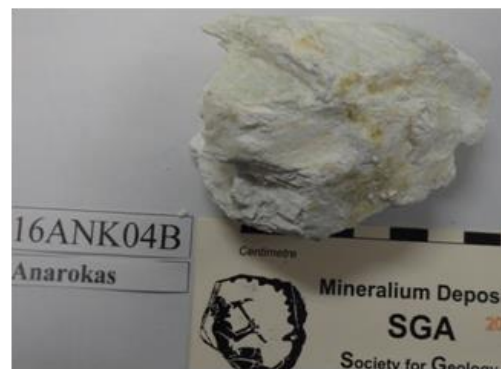


Carbonate-hosted talc deposits, 2018



List of samples from Kherwasti deposits.

Carbonate-hosted talc deposits, 2018



Carbonate-hosted talc deposits, 2018

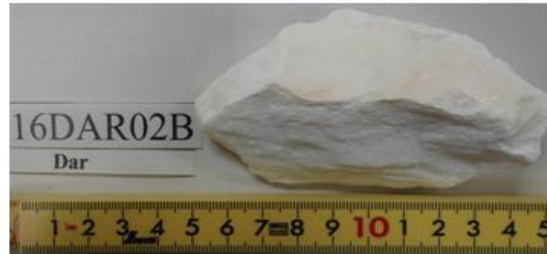


List of samples from Anarokas deposit.

Carbonate-hosted talc deposits, 2018



Carbonate-hosted talc deposits, 2018



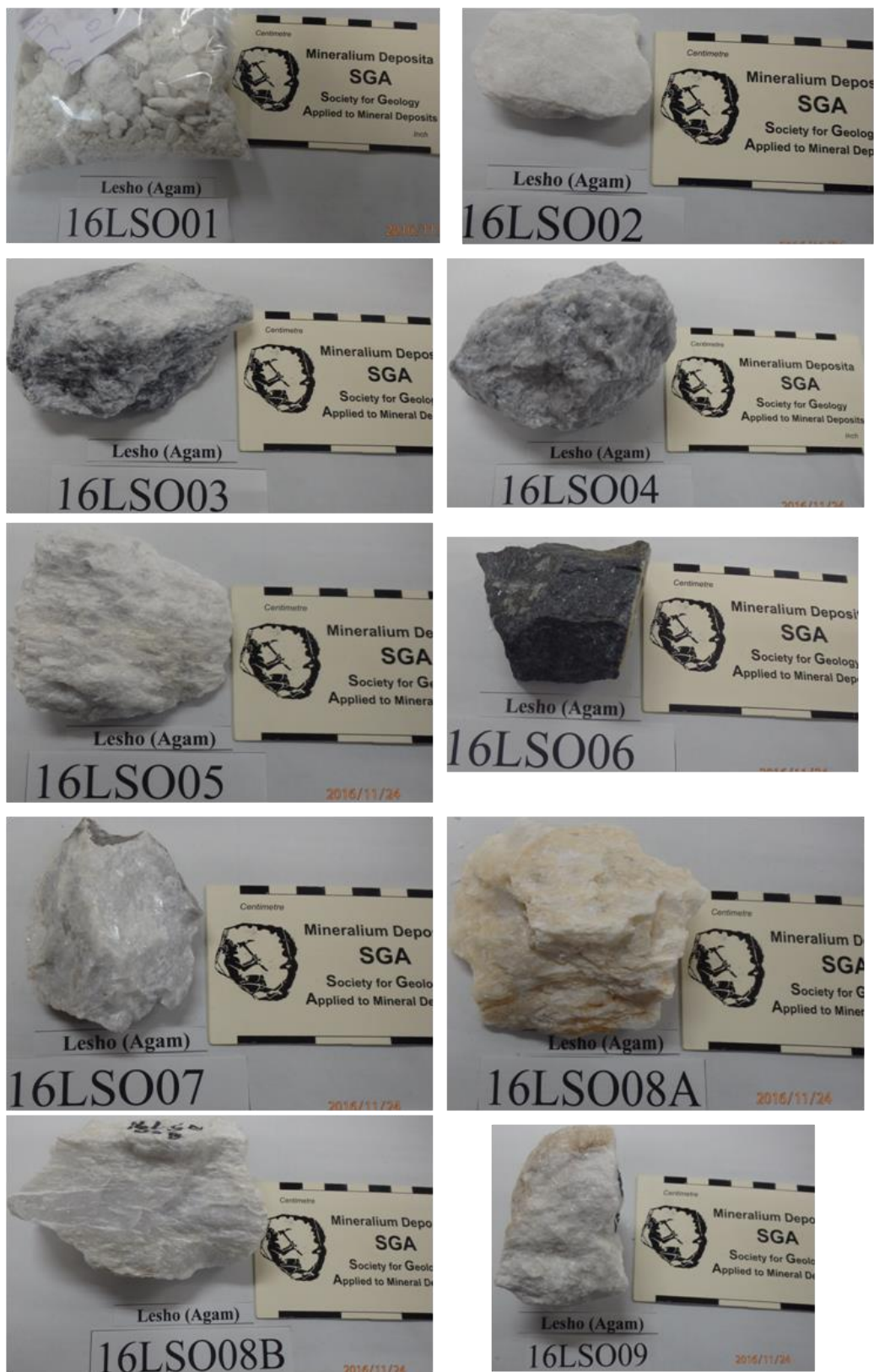
List of samples from Dar deposit.

Carbonate-hosted talc deposits, 2018



List of samples from Wachalgad prospect.

Carbonate-hosted talc deposits, 2018



List of samples from Lesho deposit.

Carbonate-hosted talc deposits, 2018



List of samples from Sargare prospect.

Carbonate-hosted talc deposits, 2018



List of samples from Mamond dara deposit.

Carbonate-hosted talc deposits, 2018

Appendix 2: List of minerals in each rock from each deposit, based on microscopy and XRD.

Kotikhel deposit

No	Samples	Type	Minerals
1	16KTI01	Talc-bearing dolomite marble	Dolomite, Talc, Calcite
2	16KTI02	Talc rock	Talc
3	16KTI03	Dolomite-bearing talc	Talc, Dolomite, Chlorite
4	16KTI04	Talc-bearing dolomite marble	Dolomite, Talc
5	16KTI05	Tremolitite	Tremolite, Dolomite, Talc, Calcite
6	16KTI06	Antigorite	Antigorite, Dolomite, Calcite
7	16KTI07	Dolomite marble	Dolomite, Tremolite, Calcite
8	16KTI08	Talc rock	Talc
9	16KTI09	Gneiss	Quartz, Muscovite
10	16KTI10	Talc rock	Talc
11	16KTI11	Quartz vein	Quartz, Talc

Janinaw deposit

No	Sample	Type	Mineral
1	14AF13A	Talc rock	Talc, Cordierite
2	14AF13B	Tremolite-bearing talc	Talc, Tremolite
3	14AF14	Dolomite marble	Calcite, Tremolite, Dolomite, Diopside
4	14AF15	Talc rock	Talc
5	14AF16	Tremolite-bearing talc	Talc, Tremolite, Dolomite, Diopside
6	14AF17	Talcose quartz vein	Talc, Qtz., Chlorite, Titanite

Kherwasti deposit

No	Sample	Type	Minerals
1	14AF06A	Magnesite rock	Magnesite, Zoisite, Chloro-apatite
2	14AF06B	Talc rock	Talc
3	14AF07A	Magnesite rock	Magnesite, Calcite
4	14AF07B	Magnesite-bearing talc	Talc, Magnesite
5	14AF08	Talc-bearing magnesite	Magnesite, Olivine, Chlorite, Apatite, Talc
6	14AF09	Altered diorite	Chlorite, Quartz., Plagioclase, Opaque mineral, Epidote
7	14AF10	Talc rock	Talc
8	14AF11	Tremolitite	Tremolite
9	14AF12	Tremolitite	Tremolite
10	16KHTI01A	Talc-bearing magnesite	Magnesite, Talc
11	16KHTI01B	Amphibolite	Quartz, Hornblende, Calcite, Chlorite
12	16KHTI01C	Talc-bearing magnesite	Magnesite, Talc
13	16KHTI01D	Talc rock	Talc
14	16KHTI01E	Tremolitite	Tremolite, Talc
15	16KHTI02A	Antigorite	Antigorite
16	16KHTI02B	Magnesite rock	Magnesite, Dolomite, Antigorite
17	16KHTI02C	Fine grained dolomite	Dolomite
18	16KHTI02D	Clinocllore	Clinocllore, Albite
19	16KHTI03	Dolomite marble	Dolomite, Calcite, Tremolite

Carbonate-hosted talc deposits, 2018

Anarokas deposit

No	Sampl	Type	Minerals
1	16ANK01	Gneiss	Quartz, Plagioclase, Biotite, Muscovite
2	16ANK02	Gneiss	Quartz, Biotite
3	16ANK03A	Magnesite rock	Magnesite, Dickite
4	16ANK03B	Amphibolite	Quartz, Chlorite, Epidote
5	16ANK04A	Talc-bearing magnesite	Talc, Magnesite, Lizardite
6	16ANK04B	Talc-bearing dolomite marble	Talc, Dolomite, Antigorite
7	16ANK05A	Talc rock	Talc
8	16ANK05B	Talc-bearing magnesite	Magnesite, Talc
9	16ANK05C	Altered carbonate rock	Lizardite, Talc, Magnesite
10	16ANK06	Amphibolite	Quartz, Chlorite, Plagioclase
11	16ANK07	Quartz vein	Quartz, Plagioclase
12	16ANK08A	Talc rock	Talc
13	16ANK08B	Talc-bearing magnesite	Magnesite, Talc
14	16ANK09	Tremolite	Tremolite
15	16ANK10	Talc-bearing dolomite marble	Magnesite, Talc
16	16ANKG01	Granite	Quartz, Plagioclase, Microcline, Biotite, Muscovite
17	16ANKG02	Quartz vein	Quartz
18	16ANKG03	Gneiss	Quartz, Muscovite, Biotite

Dar deposit

No	Sample	Type	Minerals
1	14AF01A	Chlorite	Chlorite, Ilmenite
2	14AF01B	Serpentinite	Vermiculite, Lizardite, Olivine, Pyroxene, Calcite
3	14AF01C	Talc-bearing magnesite	Magnesite, Forsterite, Talc, Pyroxene
4	14AF02A	Altered dolerite	Quartz, Mica, Plagioclase, Opaque minerals, Chlorite, Titanite, Rhodocrosite
5	14AF02B	Talc-bearing magnesite	Magnesite, Talc, Clay minerals
6	14AF02C	Tremolite-bearing talc	Talc, Tremolite
7	14AF02D	Dolerite	Plagioclase (anorthite by XRD), Olivine, Pyroxene
8	14AF02E	Talc rock	Talc
9	14AF03	Talc-bearing magnesite	Magnesite, Talc, Calcite
10	14AF04	Tremolite-bearing talc	Talc, Tremolite
11	14AF05A	Magnesite-bearing talc	Talc, Magnesite, Tremolite
12	14AF05B	Talc rock	Talc
13	14AF05C	Altered dolerite	Plagioclase, Chlorite, Opaque mineral(Pyrite), Natrolite
14	14AF05D	Talc-bearing magnesite	Magnesite, talc
15	16DAR01A	Talc-bearing magnesite	Magnesite, Talc
16	16DAR01B	Talc-bearing magnesite	Magnesite, Talc
17	16DAR02A	Dolomite marble	Dolomite, Tremolite
18	16DAR02B	Talc rock	Talc
19	16DAR02C	Tremolite-bearing talc	Talc, Tremolite

Carbonate-hosted talc deposits, 2018

Wachalgad prospect

No	Sample	Type	Minerals
1	16WCD01A	Talc-bearing magnesite	Magnesite, Talc
2	16WCD01B	Talc rock	Talc, Magnesite
3	16WCD02A	Talc-bearing magnesite	Magnesite, Talc, Chlorite
4	16WCD02B	Talc rock	Talc
5	16WCD03A	Talc-bearing magnesite	Magnesite, Talc
6	16WCD03B	Talc rock	Talc
7	16WCD04	Talc rock	Talc
8	16WCD05A	Talc rock	Talc, Magnesite
9	16WCD05B	Talc-bearing magnesite	Magnesite, Talc
10	16WCDGneiss1	Gneiss	Quartz, Biotite, Muscovite, Amphibole
11	16WCDDo	Dolomite marble	Dolomite, Tremolite, Calcite
12	16WCDqtz	Quartz vein	Quartz, Microcline
13	16WCDGneiss2	Gneiss	Quartz, Biotite, Muscovite, Microcline

Lesho deposit

No	Sample	Type	Minerals
1	16LSO01	Talc rock	Talc
2	16LSO02	Talc rock	Talc
3	16LSO03	Talc-bearing magnesite	Magnesite, Talc, Calcite
4	16LSO04	Talc-bearing magnesite	Magnesite, Talc
5	16LSO05	Talc-bearing magnesite	Magnesite, Talc
6	16LSO06	Amphibolite	Chlorite, Quartz, Plagioclase
7	16LSO07	Tremolitite	Tremolite, Dolomite, Calcite
8	16LSO08A	Talc-bearing magnesite	Magnesite, Talc
9	16LSO08B	Talc-bearing dolomite marble	Dolomite, Talc, Tremolite, Calcite
10	16LSO09	Dolomite marble	Dolomite, Tremolite

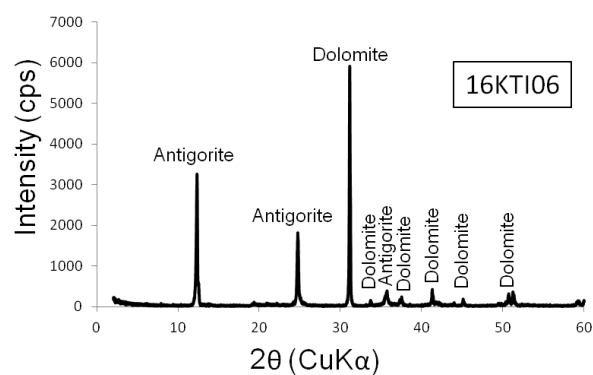
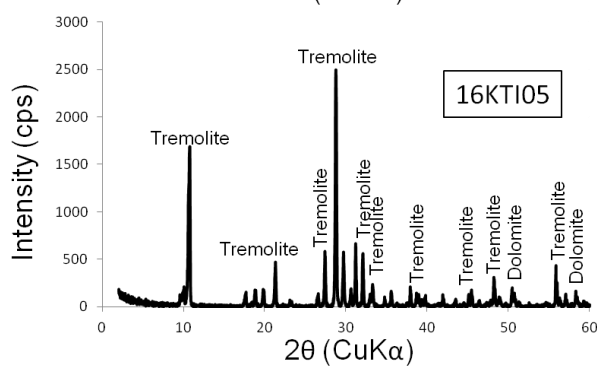
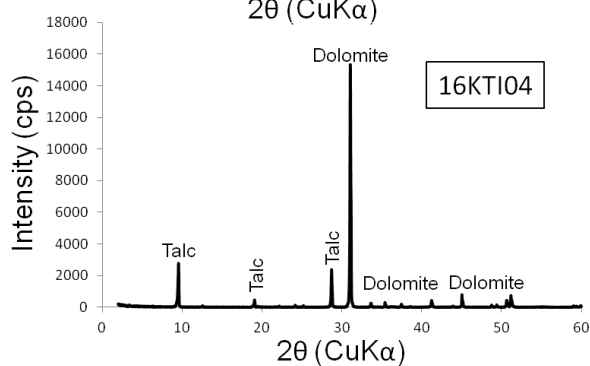
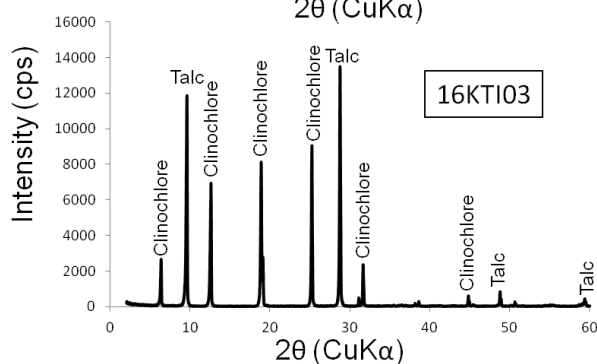
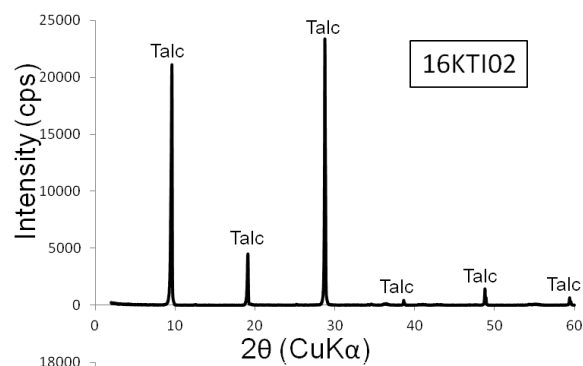
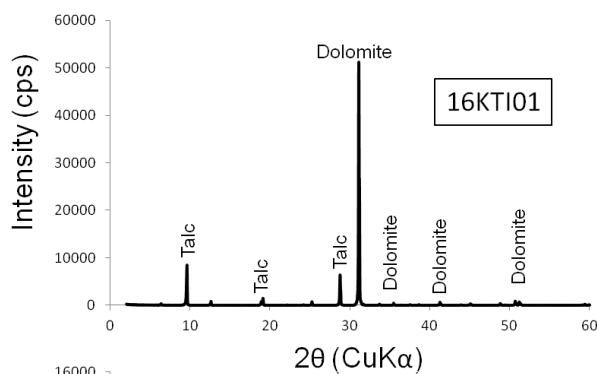
Sargare prospect

No	Sample	Type	Minerals
1	16SRG01	Talc rock	Talc
2	16SRG02	Talc-bearing magnesite	Magnesite, Talc
3	16SRG03	Talc-bearing dolomite marble	Dolomite, Tremolite, Talc

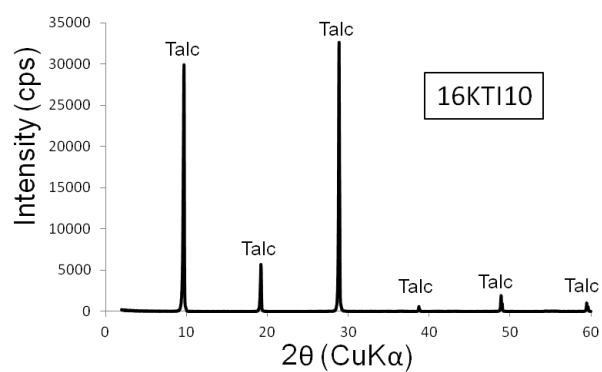
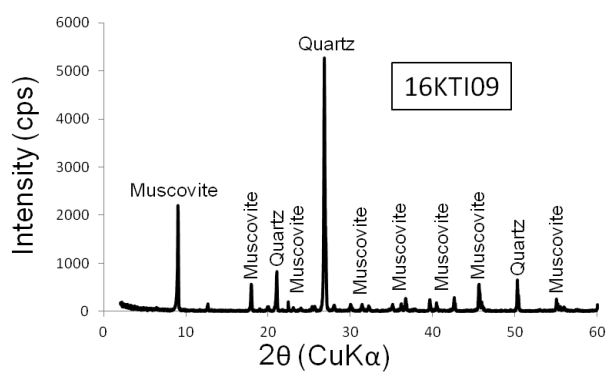
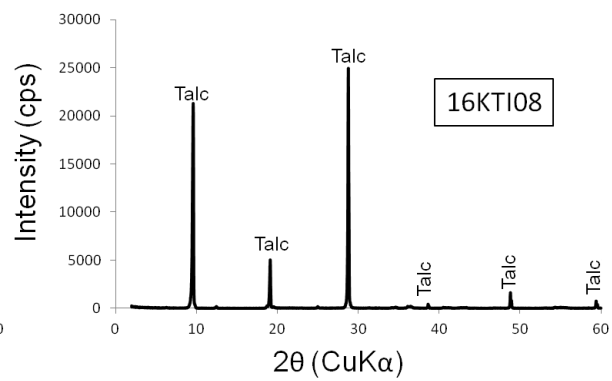
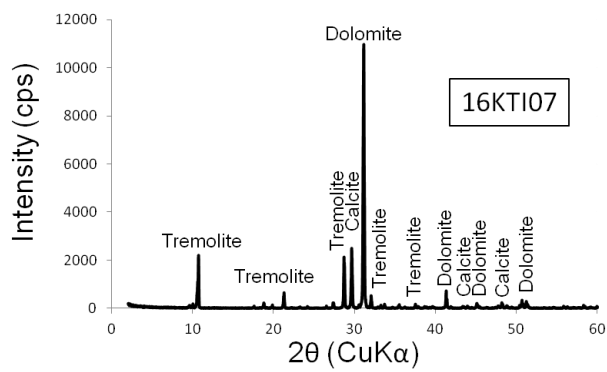
Mamond Dara deposit

No	Sample	Type	Minerals
1	14AF18A	Talc-bearing dolomite marble	Talc, Dolomite (XRD), Quartz, Calcite, Apatite
2	14AF18B	Talc rock	Talc
3	14AF19	Quartz chlorite schist	Quartz, Chlorite
4	14AF20A	Talc-bearing dolomite marble	Talc, Dolomite, Calcite
5	14AF20B	Talc rock	Talc
6	14AF20C	Talc-bearing dolomite marble	Dolomite, Calcite, Quartz, Talc, Chlorite, Apatite
7	14AF21	Schist	Quartz, Feldspar, Actinolite, Biotite
8	14AF22A	Talc rock	Talc
9	14AF22B	Talc rock	Talc

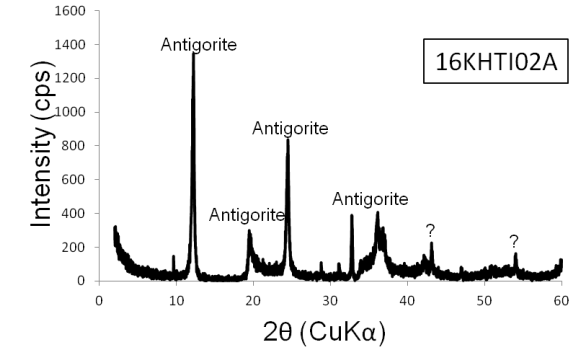
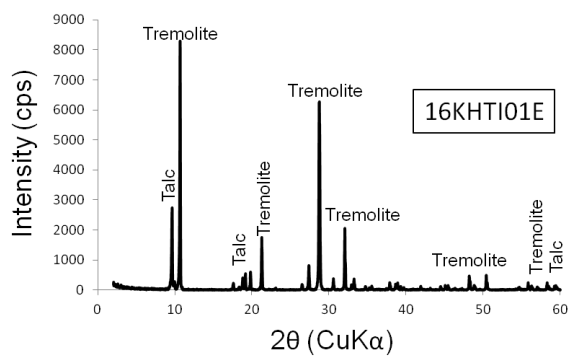
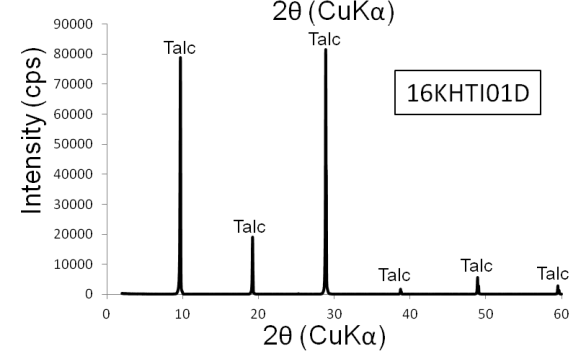
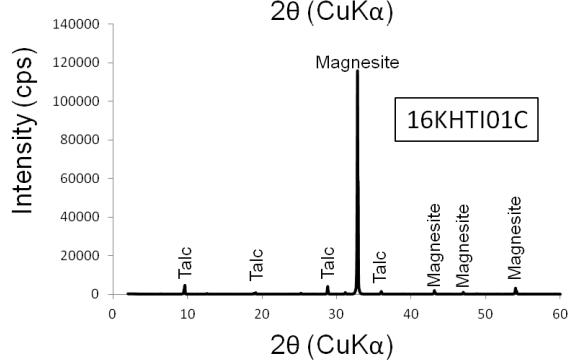
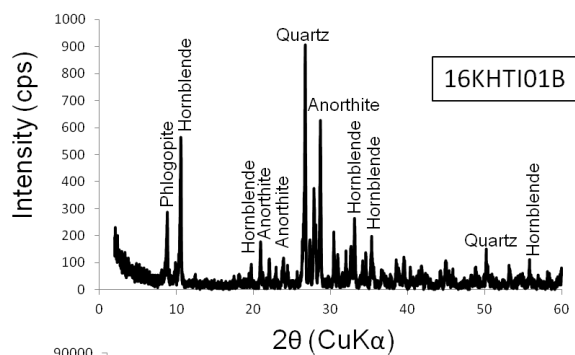
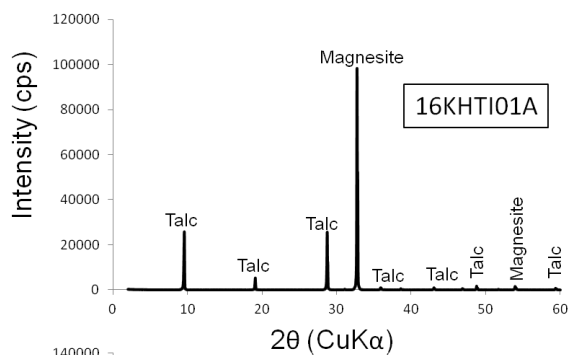
Carbonate-hosted talc deposits, 2018

Appendix 3: List of XRD analyses of each rock from each deposit.➤ **Kotikhel deposit**

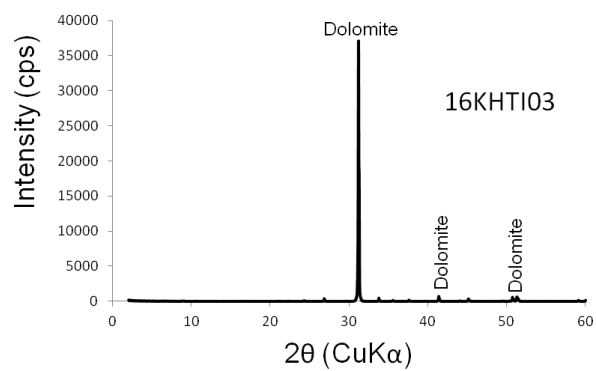
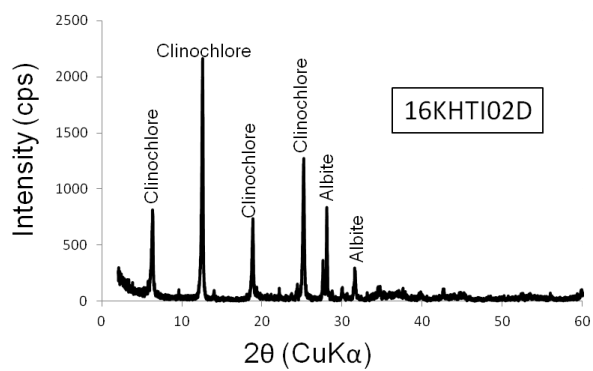
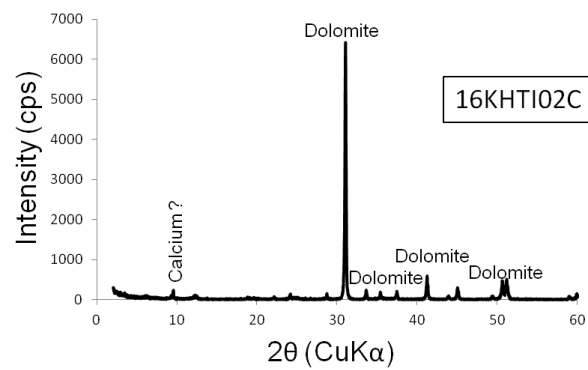
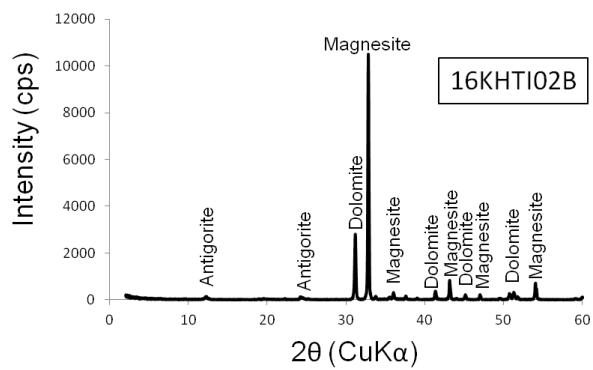
Carbonate-hosted talc deposits, 2018



Carbonate-hosted talc deposits, 2018

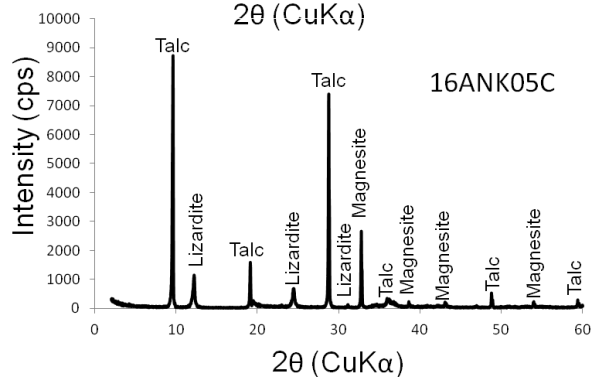
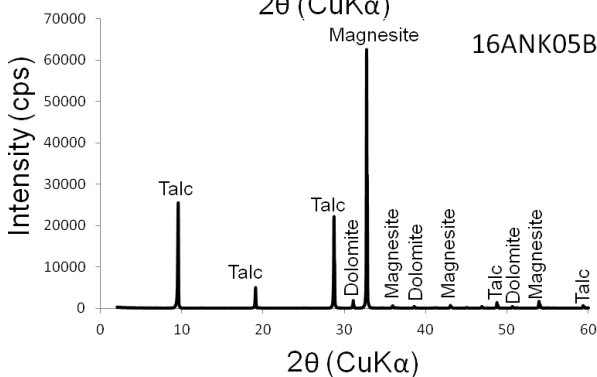
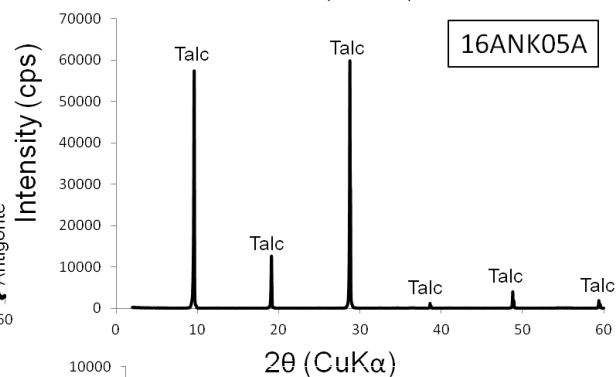
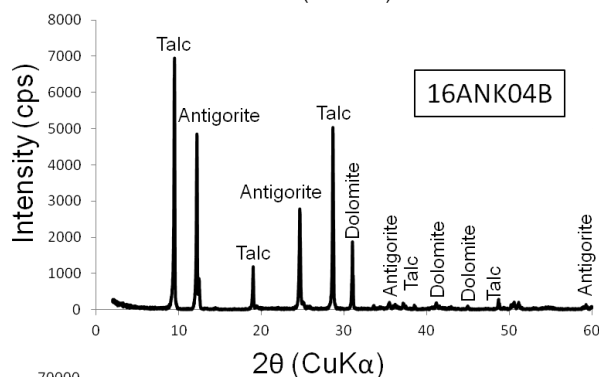
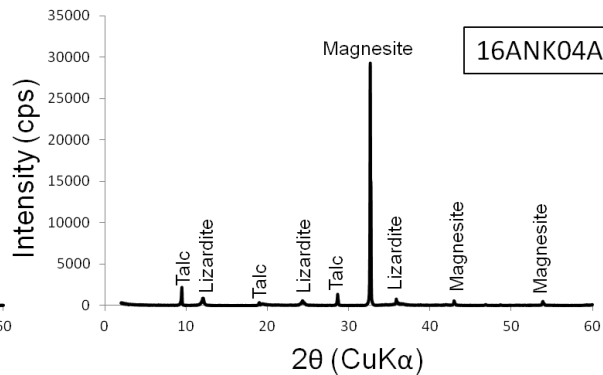
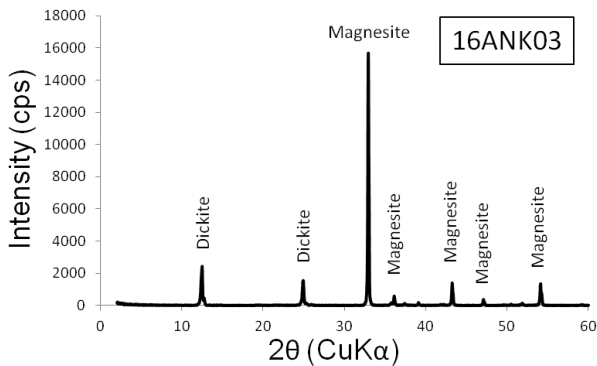
➤ **Kherwasti deposit**

Carbonate-hosted talc deposits, 2018

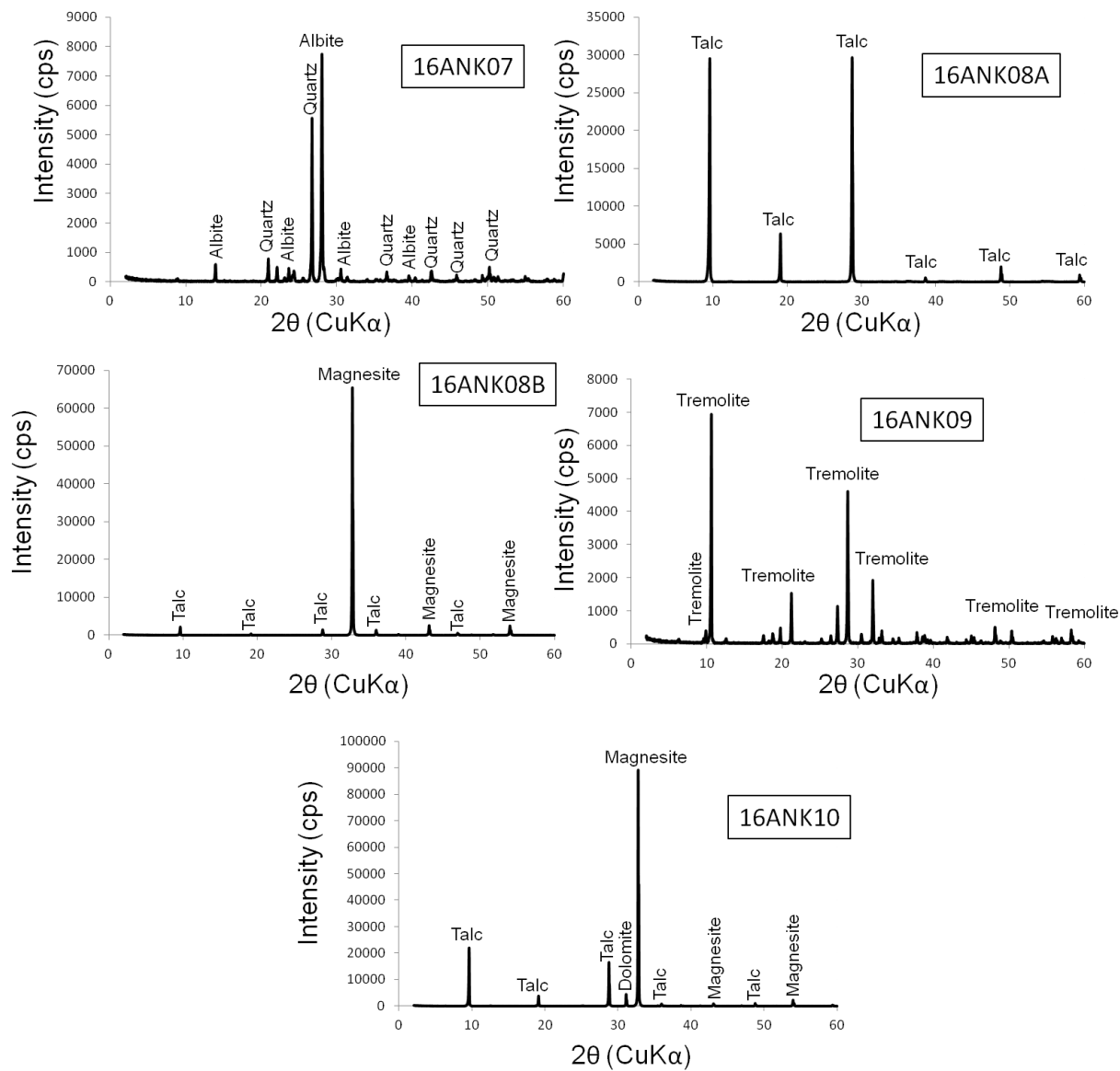


Carbonate-hosted talc deposits, 2018

➤ Anarokas deposit

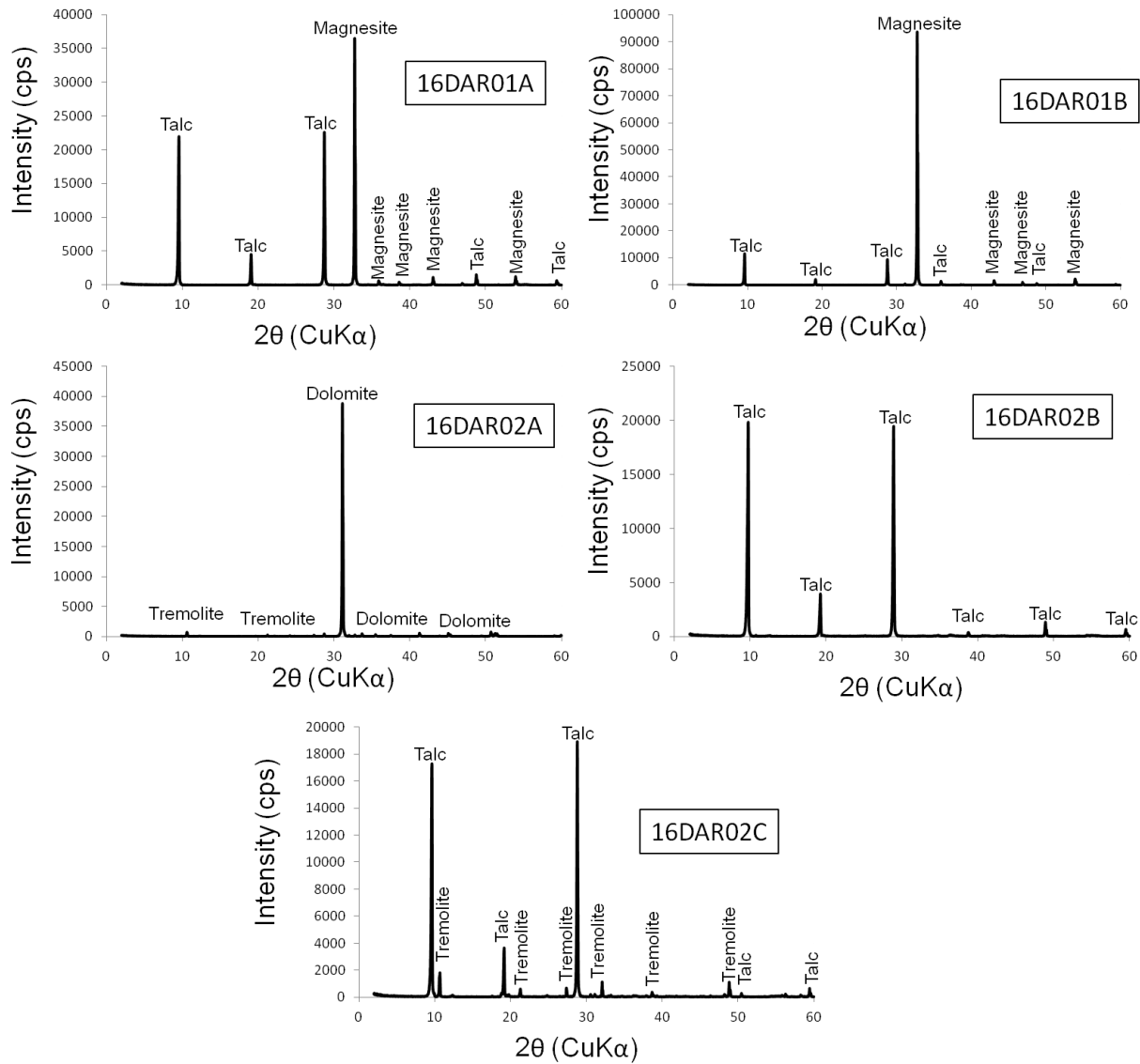


Carbonate-hosted talc deposits, 2018



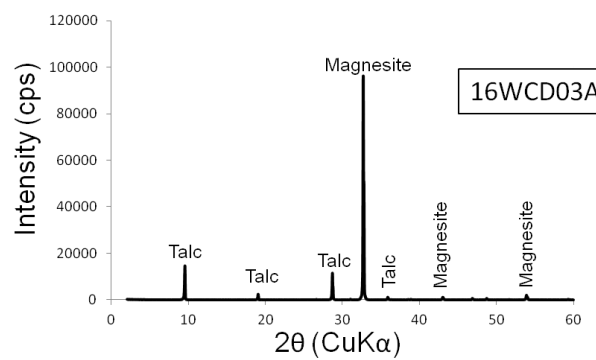
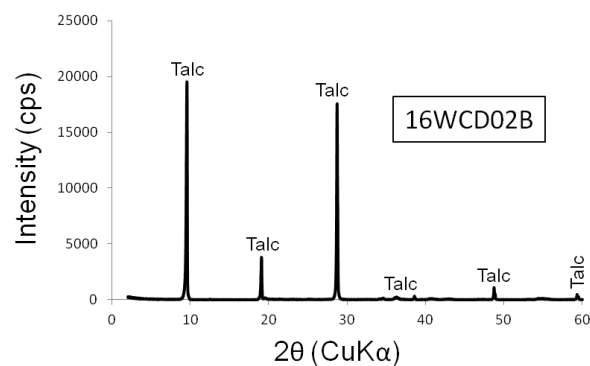
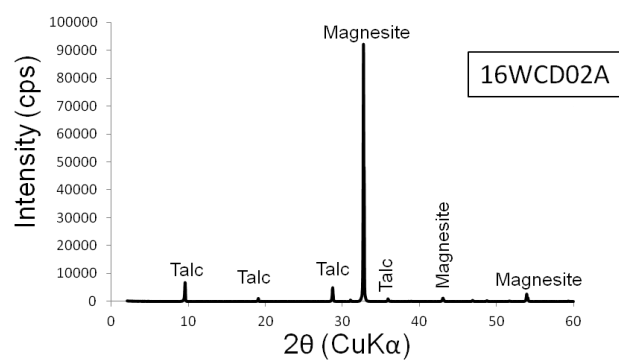
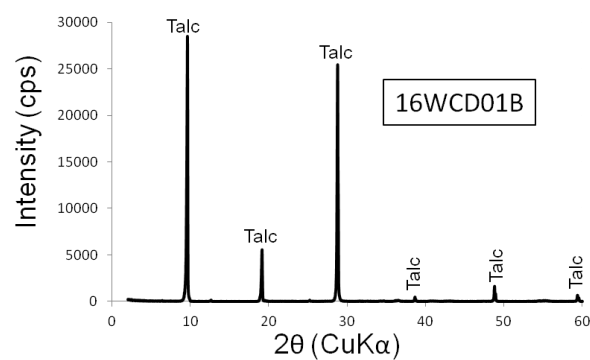
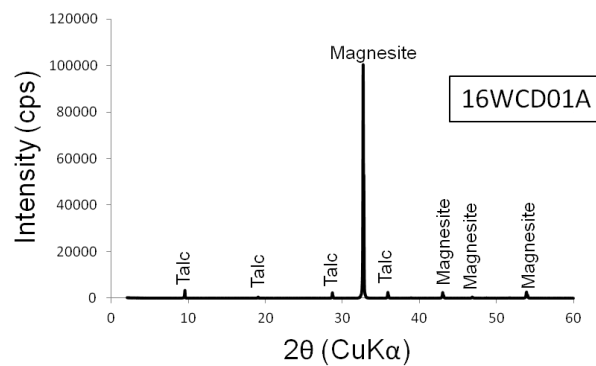
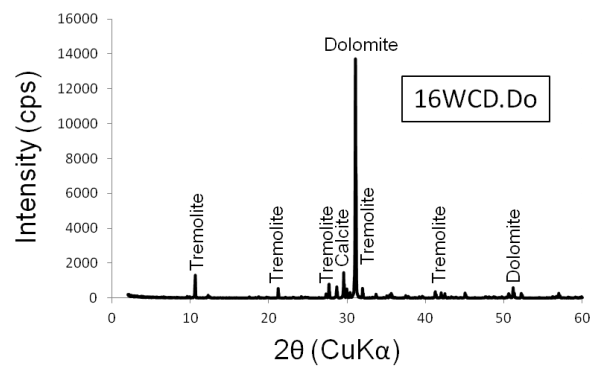
Carbonate-hosted talc deposits, 2018

➤ Dar deposit

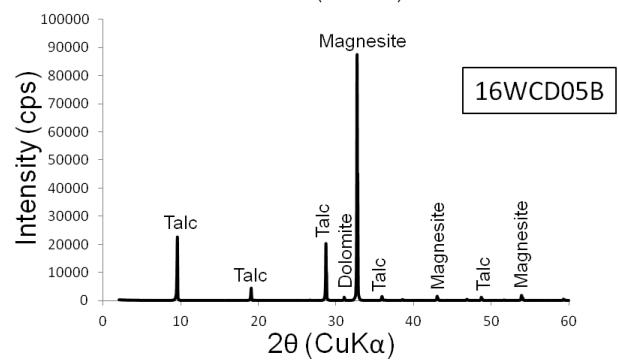
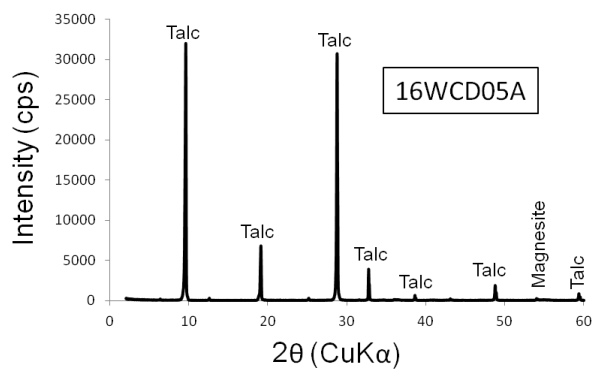
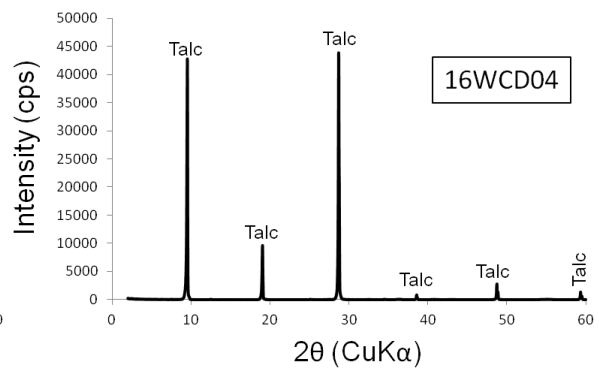
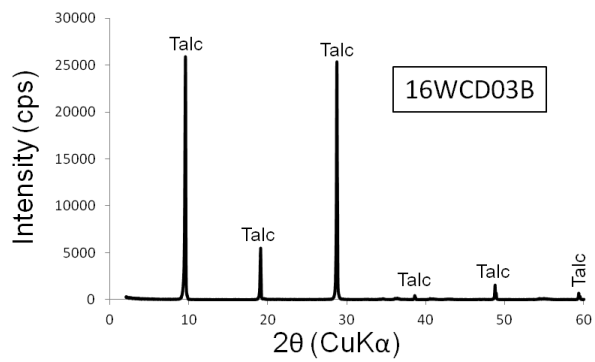


Carbonate-hosted talc deposits, 2018

➤ Wachalgad prospect

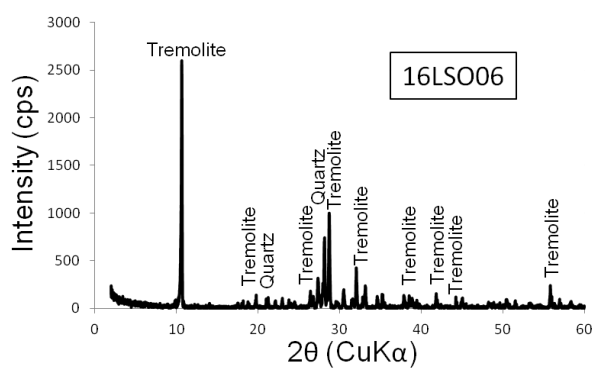
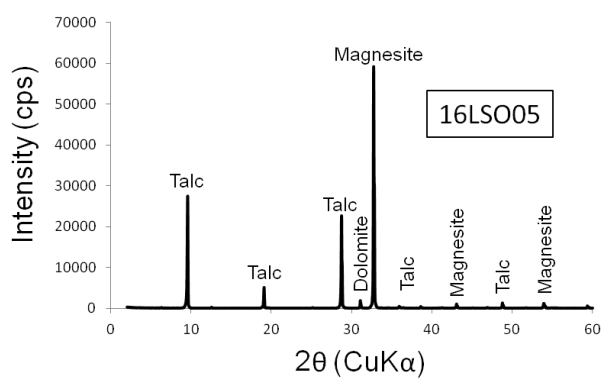
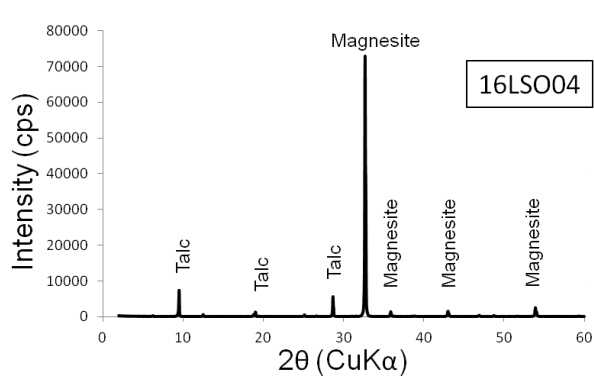
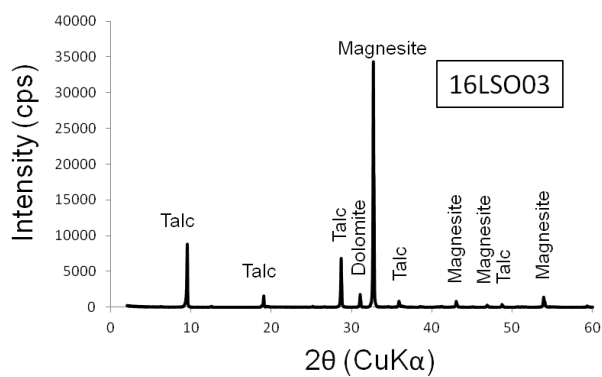
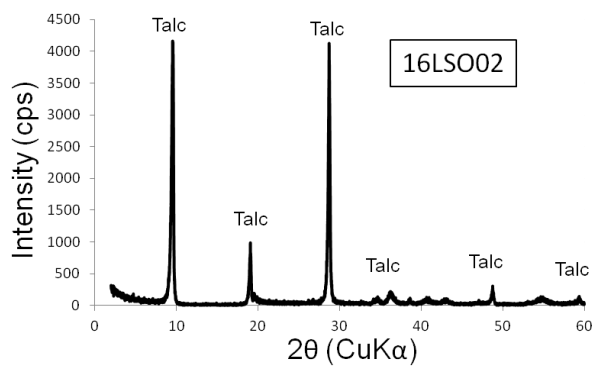
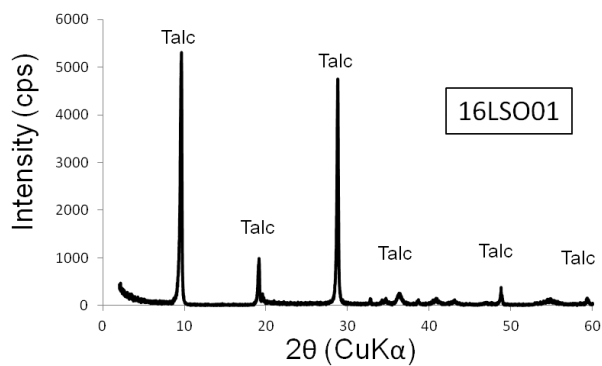


Carbonate-hosted talc deposits, 2018

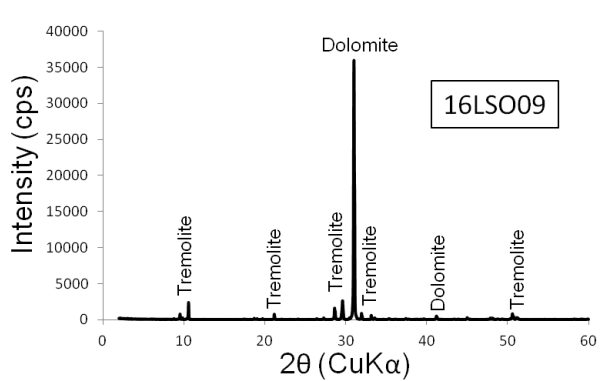
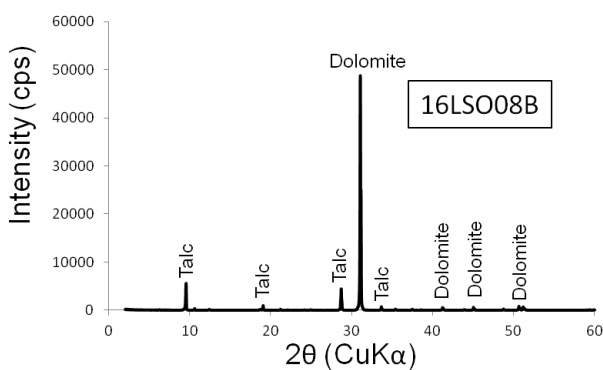
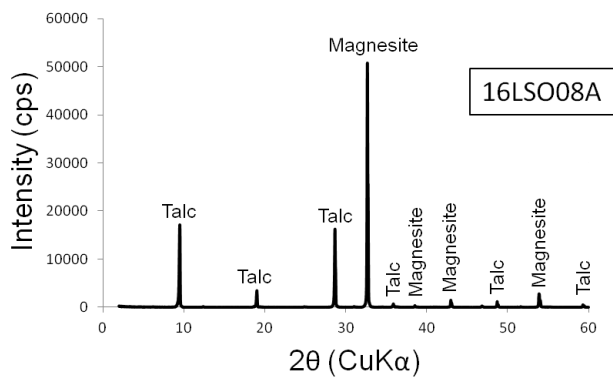
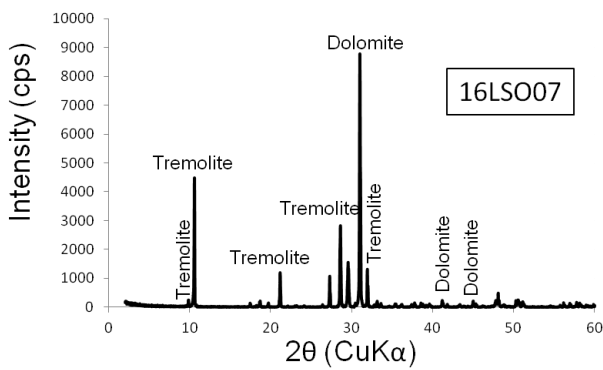


Carbonate-hosted talc deposits, 2018

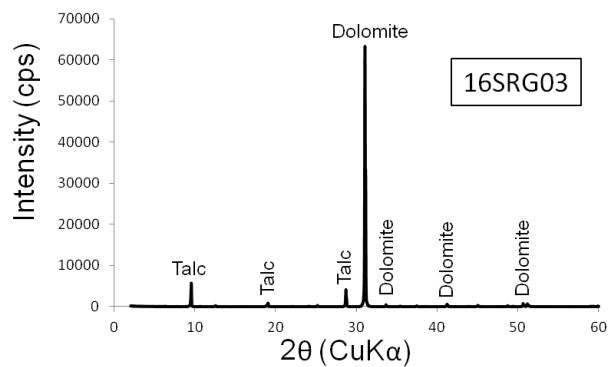
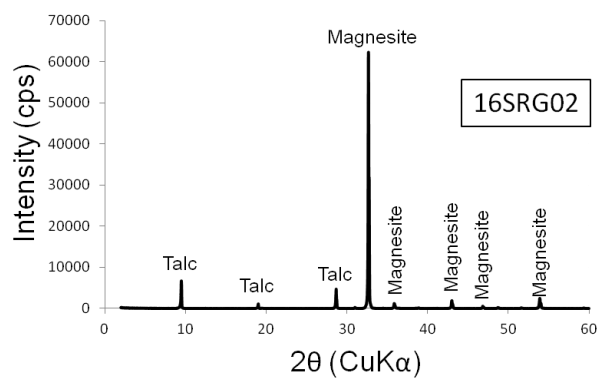
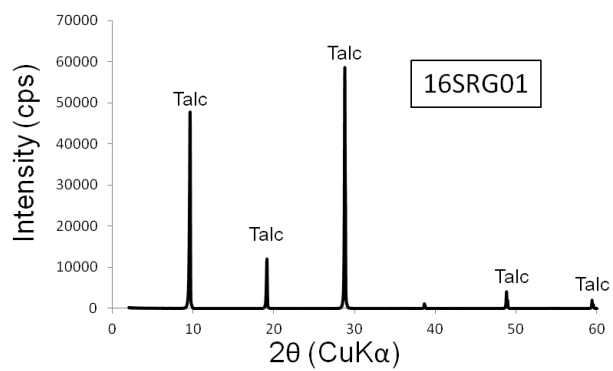
➤ Lesho deposit



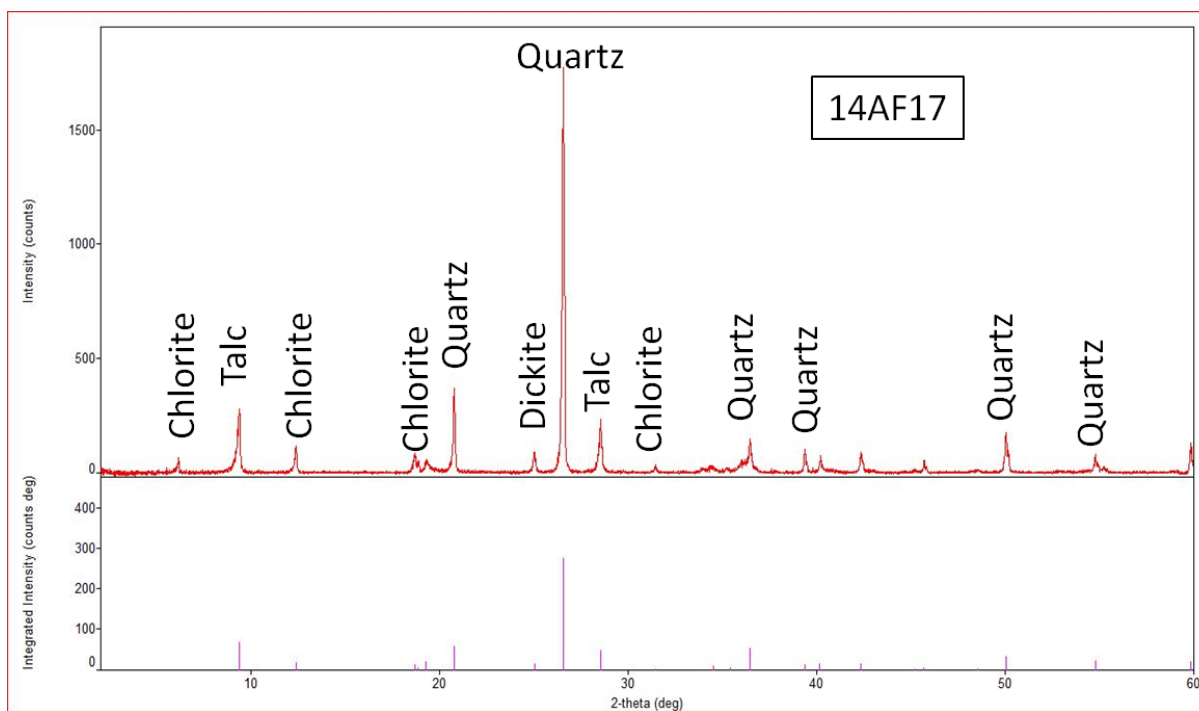
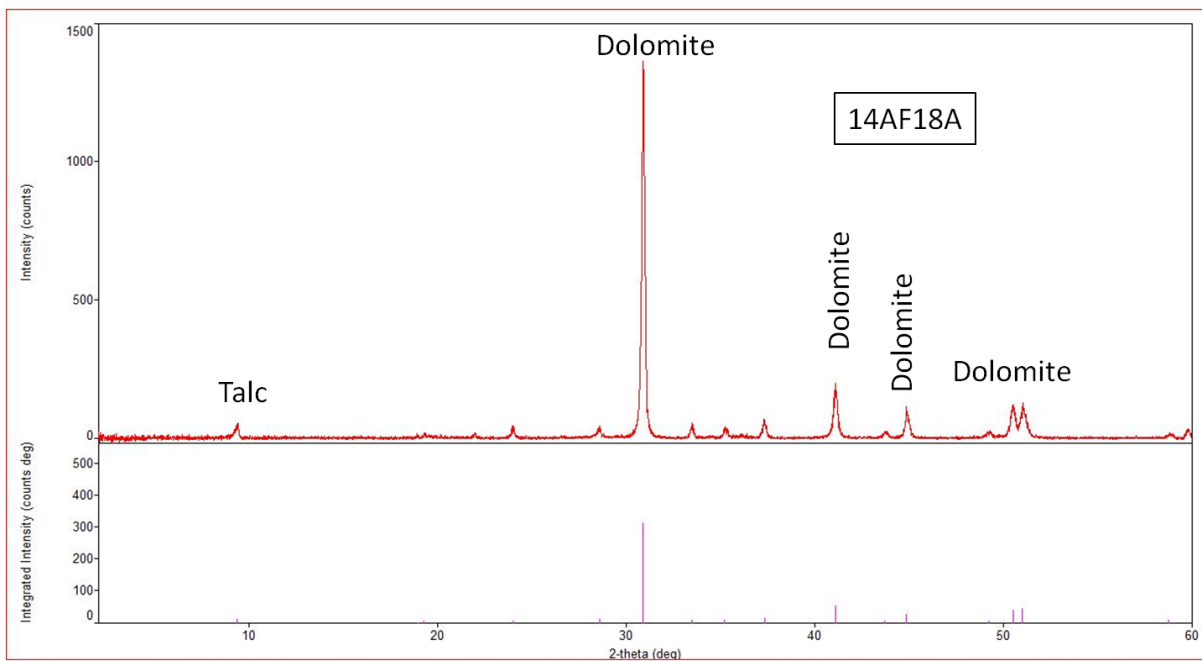
Carbonate-hosted talc deposits, 2018



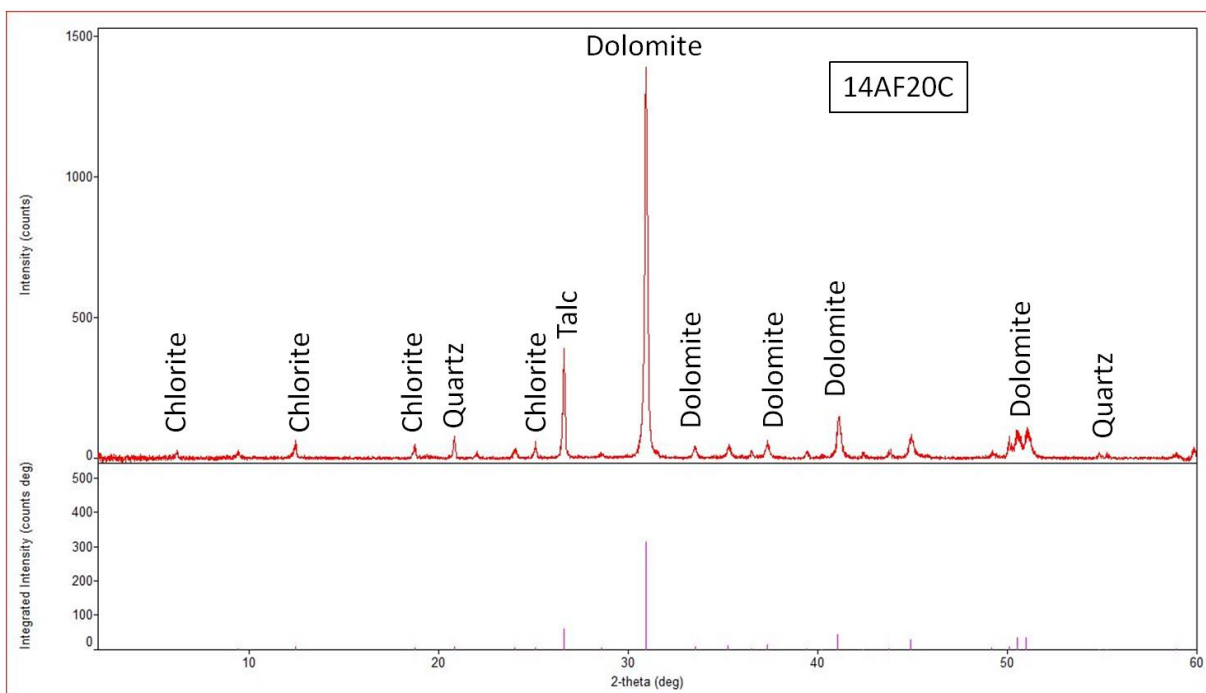
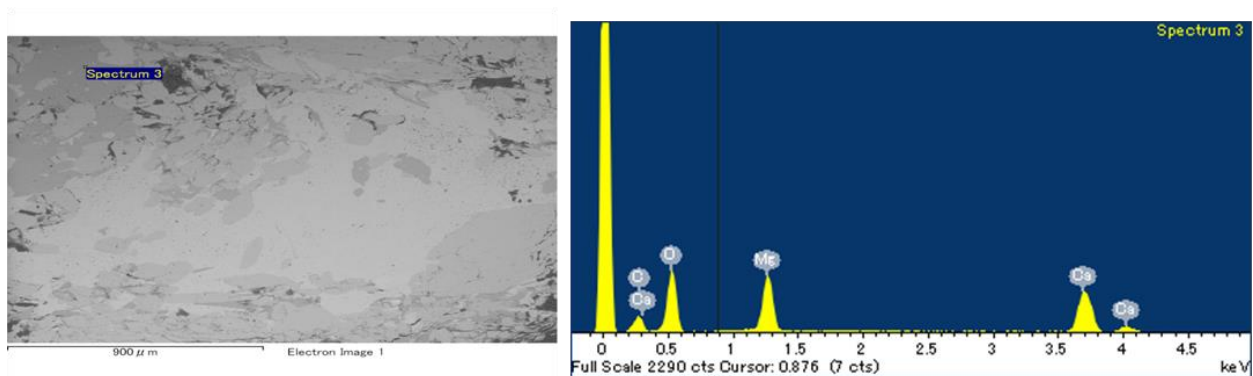
➤ Sargare prospect



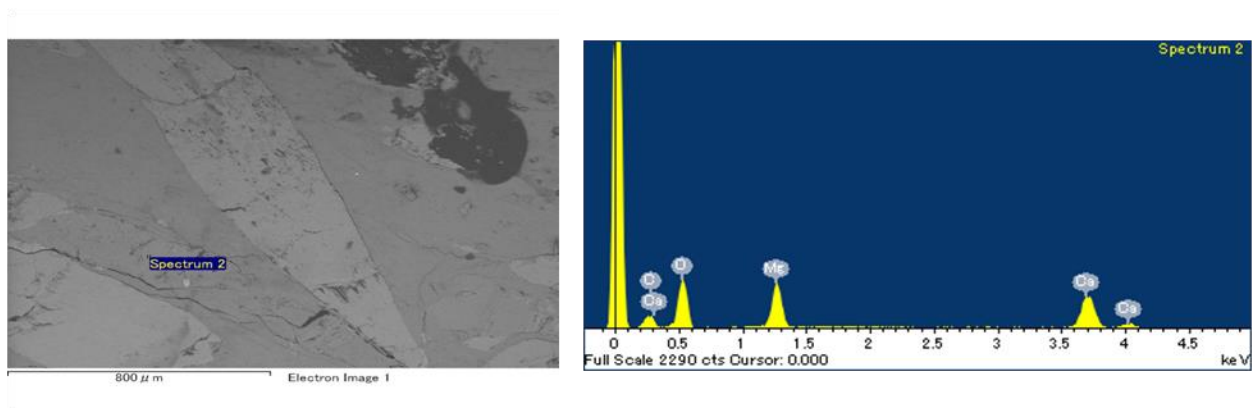
Carbonate-hosted talc deposits, 2018

➤ **Janinaw deposit**➤ **Mamond dara deposit**

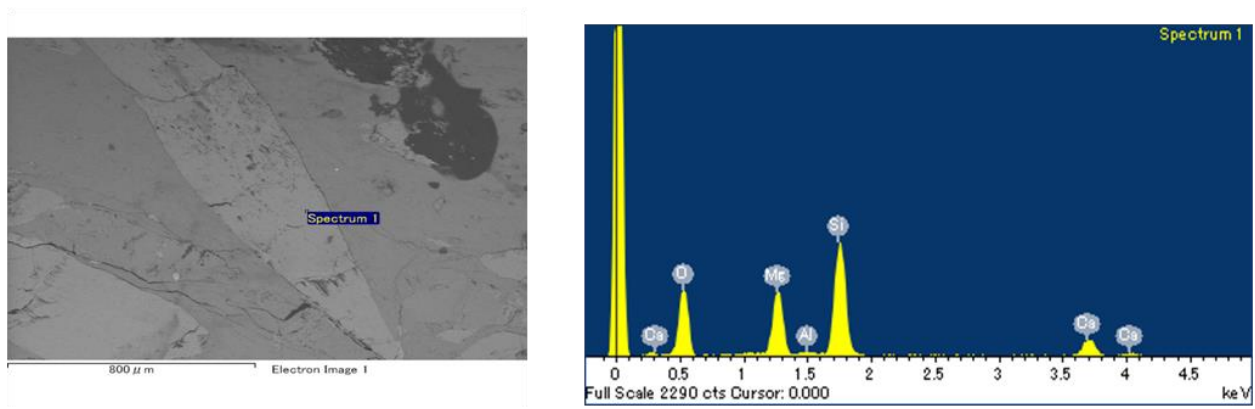
Carbonate-hosted talc deposits, 2018

**Appendix 4:** List of SEM-EDS analyses of different minerals.

SEM-EDX confirmation of dolomite in host rocks (14AF14) from Janinaw deposit.



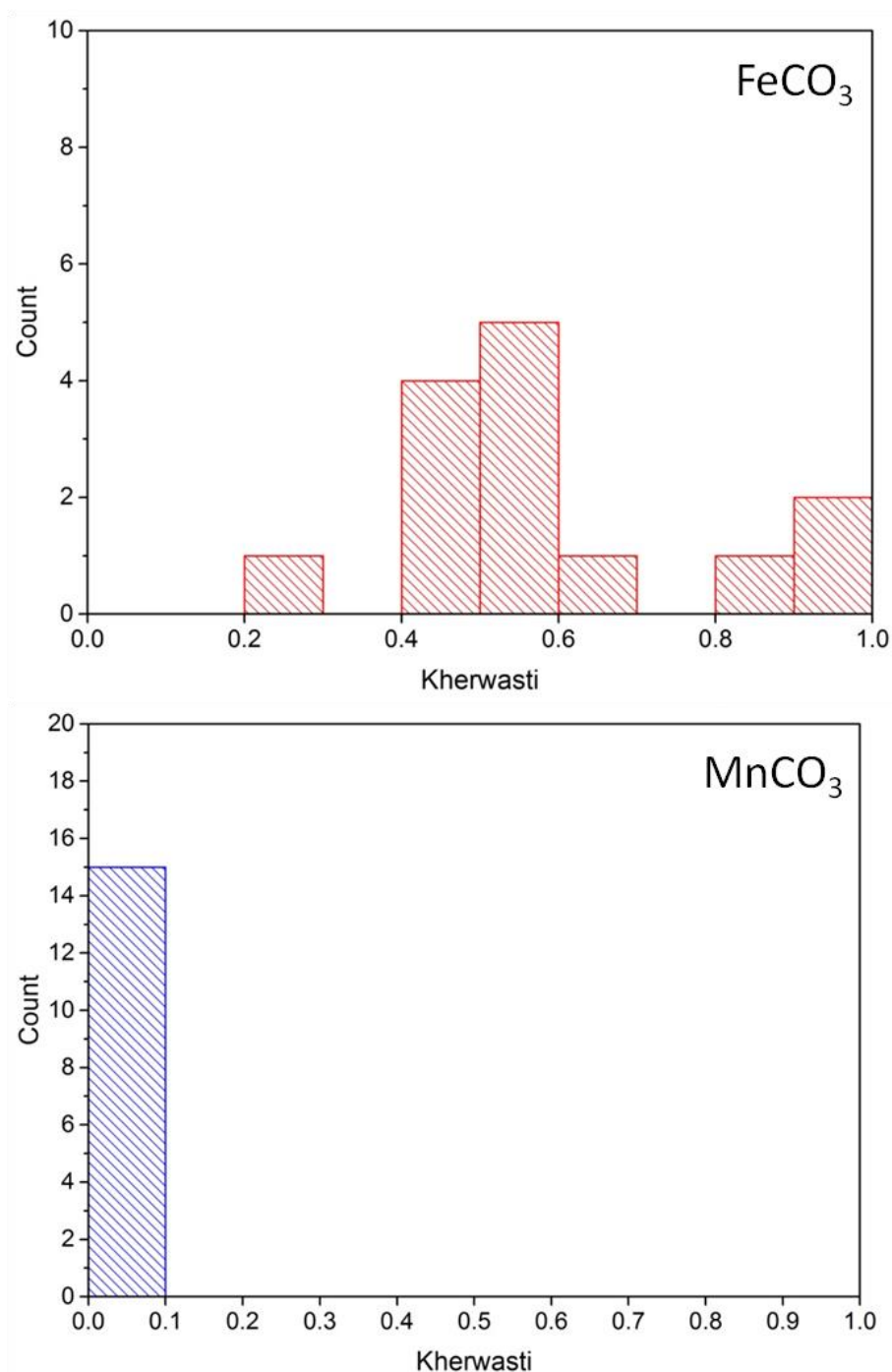
Carbonate-hosted talc deposits, 2018



SEM-EDX confirming tremolite and dolomite in sample 14AF16 from Janinaw deposit.

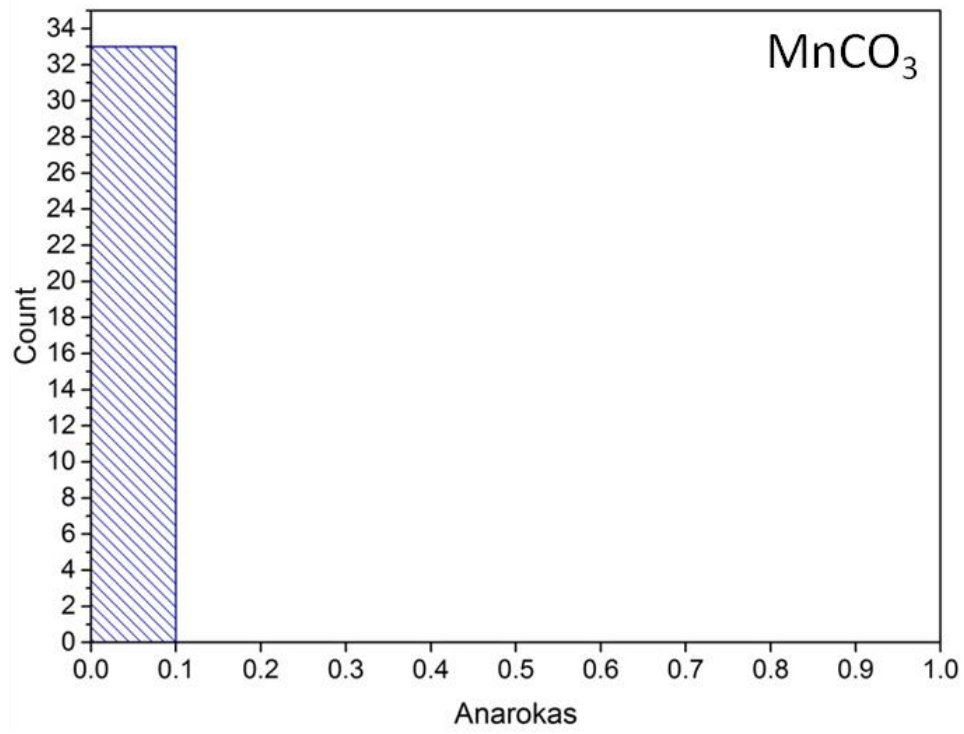
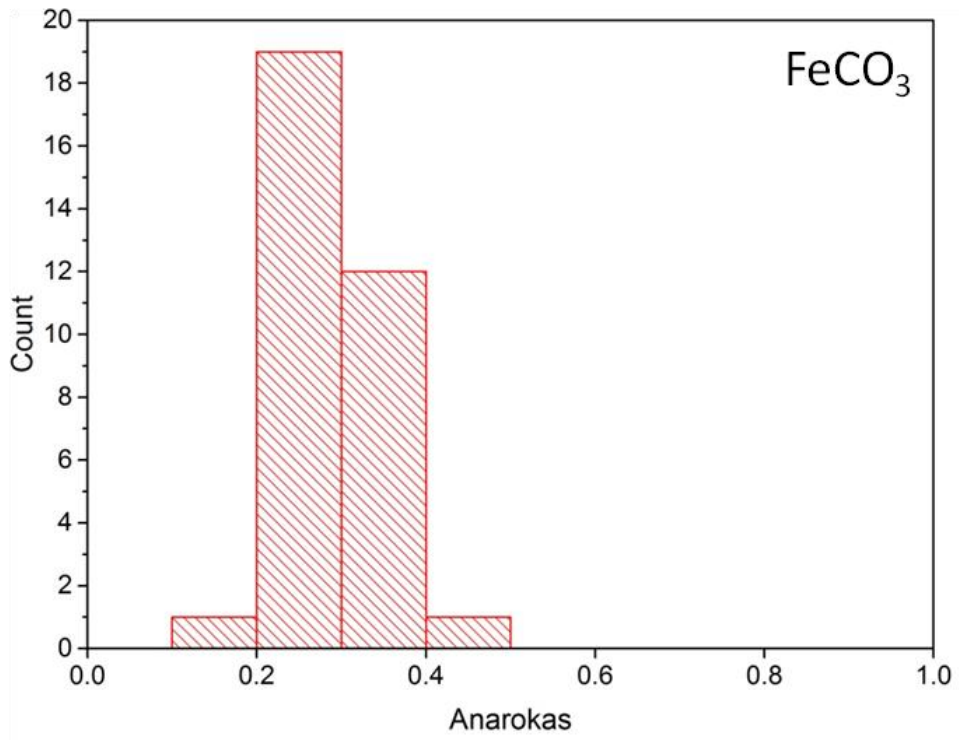
Carbonate-hosted talc deposits, 2018

Appendix 5: Histograms of Fe and Mn concentrations in magnesite, calcite and dolomite minerals from each deposit.

Magnesite mineral

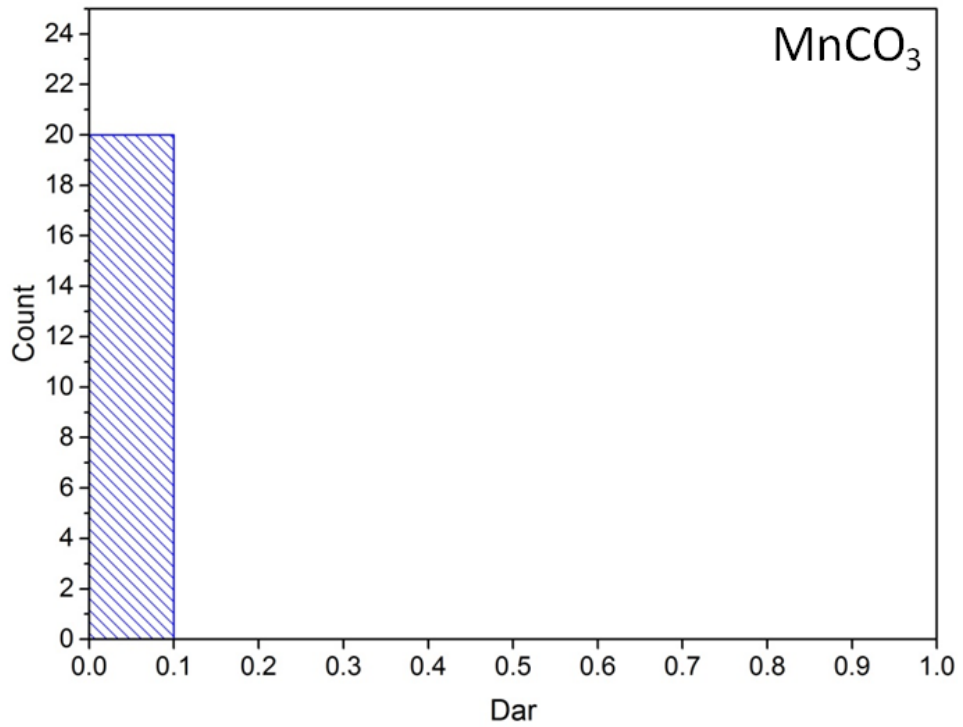
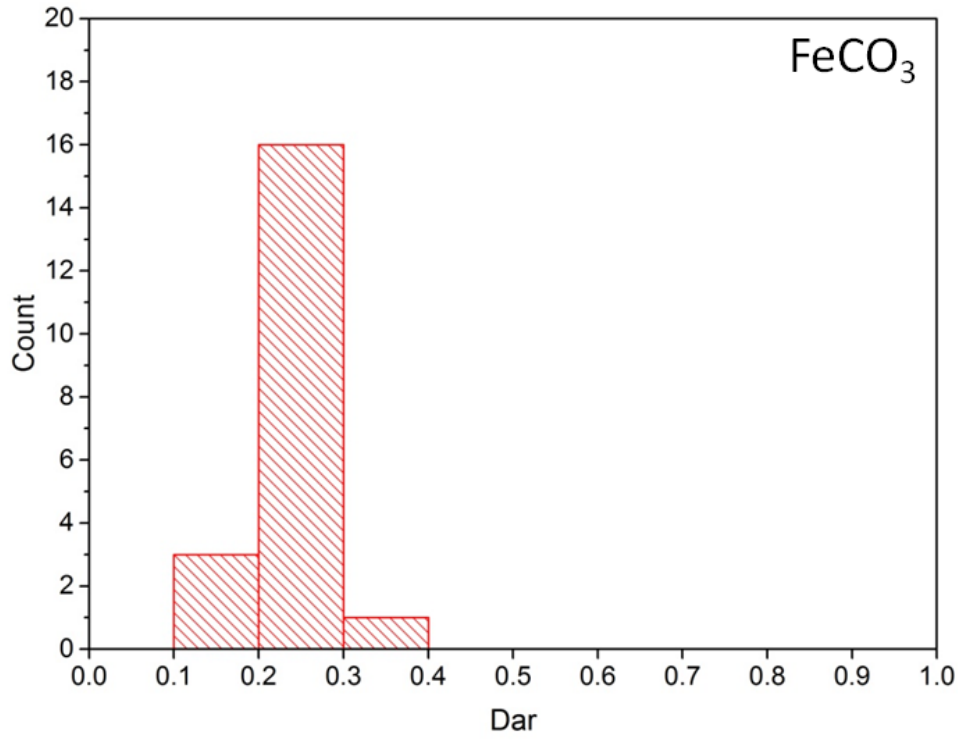
16KHTI01A

Carbonate-hosted talc deposits, 2018



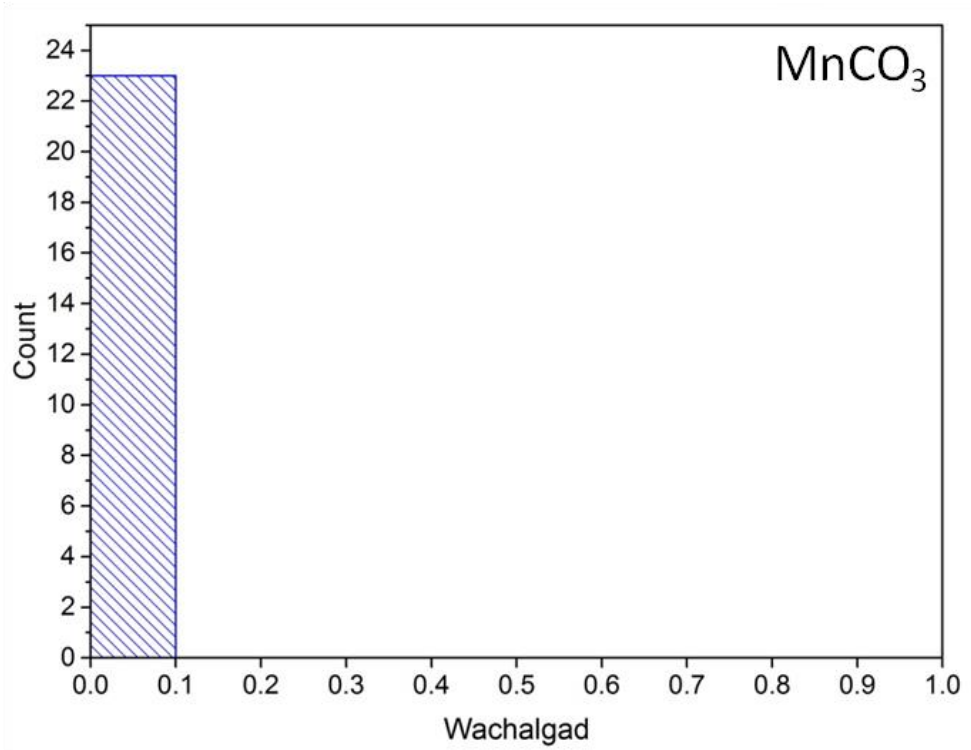
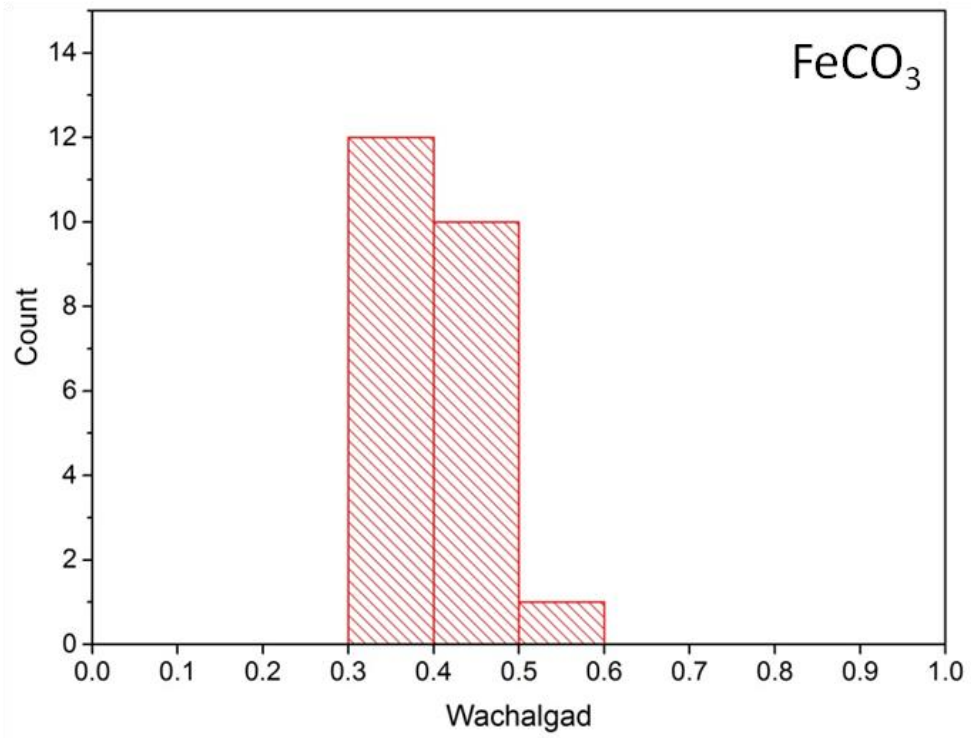
16ANK05B

Carbonate-hosted talc deposits, 2018



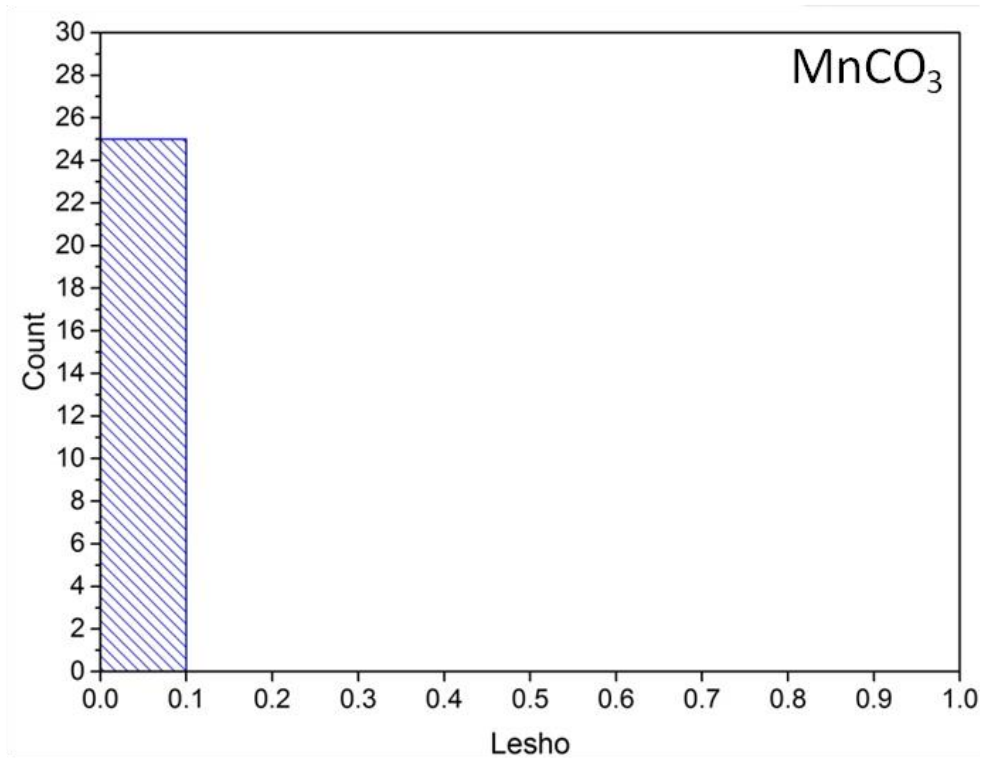
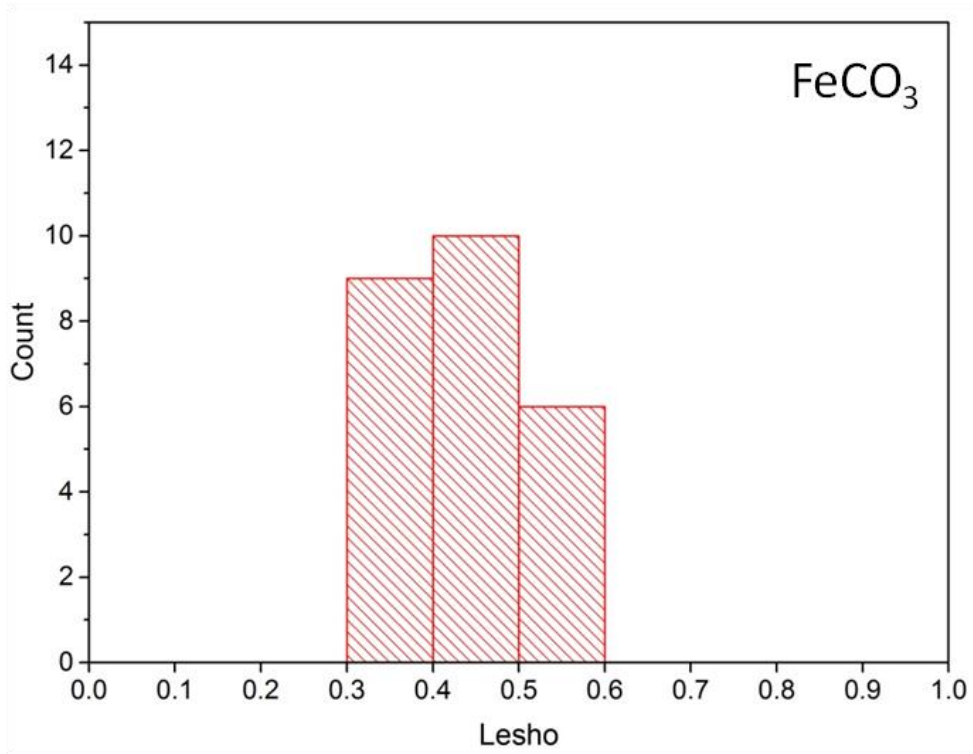
14AF01C

Carbonate-hosted talc deposits, 2018



16WCD02A

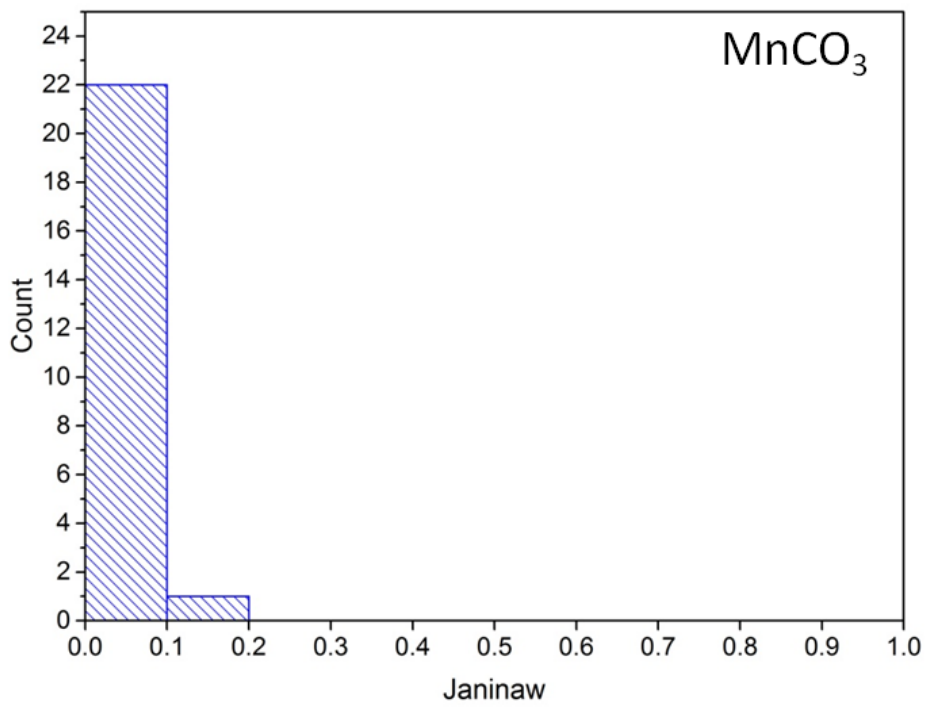
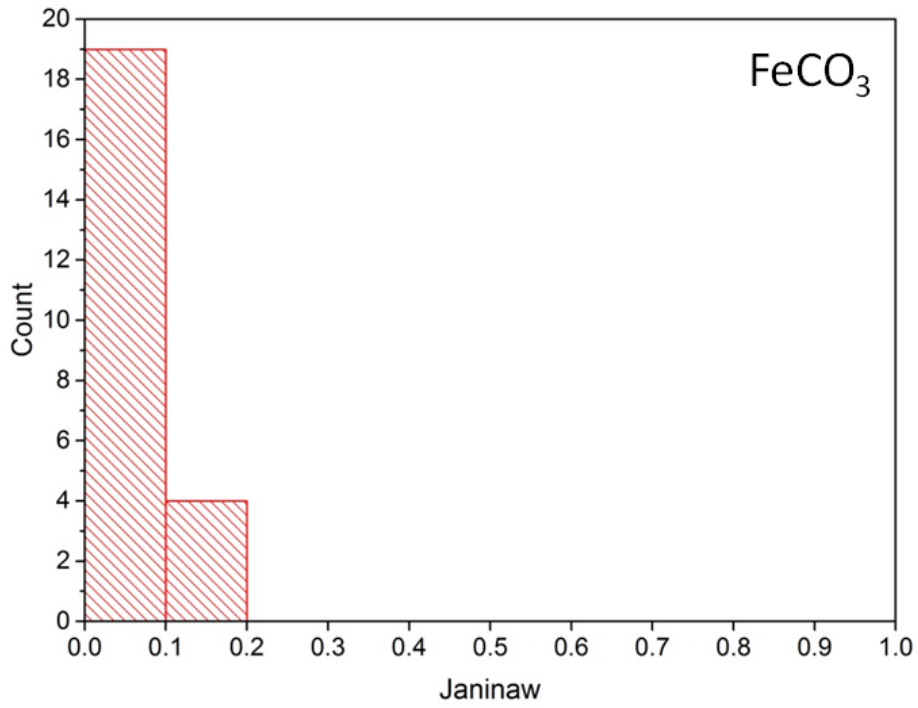
Carbonate-hosted talc deposits, 2018



16LSO03

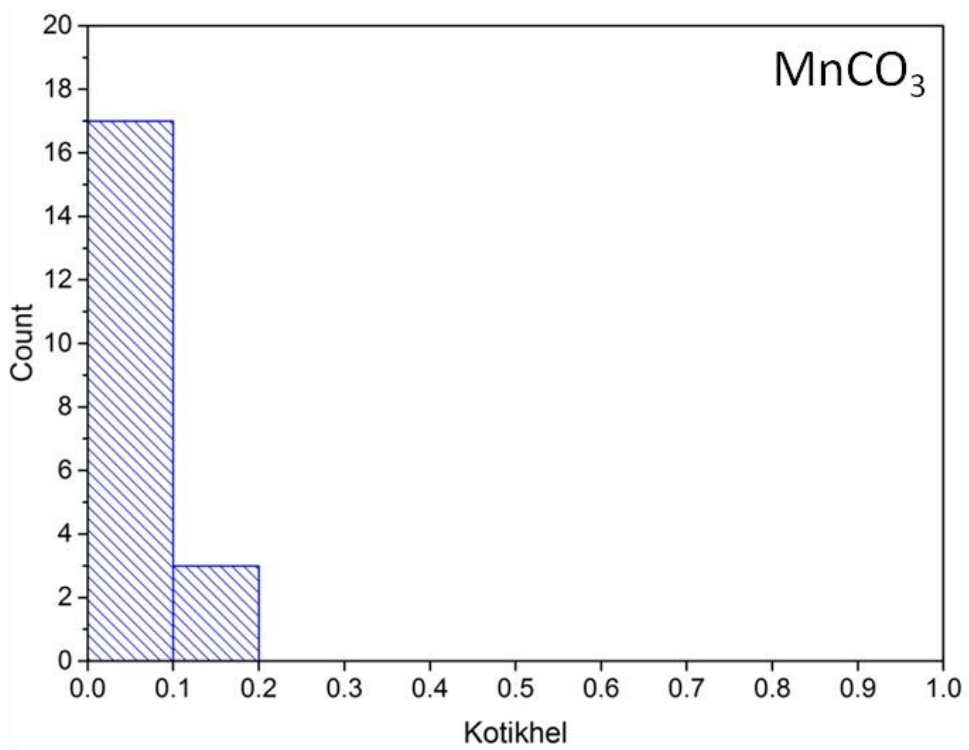
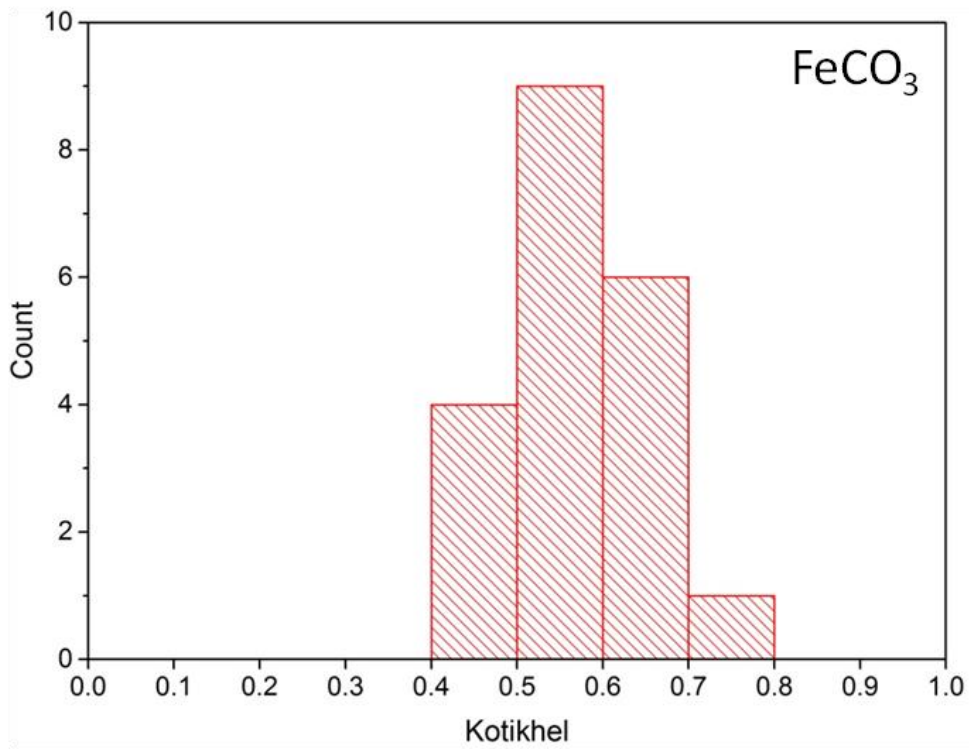
Carbonate-hosted talc deposits, 2018

Calcite mineral



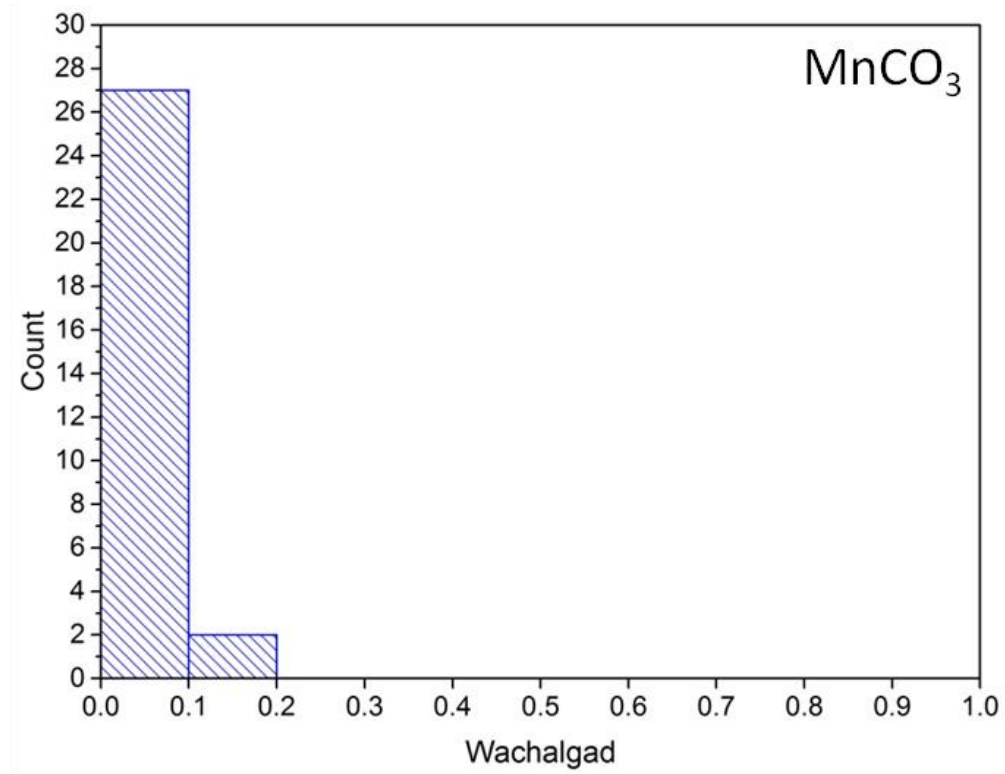
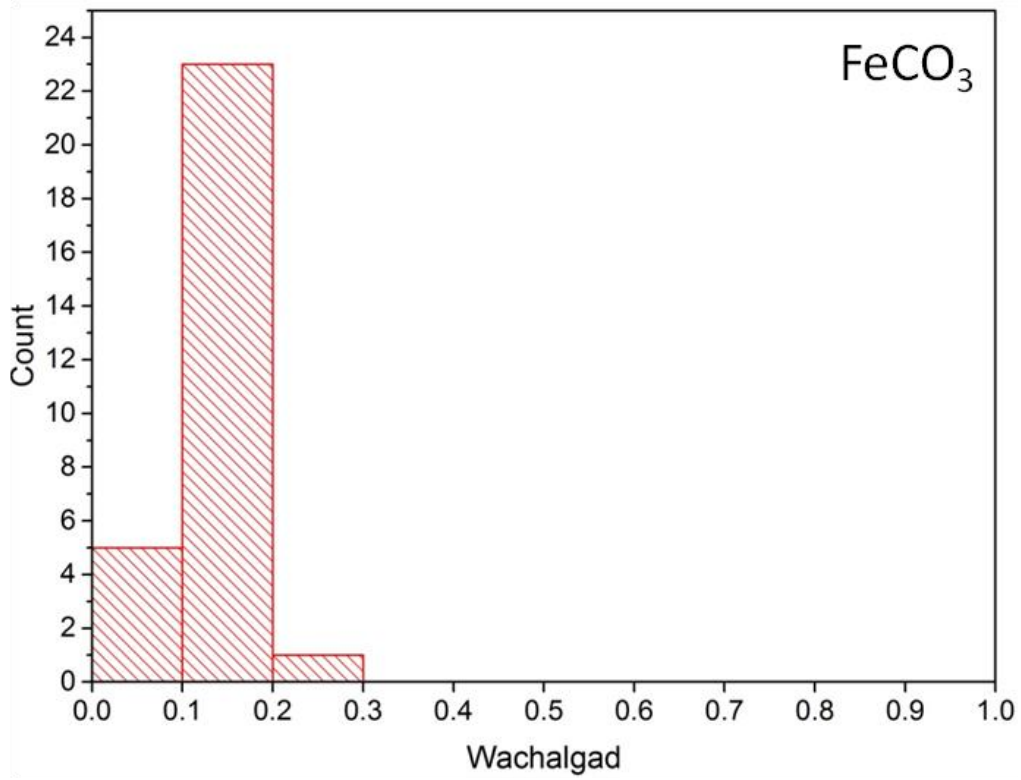
14AF14

Dolomite mineral



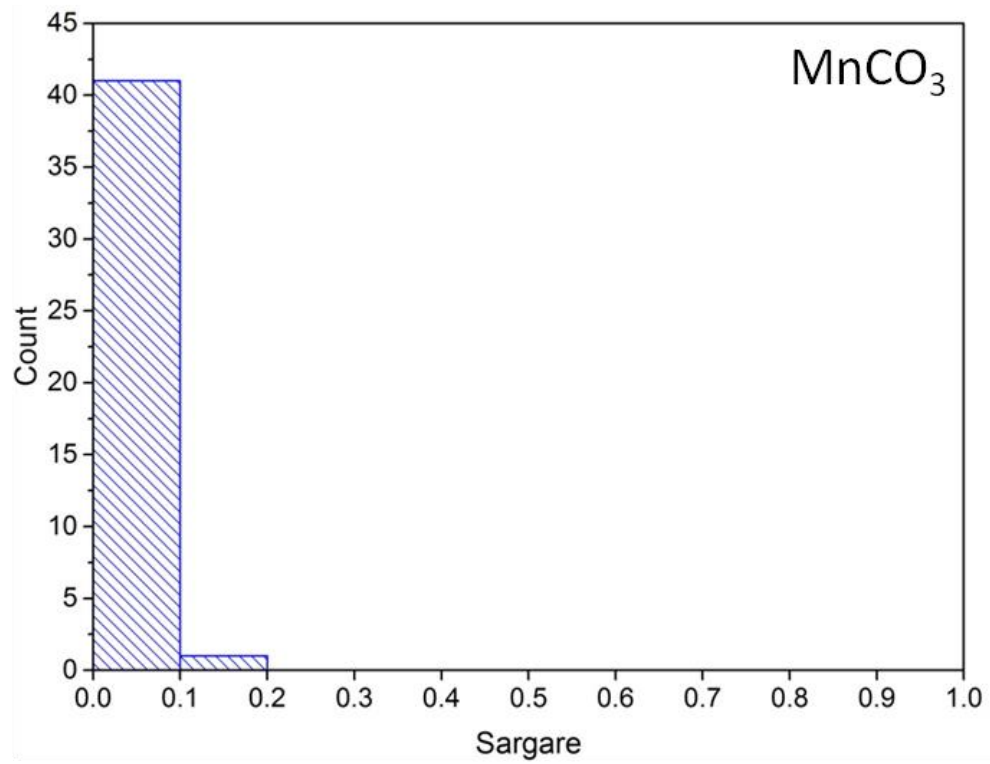
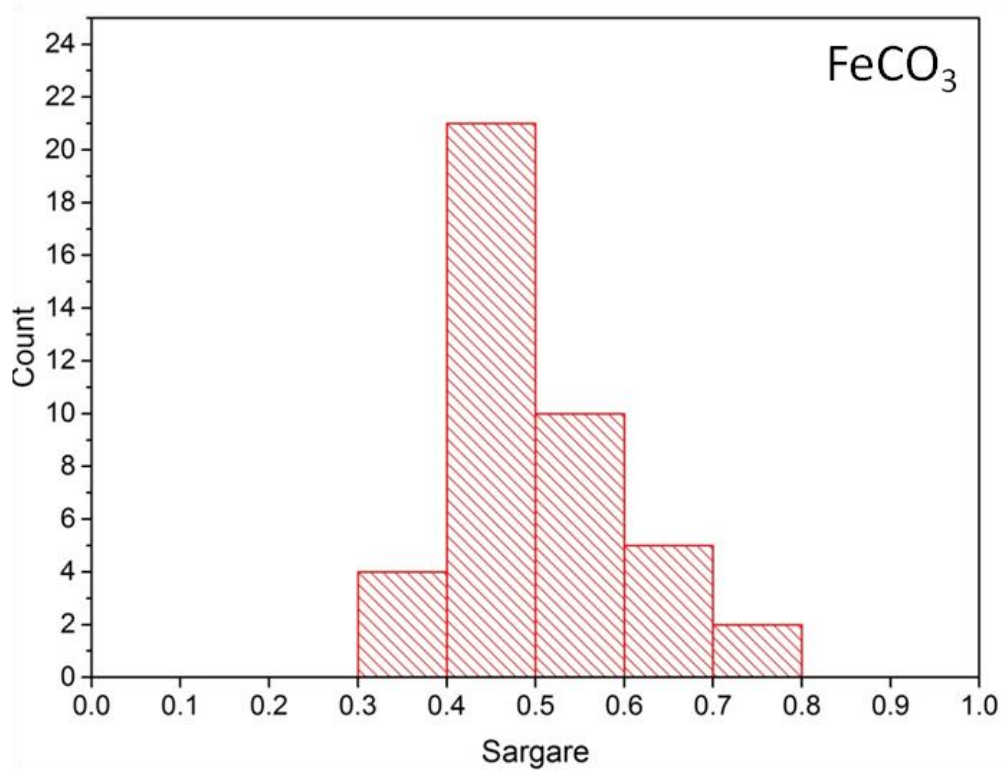
16KT101

Carbonate-hosted talc deposits, 2018



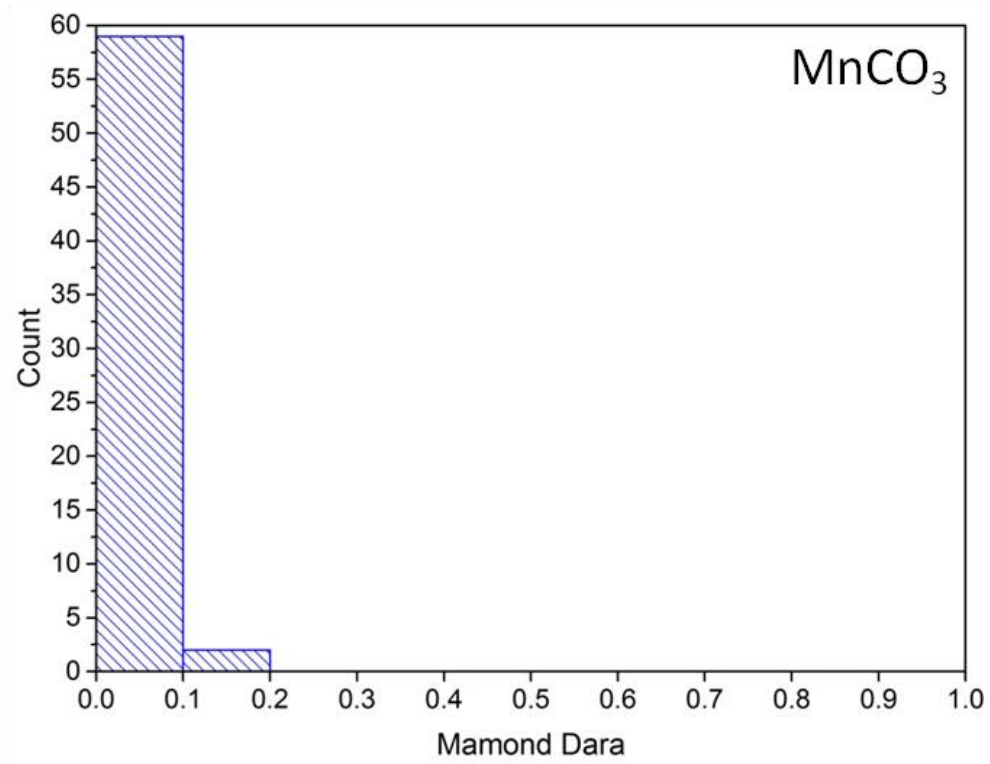
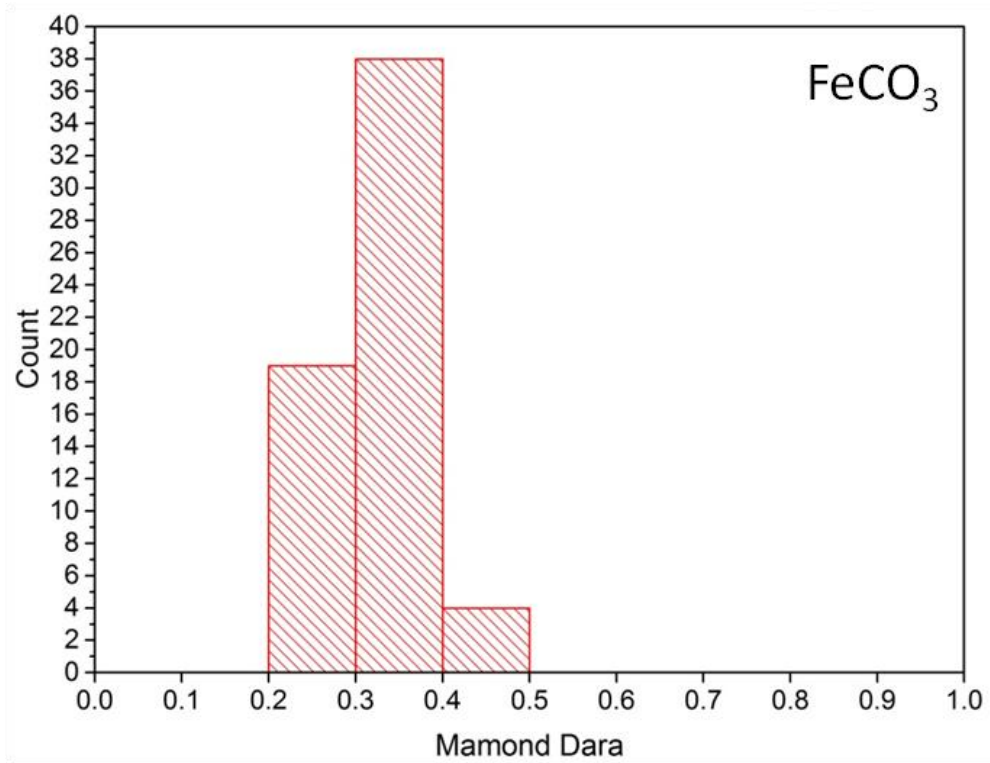
16WCD.Do

Carbonate-hosted talc deposits, 2018



16SRG03

Carbonate-hosted talc deposits, 2018



14AF18A

Carbonate-hosted talc deposits, 2018

